A METHODOLOGY FOR THE PREDICTION OF NON-VOLATILE PARTICULATE MATTER FROM AIRCRAFT GAS TURBINE ENGINE

A Dissertation
Presented to
The Academic Faculty

By

Kyung Hak Choo

In Partial Fulfillment
of the Requirements for the Degree
Doctor of Philosophy in the
School of Aerospace Engineering

Georgia Institute of Technology

August 2019

A METHODOLOGY FOR THE PREDICTION OF NON-VOLATILE PARTICULATE MATTER FROM AIRCRAFT GAS TURBINE ENGINE

Approved by:

Dr. Dimitri Mavris, Advisor
School of Aerospace Engineering
Georgia Institute of Technology

Dr. Jechiel Jagoda
School of Aerospace Engineering
Georgia Institute of Technology

Dr. Daniel Schrage
School of Aerospace Engineering
Georgia Institute of Technology

Dr. Jimmy Tai
School of Aerospace Engineering
Georgia Institute of Technology

Mr. Russell Denney
School of Aerospace Engineering
Georgia Institute of Technology

Dr. Reza Rezvani
Senior Engineer
Pratt & Whitney

Date Approved: July 15, 2019

For a successful technology, reality must take precedence over public relations, for nature cannot be fooled.

Richard P. Feynman

To my dear father and mother, to my wife and my little boy, for their endless support and encouragement. This work would have been completed earlier without them.

ACKNOWLEDGEMENTS

This work would not have been possible without support and encouragement from a great number of individuals. I would like to express my deepest appreciation to my advisor, Dr. Dimitri Mavris. His support and advice always encourage me not to give up the race in the middle. I would also like to extend my deepest gratitude to Dr. Jeff Jagoda. He has always been in my side whenever I needed his guidance. I would like to thank Dr. Jimmy Tai, who has taught and inspired me during my research, showing profound belief in my work. I thank Mr. Russ Denney, who has been my mentor with valuable insight during my long journey. I am also grateful to Dr. Daniel Schrage and Dr. Reza Rezvani for their guides, comments, and ingenious suggestions in my research.

Im deeply indebted to my parents and my wife. I would not be here without their endless support and love. I thank my little boy. He is my great pleasure, a source of my endeavor.

Last but not least, special thanks to all my friends, colleagues, faculty members, and staffs. Their advice, help, friendship, and kindness will never be forgotten.

I thank you all and wish your happiness and health.

Kyung Hak Choo

Atlanta, July 2019

TABLE OF CONTENTS

LIST OF TABLES

LIST OF FIGURES

SUMMARY

There is growing concern about the adverse effects of particulate matter emissions on human health and the environment. It is revealed that particulate emissions are responsible for cardiovascular and cardiopulmonary diseases resulting in reduced life expectancy as well as climate change. New regulation standards on aviation particulate matters are expected in the near future. For these reasons, particulate emissions become one of the important design constraints. They must be evaluated during the conceptual design of an aircraft engine.

Prediction of soot emission from gas turbine combustion is a major subject in this research. Soot is a non-volatile primary particulate matter emitted directly from the combustion chamber. As its size is extremely small, most aviation soot belongs to the PM2.5 category.

Current soot prediction methods utilize engine-specific information. They do not successfully compute combustor characteristics, which highly affects soot formation. As the current methods cannot handle engines with different cycles and sizes, they are not suitable for conceptual design.

Three hypotheses addressing air partitioning, sizing methodology, and statistical distribution are established to develop the prediction environment, capable of a variety of cycles of engines with different size and thrust. An integrated prediction environment is constructed based on these established hypotheses. The environment consists of a Combustor Flow Circuit model, Statistical Distribution Model with the unmixedness curve, Chemical Reactor Networks (CRN), and Soot Evaluation Model.

The Combustor Flow Circuit model, built on NPSS, computes air partitioning and sizes the combustor. The air partitioning model consists of NPSS elements, computing air distribution in the flow circuit via loss calculations in the combustor components. The Statistical Distribution Model is to model the imperfectly mixed primary zone over the parallelly

organized Perfectly Stirred Reactors with statistically distributed equivalence ratio. The Chemical Reactor Networks model, built on CHEMKIN, computes and provides thermodynamic properties of flow and species information from all reactors to the Soot Evaluation Model. The Soot Evaluation Model computes quantitative non-volatile PM based on the soot formation mechanism applied to the semi-empirical two-equation system. These submodels are integrated on ModelCenter and provides automated computations.

The integrated prediction environment developed with the proposed methodology shows good predictability for cycles of different size and thrust engines. The baseline environment is developed first and extended for different cycles. The unmixedness curve is generalized and embedded in the Statistical Distribution Model. The sizing model, scaling the length of combustion zones and the sizes of the holes based on the combustor requirements and input cycles, are embedded in the Combustor Flow Circuit Model. The extended prediction environment provides automated computations to predict non-volatile PM emission for given input cycles.

The predicted emissions for two engine cycles of different size and thrust are compared and validated against a group of correlations whose inputs are the Smoke Number measurement and engine operating conditions. The results demonstrate good predictability, agreeing with estimations from correlations. With the developed prediction environment, three hypotheses, the basis of the development, are evaluated via a set of experiments. The effects of air partitioning, sizing, and statistical distribution modeling on the prediction of the non-volatile PM emission are evaluated while hypotheses are proved.

A methodology for the prediction of the non-volatile particulate matter emitted from the aircraft gas turbine engine is introduced via the development of the integrated prediction environment. The air partitioning, sizing, and non-uniform mixture modelings are incorporated in the prediction environment providing the capability of handling cycles of a variety of sizes and thrust classes. As the input of the prediction environment is a cycle, the proposed methodology is adequate for the prediction of non-volatile PM during the conceptual

design of an aircraft engine.

CHAPTER 1
INTRODUCTION

1.1 Air Traffic Forecast and Emission Concerns

As a global industry expands and international exchange is growing, overall air traffic has consistently increased despite several economic crises. Due to the technology development and the effort to increase fuel efficiency, aircraft is an even more convenient option as international transportation as well as domestic transportation. For this reason, the aircraft is an attractive transportation method and even stiffer increase in air traffic in the future is expected.

Figure 1.1 shows historical data of air traffic from International Civil Aviation Organization(ICAO) data followed by the expected future traffic in the next 20 years from Airbus Global Market Forecast 2015[1] in Revenue Passenger Kilometer(RPK). In this historical data, it is observed that the air traffic was accelerated for the last decades despite several global crises. Based on the trend that air traffic has doubled every 15 years, Airbus company is expecting another double traffic in the next 15 years. This means that global air traffic will keep growing with an average annual rate of 4.6% during the 2014-2034 period.

Besides the Revenue Passenger Kilometer(RPK), the number of aircraft in service will also increase over the next 20 years, as shown in the Figure 1.2. There are currently 19,000 aircraft in service at the beginning of 2015. Among them, 13,100 aircraft, which are more than half, will be replaced and much more new aircraft will be in service.

However, the development of the aircraft industry also accompanies with the concern of emissions. There are a lot of research results showing the harmful effect of aircraft emissions on the environment as well as on human health. As the high demand for aircraft is expected, more concerns about the emissions arise.

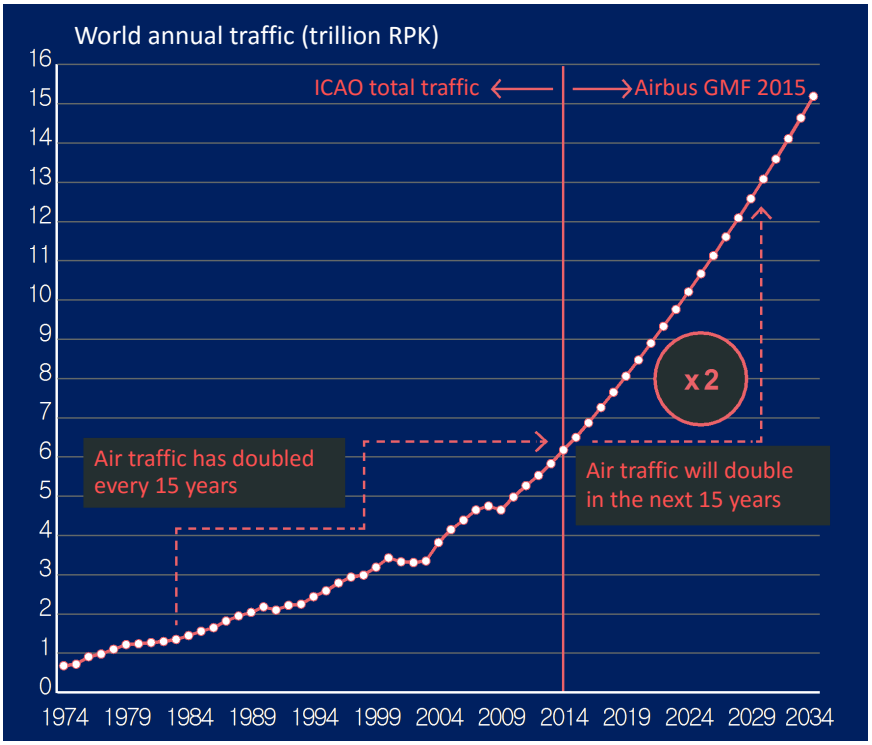

Figure 1.1: Historical Air Traffic and Forecast[1]

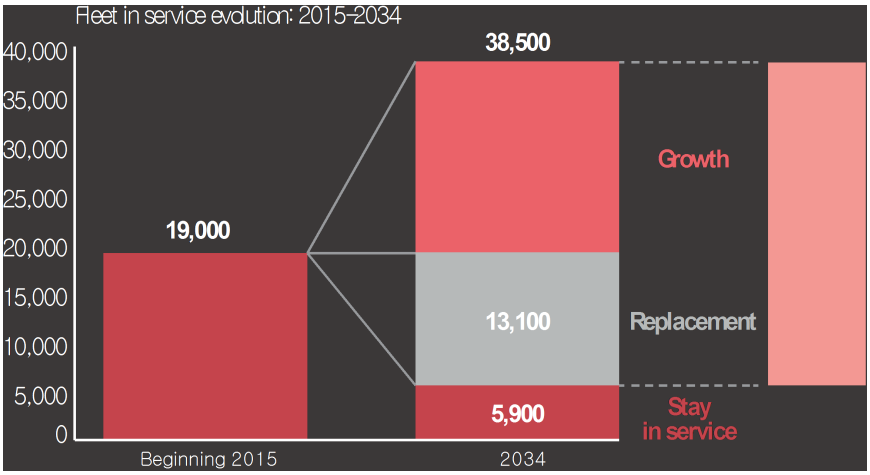

Figure 1.2: Fleet Increase over Next 20 Years[1]

To reduce the impact of aircraft emissions, ICAO sets regulations on aircraft emissions and the manufacturers must design the engines to meet the regulation requirements. These emissions include nitrogen oxides (NOx), carbon dioxide (CO), volatile organic compounds (VOC), unburned hydrocarbon (UHC), and smoke. However, the smoke emission which is the particulate matters (PM) was not well-understood when these regulations were set. It is recently revealed that the adverse effects of PM emission on the environment, climate, and human health is more serious than expected in the past. Therefore, there is an effort to set a new regulation on aircraft PM emission in the near future and the designers must consider it in the design.

1.2 Issues in the Particulate Matter Emissions

Health and Environmental Issues

The Particulate Matter (PM) has been one of the main issues for many researchers in a variety of fields due to its harmful effects on the environment as well as on human health. The World Health Organization defines the Particulate Matter (PM) as the sum of a mixture of solid and liquid (or both) suspended in the atmosphere.[2] This definition seems somewhat vague and too broad, at a glance, but this also means that PM is a very comprehensive terminology indicating all non-gaseous pollutants in the air. Dust, dirt, soil, pollen, soot, and liquid droplets are some examples of PM.[2][3]

Many recent studies have revealed that the adverse effects of PM on the health are more serious than what many researchers believed in the past. A report from World Health Organization[2] seriously warns that long-term exposure to the particulate matter ultimately reduces life expectancy. According to this report, frequent exposure to PM over a long period reduces lung function and makes people vulnerable to cardiovascular and cardiopulmonary diseases.

The U.S. Environmental Protection Agency (EPA)[3] also warns the harmful effect of PM. According to the EPA, the risk from the particulate matter is mainly due to its small

size. Because its size is so small, it reaches deep into lungs and bloodstream and causes many health issues. For this reason, EPA believes that PM is responsible for the premature death caused by heart and lung disease. More specifically, PM causes irregular heartbeat and nonfatal heart attacks. It also decreases lung function, aggravates asthma, and increases respiratory symptoms such as irritation of the airways, coughing or difficulties in breathing.

EPA also warns the environmental damage caused by PM. PM acidizes water and changes the nutrient balance of lakes and streams. On the ground, it depletes soil nutrients, damages forest and crops, and disturbs the ecosystem.[3]

Kolb[4] argues that PM is highly responsible for climate change. For the direct effect, PM affects the radiative balance of Earth. PM absorbs incoming solar and Earth radiation. This is the warming effect. However, at the same time, PM also shows the cooling effect by back-scattering solar radiation. The indirect effect is related to precipitation. PM plays a role as nuclei of cloud condensation. When clouds are formed by small particles, droplets are more likely smaller than usual and less likely to precipitate. These clouds live longer while suppressing rainfall and snowfall, and leading drought.

An article written by Tollefson[5] shows the environmental effect of the black carbon, or soot, which is one of the major pollutants in PM study. According to his article, the soot forms the haze and it spreads over all around the world by the wind because particles are so small and light, affecting the climate of many regions. As a result, it largely contributes the Arctic warming and global warming. It promotes snow melting, glacier retreats, flooding, and droughts in all around the world.

As discussed so far, there are so many pieces of evidence showing that PM is harmful to our health and Earth. Because the academic research of this field has accumulated scientific background enough to build global agreement on the need of international regulation on aircraft PM emission, engine manufacturers must consider PM emission at the early stage of design.

Categories of PM

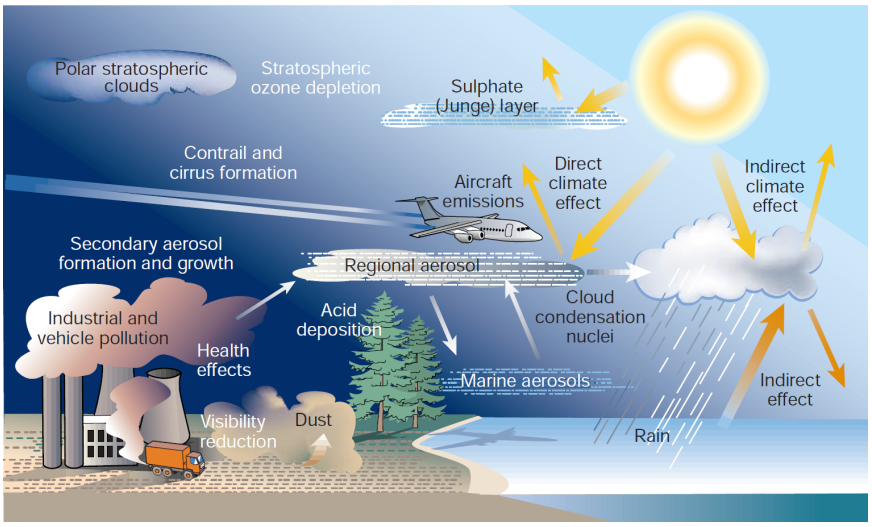

Figure 1.3: PM effects on health and environment[4]

Now that the size is an important factor which has close relationship with human health and environment, many organizations and researchers often categorize PM by size. According to the WHO report[2], two main categories are PM_{10} and $PM_{2.5}$. PM_{10} is called "fine particle" whose aerodynamic diameter is 10 micrometer or less and $PM_{2.5}$ is "ultra-fine particle" whose aerodynamic diameter is 2.5 micrometer or less. Thereforem, $PM_{2.5}$ is a subset of PM_{10}. Although the mass contribution of $PM_{2.5}$ to the total PM is very low (a few %), $PM_{2.5}$ is huge in number (over 90%)[2]. Reduced visibility is mainly due to $PM_{2.5}$ emission.[3] Because most PM emission from the aviation belongs to this $PM_{2.5}$ category[6][7], the main focus of this thesis proposal will be $PM_{2.5}$ emission.

PM can also be characterized by the source where it is emitted. When it is emitted to the atmosphere directly from the source such as the combustion of fuel, it is called "primary PM".[8] The secondary PM is formed and evolves in the atmosphere by the oxidation of gaseous precursors.[4] The main focus in aviation is the primary PM because it is the direct emission from the engine while the secondary PM experiences complicated formation path in the atmosphere with the interaction of other gaseous particles.

The PM emission from the aircraft can also be categorized by its component volatility. The two categories are the volatile PM and the non-volatile PM.[9] The sources of volatile

PM are fuel sulfur content, fuel organics, and lubrication oil. It is formed in the exit plume. The non-volatile PM is mainly the soot, or carbonaceous black carbon.[8] Although metals are also in non-volatile category, they are often ignored because of their extremely small amount.[7] The soot, or the non-volatile PM is formed inside the combustion chamber by the combustion process. As its name implies, it is thermally stable at the condition of the engine exit and shows almost no change in size and number between the combustor exit and the engine exit.[8] While the sources directly affect the amount of the volatile PM emissions, the non-volatile PM emission is highly dependent on the combustion process like other emissions such as NOx and CO. In the conceptual design stage, the non-volatile PM is of interest because the volatile PM emission is rather directly related to the detail design and the amount of source.

Based on the discussion above, this thesis proposal will focus on the non-volatile PM (soot) emission from gas turbine combustor in $PM_{2.5}$ category at the conceptual design phase.

CHAPTER 2

LITERATURE SEARCH

2.1 State-of-the-Art of Soot Prediction

Soot particles experience complicated paths through the flame. In order to simplify the problem, four main stages of the soot evolution are generally considered in the study of soot formation [10]. The first step is the inception stage, or the nucleation stage, where the initial soot particle is formed. The next stage is the surface growth stage where the initial particles grow as more carbon and other species are added on the soot particle surface. The larger surface area generally accelerates the surface growth rate. There is the oxidation stage where the soot particles are oxidized. The major oxidizers are hydroxyl radical and oxygen. Through the agglomeration (coagulation) stage, soot particles increase their size and reduce numbers. During these four stages (inception, surface growth, oxidation, coagulation), soot particles interact with other species such as acetylene species. Polycyclic aromatic hydrocarbon (PAH) path is often closely involved in the soot formation process. To "predict" the soot emission, the soot formation rates in each evolution stage are often the main research interest in many soot-related studies.

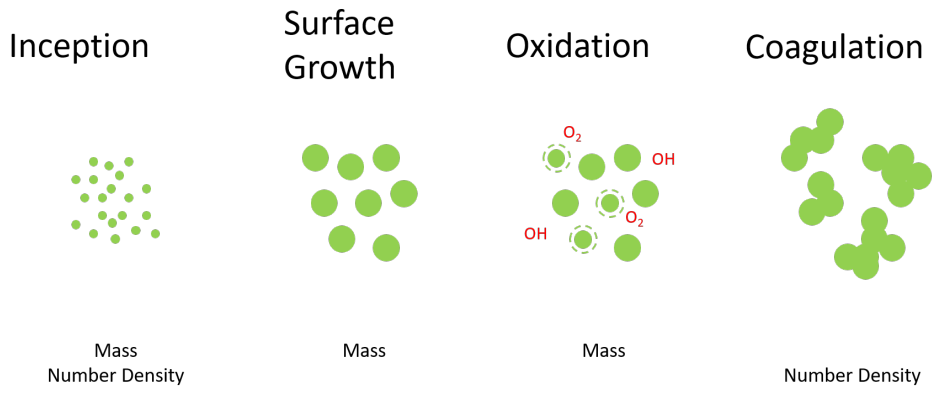

Figure 2.1: Soot evolution stages

In the early days when the emissions became a growing issue after people experience several smogs in the metropolitan cities, soot emission was also an important issue. However, it was not fully because of its harmful effect on health or environment at that time. Its adverse effects are revealed rather recently and a lot of studies are still in progress nowadays. In the early days, people focused on its visible effects. Many people thought the air was not safe for breathing when the visible pollutants made the air not clear. For this reason, the regulation and the standard procedure of measurement of the soot emission established in the early days also focused on the clarity of the air. With the lack of new regulations so far, the smoke regulation set earlier is still active although a discussion on the new standard of PM regulation is currently active. The current regulation is set the maximum level of smoke number[11]:

$$\textit{Regulatory Smoke Number} = 83.6\,(F_{oo})^{-0.274}\textit{, or a value of } 50\textit{, whichever is lower}$$

The *Smoke Number* (SN in short) in the regulation above is an empirical scale ranging from 0 to 100. 0 of SN means no smoke is measured during the engine certification process. More details on the current regulation are in the background chapter.

Another issue in soot emission is radiation. This is the issue mainly for the combustor designers. The radiation from soot is an unexpected heat source in the downstream of the combustor. Combustor designers want to burn most fuel in the front part of the combustor so that they can control the flow temperature and protect the combustor wall and turbine blades. However, the soot particles consist of many carbon molecules such that they keep the heat released by the fuel-air pyrolysis and oxidation reactions and emit it through the radiation into the downstream flow where the flow temperature is supposed to be lower than a material threshold temperature. This radiation threats the component durability. This is a very undesirable phenomenon for both designers and operators.

The early studies in the 20th century mainly targeted simple flames and light fuels

rather than real combustion of a gas turbine engine and heavy jet fuels. For example, Neoh et al.[12] used the premixed methane flame in the lab burner environment to study the oxidation of soot. They revealed that the OH radical is the primary oxidant and the O_2 molecule is the secondary one. In this study, their lab burner is far from the real practical combustion flame. Their premixed condition is also not as realistic as the actual flow in the practical combustion is non-premixed. Furthermore, this study was conducted under atmospheric condition despite the fact that the actual flow pressure and temperature are much higher than the atmospheric condition as the flow passes through the compressor. The methane fuel may be practical when it comes to the industrial ground gas turbine which uses natural gas. However, this fuel is not practical for the application of aviation combustion. The aviation fuel is generally much heavier than the methane. Their foundation can be applied to the soot prediction because they found the collision efficiency of OH radical which is one of the fundamental characteristics in soot evolution. However, their study is not enough to give confidence that their results will be the same for the actual combustor flames as their condition is not realistic.

There are a lot more similar examples of research that were conducted for the light fuels and the simple flames setup. Moss et al.[13] performed the numerical simulation and experiments for co-flowing turbulent diffusion flame with ethylene fuel under the atmospheric pressure to 3 bar condition. Their objective was to predict soot and provide property maps. They used a simplified two-equation model with laminar flamelet approach in their simulation. Their experiments and simulations environment was far from combustion in the industry, as shown in Figure. 2.2. Leung et al.[14] developed a simplified soot formation model by providing simple formation rates of soot in all four stages of the soot evolution. However, their research was also conducted for the laboratory condition which was the non-premixed counterflow with ethylene and propane fuel. Puri et al.[15] measured soot particle size and concentration and performed OH Planar Laser-Induced Fluorescence (PLIF) in the small axisymmetric laminar coannular burner with methane and butane fu-

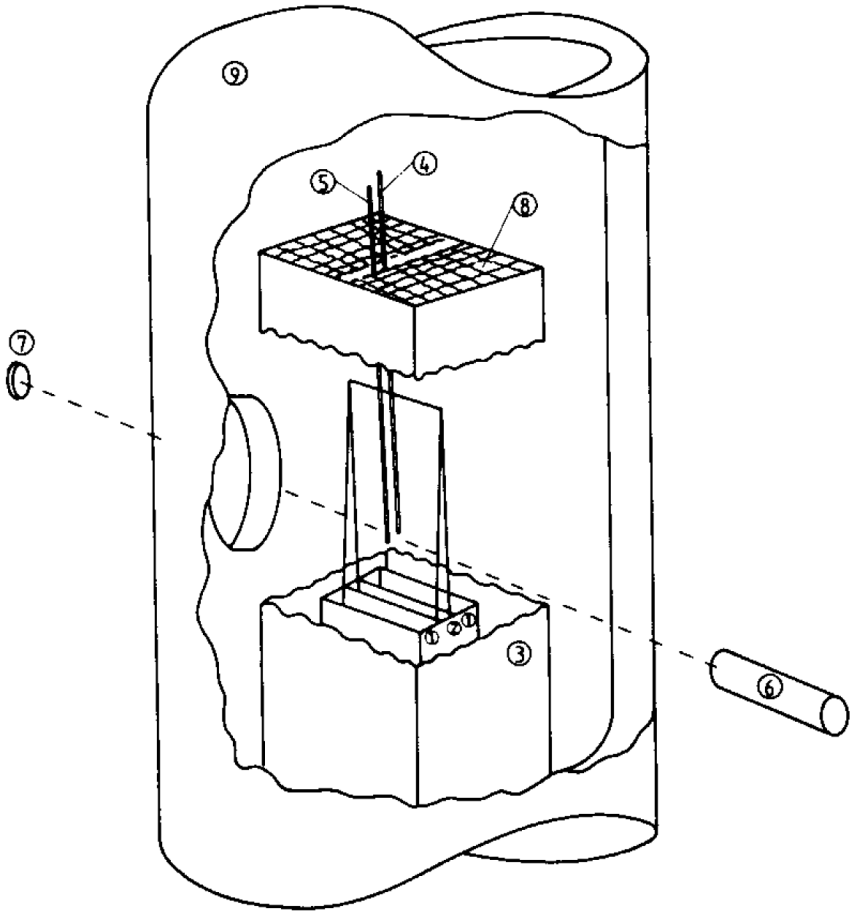

Figure 2.2: Experimental Configuration of Moss et al.(1: air slots, 2: fuel slots, 3: rectangular duct, 4: quartz microprobe, 5: thermocouple probe, 6: laser, 7: photodiode, 8: gauze, 9: pressure vessel)[13]

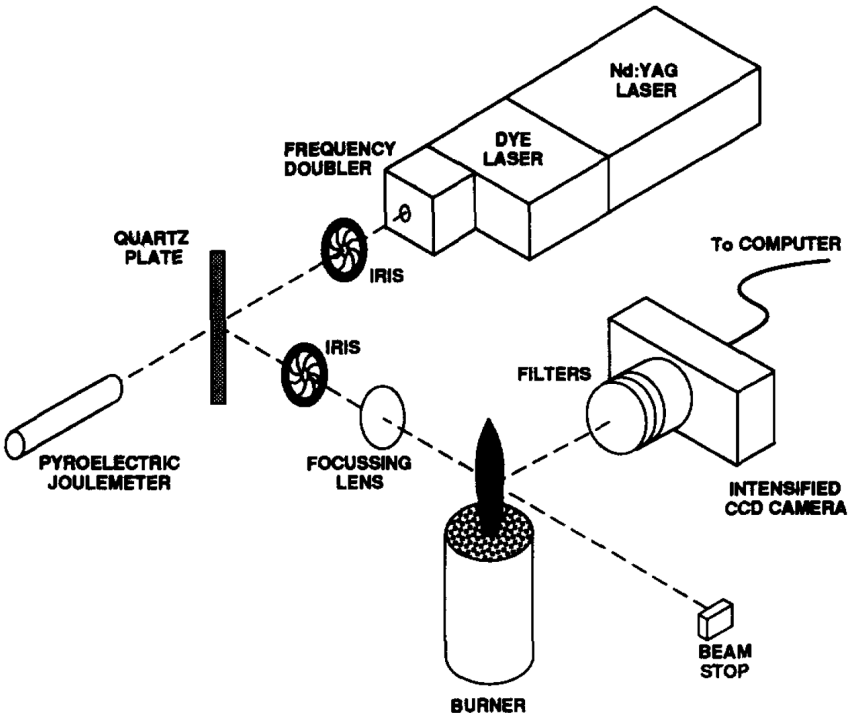

Figure 2.3: LIF Experimental Setup of Puri et al.[15]

els under the atmospheric pressure, as depicted in Figure 2.3. They studied the oxidation rate and concluded that the hydroxyl radical is the more dominant oxidizer of soot than the oxygen molecule. They revealed that the soot interrupts the reaction between the hydroxyl and carbon monoxide by reacting with hydroxyl radicals. Sunderland and Faeth[16] found some fundamental properties of soot formation rate such as acetylene and ethylene collision frequencies of growth rate and activation energy of nucleation rate from their experiment on the round laminar jet diffusion flame under the pressure of 25-99 kPa, which is lower than the atmospheric pressure, with many light fuels including ethane, propane, n-butane, ethylene, propylene, and 1, 3-butadiene. Brookes and Moss[17] simulated confined co-flowing turbulent jet flame burning methane fuel at 1 and 3 atm of pressure and 290 Kelvin flow temperature in their computational modeling of coupled soot production rate and thermal radiation loss for the prediction of soot.

As observed in the works listed above, the general strategy of early works is to work on formation rate, use it with numerical simulation, compare the simulation results with exper-

imental results, and validate their prediction. There are several limitations in these works. They cannot predict the soot emission from the real gas turbine combustion although they can predict local soot quantity when the initial condition is provided. There are several reasons for it. Because soot rate expressions highly depend on the local conditions, the correct thermodynamic properties and flow field information inside the three-dimensional combustor space as well as detail geometry information are required to simulation the real combustor. The detail geometry structure is generally not open to the public. The combustor geometry is a result of many considerations including, mixing, ignition, staging, emissions, stability, etc. Manufacturers do not want to open these company assets which are a result of their tremendous research time and budget. For the flow field information, there are not enough measurement data. Because the flow field inside the burning combustor is very complicated as well as very hot and highly pressurized, there were not many options to take for measurement in the old time. This is still true although new techniques are being developed. With the lack of detail data, researchers have to rely on numerical simulation to estimate the combustor flow field. However, these kinds of calculations usually require high computing power and calculation time. The hardware specifications were not enough to afford the computational cost for them. Therefore, early works usually focused on the fundamental characteristics of soot formation under the relatively simple flame structure rather than the real combustor flow field.

Another limitation of the early works is the fuel used in their research. Unlike the natural gas that is used in the gas turbine for the ground power plant and whose major component is the methane(CH_4), the jet fuel used in the aviation gas turbine is loosely defined and consists of many species including high C number hydrocarbons. Its pyrolysis reaction path is extremely complicated as a lot of species and their elementary reactions are related. It is a very tough task to make good representative jet fuel and generate pyrolysis mechanism. However, research on light hydrocarbon fuels of with low C numbers has been done for a long time and many combustion mechanisms are developed. For this reason,

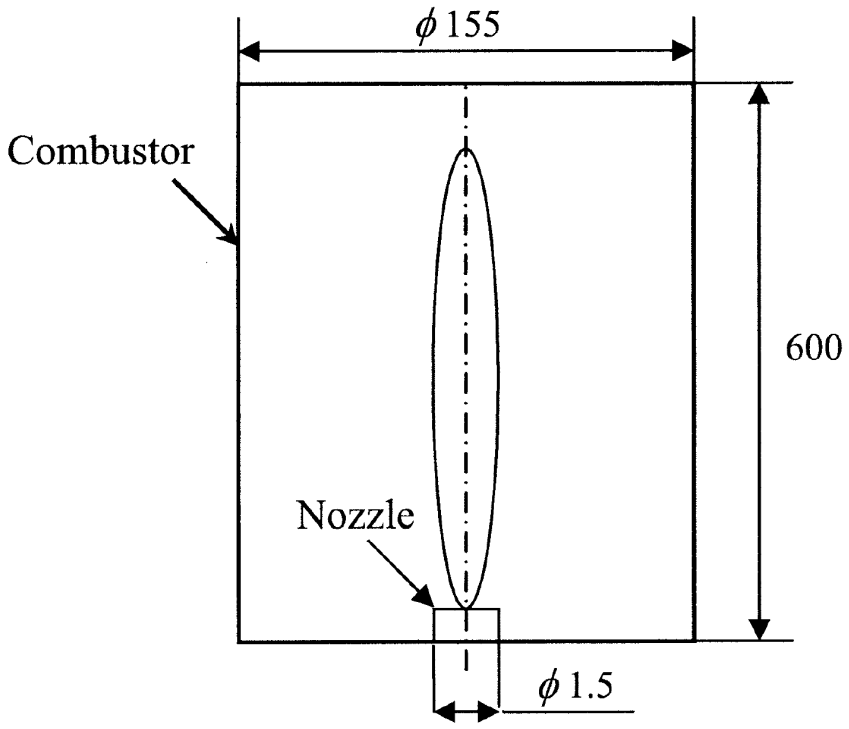

Figure 2.4: Burner and flame configuration of Wen et al.'s numerical simulation[18]

early soot works focused on the light fuels to discover the fundamental reaction path which can be also applied to the heavy fuel reactions.

As computation power is improved and more research on soot formation and jet fuel is conducted, many scholars tried studies for more complex flame condition or aviation fuel combustion. However, because these study conditions are still computationally heavy, either condition is often chosen. Wen el al.[18] compared the predictive capability of the acetylene inception model and the PAH inception model by performing a numerical simulation of co-flowing turbulent jet diffusion flame. In their simulations, they used kerosene fuel although their burner configuration was still simple and far from the actual practical combustor, as shown in Figure 2.4. Saffaripour et al.[19] measured soot and some species radial and centerline profile in the laminar co-flow diffusion flame under atmospheric pressure. They also used aviation grade fuel(Jet-A1). Franzelli et al.[20] performed Large Eddy Simulations(LES) for the model combustor with swirler with ethylene fuel. They tried to simulate the flow field closer to the practical combustor rather than the simple flame as

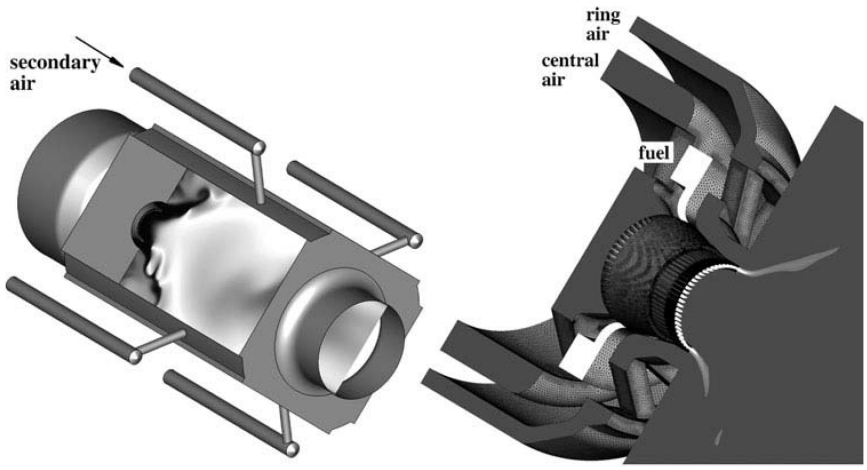

Figure 2.5: Computational domain and injector system of Eberle et al.[22]

they used the burner model and swirler. Eberle et al.[21][22] also used ethylene fuel in the numerical simulation of a model combustor which has swirler and injector. Both Franzelli et al. and Eberle et al. tried to make their condition closer to the practical combustor environment with limited computational power, they referred their burner as aero-engine model combustor, as shown in the Figure 2.5. These works used either the jet fuel with simple flame or the simple flame with the model combustor. As mentioned above, this is because of the computational cost. Although technology is improved, the calculation of jet fuel pyrolysis and reacting flow field inside the combustor require huge computing power. Even though Franzelli et al. and Eberle et al. used ethylene fuel, their strategy was to apply simple two-equation system for the calculation of soot to avoid a heavy computational load of calculation of chemical reactions involving soot. More recently, Koo et al.[23] performed LES simulation on rich-burn, quick-quench, lean-burn (RQL) type combustor and compared the soot volume fraction with experimental data. They used ethylene fuel. They referred their simulation environment as RQL type combustor, not actual RQL combustor. They replicated RQL condition by applying secondary air injection. Therefore, their simulation condition was not the same as the practical operating condition.

As the health and environmental concerns are growing, general guidelines and regulations for the particulate matters are established in many industry fields. A new regulation

on particulate emissions from aviation is also expected in the near future. This regulation is a strong motivation for manufacturers and researchers to understand the characteristics of soot emissions from a more practical perspective. Many works have been done already to discover the fundamental and basic characteristics of soot formation, as described above. Therefore, with the base of previous studies, many works for both practical fuel and combustion are attempted recently despite the complexity of jet fuel pyrolysis and practical combustion phenomena. Moriai et al.[24] performed experimental study and numerical simulation to predict NOx and soot concentration under the atmospheric pressure. They used Jet-A surrogate and 1/2 subscale aircraft gas turbine combustor. Their combustor modeled RQL combustor. Although their combustor is the laboratory combustor as shown in Figure 2.6a, they reproduce the environment similar to the practical combustor as their combustor is equipped with air blast type fuel nozzle, as shown in Figure 2.6b. Mueller and Pitch[25] tried integrated LES approach with Jet-A surrogate to simulate soot evolution in the aircraft gas turbine combustor. In this work, both practical combustor and practical fuel were used. Their simulation combustor was Pratt & Whitney RQL combustor and they did not mention about the detail of it. Figure 2.7 shows their simulation. Dupoirieux et al.[26] performed numerical simulation and experimental study with liquid kerosene to predict soot volume fraction. A square burner with a Twin Annular Premixing swirler (TAPS) injector was used to predict soot volume fraction in their research. Because of the complex flow field and chemical reactions of fuel oxidation, they used a simple two-equation system for soot volume calculation to manage reasonable CPU time. Ghose et al.[27] performed numerical simulations of a laboratory scale combustor burning Jet-A fuel. Their combustor has pressure swirl atomizer and they predicted soot volume fraction and thermal radiation for different swirl vane angle.

Many soot works are focused on the experiments and numerical simulations. An experiment is one of the most preferred methods to achieve data. Scholars analyze data and discover the underlying fundamental physics of soot formation. Numerical simulations

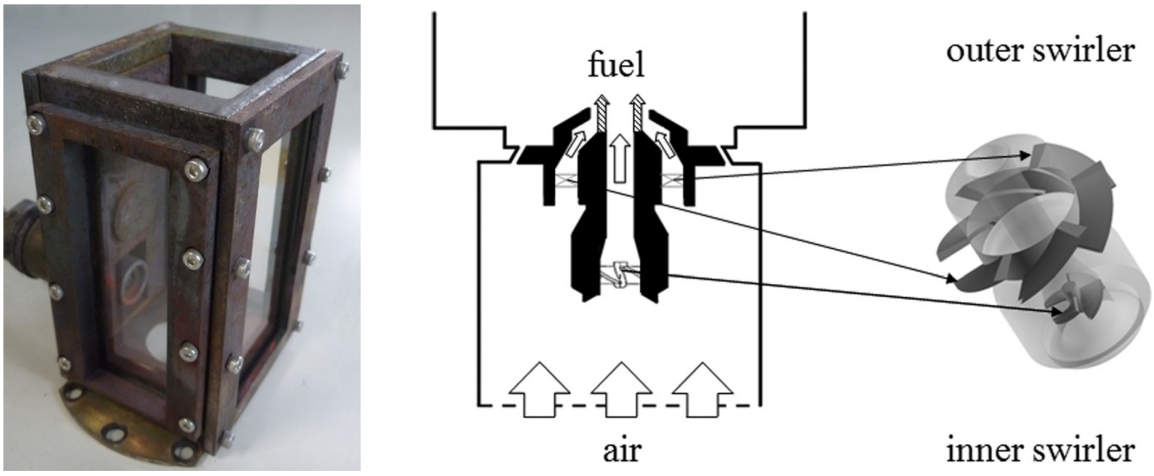

(a) Subscale combustor

(b) Nozzle configuration

Figure 2.6: Subscale combustor and nozzle configuration of Moriai et al.[24]

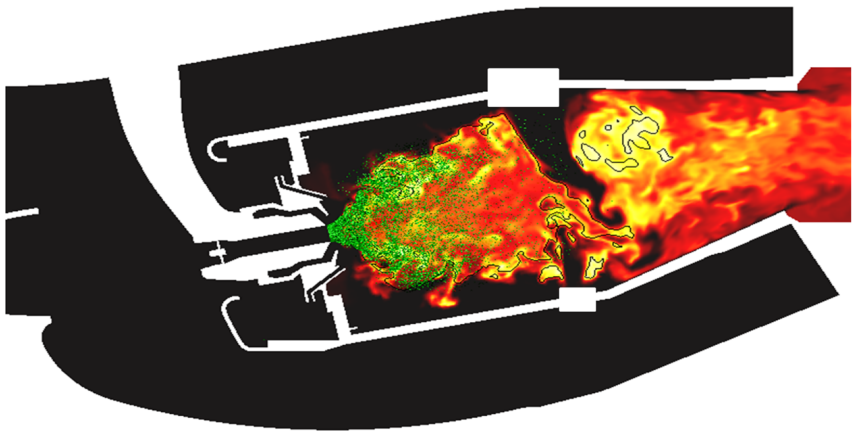

Figure 2.7: LES simulation of PW RQL combustor by Mueller and Pitch[25]

often follow the experiment. Scholars can broaden their understanding by comparing the results of the experiment and numerical simulation. Moreover, with confidence in their new theory on soot formation theory, numerical simulation is used to predict soot and experimental data provides the validation data of prediction. This strategy is very common in soot study because the validity of this strategy is historically proven in many combustion studies. However, it is also true that this strategy accompanies a lot of time and cost due to the complexity of the flow field and the chemical mechanism of jet fuel. That is why many works were not performed for practical jet fuel or practical combustor.

There are a few works performed with a different approach to overcome this issue. They tried reactor networks instead of detailed numerical simulations. The reactor networks approximate the complex flow field and represent it as an equivalent network form. This approach was developed earlier for NOx study when the computing power was not high enough to perform CFD simulations. Although the accuracy of reactor networks is less than CFD simulations, many scholars insist that its accuracy is still reasonable to capture physical and chemical trends of combustion phenomena with dramatic reduction of computation time. For this reason, this method is still actively used in many NOx studies. With success in NOx problems, some scholars adopted network reactor approach in soot problem.

Martini[28] applied a chemical reactor network (CRN) to predict soot from CRM56-2C and PW4090 engines. His CRN was originally developed for previous NOx study by utilizing real data of modeled engines. His model consists of parallel perfectly stirred reactors (PSR) to describe unmixed flow in the primary zone with statistical distribution and a series of plug flow reactor (PFR) to describe the downstream flow. He used a model aviation jet fuel developed based on the GRI mechanism. Moniruzzaman and Yu[29] predicted many combustion products and species including soot from the simulation of their reactor network. Their reactor network consists of multiple unmixed gas parcels and one mixed gas parcel. The unmixed gas parcels in their model are described in a statistical

distribution and continuously mixed into the mixed gas parcel. They specifically targeted the idle power condition of CFM56-2-C1 engine burning Jet-A1 fuel. By utilizing detailed information of target engine with lots of gas parcels from upstream to downstream of the combustor, they could achieve detailed species profile through the combustor. Choo et al.[10] made chemical reactor network (CRN) consisting of three series of parallel PSRs to describe time-evolving statistical distribution of non-uniform flow at the primary zone of the RQL combustor to predict soot emission from PW4168 engine burning Jet-A1 fuel. By doing so, they could avoid the issue of detailed geometry that is essential in many numerical simulations. However, required reactor information such as residence times of local combustion zones was taken from their previous NOx prediction model although they build a new CRN for this research. As the combustion process is highly affected by the initial condition of the flow, errors due to approximated cycle information can cause high uncertainties in soot evaluation. They resolved this issue by acquiring thermodynamic cycle information at station 3 from detailed engine cycle analysis. However, deep analysis of engine cycle is another complex project that is not easily accessible to the public in many cases. For this reason, cycle inputs are calculated from simple approximation or real data are used in many works. Bisson et al.[30] also achieved operating conditions of target engine from simple calculations with several assumptions and from real data. They generated CRN with a set of parallel PSRs and a series of PFRs. One interesting characteristic of their study is the inclusion of post-combustor region. They applied a statistical distribution of non-uniform flow at the primary zone with parallel PSRs like many other studies and they described downstream components with PFRs from the secondary zone of the combustor to the nozzle of the engine. They calibrated their model against NOx and CO emissions of CFM56-2C1 engine with jet-A1 fuel surrogate. Then, they compared predicted soot results against measurement data. They used geometry information and air partitioning information of a prototype combustor of single annular combustor (SAC) combustor which is the Energy Efficient Engine (E^3 engine) whose length to height ratio is similar to that of the

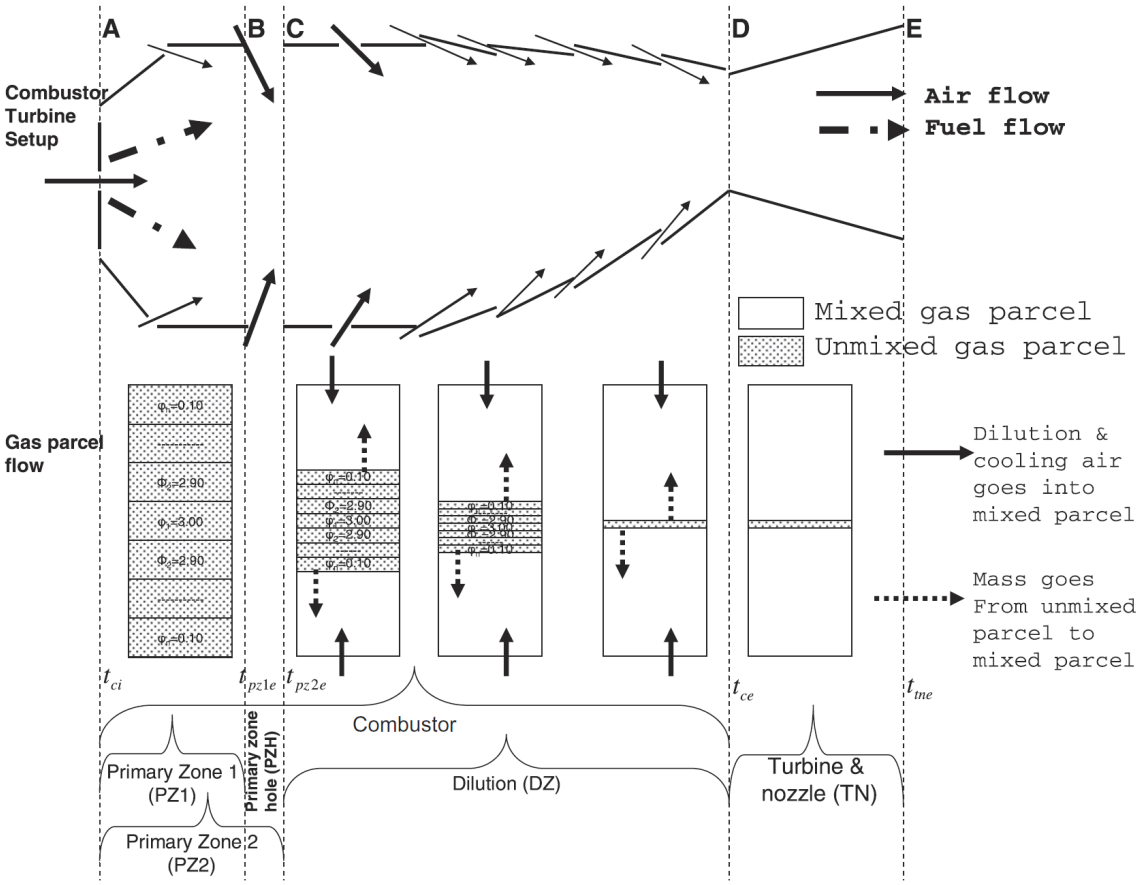

Figure 2.8: Schematic of reactor network model of Moniruzzaman and Yu[29]

target engine(CFM56-2C1).

Many scholars have devoted to discovering fundamental characteristics of soot formation in combustion to predict soot in practical operating conditions. As concerns on health, climate, and environment are growing, regulations will be more stringent and the soot prediction during the design process will be a more important constraint for engine designers. However, at the current level of technology, soot problems in practical operating conditions are still difficult due to not enough computation power. Although some recent works achieved good results by applying new approaches instead of complicated numerical simulations, current methods are not fully enough to be utilized when it comes to the conceptual design of aircraft gas turbine engine despite lots of efforts to predict soot. In the next section, requirements of soot prediction methods for the use in the conceptual design of

Table 2.1: Some examples of soot prediction research

Author	**Fuel**	**Combustion type**	**Year**
Neoh et al.[12]	methane	premixed flame, lab burner	1985
Moss et al.[13]	ethylene	co-flowing turbulent diffusion flame	1989
Leung et al.[14]	ethylene, propane	non-premixed counterflow flame	1991
Puri et al.[15]	methane, butane	axisymmetric laminar coannular burner	1994
Sunderland and Faeth[16]	ethane, propane, n-butane, ethylene, propylene, 1, 3-butadiene	round laminar jet diffusion flame	1996
Brookes and Moss[17]	methane	confined co-flowing turbulent jet flame	1999
Wen el al.[18]	kerosene	co-flowing turbulent jet diffusion flame	2003
Saffaripour et al.[19]	Jet-A1	laminar co-flow diffusion flame	2011
Franzelli et al.[20]	ethylene	aero-engine model combustor with swirler	2015
Eberle et al.[21][22]	ethylene	aero-engine model combustor with swirler and injector	2015
Koo et al.[23]	ethylene	RQL type combustor	2017
Moriai et al.[24]	Jet-A	1/2 subscale aircraft gas turbine combustor	2013
Mueller and Pitch[25]	Jet-A	Pratt & Whitney RQL combustor	2013
Dupoirieux et al.[26]	liquid kerosene	square burner with TAPS injector	2016
Ghose et al.[27]	Jet-A	laboratory scale combustor with pressure swirl atomizer	2016
Martini[28]	model aviation jet fuel	CRM56-2C, PW4090 engines	2008
Moniruzzaman and Yu[29]	Jet-A1	idle power condition of CFM56-2-C1 engine	2012
Choo et al.[10]	Jet-A1	primary zone of RQL combustor (PW4168 engine)	2015
Bisson et al.[30]	Jet-A1	CFM56-2C1 engine	2016

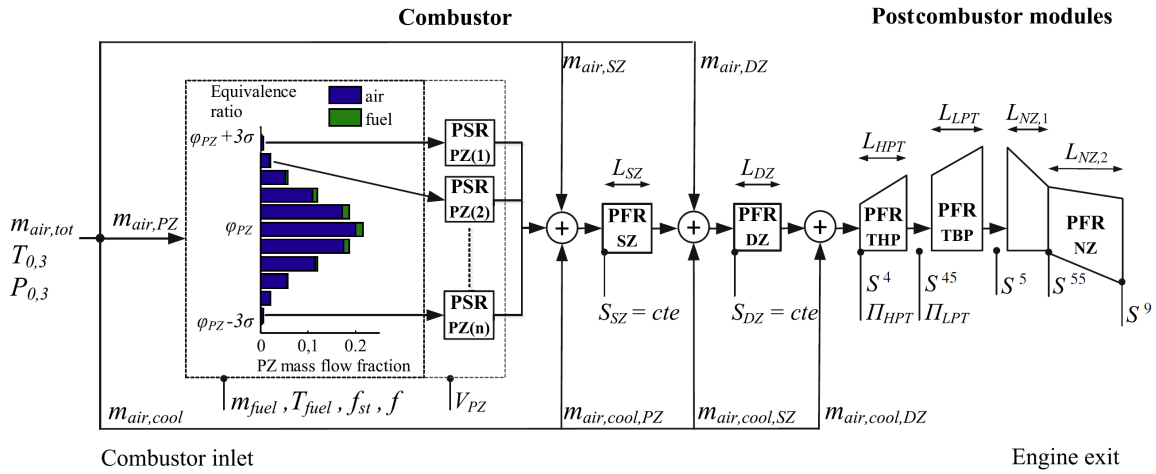

Figure 2.9: Schematic of chemical reactor networks of Bisson et al. and input parameters[30]

aircraft gas turbine engines will be discussed and current soot prediction methods will be evaluated against requirements of conceptual design.

2.2 Requirements of Soot Prediction during Conceptual Design

Design process starts from the conceptual design phase. The preliminary design phase is the next. These two are the early design phases. After these phases, the detailed design phase starts. Figure 2.10 shows this series of processes. In this figure, the conceptual design phase takes a relatively small portion of the total process time. Nevertheless, several interesting characteristics are observed in this figure. Because this is the beginning of the whole design process, there is a lot of design freedom at this phase (blue line). With the same reason, the level of knowledge on the design product is very low (black line). However, despite its short process period and low knowledge level, a huge amount of cost is committed during this phase (red line). In short, the conceptual design phase can be described as high freedom of design, low knowledge on the product, and high expenditure of budget. This is because the conceptual design is the step where requirements and constraints are defined and a lot of combinations of design alternatives are reviewed and evaluated. This is to decide the direction of the design process and the expected final product.

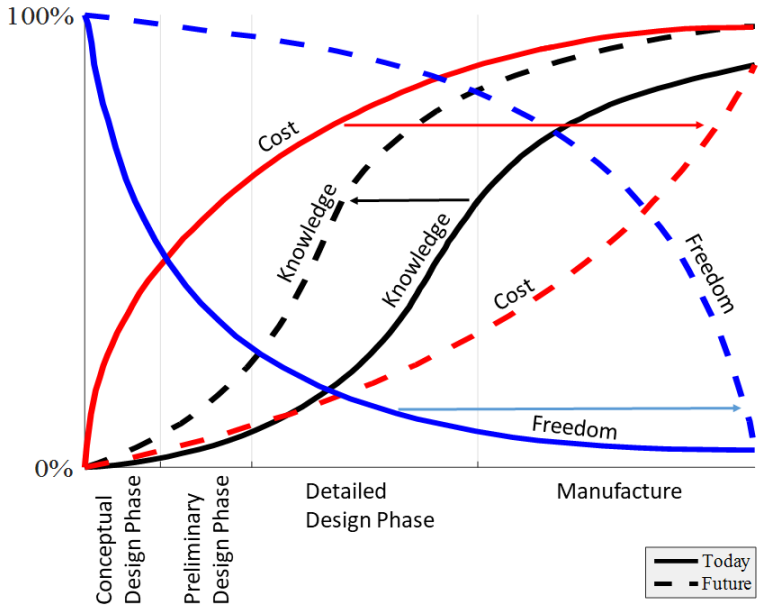

Figure 2.10: Design steps and cost, knowledge, freedom relations, redrawn from Fabrycky and Blanchard(1991)[31]

Decision makers review possible options among the available alternatives such that requirements and constraints are satisfied. For example, decision makers may need to evaluate options to see if fixed wing type will be appropriate or rotorcraft type will be appropriate for given performance requirements when it comes to the aircraft design. They also need to decide what type of wing and body will be appropriate in the next step when they decide to design a fixed-wing aircraft. They need to review and evaluate the traditional tube-and-wing design and the hybrid wing body design. They also need to decide how big the aircraft should be and what engines are appropriate. When it comes to engine design, the types of an engine such as turboshaft, turbofan, and turbojet are alternatives to be evaluated. Also, the cycle such as pressure ratio, bypass ratio, combustor types, etc. are alternatives to be evaluated. The type of compressor, the number of stages of the compressor, the number of spools, thermodynamic cycles and properties at stations, bleed flow, nozzle type, etc. should be addressed during the early phase of the design.

As shown in the examples above, there are so many combinations of alternatives pos-

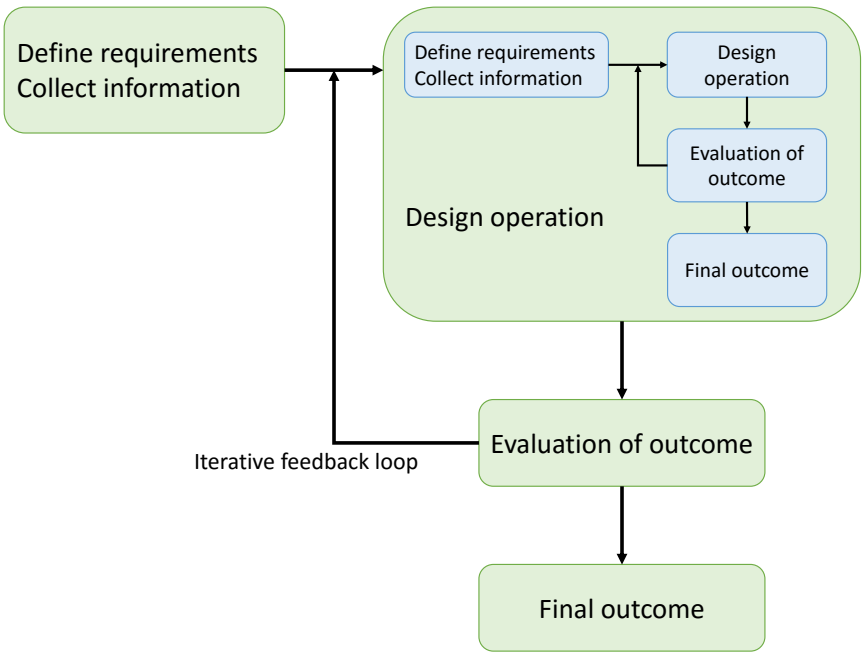

Figure 2.11: Iterative design loop

sible during the conceptual design. However, due to the lack of knowledge, the quality of the product often deviates from the design standards during the later phase of the design process. When it happens, designers alleviate the requirements and constraints standard if possible. If the deviation is not small, then they go back to the early phase of the design, make some modifications, and repeat the design process to satisfy the design standards. This trial-and-error type feedback iteration is very common during the design. Figure 2.11 shows the iterative feedback loop of the design process. As the knowledge is not enough, lots of uncertainties are inherently embedded in the decisions made during the conceptual design and unexpected outcomes are achieved by the accumulated uncertainties at the later phase of the design. As this iteration is repeated and repeated, the cost and time to finish design and manufacture the final product drastically increase. Therefore, designers put a lot of effort to make an adequate decision that will lead the overall design process in the right direction and reduce the iterative loop of design.

To achieve the right decisions at the conceptual design phase, one of the most important things is to increase the knowledge as much as possible. By doing so, cost expended can be

reduced with more freedom in design during the conceptual design, as dotted lines in Figure 2.10 imply. Therefore, understanding of factors affecting requirements and constraints is crucially important in making decisions.

In this perspective, the soot prediction model must be parametric for use during the conceptual design phase. This means that the model should show the correct relationship between inputs and outputs. When a set of inputs are given to the parametric soot prediction model, the model should return the corresponding soot outputs that physically make sense. If the input variables are varied, then the model should also return a new set of correct output values. For instance, for the given pressure, temperature, and fuel-to-air ratio, the parametric model must return the correct soot outputs. The model must be able to predict correct soot values regardless of the size of combustors or the architecture of combustors if the model is truly parametric. The architecture of a combustor in this context means mainly the staging characteristics of a combustor. The examples of combustor architectures are the single annular combustor (SAC), the duel annular combustor (DAC), the rich-burn, quick-quench, lean-burn (RQL) combustor, lean direct injection (LDI) combustor, twin annular premixing swirler (TAPS) combustor, etc. In summary, the parametric soot prediction model needs to be able to handle different thermodynamic cycles, different sizes of a combustor, and different combustor architectures. To achieve these requirements, the model must capture the physical relationships of parameters and be able to work for large design space.

Another important requirement for the soot prediction model for the use in the conceptual design phase is the short execution time. More specifically, the model must be fast enough to evaluate a lot of combinations in a large design space. To increase the understanding of the design space and make the right decision, deep analyses on the design space are required. The more cases are desirable to be run for the prediction model. If the problem is very complex and shows high nonlinearity, the number of cases required to be run for better understanding dramatically increases. As discussed above, the design process

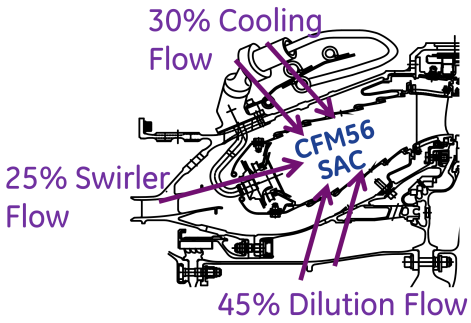

(a) Single annular combustor[32]

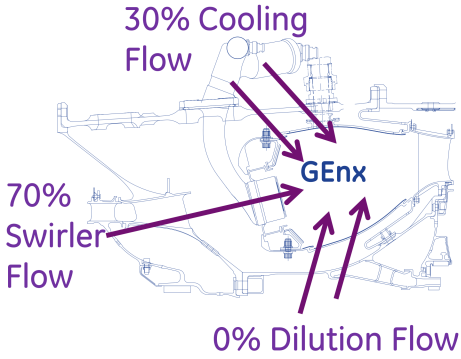

(b) Twin annular premixing swirler combustor[32]

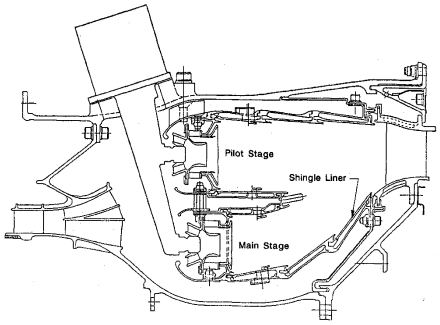

(c) Dual annular combustor[33]

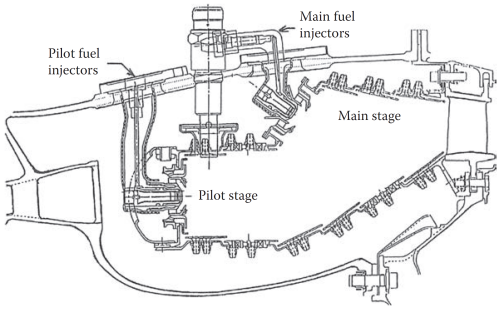

(d) Axially staged combustor[34]

Figure 2.12: Some examples of different combustor architectures

inherently involves iterative nature. As more time is required during the conceptual design, the whole design time to manufacture the final product is delayed a lot. Of course, this is a very undesirable situation for the designers as it causes huge losses in time and budget.

The statement that the soot prediction model must be parametric and fast enough to handle a lot of design combinations in a short time seems very straightforward. Nevertheless, this mission is often not successfully accomplished due to the lack of knowledge. The conceptual design is the very beginning of the whole design process. The conceptual design often aims a few years of the future to a few decades of future. The details of sub-components are not available yet in this step. However, many issues in design including soot problem often depend on the component details. For example, the soot emission is not simply determined by the inlet condition. The local thermodynamic properties inside the combustor affect the instantaneous formation and oxidation rates. Therefore, combustor characteristics such as geometry are required for accurate prediction. However, the development of sub-components is usually not completed in the conceptual design. For this reason, a simple correlation is desired for designers. However, correlation is based on the historical data and usually not available for new concepts. To satisfy emission constraints, combustor technology keeps evolving and new architecture is a design consideration in many cases. In this case, a designer at the conceptual design phase cannot wait until new hardware is developed and tested for the correlation of new concepts. Knowledge is limited and the time is running out. Development of a soot prediction model for the conceptual design phase is a very challenging task.

In summary, a soot prediction model for the use during the conceptual design of engine must be parametric and fast enough to handle a large design space with limited information on combustors. Then, one reasonable question will be if the current state-of-the-art of the soot prediction methods is suitable for conceptual design in spite of limited information.

The rise of the computational fluid dynamics (CFD) simulation changed the paradigm in engineering design. It replaced the physical experiment in many areas. The physical

experiment has its own irreplaceable value. It is usually considered the most accurate way to acquire data. However, some amount of errors are always in the acquired data whether they are small or large. Sometimes, the measurement is not easily done. Noise in the data, low signals, harsh measurement condition such as extreme temperature and pressure, insufficient measurement hardware technology, etc. are the factors making measurement difficult. Even if the measurement technique and hardware are sufficient, the time and cost are very important factors making physical experiments not attractive for designers and engineers. A lot of devices need to be prepared and installed even for a small physical experiment in the design process. For example, if someone wants to measure the flow field of reacting combustor, so many devices are required. The combustor, pipelines, fuel and air supply, flowmeters, thermocouple, laser, lenses, mirrors, photo-multiplier, high-speed camera, thermometer, barometer, exhaust system, isolation room, and a lot more devices need to be prepared and installed. This setup process takes lots of time and effort with expensive cost. Once the setup is done, the real experiment also takes time and cost. If some modifications are required, another time and cost are expended again for repeated device setup and experiment. Small changes in experimental conditions always cause not-small cost. However, the CFD simulation does not require complicated setup environment. The setup and simulation time is usually much shorter than the time required for the real physical experiment. The modification of the experimental condition is also easy and fast. Furthermore, it does not require a special device or technique for measurement. With these strong advantages, CFD simulation is a virtual experiment and a currently attractive alternative to physical experiment. In gas turbine combustion study, the real physical experiment is not easy due to difficult measurement environment. The operating condition is not easily reproduced in the ground laboratory environment, inside of burning combustor is so hot and pressurized that installation and operation of measurement devices are not easily achieved. These difficulties are not a problem for the CFD simulation. For this reason, many soot studies also utilize the advantage of CFD simulation. The use of the CFD simulation makes

it possible to achieve the axial and radial profile of thermodynamic properties and the concentration of soot indicator species inside the combustor. Scholars make some hypotheses and theories, validate them by comparing results experimental results and CFD results for a simple experimental condition where data are available, and apply theories to the more complex condition for soot prediction. This process is commonly used in soot research and many studies in Table 2.1 are good examples of research following this procedure.

Despite the advantages mentioned in the previous section, there are some limitations of CFD simulations to be utilized for the prediction of soot emission during the conceptual design of the aircraft gas turbine engine. As the results of CFD simulations are achieved by solving Navier-Stokes equations and a set of chemical reactions in the flow field, the initial conditions and boundary conditions are critical factors in acquiring solutions. In combustion studies, these conditions are thermodynamic properties and geometry information. The thermodynamic properties may be given from the cycle analysis. The detailed geometry information, however, is not usually available during the conceptual design. As shown in Figure 2.10, the conceptual design is the phase where the knowledge is most limited among the whole design process. The detailed shapes of sub-components are available as the design process goes to the later stage. If the conceptual design deals with the currently available combustor geometry, this factor may not be a problem. However, aircraft engine has a long lifetime. Once it is developed, it is used at least for a few decades. Some engines have so long lifetime as the upgraded variations are developed. Therefore, the conceptual design of an aircraft engine targets future engines with the technology that is not fully mature yet in many cases. Of course, the geometry of low TRL (Technology Readiness Level) combustor is not available in this case. Furthermore, because the geometry information is essential in CFD simulations, separate CFD model for different sizes, different architectures, and different thermodynamic cycles of engines need to be developed to predict soot emission. For example, the CFD model for the GE90 engine cannot correctly predict soot emission from the CF6 engine even if the CF6 engine cycle is provided. This means that

CFD simulation is engine-specific and not parametric in soot prediction during conceptual design.

Another limitation of CFD is its simulation time. Although its simulation speed is faster than the actual physical experiments, it is still slow for the conceptual design. The simulation time often takes at least for several hours for a simple problem and sometimes it takes more than a few days or weeks in many cases. This execution time is not suitable for the conceptual design phase where a lot of combinations of design alternatives are compared and evaluated. If one imagines that he/she runs 10,000 cases of CFD simulations, this is not a realistic task. The number of cases to be evaluated in the conceptual design phase is much more than this number. Therefore, the CFD simulation is not a suitable method for use during the conceptual design in terms of parametric capability and simulation time.

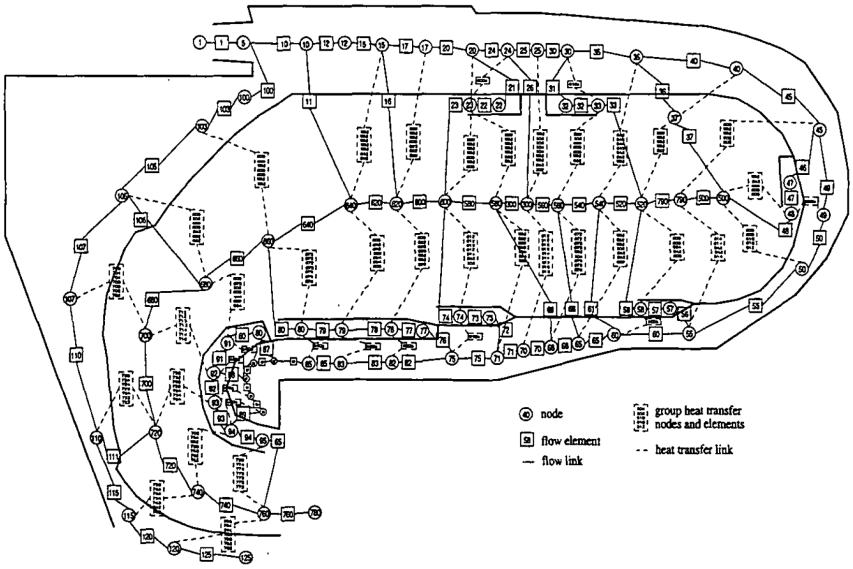

Figure 2.13: An example of geometry-based network[35]

As an alternative method to CFD simulation, the parcel-box method is often used in gas turbine combustion study. It approximates the complex reacting flow field into multiple parcels. As discussed earlier, this method was developed when the computation power was not enough to perform a complex numerical simulation. Although numerical simu-

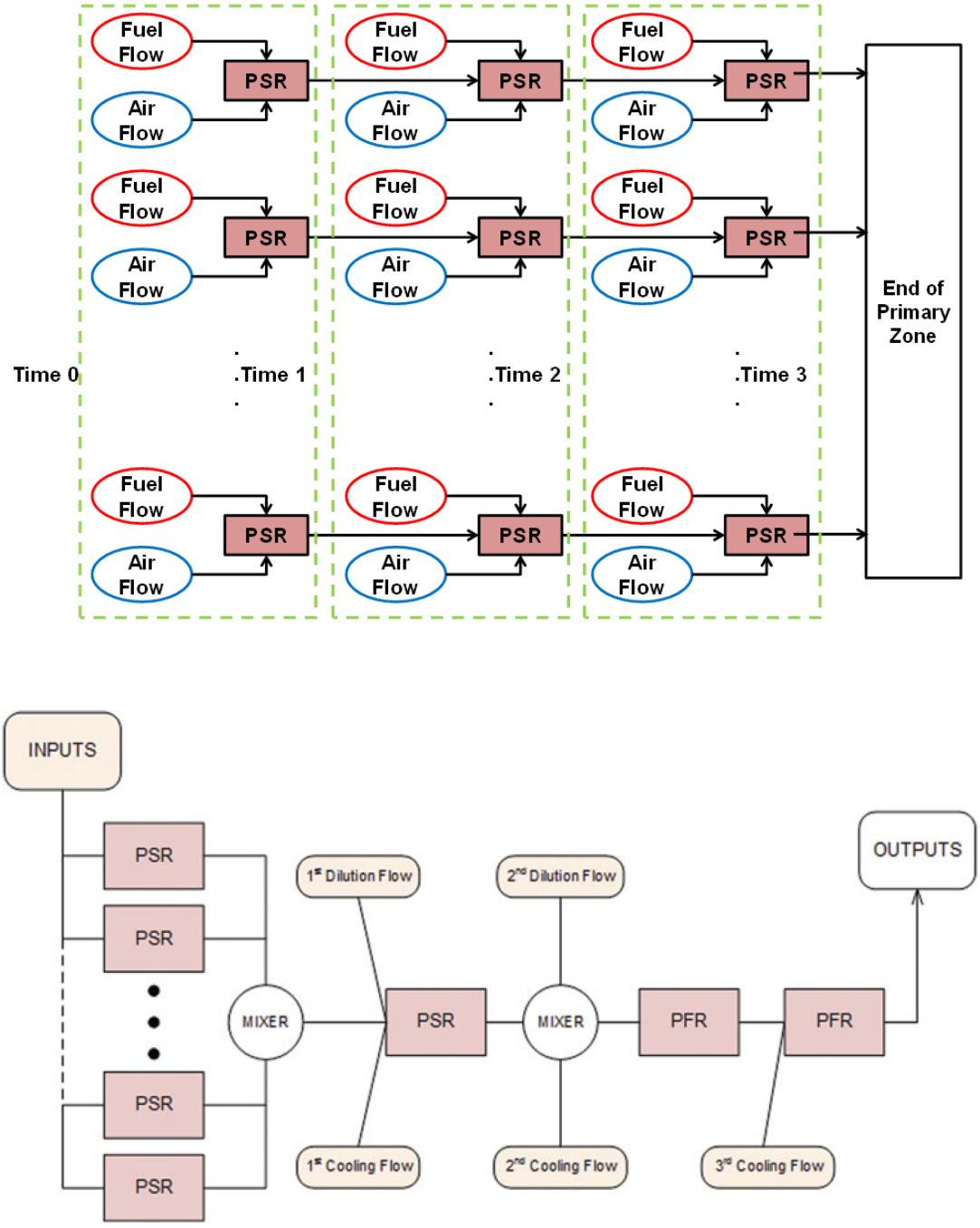

Figure 2.14: Examples of mixing-based network[10][36]

lations are widely used as computation power has dramatically increased, the parcel-box approaches such as the chemical reactor networks(CRN) are still used because of its simple structure and fast calculation time in reacting flow problems. Even if the complex chemical mechanism is applied, the calculation of one parcel-box or one reactor generally takes only a few seconds or less. There are two types of parcel-box approach. One is the geometry-based method. Many parcels are allocated along the given geometry to represent networks of local flows. The calculation scheme of this method resembles the CFD simulation with coarse grids or meshes as the parcels represent the flow characteristics in a physical location, as shown in Figure 2.13. The hybrid method is also often used. In this case, CFD takes a complex turbulent flow field and CRN takes chemistry calculations. Another form of parcel-box method is the mixing-based approach. This method focuses on the non-uniform fuel/air mixing characteristics of reacting flow. Several parallel reactors are generally used to represent a distribution of the non-uniform fuel-to-air ratio of local flow in this approach. Figure 2.8 and Figure 2.9 in the previous discussion and Figure 2.14 are the examples of this approach. The details of geometry are less important in this case. However, each reactor or each parcel still requires some geometry factors such as volume, length, and cross-sectional area. These characteristics make parcel-box approach or CRN still engine-specific. The studies discussed earlier also focused on some target engines. They utilized engine-specific detailed information while they built their prediction models (see Table 2.1). Therefore, the parcel-box approach is also not fully parametric thus not suitable for conceptual design although its calculation speed is very fast.

There have been a lot of efforts to understand and predict soot emission from gas turbine combustion as discussed so far. Thanks to their contribution, fundamental mechanisms of soot formation are keep being discovered and soot prediction capability keeps growing. However, soot prediction at the early stage of design is not fully achieved yet in terms of parametric capability. This is a strong motivation of this research as a new regulation on particulate matters is expected in the near future and soot emission will be an essential

design constraint in aviation engine design. In this chapter, the gap between the requirement and the current state-of-the-art is identified. This leads to a research objective in the next chapter.

2.3 Problem Statement and Research Objective

In this section, there will be a brief summary of the issues discussed in the previous sections. Then, a gap between the requirement of the soot prediction method for the use in the conceptual design of an aircraft gas turbine engine and the state-of-the-art soot prediction method will be identified based on the observations. This gap will lead to a problem statement and a research objective will be finally established.

As discussed in the beginning, aviation emissions are apparently harmful to the environment, climate, and human health. Among many emissions, the adverse effect of particulate matters(PM) is discovered rather recently. The adverse effects of these emissions including PM are seriously threatening our lives and many scholars have contributed to technology improvement to overcome this issue. However, the aviation market will keep growing as there are continuously increasing demands on new aircraft in the future. This will compensate for the efforts to reduce emissions and cannot resolve the concern. Based on this discussion, observation 1 is derived.

Observation 1: There are growing concerns about the adverse effects of aviation emissions including PM as the aviation market is growing.

The current regulation on PM is effective under the form of SN(smoke number) regulation. The purpose of this regulation is focused on the removal of visible smoke from the exhaust of the engine. This is because there was not much evidence to show the harmful effect of PM on human health and the environment. PM was not well understood at that time. This is also true for the engine design perspective. The soot formation characteristics in the aviation engine were not understood enough to perform trade-off study between

soot and other design factors[37]. However, many studies on the effects of PM on health, environment, and climate have been performed so far. It turns out that PM has a high correlation with human health and the environment. It reduces expected life expectancy and contributes to global warming. Figure 1.3 in the earlier chapter shows the PM effects on health and the environment. Because extremely small particles can penetrate deep into the lungs when they are inhaled, they can cause cardiovascular and cardiopulmonary diseases[2]. For this reason, PM emission is one of the emission pollutants catching scholars' attention. Therefore, observation 2 comes here.

Observation 2: PM has a significant impact on human health and the environment.

Based on these discussions in the previous paragraphs, two conclusions are derived. The first one is that the soot emission is one of the important design constraints for aircraft gas turbine engines. This is not only because the PM is a harmful pollutant for health and environment but also because the new regulations will be effective in the near future. Once the regulation is effective, no engines cannot be in the market unless the regulatory emission level is satisfied. Therefore, engine manufacturers need to consider the level of soot emission during the engine design process. This leads to another conclusion: The soot emission must be evaluated during the conceptual design of aircraft gas turbine engines. The conceptual design is the first step in the design process(see Figure 2.10). Because the design is a series of iterative processes(see Figure 2.11), the right decision made during the conceptual design highly affect the rest of the design processes as well as cost and time. Therefore, to design engines satisfying the regulatory PM level, the soot emission must be evaluated during the conceptual design phase.

With these two observations, the current state-of-the-art methods of soot prediction were reviewed in this chapter. Thanks to many efforts and researches, deeper understanding on soot formation mechanism has been achieved. Based on this achievement, there have been many efforts to predict soot emission from the gas turbine combustion. Many scholars

approached with a detailed numerical simulation scheme or parcel-box model. However, their approaches utilize detailed design information of engine and combustor which are not available during the conceptual design. Therefore, the prediction models that they developed are valid only for their target engines and power conditions. This leads to the third observation:

Observation 3: Current soot evaluation methods are engine-specific

This means that the current soot evaluation methods are not suitable for conceptual design of engine because they are not fully parametric. They cannot handle engines with different cycles and sizes. Their usage is limited. To be able to address a wide design space, the prediction model must be parametric such that the model responds to the variation of input values correctly. In this context, a clear gap between the requirement in the conceptual design and the current state-of-the-art soot prediction methods is identified, as below.

Problem statement: Current soot evaluation methods cannot adequately predict soot emission for conceptual design of aircraft gas turbine engines

A lot of cycles are reviewed and evaluated during the conceptual design phase. They have a variety of sizes. The engines for small business jet will be small sizes and the engines for large twin-aisle will have much bigger sizes. They also have different combustion architectures. Many current aviation engines have simple rich-dome type single annular combustors(SAC). Some of them have more advanced rich-burn, quick-quench, lean-burn(RQL) combustors. In the future, more engines will have staged lean combustor, lean direct injection(LDI) combustor, and twin-annular premixing swirler (TAPS) combustor. The soot prediction model should be also able to address different combustion architectures. Therefore, to fill the observed gap, a research objective of this thesis research can be established as below.

Research Objective: Establishing a methodology to develop a parametric environment to

Table 2.2: Summary of observations, problem statement, and research objective

Observation 1:	There are growing concerns about the adverse effects of the aviation emissions including PM as the aviation market is growing
Observation 2:	PM has a significant impact on human health and the environment
Conclusions from observation 1 and 2	a. The soot emission is one of the important design constraints for aircraft gasturbine engines b. The soot emission must be evaluated during the conceptual design of aircraft gas turbine engines
Observation 3:	Current soot evaluation methods are engine-specific
Problem statement:	Current soot evaluation methods are not suitable for predicting soot emission during conceptual design of aircraft gas turbine engines
Research objective:	Establishing a methodology to develop a parametric environment to evaluate and predict non-volatile particulates emission level of aircraft gas turbine engines during conceptual design for different thermodynamic cycles and scalable for different combustor sizes

evaluate and predict non-volatile particulates emission level of aircraft gas turbine engines during conceptual design for different thermodynamic cycles and scalable for different combustor sizes

In this chapter, a gap between the requirement of the soot prediction method for the use in the conceptual design of an aircraft gas turbine engine and the state-of-the-art soot prediction method was identified. Based on several discussions and observations, the problem statement was addressed and the research objective was established. A summary of them is listed in Table 2.2. In the next chapter, several basic concepts that might be useful in understanding topics that will be discussed in this thesis research will be introduced. Then, several research questions will be asked based on the research objective and hypotheses will be suggested to answer the questions.

CHAPTER 3

BACKGROUND

In this chapter, several background information is provided to help the readers understanding. The addressed information in this chapter is related to the regulations, metrics, and combustor.

3.1 ICAO LTO Cycle

International Civil Aeronautics Organization(ICAO) landing and take-off(LTO) cycle is a standard cycle set by ICAO for the purpose of the regulation of aviation-emitted emissions near the airport areas. As its name indicates, this cycle describes the landing and take-off actions taken by the aircraft near the airport area below 3000ft under International Standard Atmosphere(ISA) sea level static(SLS) condition. It consists of four phases that are take-off, climb out, approach, and idle(or taxi) operating modes, as described in Figure 3.1.

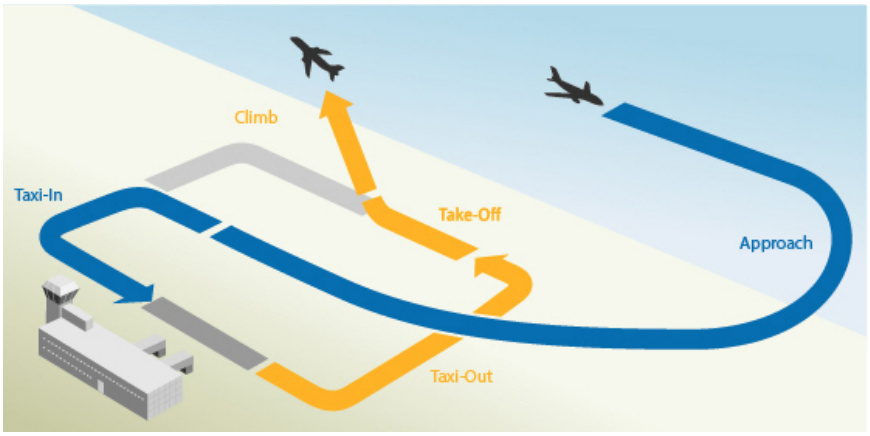

Figure 3.1: Reference Landing and Take-Off (LTO) cycle[38]

Each mode is defined by the rated output(Foo) and duration. The rated output, or Foo, is a metric meaning the maximum thrust for take-off under ISA SLS conditions for the

purpose of the engine certification process. The duration means the time taken by each mode. Defined thrust settings and durations are listed in Table 3.1. For example, the approach mode in LTO cycle is defined as the 30% of take-off thrust for 4 minutes. The duration of idle mode is much longer than other modes. This is because the idle mode in the ICAO LTO cycle includes the taxi-in and taxi-out actions. Duration of mode is important because the total emissions during the mode are regulated.

Table 3.1: Definition of ICAO Landing and Take-off(LTO) Cycle[11]

Mode	Thrust	Duration(min.)
Take-off	100% of take-off thrust	0.7
Climb out	85% of take-off thrust	2.2
Approach	30% of take-off thrust	4.0
Idle	7% of take-off thrust	26

The gaseous emissions such as hydrocarbons(HC), carbon monoxide(CO), and oxides of nitrogen(NOx) are measured over the LTO cycle for the engine certification. This process follows the Annex 16, Volume II[11]. The metric used in this procedure is Dp/Foo. Dp is the mass of the pollutant emitted during the LTO cycle, in gram unit. Emissions index(EI) introduced earlier is utilized in the calculation of Dp. Because the emissions index is the mass of the pollutant emission per unit fuel, the emitted mass per unit time(g/s) can be calculated by multiplying the emissions index($g/kg - fuel$) by fuel flow rate($kg - fuel/s$). Because the LTO cycle defines time, the mass of emitted pollutant for each duration of mode can be calculated by multiplying the emitted mass per unit time by duration. If this is repeated for all four operation modes, the sum of them is the total mass of pollutant emitted during the LTO cycle, that is Dp. Foo is the rated thrust introduced in the previous paragraph. Dp/Foo is the total mass of pollutant emitted during the LTO cycle normalized by the take-off thrust. It can be calculated simply by dividing Dp by Foo. This relationship

is described in Equation (3.1) through Equation (3.4).

$$Dp = (EI_i \times W_f \times t)_{TO} + (EI_i \times W_f \times t)_{CO} + (EI_i \times W_f \times t)_{AP} + (EI_i \times W_f \times t)_{ID} \tag{3.1}$$

or simply

$$\sum_{TO,CO,AP,ID}^{j} (EI_i \times W_f \times t)_j \tag{3.2}$$

where i is the type of pollutant emission.

Therefore, Dp/Foo is

$$Dp/Foo = \frac{(EI_i \times W_f \times t)_{TO} + (EI_i \times W_f \times t)_{CO} + (EI_i \times W_f \times t)_{AP} + (EI_i \times W_f \times t)_{ID}}{\textit{take-off thrust}} \tag{3.3}$$

or simply

$$Dp/Foo = \frac{\sum_{TO,CO,AP,ID}^{j} \left(EI_i \times W_f \times t\right)_j}{\textit{take-off thrust}} \tag{3.4}$$

The smoke number (SN) is also measured over the LTO cycle for its regulation standard. As discussed earlier, the emissions index of non-volatile PM can be estimated by the First Order Approximation(FOA) method from the measured smoke number. Therefore, Dp/Foo of soot emission can also be estimated from measured LTO smoke numbers by Equation (3.4).

3.2 Metrics of PM and Current Regulation

Smoke Number

The smoke number(SN) is an empirical metric ranging from 0 to 100. It is measured through a filter-based optical method. The current regulation on the aviation emitted PM limits the maximum level of SN through the ICAO LTO cycle.

The smoke number is a measure of the stain of the filter after flowing exhaust gas through a filter. 0.5 cfm of the exhaust gas is flown through the #4 Whatman filter with the flow rate of 0.023 lbm per unit square inch of filter area and the reflectance of the filter is converted to the smoke number. 100% reflectance means 0 in SN and 0% reflectance means 100 in SN. The measurement error is typically $\pm$3[37].

According to the Annex 16, Volume II[11], the smoke number of the aircraft must not exceed:

$$\textit{Regulatory Smoke Number} = 83.6\,(F_{oo})^{-0.274}\textit{, or a value of } 50\textit{, whichever is lower}$$

The primary purpose of the regulation is to avoid the visible plume at the engine exit. When this regulation was initially introduced, there was no clear evidence correlating particulate matter to human health and the environment. Particulate emission was not a primary interest in trade-off studies for the regulation and engine design[37]. For this reason, the regulation targets visible plume rather than health and climate effect.

The smoke number is an empirical dimensionless parameter. Because it is not a direct measure of PM quantity,

Because the smoke number is not a direct measure of PM quantity but an empirical dimensionless parameter, it is not an appropriate parameter to be related to health and environmental effects. For this reason, many studies have been conducted to estimate aviation emitted PM from measured SN data. The First Order Approximation(FOA) method is one of the famous examples correlating SN to the mass quantity of PM. More correlation efforts to estimate the aviation PM are introduced in the latter part of this thesis.

ppm/ppb

"Parts per" unit is often used in the experiment. The volume fraction of soot (f_v). is commonly measured in many experimental soot studies. Because the amount of soot is tiny relative to other species in the combustion product gas, parts per million (or sometimes parts per billion due to the extremely small amount of soot) unit is commonly used. The ppm(or ppb) unit can be easily converted into mass when the density of the solid soot particle (ρ_s) is applied. The density of soot in literature generally ranges from 1,800 kg/m^3 to 2,000 kg/m^3.

Emission Index

Emission Index (EI) is the measure of the mass of emissions normalized by the mass of fuel. The regulations set by the International Civil Aeronautics Organization (ICAO) limiting gaseous emissions at near-ground area uses this metric. Regulated gaseous emissions are nitrogen dioxides (NOx), carbon monoxide (CO), unburned hydrocarbons (UHC), volatile organic compounds (VOC), etc. The unit is generally gram emission per kilogram fuel ($g/kg-fuel$).

While soot studies in flame scale prefer the volume fraction, the many studies on aviation PM in engine scale adopt the emission index as a metric. Due to the small amount of PM from the engine, the unit is usually milligram of PM per kilogram of fuel ($mg/kg-fuel$). Many correlations developed to estimate aviation PM adopt EI metric. In addition to the mass of particulate matter, the number of particles is also often one of the interests due to its adverse effect on health. In this case, the number of particles is also expressed in EI metric ($\#/kg-fuel$).

3.3 Combustor Basics

3.3.1 Stoichiometry

The combustion occurs when the fuel and oxidizer meet and react together. The gas turbine engine uses kerosene fuel, which is one of the hydrocarbon fuels. The oxidizer in the gas turbine combustion is the air whose major components are nitrogen and oxygen. When carbon and hydrogen in the hydrocarbon fuel and the oxygen in the air react, the most probable products are carbon dioxide(CO_2) and water vapor(H_2O). The nitrogen(N_2) in the air has very low reactivity in this pyrolysis process. When there is the exact amount of oxidizer to burn the given fuel completely, the ratio of fuel to oxidizer is called stoichiometric fuel-air ratio(f_{st}). For hydrocarbon fuels, the stoichiometric fuel-air ratio is achieved when there is the exact theoretical amount of fuel and air such that all fuel and oxygen are consumed and carbon dioxide and water can be the only products from the reaction. This relationship can be expressed in an equation form from the atom balance, as shown in Equation (3.5).

$$C_xH_y + \left(x + \frac{y}{4}\right)(O_2 + 3.76N_2) \rightarrow xCO_2 + \frac{y}{2}H_2O + 3.76\left(x + \frac{y}{4}\right)N_2 \qquad (3.5)$$

The hydrocarbon fuel in this reaction equation is expressed as C_xH_y where x and y are the numbers of carbon and hydrogen atoms in the fuel molecule, respectively. In this relationship, the air is assumed to have 21% of oxygen and 79% of nitrogen by volume. This ratio derives 3.76 moles of nitrogen molecules per one mole of oxygen molecules in the air. The nitrogen molecules do not participate in the theoretical complete combustion reactions, as N_2 term stays the same in both sides of Equation (3.5).

The stoichiometric fuel-air ratio of the combustion of the hydrocarbon fuel and the air

can be calculated from this Equation (3.5).

$$f_{st} = \left(\frac{m_{fuel}}{m_{air}}\right)_{stoic} = \frac{x \times MW_C + y \times MW_H}{\left(x + \frac{y}{4}\right) \times (MW_{O_2} + 3.76 \times MW_{N_2})} \tag{3.6}$$

The molar weights of carbon and hydrogen atoms are 12.01 g/mol and 1.01 g/mol, respectively, and the molar weights of oxygen and nitrogen molecules are 32.0 g/mol and 28.01 g/mol, respectively[39]. Therefore, the stoichiometric fuel-air ratio from Equation (3.6) is

$$f_{st} = \frac{12.01x + 1.01y}{\left(x + \frac{y}{4}\right) \times (32.0 + 3.76 \times 28.01)} \tag{3.7}$$

According to Dryer et al., the molecular formula of Jet A POSF 4658 fuel is $C_{10.17}H_{19.91}$[40]. Walsh and Fletcher's represention of kerosene(JP3, JP5, Jet-A1, AVTUR, etc.) is $C_{12}H_{23.5}$[41]. If the jet fuel is expressed as $C_{12}H_{23}$, $x = 12$, $y = 23$, and therefore, the stoichiometric fuel-air ratio is about 0.06865958.

The jet fuel is somewhat loosely defined with requirements in several fuel specifications. The jet fuel consists not only of a single molecule but also of the mixture of various molecules. For this reason, the stoichiometric fuel-air ratio can slightly vary by studies. Nevertheless, variations are very small within a narrow range. Henderson and Blazowski's value for the aircraft propulsion system is 0.067[42]. Lefebvre and Ballal's value is 0.0676 for kerosene fuel when it is represented as $C_{12}H_{24}$[34] and Mattingly et al.'s value is 0.0685 when the fuel is represented as $C_{12}H_{23}$ [43]. McKinney and Hoke's value is around 0.068 for jet fuel[44]. The reason why Mattingly et al.'s value is different from the values calculated in the previous paragraph may be due to the small difference in molecular weight. If the molecular weights are set to 12.0, 1.0, 32.0, and 28.0 for a carbon atom, hydrogen atom, oxygen molecule, and nitrogen molecule, the stoichiometric fuel-air ratio of $C_{12}H_{23}$ is about 0.0685348.

When there is more air than the stoichiometric amount, this mixture is fuel lean and

the fuel-air ratio is lower than the stoichiometric value. When there is less air than the stoichiometric amount, this mixture is fuel rich and the fuel-air ratio of this mixture is higher than the stoichiometric value. Because all fuels have a different stoichiometric fuel-air ratio as their x and y values are different, the stoichiometric fuel-air ratio that divides the rich and lean condition is also different for a different fuel. In order to capture the common physics in fuel-air ratio, there is a normalized non-dimensional parameter for fuel-air ratio. When the fuel-air ratio of the mixture is normalized by the stoichiometric fuel-air ratio of the fuel, this value is called the equivalence ratio and commonly expressed with a symbol of ϕ. The stoichiometric air-fuel ratio divided by the mixture air-fuel ratio also leads to the equivalence ratio. Therefore, the equivalence ratio can be defined as

$$\phi = \frac{(F/A)}{(F/A)_{stoic}} = \frac{(A/F)_{stoic}}{(A/F)} \tag{3.8}$$

where (F/A) is the fuel-air ratio and (A/F) is the air-fuel ratio.

From this definition, the equivalence ratio is unity ($\phi = 1$) for stoichiometric mixture, the equivalence ratio is larger than unity for fuel rich mixture ($\phi > 1$), and the equivalence ratio is lower than unity for a fuel-lean mixture. Among many thermodynamic parameters affecting reactions, the temperature has a close relationship with the equivalence ratio. When the mixture is rich, there is excess fuel that cannot be burnt completely due to the lack of enough air. When the mixture is lean, there is excess air than required for complete combustion. In both cases, excess amount works as a diluent flow that takes some portion of heat energy released from the exothermic reaction of fuel and air. Therefore, the temperature in the off-stoichiometric region is lower than the temperature of the near-stoichiometric region. Theoretically, the temperature of the mixture is the highest when the equivalence ratio is unity($\phi = 1$). However, in reality, the peak temperature is slightly on the richer side than the stoichiometric fuel-air ratio. This trend can be observed in Figure 3.2.

Several factors are affecting the temperature of the reacting mixture in this Figure 3.2.

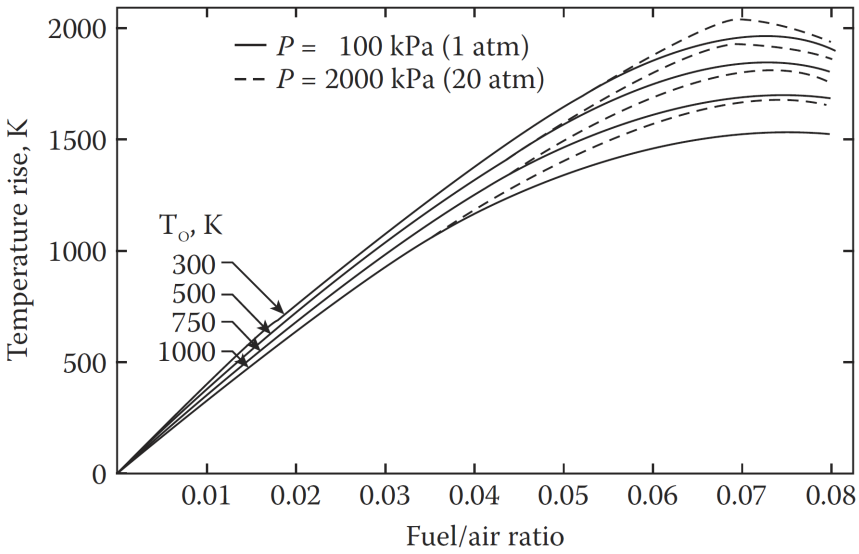

Figure 3.2: Temperature and fuel-air ratio for kerosine (JP-5) fuel[34]

Among them, it is obviously shown that the fuel-air ratio is the most affecting factor. The temperature increases as the fuel-air ratio approaches to the near-stoichiometric value (around $f_{st} \cong 0.068$). After this region, the mixture is rich and the temperature decreases as the fuel-air ratio of mixture increases.

The equivalence ratio is also closely related to some emission pollutants. Oxides of nitrogen and carbon monoxide are the pollutants that are in a trade-off relationship with each other. This is because the equivalence ratio is related to the temperature as we already discussed. The reaction producing carbon dioxide from carbon monoxide and hydroxyl radical(Equation (3.9)) is a major reaction releasing a large amount of heat in the combustion process. Therefore, the oxidation of carbon monoxide must be achieved as much as possible to achieve high combustion efficiency.

$$CO + OH \rightarrow CO_2 + H \tag{3.9}$$

The reaction rate is exponentially related to the temperature. The higher temperature promotes the faster reaction rates, as shown in the Arrhenius expression(Equation (3.10) and

Equation (3.11)).

$$k = Ae^{-E_a/RT} \tag{3.10}$$

or sometimes

$$k = AT^b e^{-E_a/RT} \tag{3.11}$$

where k is the specific reaction rate constant, E_a is the activation energy of reaction, R is the gas constant, T is the temperature, and A and b are constants. To completely burn all fuel within the given residence time before the reacting mixture flow leaves the combustor, the reaction rate must be high enough. If the temperature is too low, carbon monoxide in the reacting gas cannot be fully oxidized and CO emission will increase. Therefore, the fuel-air ratio near stoichiometric value is desired to minimize CO emission.

However, when it comes to the emission of oxides of nitrogen, the near-stoichiometric region should be avoided. Among many paths to generate NO, the most contribution is from the thermal mechanism. Equation (3.12), (3.13), and (3.14) are extended Zeldovich mechanism[45]. Activation energies are in kJ/mol. The first step in these chain reactions is that the oxygen atom attacks the nitrogen molecule. As the nitrogen molecule has a strong triple bond, this step is a rate-limiting step in the NO formation via the thermal mechanism, requiring relatively high activation energy. For this reason, the high temperature achieved near the stoichiometric fuel-air ratio is a key factor activating the first step of the NOx-producing chain reactions.

$$O + N_2 \rightleftharpoons NO + N \qquad k_f = 2 \times 10^{14} exp(-315/RT) \tag{3.12}$$

$$N + O_2 \rightleftharpoons NO + O \qquad k_f = 6.4 \times 10^{9} exp(-26/RT) \tag{3.13}$$

$$N + OH \rightleftharpoons NO + H \qquad k_f = 3.8 \times 10^{13} \tag{3.14}$$

The formation of soot, which is a major issue in this thesis, is also related to the equivalence ratio of the mixture. The rich fuel-air ratio is favorable for the formation and growth of soot particles. For the oxidization of soot, the concentration of oxidizers as well as the high temperature is an important factor. The main oxidizers of soot are hydroxyl radical and oxygen. These two species are usually abundant in the lean mixture. However, as the high temperature also plays an essential role in soot oxidization, the region where soot particles are oxidized covers from lean to near stoichiometric region. In Colket's virtual experiment utilizing a chemical reactor network(CRN), soot particles were formed and grew at the region where the equivalence ratio was above 1.5 up to 3.0 and oxidized at the region where the equivalence ratio was between 0.7 and 1.5[46].

3.3.2 Residence Time

The flow takes time to pass through a specific length. In other words, the flow stays for some amount of time in this region. This time is the residence time. The combustor is designed to allow enough residence time to the flow for complete combustion to achieve high efficiency. This is because the reaction takes time. If the residence time is too short, then the fuel cannot be completely burned and the efficiency is low. However, at the same time, the combustor is designed not to spend too much time in a specific region due to pollutant emissions. For example, lots of NOx and soot emissions are generally produced at the primary zone during the high power operation. This is because the rates of reactions that produce these pollutants are higher than the rates of reactions that consume them. In this case, if the residence time is too long, then a huge amount of pollutants will be emitted from the combustor. Additionally, the unnecessarily long residence time in combustor design leads to the additional length which accompanies additional weight. Therefore, the

residence time must be determined carefully with trade-off study of design factors.

The residence time of the flow(τ_{res}) can be defined as:

$$\tau_{res} = \frac{length}{\textit{flow velocity}} \tag{3.15}$$

The length can be the total combustor length if the residence time is for the entire combustor or some specific length such as the length of a primary zone if the residence time is for a specific zone. The flow velocity is the average velocity because the flow velocity changes with reactions. The reactions change the volume and temperature of the flow; thus, they change the density of the flow. The cross-sectional area of the combustor also often varies along the downstream direction. Because the mass flow rate is constant for a steady state operation, the flow velocity also changes with the variations of the density of the flow and the combustor cross-sectional area. This relationship can be found in Equation (3.16). The mass flow rate is $\dot{m}$, the density of the flow is ρ, the cross-sectional area of the combustor is A, and the flow velocity is U in this equation.

$$\dot{m} = \rho A U \tag{3.16}$$

The residence time in Equation (3.15) can be differently defined. Multiplying density(ρ) and cross sectional area(A) terms to both numerator and denominator of Equation (3.15) leads to a different form of residence time.

$$\tau_{res} = \frac{length}{U} \times \frac{\rho A}{\rho A} = \frac{\rho(length \times A)}{\rho A U} = \frac{\rho V}{\dot{m}}$$

Because the length multiplied by the area is the volume(V) and the flow velocity multiplied by the area and the density is the mass flow rate(Equation (3.16)), the residence time in Equation (3.15) is now consisting of density, volume, and mass flow rate terms.

Therefore,

$$\tau_{res} = \frac{\rho V}{\dot{m}} \tag{3.17}$$

In this expression, the density is the average density of the flow in a given control volume, V.

3.3.3 Combustor Configuration

Types of Combustors

There are three types of combustors for the gas turbine engines when they are categorized by the shape. The earliest type is the can combustors. It is often called the tubular combustor. The type of combustor that is installed on most of modern aviation gas turbine engines is the annular type combustor. The cannular(or tuboannular or can-annular) combustor is between these two extremes. The schematic shapes of three types of combustors are described in Figure 3.3.

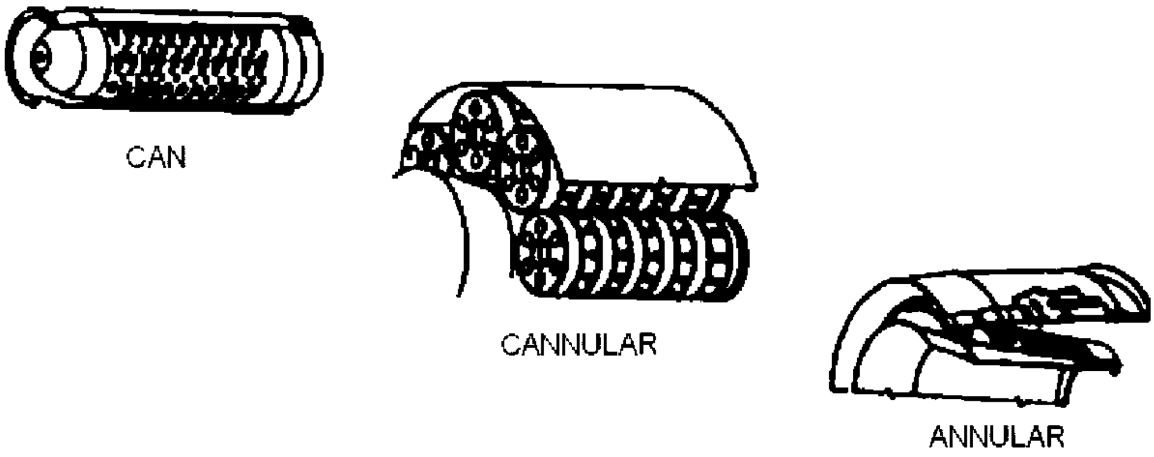

Figure 3.3: Types of combustors

Although a small engine has only one can combustor, 6 - 16 cans are usually installed around the shaft of the engines taking a can type combustor(Lefebvre). The most strong benefits of a can combustor are the ease of maintenance and the low cost and time in

development[34]. Because a can combustor consists of a can- or tube-like liner with its own casing, cans are relatively independent each other. For the aspect of maintenance, they can be taken out of the engine separately. Therefore, the issues in one can do not affect other cans or components in the engine such as a turbine for maintenance. For the development, as all cans are in the same structure, replicated cans can be easily installed on engines once one can is developed and tested. Despite its many advantages, there are several weak points that make it not used in aviation engines. Because the combustion occurs only inside cans, volume outside cans is wasted in the combustion point of view. Therefore, to maintain the same volume with annular type combustor, the can type combustor has a longer length which causes relatively heavier weight. Due to its multiple-can structure and longer length, the wetted area and resultant losses in total pressure are also relatively larger and higher[34][47][41][37].

A cannular (or also known as tuboannular or can-annular) combustor was introduced in the late 1940s as the pressure ratio of gas turbine engines increased. About six to ten cans are generally arranged around the axis of an engine in a single annulus casing while a can type has an individual casing for each can, as shown in Figure 3.3. Many disadvantages of can combustors such as pressure losses and weight have been improved in the cannular type while keeping the advantages in maintenance and development cost and time. As this type still uses a multiple can structure, it has a strong advantage in the size and cost of the rig test facility. However, when it is compared with the annular combustor, the cannular type is still heavier with higher diameter. Because the length and weight are important design considerations for aircraft engines while they are less important in the ground application, the cannular type combustors are mainly used in the industrial gas turbines[41].

In the annular combustor that most modern aviation gas turbine engines take, there are no cans around the engine. It consists of a single liner inside a single annulus casing, as shown in Figure 3.3. Therefore, the combustion process is not confined in the can but it occurs all around the annular liner volume. This means that the control volume of

the combustor is more efficiently utilized. In the design perspective, a more simple and compact design is achieved as the liner surface area is smaller and the system length is shorter. As a result, the system weight is lighter and the pressure loss is reduced with lower wetted area[34][37][42][47].

Typical values of the pressure loss factor(PLF) enables to compare pressure losses among three different combustor types. The pressure loss factor is defined as a ratio of the losses of total pressure to the reference dynamic pressure of flow through the system. It is often expressed with empirical coefficients for cold loss and hot loss, as shown in Equation (3.18)[48].

$$PLF = \frac{\Delta P_t}{\frac{1}{2}\rho U_{ref}^2} = K_1 + K_2 \left(\frac{T_{t4}}{T_{t3}} - 1 \right) \tag{3.18}$$

where ΔP_t is the total pressure loss through the system, ρ is the density of incoming flow to the combustor inlet, $\frac{T_{t4}}{T_{t3}}$ is the total temperature ratio at the outlet of the combustor to at the inlet of the combustor. U_{ref} is the reference velocity of the flow at the reference cross-sectional area of the combustor. The reference cross-sectional area is usually the maximum cross-sectional area of the combustor and the flow condition is the combustor inlet condition. The first K_1 is the empirical coefficient for the cold loss and K_2 is the empirical coefficient for the hot loss.

The hot loss is also called the fundamental loss. It is caused by the heat addition to the flow. This flow is often called Rayleigh flow and the loss is higher for faster flow. All other losses that are not related to heat in the combustor are cold loss such as losses due to the friction and turbulence dissipation when the flow is injected through the holes. The empirical coefficients K_1 and K_2 are usually determined by experimental test. Further details about the pressure losses in the combustor will be discussed in the later chapter.

The pressure loss factor is a combustor characteristic. The PLF is the total pressure loss relative to the dynamic pressure. The higher value generally implies the more pres-

sure loss through the combustor. Typical values are 35 for the can combustor, 25 for the cannular combustor, and 18 for the annular combustor. The PLF of the annular combustor is almost half of the can combustor. This means that about half of the total pressure loss can be improved by using an annular type combustor if the inlet cycle and the design of the maximum cross-sectional area are the same with a can type combustor. Typical values are listed in Table 3.2.

Table 3.2: Typical pressure loss factor[48]

Combustor Type	PLF
Can	35
cannular	25
Annular	18

Another advantage of the annular design is the more uniform temperature profile in a circumferential direction. This is a positive design improvement for the turbine blades. For the can combustor, the combustion process occurs only inside the cans and the efflux of the hot gas forms non-uniform circumferential profile of temperature at the turbine entrance from the combustor exit. Then, the rotating turbine blades experience a high variation of temperature and it reduces the life of materials. However, by eliminating cans and utilizing all volume inside the annular liner, the annular design achieves more uniform circumferential temperature profile.

Now that the annular structure is the most common design of the modern combustors of the aircraft gas turbine engines, this thesis research will work on this type.

Basic Structure of Combustor

The traditional gas turbine combustor consists of three main zones; the primary zone, the secondary zone (or intermediate zone), and the dilution zone. Figure 3.4 shows the

schematics of this configuration. Although there are some combustors that have more complex configurations as more staging technologies are developed, they are extended forms of this traditional configuration.

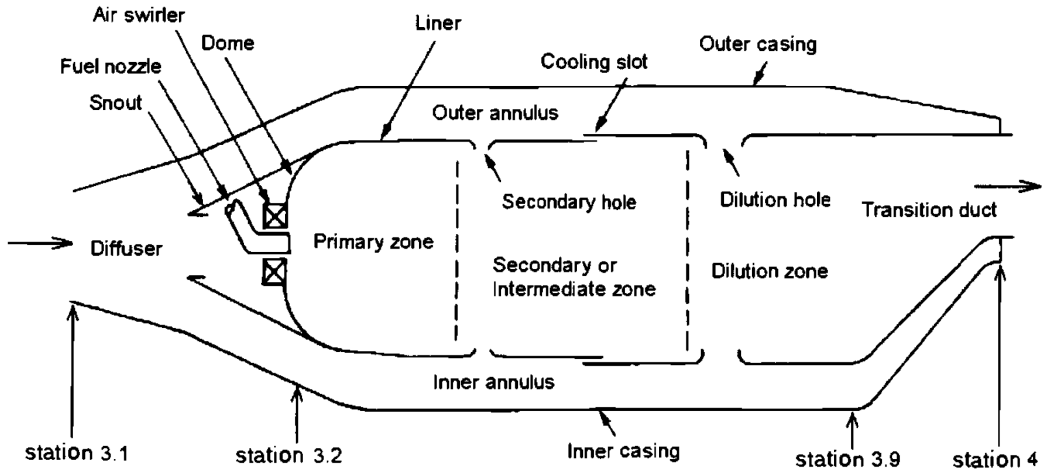

Figure 3.4: Basic configuration of combustor

The diffuser is the first component that flows from the compressor meet. The Mach number of the discharge flow from the compressor exit is the order of 0.2-0.32[41] and the typical value suggested by Hawthorn[49] is 0.28. The goal of the diffuser is to slow down the flow speed. This is to prevent a high level of pressure losses in the combustor. Both cold and hot pressure losses discussed earlier are a function of flow Mach number. As the flow is faster, the more pressure losses are caused. When the heat is added into the flow, this flow is called Rayleigh flow. When the flow is flowing with friction, this flow is called Fanno flow. The losses in total pressure are caused to both flows. The total pressure losses are expressed in Equation (3.19) for the Rayleigh flow and in Equation (3.20) for the Fanno flow[50].

$$\frac{P_{t2}}{P_{t1}} = \frac{1+\gamma M_1^2}{1+\gamma M_2^2}\left(\frac{1+\frac{\gamma-1}{2}M_2^2}{1+\frac{\gamma-1}{2}M_1^2}\right)^{\gamma/(\gamma-1)} \tag{3.19}$$

where P_t is the total pressure, γ is the specific heat ratio, and M is the Mach number. The

subscript 1 denotes the flow condition before the heat addition and the subscript 2 denotes the flow condition after heat addition,

$$\frac{P_{t2}}{P_{t1}} = \frac{M1}{M2}\left[\frac{2+(\gamma-1)M_2^2}{2+(\gamma-1)M_1^2}\right]^{(\gamma+1)/[2(\gamma-1)]} \tag{3.20}$$

where the subscript 1 denotes the flow condition before the friction is applied to the flow and the subscript 2 denotes the flow condition after the friction is applied.

These two equations are approximated for the thermally and calorically perfect gases. The general relationship with Mach number is that the higher M_1 causes the more total pressure losses for the subsonic flow. The Figure 3.5 shows the variation of the percent total pressure loss of Rayleigh flow for the variation of incoming flow Mach number(M_1) with outgoing Mach number(M_2). The lower heating value in this simulation is 43124 kJ/kg as it is the lower heating value for the jet fuel and the specific heat ratio(γ) is 1.33 and the specific heat for constant pressure is 1156.9 $kJ/kg-K$ as Walsh and Fletcher suggested for the hot end gas[41]. The fuel mass was neglected in this simulation due to its small contribution to the total mass. As M_1 increases, the Rayleigh loss increases significantly. The typical Mach number of the flow at the compressor exit 0.2-0.32[41] corresponds to a significant loss in this Figure which is unacceptably high. For example, when M_1 is 0.2, the flow is accelerated to $M_2 = 0.52$ and the total pressure loss is 58.0%. However, if the flow is successfully decelerated to 0.025 which is a typical Mach number inside the combustor[41], the Rayleigh loss is just 0.93% in this simulation. For this reason, there is a diffuser at the first stage of the combustor. The diffuser usually decelerates the flow to around M_1 = 0.05-0.1 around the liner[41].

The primary zone is the first combustion zone in the combustor. In this region, the fuel is injected and reacts with the fresh air. The injected fuel is atomized and sprayed to this zone and high swirls are generated when some portion of the fresh air from the diffuser passes through the swirler at the liner entrance. These swirls generate strong turbulence

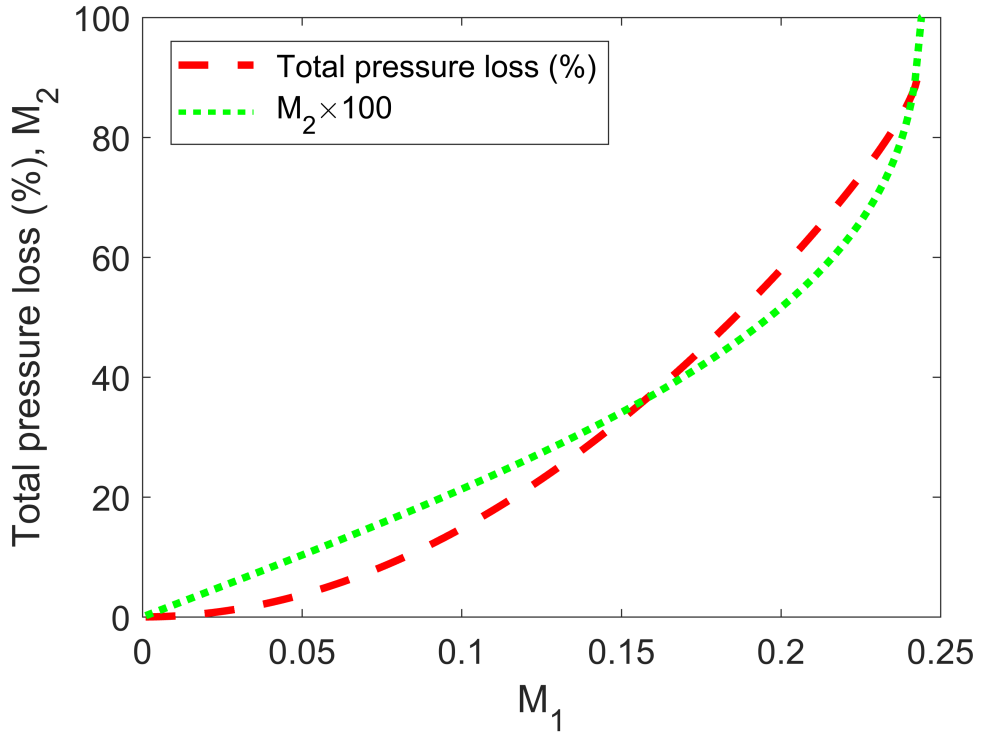

Figure 3.5: Hot loss and Mach number relationship

that promotes the mixing process of fuel and air as well as recirculation of hot gas. The recirculating toroids provide heat to the fresh reactants so that the combustion is stable and continuous. They also provide sufficient time for combustion[34]. In this primary zone, the equivalence ratio is usually near the stoichiometric value to achieve stable and efficient combustion. The design guideline from Walsh and Fletcher[41] about the equivalence ratio at the primary zone is 1.02 and the temperature at the primary zone is 2300K. Although this high temperature is to achieve high reaction rate for the stability and efficiency considerations, it is highly favorable for the formation rate of the oxides of nitrogen(NOx) as discussed previously. For this region, there are some staging techniques keeping the equivalence ration richer or leaner than the traditional primary zone stoichiometry. These staging techniques will be discussed later. The flow experiences a small pressure drop as the heat is added. This is the Rayleigh flow discussed earlier. The Mach number of the flow leaving the primary zone is about the order of 0.02-0.05[41].

The hot products from the primary zone keep combusting with additional fresh air injected through the holes at the secondary zone. This secondary zone is often called the intermediate zone. Although the majority of heat stored in the chemical bonds of the fuel is released at the primary zone, there are relatively high concentrations of hydrogen(H_2) and carbon monoxide(CO) species in the hot gas from the end of the primary zone. This is due to the high temperature in the primary zone. To keep the fast reaction rate, the primary zone temperature is maintained to be above 2000K. In this temperature, some of CO_2 and H_2O molecules are dissociated and CO and H_2 species are produced[34]. These processes are endothermic reactions. This is the inefficient use of energy for engine users. Therefore, the further combustion process is required to burn CO and H_2 species contained in the hot gas from the primary zone. For this reason, additional air is injected into the secondary zone through holes and lower the overall temperature and equivalence ratio of the flow. In this process, unburned fuel and soot produced in the primary zone are also burned together[34][42]. To keep the combustion process to burn CO, H_2O, unburned fuel, and soot while the NOx chemistry is suppressed, the typical equivalence ratio at the secondary zone is around 0.6 and the temperature is around 1700K[41]. The combustion process is completed at the secondary zone[41][42].

To protect the turbine materials, the flow temperature needs to be lowered before it enters the turbine stage. For this reason, leftover air is injected into the dilution zone. This fresh air does not participate in the combustion. The combustion process is already completed at the primary and secondary zones. The dilution air is mixed with hot products from the upstream and lowered the temperature. In addition, it makes the uniform temperature profile at the combustor exit so that the turbine blades do not experience temperature fluctuation.

There are two factors describing the uniformity of flow temperature at the combustor exit. One is the te pattern factor. The pattern factor characterizes the deviation of the maximum temperature at the exit plane from the overall exit tempetarue. It is defined

as[34]:

$$\textit{Pattern factor} = \frac{T_{max} - T_4}{T_4 - T_3} \tag{3.21}$$

where T_3 is the overall temperature entering the combustor from the compressor exit, T_4 is the overall temperature entering the turbine from the combustor exit, and T_{max} is the maximum temperature at the combustor exit.

The other factor is the profile factor. The profile factor characterizes the deviaion of the maximum mean circumferencial temperature at the exit plane from the overall temperature at the exit. It is defined as [34]:

$$\textit{Profile factor} = \frac{T_{mr} - T_4}{T_4 - T_3} \tag{3.22}$$

where T_{mr} is the maximum circumferencial mean temperature. Figure 3.6 is the visual explanatino of terms in Equation (3.21) and (3.22).

The main goal of the dilution zone is to achieve good pattern factor and profile factor. As the mixing process takes time, some length from the injection of dilution air is required. The typical length to diameter ratio of the dilution zone is about 1.5-1.8 for this purpose[34].

Staging

When staging technique is applied, each zone is specifically optimized for different combustion performance goals. In this section, several types of staged combustors will be briefly introduced as one of the research objectives of this thesis is to develop a soot prediction environment applicable to different combustor architectures.

Rich-burn, quick-quench, lean-burn(RQL) combustor is an air-staged combustor. It is an extended form of a traditional combustor with differently controlled stoichiometry.

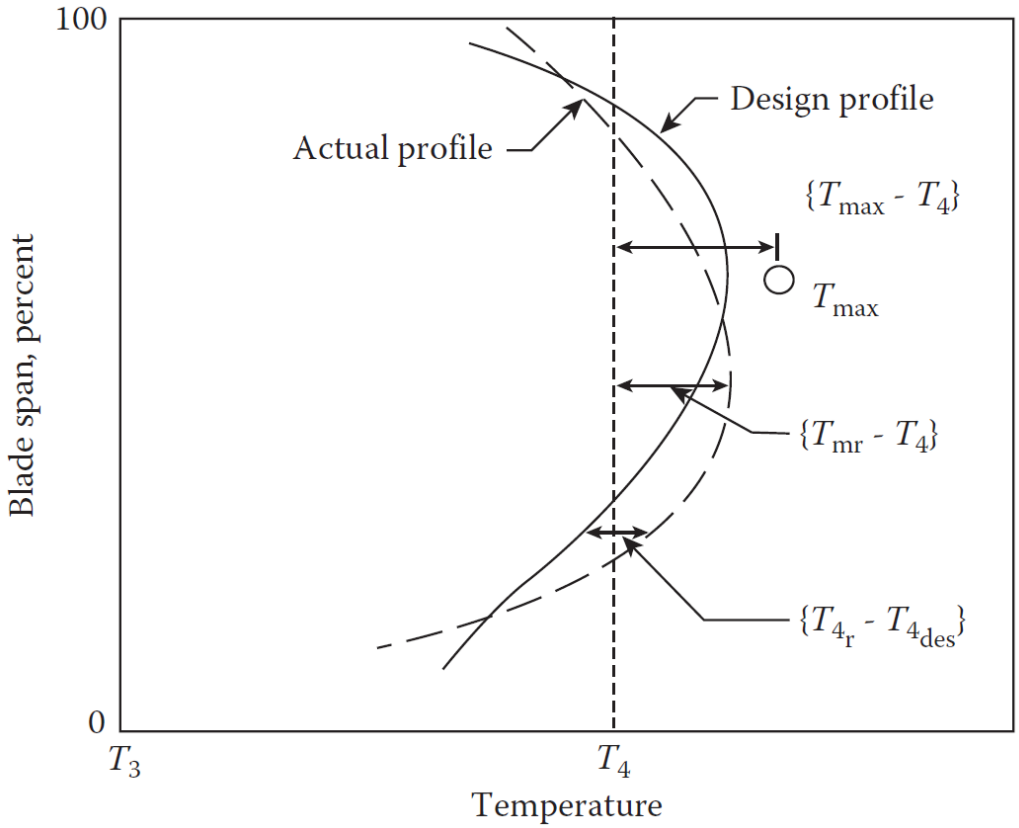

Figure 3.6: Visual explanation of terms in temperature profile parameters[34]

Therefore, its overall shape is still similar to the traditional ones. The main idea of this combustor is to lower the flow temperature by burning fuel at rich and lean equivalence ratios and suppress the NOx formation mainly at the high power. The primary zone of RQL combustor is called ”rich zone.” The equivalence ratio of this zone is much higher than the traditional combustor. It is around 1.8[51]. Because the equivalence ratio is high, the temperature is low enough to suppress NOx formation. However, the combustion efficiency is not high such that a large amount of fuel is not completely burnt yet due to the low reaction rate. In the quench zone, a large amount of air is injected and mixed with hot product gas in a short time. Then, in the lean zone, the rest of the combustion process is continued at low equivalence ratio. The temperature is also low enough to prevent NOx formation. The basic scheme is illustrated in Figure 3.7.

The RQL combustor introduced in the above is the air-staging combustor. This is an

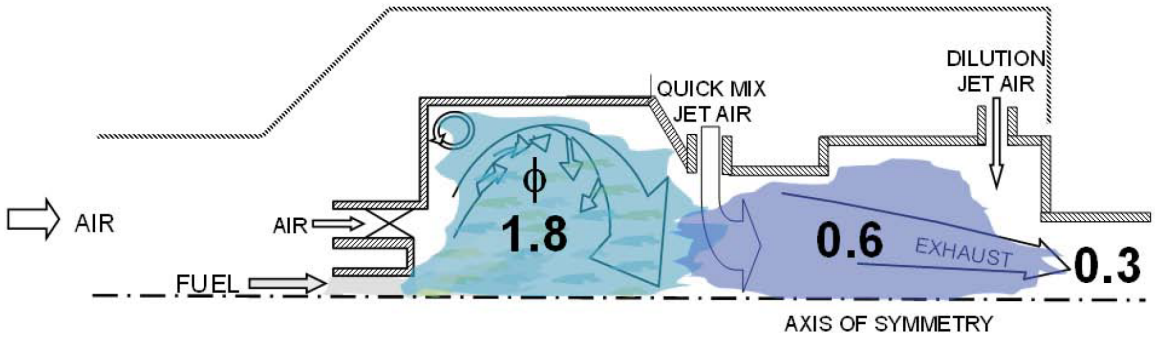

Figure 3.7: Basic scheme of Rich-Burn, Quick-quench, Lean-burn(RQL) combustor with stoichiometry[51]

extension of the traditional combustor. It passively controls the stoichiometry of each local combustor zone once the air injection holes are designed. However, the combustors will be in introduced now are more actively control the local stoichiometry with fuel staging techniques. The first one is the double annular combustor(DAC). It is often called the dual annular combustor. Its basic configuration is illustrated in Figure 3.8.

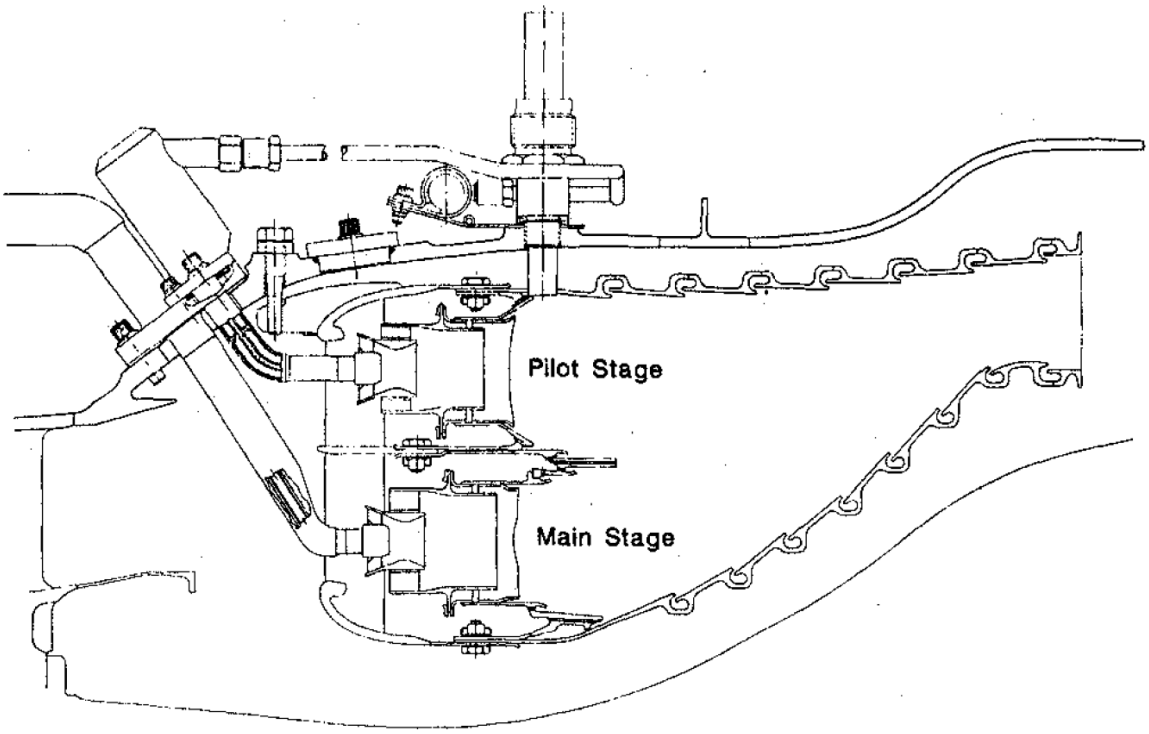

Figure 3.8: Basic configuration of Double Annular Combustor(DAC)[33]

Unlike the traditional single annular combustor(SAC) or RQL combustor that has serial

combustion zones, the DAC combustor has parallel combustion zones at the front side. The primary zone of the DAC combustor is called pilot zone. This zone is responsible for all combustion required at the low power. The other zone is called the main zone. The main zone is turned on during the low power setting. At the high power condition, the fuel is also injected at the main zone with air and the pilot zone provides heat to the main zone so that the combustion at the main zone is stable and continuous. The pilot zone is optimized for stable and efficient combustion at low power and the main zone is optimized for low NOx production and high efficiency at the high power[34]. As the fuel is injected and mixed with the air and as the initial combustion process is activated at both zones, they can be treated as the primary zones sharing common parameters with different values for modeling perspective.

Figure 3.9 shows the axially staged combustor. This is another type of fuel staging combustors. Like the radially staged combustor, the axially staged combustor also consists of the pilot zone and main zone. The primary zone is the pilot zone which is responsible for low power load optimized for stable combustion. At high power, the hot product from the pilot zone delivers heat to the fuel and air mixture injected at the main zone. This enables immediate combustion. Both zones are operated at low equivalence ratio so that the NOx and soot formations are suppressed.

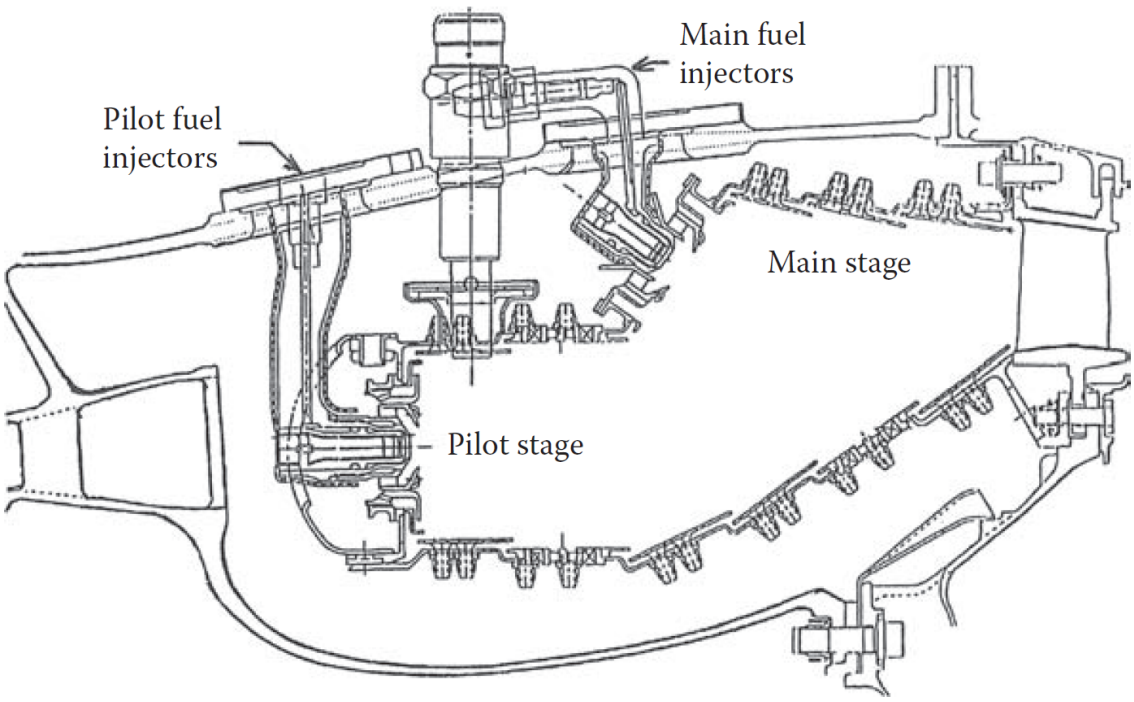

Figure 3.9: Basic configuration of axially staged combustor[34]

GE Aviation Twin Annular Premixing Swirler(TAPS) combustor can be categorized as a radially staged combustor. Its injector consists of a pilot and main injectors. The pilot injector is at the center and the main injector is around the pilot(see figure 3.10). Like other staged combustors, the pilot is responsible for the low power. At the high power, fuel and air are injected from both injectors. The main combustion is ignited by the heat from the pilot one. By generating high swirls through the injectors, the combustion can be stable while operating with low equivalence ratio[32].

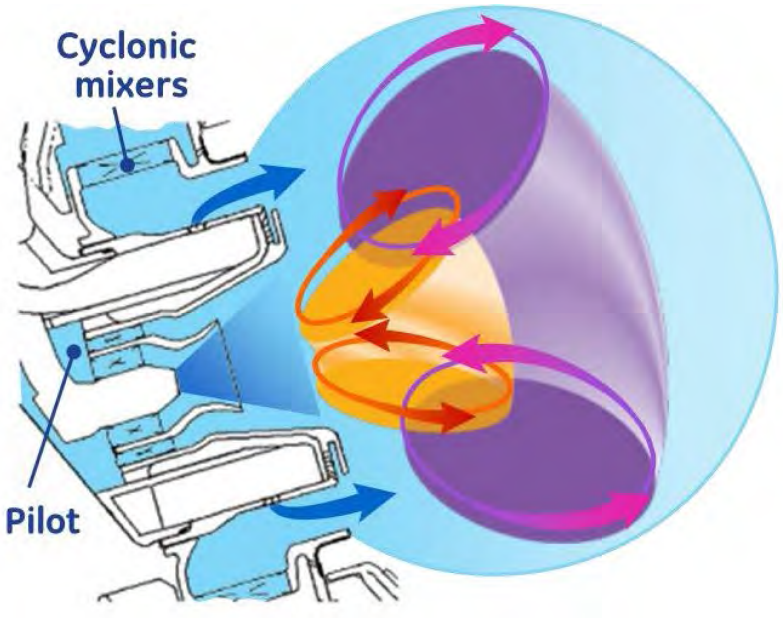

Figure 3.10: TAPS injector concept[32]

The lean Direct Injection LDI combustor is a radially staged combustor. In this combustor, a relatively large number of small injectors are radially distributed at the front plane of the combustor. Its injector concept is described in Figure 3.11. The main idea of this type is that the fuel is rapidly atomized and mixed with air at lean fuel/air ratio prior to burning.

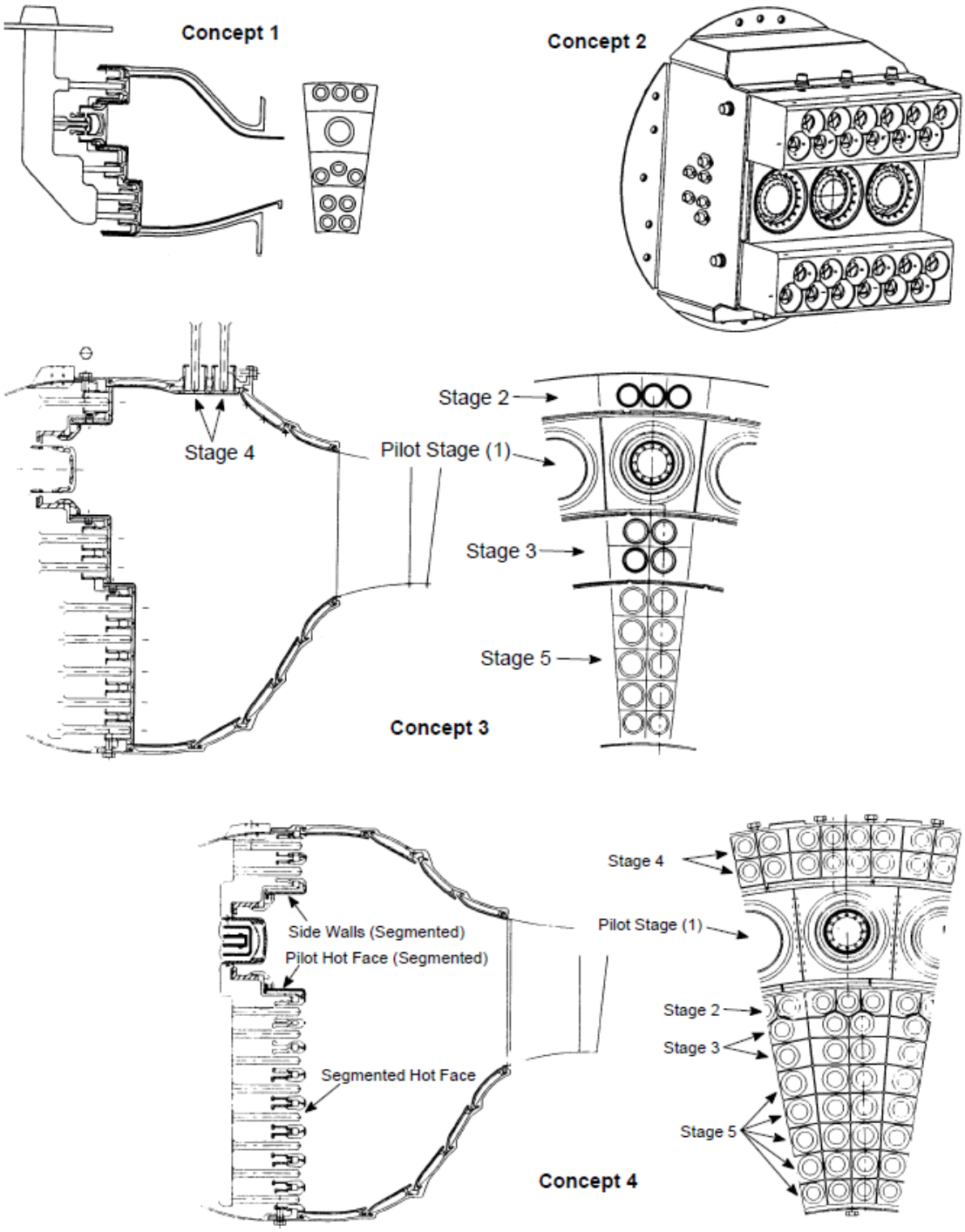

Figure 3.11: LDI injector concepts[52]

Staged combustors such as RQL, DAC, axially staged, TAPS, and LDI combustors are briefly introduced in this section. They are categorized and listed in Table 3.3 by staging

types.

Table 3.3: Staged combustors

	Air staging only	Fuel staging
Axial Staging	RQL	Axially staged
Radial Staging	TAPS	DAC LDI

CHAPTER 4

PROBLEM FORMULATION

4.1 Research Questions and Hypotheses

The problem statement was identified and the research objective was established in the earlier chapter. The main issue in this thesis research is the soot prediction. To achieve this goal, several steps of research questions should be addressed. The first one is:

RQ1: What are the important factors in soot prediction?

This is the most fundamental question. To create a soot prediction model, the important factors affecting soot must be identified.

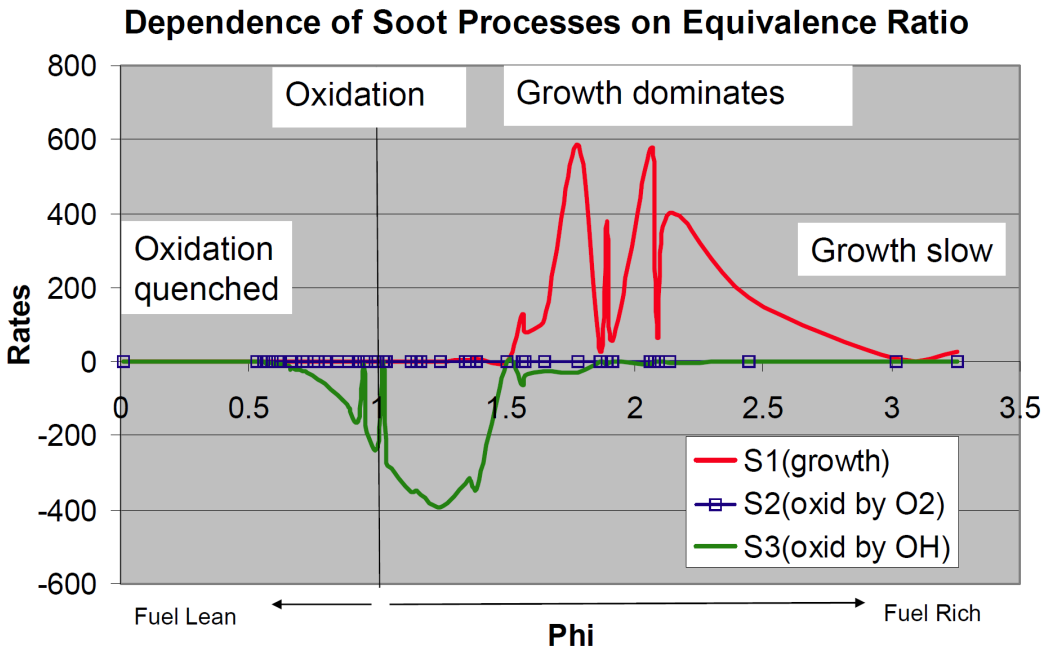

Figure 4.1: Dependence of soot processes on equivalence ratio[46]

Local fuel-air ratio

Now that the soot formation is not a simple process, there are several factors involved. One of them is the fuel-air ratio. According to Colket's CRN simulation of a rig combustor at take-off condition($T_3 = 811K$ and $P_3 = 16.3\ atm$), soot is formed at the region where the equivalence ratio is over 1.5 and oxidized at the region where the equivalence ratio is between 0.7 and 1.5[46]. Figure 4.1 shows this result. This figure implies that the soot formation and oxidization processes are highly affected by the fuel-air ratio of the combusting flow.

As already discussed earlier, the soot evolution consists of four stages: inception(or nucleation), surface growth, oxidization, coagulation(or agglomeration). The balance between formation and oxidization determines the amount of soot produced through the combustion process. The formation processes are active in the fuel-rich region while the oxidization processes are usually active at the fuel-lean and near stoichiometric region.

This relationship can be also found in the soot formation mechanism. Leung et al.'s soot formation mechanism[14] is one of the examples. Their mechanism is listed in Table 4.1. They applied this mechanism to their simulation.

Table 4.1: Leung et al's soot formation mechanism[14]

rate of inception	$R_1 = 0.1 \times 10^5 e^{-21100/T}[C_2H_2]$
rate of surface growth	$R_2 = 0.6 \times 10^4 e^{-12100/T} S[C_2H_2]$
rate of oxidization	$R_3 = 0.1 \times 10^5 T^{1/2} e^{-19680/T} S[O_2]$
rate of coagulation	$R_4 = -2C_a \left(\frac{6M_{C(S)}}{\pi\rho_{C(S)}},\right)^{\frac{1}{6}} \left(\frac{6\kappa T}{\rho_{C(S)}}\right)^{\frac{1}{2}} [C(S)]^{1/6}[\rho N]^{11/6}$
surface area	$S = \pi \left(\frac{6}{\pi}\frac{1}{\rho_{C(S)}}\frac{Y_{C(S)}}{N}\right)^{\frac{2}{3}} (\rho N)$

The species involved in the soot formation phases mainly come from the fuel. The

inception and surface growth models usually include many hydrocarbon species such as acetylene, benzene, and many different kinds of polycyclic aromatic hydrocarbons. The concentration of these species which promotes the soot formation processes from the fuel. Therefore, the richer mixture leads to more soot formation. For example, Leung et al.'s mechanism in Table 4.1 shows that the more acetylene species in the reacting gas leads to the more formation of soot. The carbons and hydrogen consisting of the acetylene species in the inception and surface growth phases of Leung et al.'s mechanism come from the hydrocarbon fuel. Therefore, it is obvious that the fuel-rich condition of the flow is more favorable for the formation of soot.

In the oxidization expression, the concentration of the soot oxidizers such as hydroxyl radical and oxygen species shown in the oxidization phases in Leung et al.'s mechanism plays an important role. The simulation result by Colket's[46] in Figure 4.1 also support it. Hydroxyl radical and oxygen are abundant in the fuel-lean flow because the oxygen atoms in both species are from the air.

In Leung et al. 's mechanism listed in Table 4.1, the activation temperature of the oxidization stage is 19680K while the activation temperature of the growth stage is 12100K. These two stages are the stages where the mass of soot is highly affected. The soot gains its mass by surface growth and the mass is decreased as the soot is oxidized. Therefore, it can be expected from the high activation temperature of the oxidization step that the oxidization of soot is also active in the near-stoichiometric region. In addition to the exponential term, the oxidization rate includes the square root of temperature term. This high dependency on temperature implies the high-temperature effect on soot oxidization. Furthermore, the concentration of hydroxyl radical is also relatively high in the near-stoichiometric region. As discussed in the Stoichiometry section in Background chapter, the high temperature at the near-stoichiometric equivalence ratio causes dissociation of H_2O and increases the concentration of OH which is a major oxidizer of soot. Therefore, the oxidization of soot is expected at the fuel-lean and the near-stoichiometric region, and this is in agreement with

the result of Colket's experiment(Figure 4.1).

These observations give strong confidence on the effect of fuel-air ratio on the soot formation. Therefore, the fuel-air ratio is apparently one of the important factors in soot prediction.

Air partitioning

The fuel-air ratio is the ratio of the mass of fuel to the mass of air. The fuel is injected at the front part of the combustor for many typical gas turbine combustors. As the flow goes to the downstream, the air is injected through the swirler and holes and mixed with fuel and hot gas. As the air is injected and mixed with the fuel and the hot product stream, the local fuel-air ratios keep changing. The local equivalence ratio of traditional combustors such as SAC and RQL combustors go leaner as air is mixed. Because the fuel is injected once, the amount of air injected is the driving factor determining local equivalence ratio of the combustion zone. Therefore, distribution of air flow into different combustion zones, or air partitioning is a key factor in determining the local fuel-air ratio, thus one of the key factors in soot prediction. The air partitioning is an important design factor even for the fuel-staging combustors because the local equivalence ratio and temperature profile are controlled mainly via air partitioning. The designs of swirler and hole geometry that take a huge part of combustor design are to achieve the appropriate air partitioning whether they are for the traditional SAC combustor or for the staging combustors. Therefore, the air partitioning that is highly affecting local fuel-air ratio is apparently one of the important factors in soot prediction.

Local flow properties and species concentrations

The temperature of flow is also an important factor in soot prediction. The temperature indicates the energy of molecules in the flow. When the temperature is higher, the more particles are likely to be above the chemical barrier and the reaction rate becomes higher.

This is the same for the soot formation phenomena. As shown in Table 4.1, all expressions in the soot mechanism show temperature dependence. As temperature increases, all rates become higher. In addition to the direct effect, these rates are also indirectly affected by the temperature as the terms included in them also depend on temperature. For example, the concentration of acetylene species included in the inception and surface growth rates is a result of chemical reactions that depend highly on the temperature. The density in the surface expression also depends on the chemical reactions and the temperature. Therefore, the temperature is one of the most important flow properties in soot prediction.

It is well known from many studies that some species have a close correlation with soot formation process. As a result, many semi-empirical soot formation mechanism includes the concentration of soot indicating species. Examples are C_2H_2 and C_6H_6 in Lindstedt's nucleation rate expressions[53], $C_{10}H_7$ and $C_{14}H_{10}$ in Hall et al.'s nucleation rate expressions[54], and C_2H_2 and H in El-Leathy et al.'s surface growth rate expression[55].

Table 4.2: Examples of soot formation mechanism involving soot indicators

Lindstedt[53]	nucleation rate	$r_{27.10} = k_{27.10}(T)[C_2H_2]$ $r_{27.11} = k_{27.11}(T)[C_6H_6]$
Hall et al.[54]	nucleation rate	$S = 127 \times \frac{d[C_{10}H_7]}{dt}$ $+178 \times \frac{d[C_{14}H_{10}]}{dt}$
El-Leathy et al.[55]	surface growth rate	$w_g = k_H[H][C_2H_2]$

Not only soot indicators but also oxidizers are included in the soot mechanism. One example is the O_2 in the oxidization rate expression of Leung et al.'s soot formation mechanism, already introduced in Table 4.1. Based on these relationships, some species concentrations are an important factor in soot prediction.

Mass flow rate is also one of the important factors in soot prediction. It has a direct relationship with the total amount of soot. The more soot exists as the more mass flows through the combustor for a given soot formation rate. For example, the unit of formation

rates in Leung et al's soot formation mechanism introduced in Table 4.1 is $kmol$ per unit volume and time($kmol/m^3/s$). The volume can be easily converted into mass simply by multiplying density. Therefore, in addition to a set of soot formation rates, the mass of the flow is essential in the prediction of soot.

Not only the temperature, mass, and species concentration but also other flow properties such as pressure and density do need to be considered as affecting factors. The higher pressure means the higher density. This relationship is easily found in the state equation(Equation 4.1).

$$p = \rho RT \tag{4.1}$$

When the density is higher, the molecules in the gas are closer to each other. This means that the mean free path of species is shorter and they have more chances to collide each other. Therefore, the reaction rate is increased and the species concentration and the temperature are affected as a result. Therefore, soot formation is affected by some flow thermodynamic properties such as pressure and density although they are generally not found in the soot formation mechanism. As temperature and species concentrations are affected by these properties, they must be considered for the calculations of chemistry.

Residence time

The residence time is another factor crucial in soot prediction. The flow takes time to flow through the combustor or a specific length of the combustor. The average time for which the flow stays in this region is the residence time. It can be roughly calculated by Equation 3.15 or 3.17. Because chemical reactions occurred inside the combustor change the density and velocity of the flow, these expressions are a rough estimation.

$$\tau_{res} = \frac{length}{\textit{flow velocity}} \tag{3.15 revisited}$$

$$\tau_{res} = \frac{\rho V}{\dot{m}} \qquad \text{(3.17 revisited)}$$

The longer the flow stays, the more soot formations and oxidization occur. If the region where flow stays is favorable for soot formation, a lot of soot will be produced when the residence time is too long. In contrast, if the region is favorable for the oxidization of soot, there will be almost no soot in the flow for long residence time. Therefore, the residence time is one of the factors important in soot prediction in addition to the soot formation mechanism.

Several essential factors affecting the soot formation are identified while the first research question is answered. These are the local fuel-air ratio, air partitioning, local thermodynamic properties and species concentrations, and the flow residence time. The soot formation mechanism shows that the concentration of soot indicating species, flow temperature, and residence time are essential in soot prediction. They are calculated from the chemistry. To correctly calculate them, the fuel-air ratio must be correctly evaluated. Therefore, these factors discussed here are of importance in the soot prediction.

The research objective in this thesis research addresses the different thermodynamic cycles. The soot prediction model pursued in this research is expected to be applicable to the different thermodynamic cycles. From this goal, the second question arises as:

RQ2: How do the different thermodynamic cycles affect soot formation?

This question is closely related to the first question. One simple answer to the second question is that factors important in soot prediction that are reviewed in the first question are affected by the thermodynamic cycle of the engine, thus the soot formation process is also affected. The different thermodynamic cycle means a different engine. When it comes to the combustor, the different thermodynamic cycle means the different inlet values such

as the total pressure, the total temperature, the mass flow rate, and the fuel-air ratio of the flow at station three(P_{t3}, T_{t3}, W_3, f/a). These parameters have a significant impact on the chemical reaction inside the combustor. When the mass flow rate is different, the way of air distribution is also different. Then, the local fuel-air ratios are different and the combustion reactions are affected. When the pressure is different, the pressure distribution inside the combustor is different and the air distribution is affected, thus the chemical reaction processes are affected. The different initial temperature significantly changes the flame temperature. Then the reaction rates are changed and the flow properties including species concentrations are changed. When the chemical reactions inside the combustor are affected by the different cycles, the residence time of the flow is also changed due to the variation of flow density and volume. Therefore, it can be concluded that the different thermodynamic cycle affects many factors important in soot prediction and eventually changes the soot emission output. For this reason, it is of importance that the factors discussed in the first question should be correctly achieved so that the soot prediction model is truly parametric and can handle the different thermodynamic cycles.

As the influential factors in soot prediction are identified, the next question is about the state-of-the-art treating these factors.

RQ3: How do the current soot prediction methods treat these parameters?

For the local thermodynamic properties and species concentration, they are directly achieved by solving a set of chemical reaction equations. There are a lot of well-made chemical mechanisms for fuel pyrolysis and oxidation reactions. Examples are GRI mechanism[56] for methane fuel and Kollrack's mechanism for jet fuel[43]. Some mechanisms are complex while other mechanisms are simple. Many CFD simulations prefer simple global reactions to avoid heavy computational loads. However, the soot mechanism involves minor species that are not included in many simplified mechanisms. For this reason, the soot studies generally adopt mechanisms involving many elementary reactions.

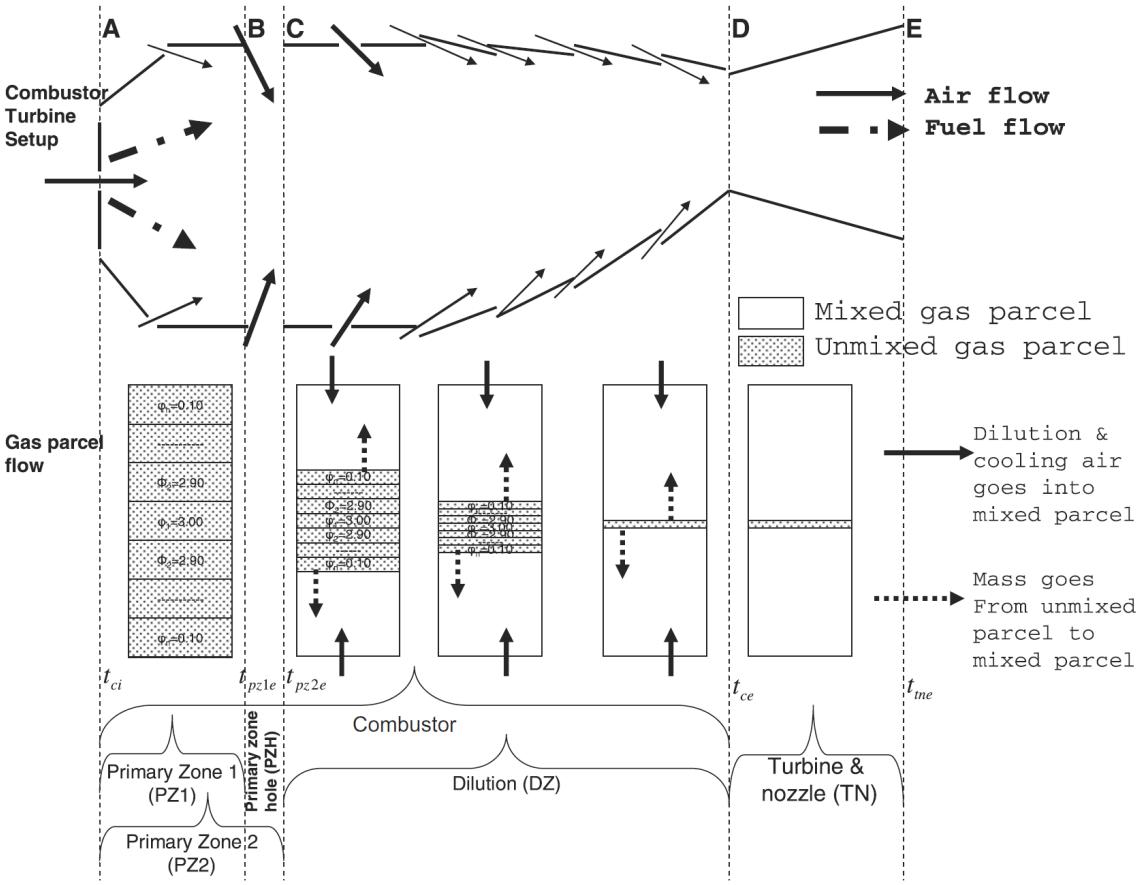

Parcel-box approach of Moniruzzaman and Yu[29] (repeated from Figure 2.8)

For example, Moniruzzaman and Yu calculated flow properties and species information from CHEMKIN code and a combined mechanism that involves 269 species and 2657 reactions[29]. Because the complex chemical mechanism is computationally heavy, soot research often takes CRN or similar approach such as the parcel-box approach. These approaches simplify the combustor flow field with multiple ideal reactors such as Perfectly Stirred Reactor(PSR) and plug Flow Reactor(PFR) or with multiple parcels. With the aids of these techniques, thermodynamic properties of the flow and species concentrations are computed from a complex chemical reaction mechanism in the current soot prediction methods.

For the air partitioning and residence time, there are mainly three approaches taken by the current soot prediction methods.

1. Assumed values for specific engines and/or specific powers are used

2. Calibrated values for specific engines and/or specific powers are used

3. Real data of specific engines and/or specific powers are used

Examples are soot prediction models of the gas turbine engine developed by Moniruzzaman and Yu[29], Bisson et al.[30], and Martini[28].

Moniruzzaman's group[29] developed an emissions prediction model of CFM56-2C1 engine. Note that they specifically focused on the modeling of idle operation. For the cycle inputs, some of them were taken from the real data available. For unknown cycle inputs, they were approximated from assumed properties such as compressor efficiency. They also utilized trial-and-error type calibration to determine the values of unknown properties. The residence time was one of them determined by this approach. The total residence time was an input parameter for their model. They assumed 10ms for the total residence time and its breakdown to local zones was determined by trial-and-error calibration. For the air partitioning, it was determined from the correlation of the equivalence ratio at the end of the primary zone after new fresh air was introduced through the hole. Bisson's group[30] modeled soot prediction model for CFM56-2C1 engine. Unlike Moniruzzaman's group, they targeted all four LTO cycles. In their modeling of a combustor, geometry factors such as length, cross-section area, and volume and air partitioning that were required for CRN model were taken from the combustor of Energy Efficient Engine(E^3) that whose length to height ratio is similar to the target combustor. Martini[28] developed a soot prediction model for the LTO cycle of PW4090 engine and CFM56-2C engine in his master thesis research. His model utilized previously developed CRN model for NOx and CO prediction purposes. For soot prediction, he recalibrated unmixedness that represented a non-uniform mixture of fuel and air at the primary zone.

In addition to these three approaches treating air partitioning and residence time, there is the fourth case for CFD simulations that calculate these two properties while other prop-

erties are calculated during the simulation. However, the CFD simulation requires detailed geometry information that is not available at the early stage of the design. Furthermore, the CFD simulation generally takes a long time that is not acceptable for the conceptual design. For these reasons, this method is not suitable for conceptual design and not reviewed here.

Based on the research objective pursued in this thesis research, there are two requirements for a parametric soot prediction method for the use during the conceptual design. First, the method ought to be able to handle different thermodynamic cycles. Second, the method ought to be scalable for different combustor sizes. In other words, they can also be addressed as

1. applicable to different engine cycles

2. applicable to off-design operating cycles

It is required to review three examples again in terms of these two requirements to identify the limitations of current methods that can be improved. In Moniruzzaman group's modeling, several properties were from real engine data and/or calibrated for the specific engine. Assumed values and calibrated values were also used in the determination of residence times. The way of achieving equivalence ratios needs more justification to be generalized. The correlation that they applied was created from the data of three Pratt & Whitney engines while their target engine is one of CFM series. The air fraction of the primary zone of these three engines is 19% of the total air. Therefore, although the correlation contains a fourth order term, all sample data points are lying in one simple line that makes the constant air fraction of the primary zone as 19% of the total. This method is equivalent to assuming air partitioning for all engine cycles and all operating conditions. Furthermore, the small number of samples are biased. Because of their approach to achieve residence times and air partitioning, their model cannot adequately handle different engine cycles and off-design operating cycles. The model developed by Bisson's group shows the results for the LTO cycle. However, the air partitioning and geometry factors utilized in the calcu-

lation of residence times were adopted from a prototype engine that is different from the target engine. As this model utilizes specific engine data, the model cannot be generalized for different engine cycles. In addition, their assumption of constant air partitioning for all power modes degrades the credibility of their results at off-design power modes. Martini used an optimizer to determine the volume and air partitioning of the local combustion zones for LTO cycle of PW4090 engine and CFM56-2C engine. The values of the two engines were independently determined. This means that this method is engine-specific and cannot be generalized for different engine cycles. In addition, the constant air partitioning assumption was also adopted by applying determined values to off-design cycles.

From these handling of air partitioning and residence times in the current soot prediction methods, two issues to be addressed are found as:

RQ4: How can a soot prediction model be applicable to different engines?

RQ5: How can a soot prediction model handle off-design operating cycles?

To find the answer to these questions, it is worth to revisit three cases of current soot prediction methods. In order to apply Moniruzzaman and Yu's approach to different operating power modes, another value for the total residence time is required and its breakdown needs to be recalibrated for a new power mode. Even if the originally determined values are used while the idle mode is assumed to be a design condition, a valid method to determine the air partitioning is required. Therefore, unless a method to determine air partitioning for different operation cycles is prepared, their soot prediction method cannot be applied to the soot prediction for off-design operation cycle. This conclusion is also applied to the soot prediction methods of Bisson et al. and Martini. Their soot results for LTO cycle was due to the assumption of constant air fraction. In order to increase the credibility of their results for different off-design operation modes, a reasonable method to determine the corresponding air partitioning is required. From this discussion, one possible conclusion answering the research question 5 is that a soot prediction model can handle off-design

operating cycles if it calculates air partitioning for different off-design operation cycles instead of adopting engine-specific and power-specific values

To justify this conclusion, it is necessary to evaluate the sensitivity of soot to the air fraction. If the air partitioning has little effect on soot formation, it may not be a key factor in soot prediction. For this reason, a preliminary experiment on air fraction is conducted.

In this preliminary experiment, the Rich-burn, Quick-quench, Lean-burn(RQL) combustor model[57] is used. This model was developed by Aerospace Systems Design Laboratory for the purpose of Oxides of Nitrogen(NOx) prediction. The NOx emission of 30% below from CAEP/6 regulation level for PW6124A engine is the calibration point of this model. Therefore, this engine cycle is used in this preliminary experiment. Among four LTO cycles, the climb out cycle is selected as an experimental point because this cycle is one of the off-design cycles and this power mode is free from the droplet effect that is activated at low power modes in the selected combustor model. The chemical mechanism that this model uses is based on the GRI 3.0 mechanism with an additional two global reactions for jet fuel pyrolysis.

The acetylene species is a well-known soot indicator. This species is involved in the soot inception and growth processes. The expression for soot nucleation rate(R_1) suggested by Leung et al.[14] takes the form as

$$R_1 = k_1 (T) [C_2H_2]$$

and the soot growth rate(w_g) suggested by El-Leathy et al.[55] takes the form as

$$w_g = k_H [H] [C_2H_2]$$

The square bracket abound the species name means the molar concentration of that species. The species concentration is the number of moles per unit volume($\frac{mol}{m^3}$). It can be found that the acetylene species is directly involved in both formation processes. The hydrogen

term is also directly involved in the soot surface growth process. For the oxidation of soot, Puri et al.[15] suggested this expression:

$$\frac{d\,[C_s]}{dt} = 4.6 \times 10^{-23} \eta_{OH} N_{av} d_p^2 N_s \sqrt{T}\,[OH]$$

In this expression, the hydroxyl radical is the species directly related to the oxidization of soot.

As the model used in this preliminary experiment does not have a capability to predict soot emission, these species concentration parameters($[C_2H_2]$, $[H]$, $[OH]$, $[H]\,[C_2H_2]$) are evaluated as indicators of soot in order to evaluate the sensitivity of soot to air partitioning. More specifically, the sensitivities of these parameters are evaluated for the variation of the air fraction at the primary zone. Although the combustor model used in this preliminary experiment is calibrated for NOx emission, this model is still useful for this experiment because the species of interest are fundamental species that are generally involved in the chemical kinetics of hydrocarbon fuels including the GRI 3.0 mechanism. Regardless of the type of emissions, the physical and chemical trends of these species are correct for well-arranged chemical mechanisms such as GRI 3.0. Therefore, it is concluded that the use of this model in this preliminary experiment is suitable for the purpose of the experiment.

The species concentrations are dependent variables in this preliminary experiment. However, it is not one of the outputs of this combustor model. Instead, the mass fraction of the species is one of output. In the conversion of the mass fraction into the species concentration, the following expression can be used.

$$[M]_i = \frac{p_i}{\bar{R}T} = \frac{p}{\bar{R}T} y_i \frac{MW_{tot}}{MW_i}$$

where $[M]_i$ is the concentration of species i, p and p_i is the pressure and partial pressure of species i respectively, bar_R is the universal gas constant, T is the temperature, and MW_tot

and MW_i is the average molecular weight of the mixture and the molecular weight of species i respectively.

The independent variable is the air fraction of the primary zone air to the total air(W_3). This term is denoted as "$fracPZ$" in the model. The value of this term is fixed to be 0.2458 regardless of power setting as this model assumes constant air partitioning. This term is varied by $\pm 15\%$ from the baseline case which is the case with zero percent perturbation in air fraction.

The results of this experiment are shown in Table 4.3 and 4.4 and Figure 4.3 and 4.4. Table 4.3 shows the variations of species concentration terms ($[C_2H_2]$, $[H]$, $[OH]$, $[H]$ $[C_2H_2]$) for the variation of the primary zone air fraction with corresponding equivalence ratio. The percent change of the primary zone air fraction is from the baseline value which has no perturbation in air fraction. Monotonic relationship between air fraction and species concentration is observed for all four terms. This relationship is visualized in Figure 4.3 with percent changes of terms from the baseline value. As the air fraction increases, the air mass amount is larger than given fuel mass and the equivalence ratio changes to leaner. Therefore, the left side in the figure is richer equivalence ratio region and the right side is the leaner region within the given ranges. The corresponding equivalence ratio at the primary zone changes between 1.307 and 1.768. Note that this range lies in the rich equivalence ratio even for the leanest experimental point. In this experimental region, all terms show high changes for the variation of air fraction. The correlations of the terms with air air fraction are 0.9805, -0.9804, 0.9771, and -0.9919 for $[C_2H_2]$, $[H]$, $[OH]$, and $[H]$ $[C_2H_2]$ terms, respectively. This is the Pearson correlation coefficient that shows the strength of the linear association of two parameters. This correlation is defined by the covariance of two parameters divided by the product of standard deviations of each parameter, as shown in Equation (4.2) and (4.3)[58].

$$r = \frac{cov(X, Y)}{\sigma_x \sigma_y} \tag{4.2}$$

Table 4.3: Variation of species concentration terms for variation of air fraction of primary zone

% change of fracPZ	fracPZ	ϕ_{PZ}	$[H]$	$[C_2H_2]$	$[OH]$	$[H]\,[C_2H_2]$
+15	0.2827	1.307	0.0882	0.897	0.305	0.079
+10	0.27	1.366	0.0869	1.052	0.299	0.091
+5	0.258	1.431	0.0834	1.241	0.292	0.104
0	0.246	1.503	0.0768	1.413	0.281	0.108
-5	0.234	1.582	0.0721	1.596	0.269	0.115
-10	0.221	1.67	0.0706	1.85	0.253	0.131
-15	0.209	1.768	0.0614	2.314	0.231	0.142

Table 4.4: Local sensitivity of species terms to air fraction of primary zone

% change of fracPZ	fracPZ	ϕ_{PZ}	$S_{[H]}$	$S_{[C_2H_2]}$	$S_{[OH]}$	$S_{[H][C_2H_2]}$
+10	0.27	1.366	0.623	-2.438	0.462	-2.254
+5	0.258	1.431	1.328	-2.552	0.636	-1.563
0	0.246	1.503	1.475	-2.512	0.823	-1.063
-5	0.234	1.582	0.797	-3.092	1.028	-2.049
-10	0.221	1.67	1.398	-5.081	1.336	-2.483

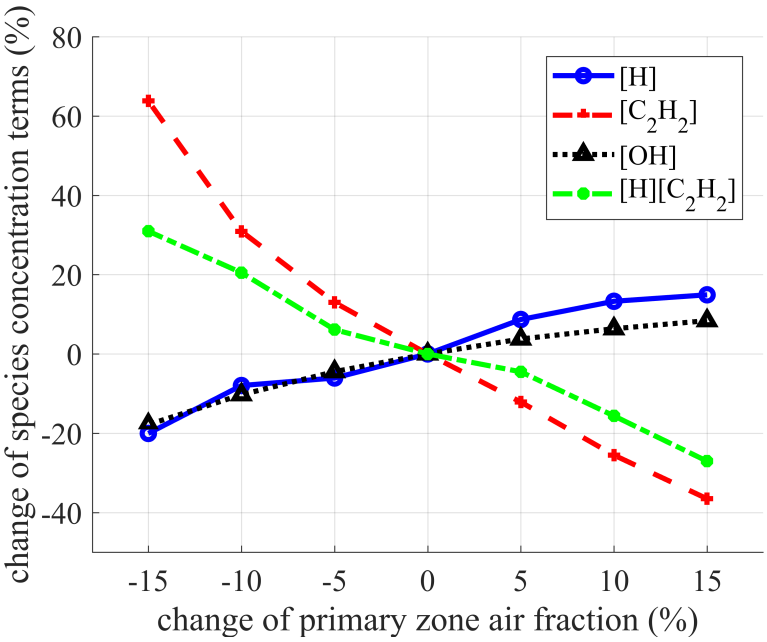

Figure 4.3: Variation of species concentration terms - air fraction

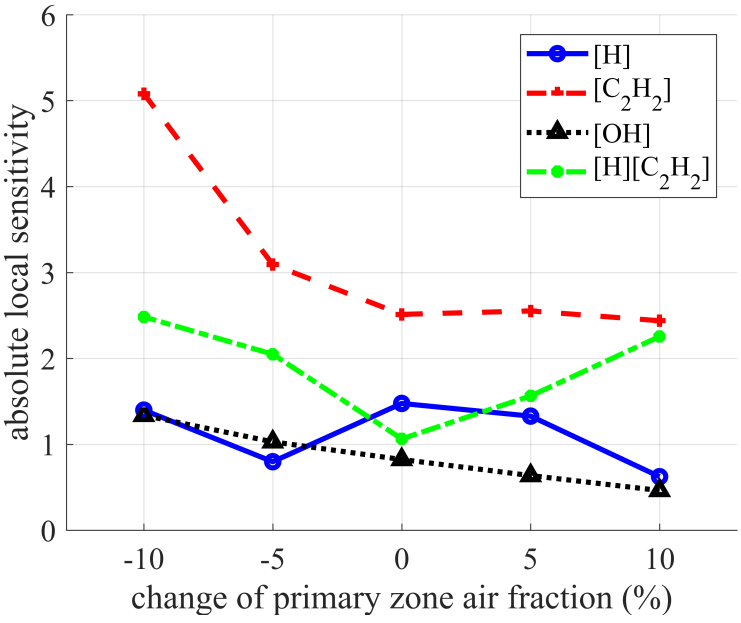

Figure 4.4: Local sensitivity of species - air fraction

or

$$r = \frac{\sum_{i=1}^{n}(x_i - \bar{x})(y_i - \bar{y})}{\sqrt{\sum_{i=1}^{n}(x_i - \bar{x})^2}\sqrt{\sum_{i=1}^{n}(y_i - \bar{y})^2}} \tag{4.3}$$

where r is the Pearson correlation coefficient of the sample groups X and Y, $cov(X, Y)$ is the covariance of X and Y, σ_x and σ_y are the standard deviations of X and Y, x_i and y_i are the i^{th} samples in the groups X and Y, and $\bar{x}$ and $\bar{y}$ are the mean of samples. The scale of this correlation is from zero to unity. The zero means no correlation between two parameters and the one means the perfect correlation. The positive sign means positive correlation and the negative sign means the negative correlation. The correlation values of all four terms are close to unity. This means that the air fraction is highly correlated with the terms directly related to soot formation and oxidation processes.

The same conclusion is derived from the sensitivities of these four terms to the air fraction. In this experiment, the sensitivity, S_i , is defined as the percent change of the i term divided by the percent change of the air fraction, as shown in Equation (4.4)

$$S_i = \frac{\%\ change\ of\ the\ term\ i}{\%\ change\ of\ fracPZ} \tag{4.4}$$

The local sensitivity that is calculated for $\pm 5\%$ range is listed in Table 4.4 and visually illustrated in Figure 4.4. With the definition in Equation (4.4), $S_i > 1$ implies that i term varies more than the variation of air fraction and $S_i < 1$ implies that i term varies less than the variation of air fraction. Note that the sensitivity less than unity does not mean that the term is not sensitive. It can be concluded that the term is not sensitive only when is the sensitivity close to zero. In this perspective, it can be concluded that all four terms highly affecting soot formation and oxidation are sensitive to air fraction as none of the local sensitivities are close to zero. The overall sensitivities of terms are 1.1653, -3.3436, 0.8738, and -1.9335 for $[C_2H_2]$, $[H]$, $[OH]$, and $[H]\,[C_2H_2]$ terms, respectively, and the absolute values are shown in Figure 4.4. It is easily observed that four evaluated terms

show high sensitivity at many experimental points. The overall sensitivities of them for the whole experimental range that is $\pm$ 15 % fracPZ are listed in Table 4.5 with Pearson correlation coefficients. This table also helps to derive the same conclusion.

Table 4.5: Pearson correlation coefficient and overall sensitivity

	Correlation with fracPZ	Overall sensitivity to fracPZ
$[H]$	0.9805	1.1653
$[C_2H_2]$	-0.9804	-3.3436
$[OH]$	0.9771	0.8738
$[H]\,[C_2H_2]$	-0.9919	-1.9335

This Table 4.5 and previously introduced tables and figures in this preliminary experiment are strong evidence showing that the air partitioning will highly affect soot prediction. Despite the importance of air partitioning in soot prediction, previous soot prediction methods achieved air partitioning by assuming it or by calibrating it for specific engine and power or from the engine- or power-specific data. From this observation, a hypothesis can be established as

Hypothesis I

Air partitioning in different combustion zones must be modeled
in order to predict soot in different cycles

By incorporating a model to calculate air partitioning adequately corresponding to the input cycle, more accurate prediction of soot for the operation at off-design cycle is expected. This conclusion of the necessity of calculation of air partitioning in soot prediction at off-design cycle is derived while the limit of current methods is investigated to answer the research question 4 and 5. If these two research questions are introduced again,

RQ4: How can a soot prediction model be applicable to different engines?

RQ5: How can a soot prediction model handle off-design operating cycles?

The hypothesis I is established while the research question 5 is addressed. As this hypothesis is limited to the application to off-design operation cycles, it cannot give an answer to the research question 4. However, similar reasoning is valid for the soot prediction for different engine cycles. In order for a soot prediction model to be applied to different engine cycles, adequate air partitioning and residence times for local combustion zones corresponding to the input cycle may need be calculated instead of achieving them by assuming them or by calibrating them or from real engine data. The necessity of calculation of air partitioning is already addressed by the hypothesis I. The next step will be the evaluation of the effect of residence time on soot emission.

The processes that involve in the mass of soot are inception, surface growth, and oxidization processes. This can be expressed as shown in Equation (4.5).

$$M_{soot} = \int \int \left(R_{inc} + R_{gr} - R_{ox}\right) dV dt \tag{4.5}$$

where M_{soot} is the mass of soot, R_i is the rate of the soot mass change in i process, V is the volume, t is the time, and the subscripts inc, gr, and ox are inception, surface growth, and oxidization processes, respectively. The processes that involve in the number of soot particles are inception and coagulation process. This relationship is expressed in Equation (4.6).

$$N_{soot} = \int \int \left(r_{inc} - r_{coag}\right) dV dt \tag{4.6}$$

where N_{soot} is the number of soot particles, r_i is the rate of the soot particle number change in i process, and the subscript $coag$ is the coagulation process. In both expressions, the volume and the time are directly involved in the mass and the number of particles of soot.

The volume V is the control volume where the combusting mixture stays and the time t is the residence time for which the flow stays in the control volume.

The overall time for which the flow stays in the local combustion zone is determined by the volume and the mass of the flow relationship. The mass of the flow is mainly determined by the air partitioning. Once the flow properties are given, the residence time is equivalent to the control volume, as already shown in Equation (3.17).

$$\tau_{res} = \frac{\rho V}{\dot{m}} \qquad \text{(3.17 revisited)}$$

The different engines often have different combustor volumes. The volume corresponding to the different engine cycle may need to be calculated in order for a soot prediction model to be applied to different engine cycles because there is a clear positive correlation between the volume and the residence time, as shown in Equation (3.17). Because the larger volume means more residence time for the given conditions, the more soot is expected for the larger volume if the conditions are favorable to the soot formation. However, there is one condition for this statement. This statement is true when the increased residence time does not affects other factors in the adverse way of soot formation. The same reasoning and condition similarly apply to the case of soot oxidization or the case of the decreased volume or residence time. To confirm the intuitive relationship of volume and soot, the second preliminary experiment is performed on the combustor volume and the four parameters investigated in the first experiment.

The basic experimental condition is the same as the first experiment. The current ASDL RQL combustor model developed for NOx prediction[57] is used. The cycle is the climb out operating cycle of PW6124A engine. The dependent parameters are four terms evaluated in the first experiment($[C_2H_2]$, $[H]$, $[OH]$, $[H]\,[C_2H_2]$). Although the temperature is also one of the factors that may be affected by the change of the volume and residence time, clear direction of its effect cannot be identified in the simple preliminary experiment

as it affects all four phases of soot evolution. For this reason, the four parameters are the only dependent variable to be investigated. The independent variable is the volume of the primary zone, denoted as V_{PZ} in this model. The size of the combustor may vary within a wide range for different engine cycles. $\pm 60\%$ range is varied from the primary zone volume of the combustor for PW6124A engine for this preliminary experiment although the actual variation can be wider than this range. This variation will lead to the variation in residence time and eventually change the species concentrations.

Table 4.6 and 4.7 and Figure 4.5 and 4.6 are the results of this experiment. The change of species concentration terms are listed in Table 4.6 and the percent change of terms are visualized in Figure 4.5. Three parameters, $[H]$, $[OH]$, and $[H][C_2H_2]$ show large variation with the variation of the primary zone volume. The variation of acetylene term is not clear when the volume changes to a larger size. However, this term shows non-negligible variation when the primary zone volume changes to the lower size. The direction of the volume effect is clear. The increased volume decreases both the growth rate and the oxidization rate. It seems the decrease in growth rate is a little more than the decrease in the oxidization rate. However, it cannot be concluded that the increase in volume adversely affects the soot formation with this result. For more evaluation, the local sensitivity of these terms are calculated, as shown in Table 4.7 and Figure 4.6. The overall sensitivities and the Pearson correlation coefficients are also listed in Table 4.8.

Table 4.6: Variation of species concentration terms for variation of volume of primary zone

% change of V_{PZ}	$[H]$	$[C_2H_2]$	$[OH]$	$[H]\,[C_2H_2]$
+15	0.0682	1.419	0.265	0.097
+10	0.0704	1.419	0.269	0.100
+5	0.0732	1.417	0.275	0.104
0	0.0768	1.413	0.281	0.108
-5	0.0818	1.403	0.291	0.115
-10	0.0894	1.383	0.304	0.124
-15	0.1024	1.342	0.325	0.137

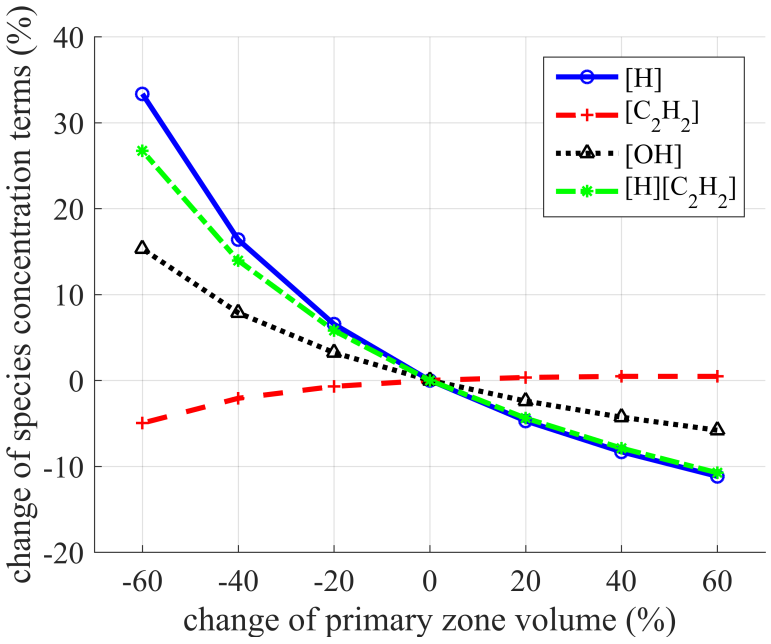

Figure 4.5: Variation of species concentration terms - volume

Table 4.7: Local sensitivity of species terms to volume of primary zone

% change of V_{PZ}	$S_{[H]}$	$S_{[C_2H_2]}$	$S_{[OH]}$	$S_{[H][C_2H_2]}$
+10	-0.161	0.003	-0.085	-0.159
+5	-0.208	0.012	-0.107	-0.197
0	-0.282	0.026	-0.141	-0.255
-5	-0.41	0.052	-0.196	-0.349
-10	-0.67	0.107	-0.302	-0.523

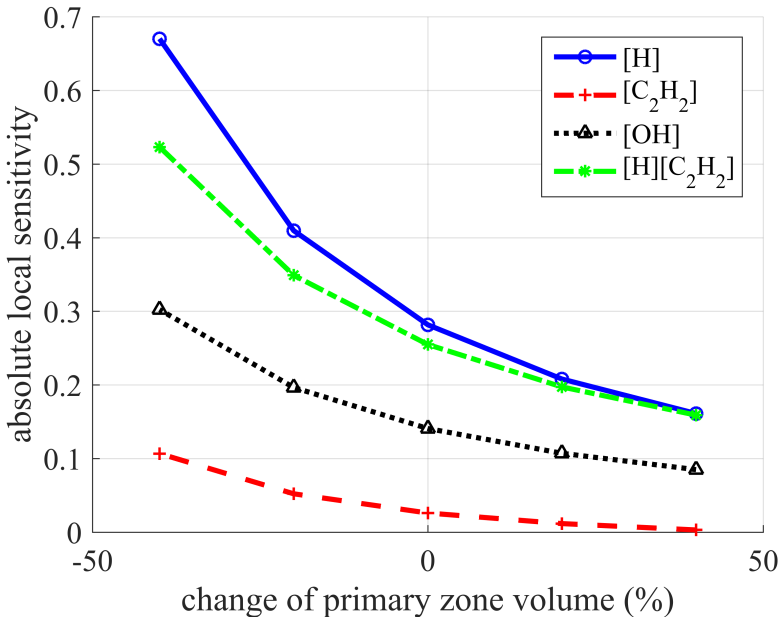

Figure 4.6: Local sensitivity of species - volume

Table 4.8: Pearson correlation coefficient and overall sensitivity - volume of primary zone

	Correlation with V_{PZ}	Overall sensitivity to V_{PZ}
$[H]$	-0.9500	-0.3710
$[C_2H_2]$	0.8643	0.0453
$[OH]$	-0.9603	-0.1760
$[H]\,[C_2H_2]$	-0.9648	-0.3123

In these results, all parameters show sensitivities lower than unity. In this case, the soot is more likely to be produced when the volume increases due to the increase in residence time. However, due to the non-negligible sensitivities of growth and oxidization related parameters and the clear direction of effects also shown in the correlations, the final effect of the volume change is not easily identified. To identify the effects on soot, the actual calculation on soot formation is required for a given volume. This means that the correct physics of the soot formation may be captured when the correct volume of the combustor is applied. From this conjecture, the second hypothesis can be established as:

Hypothesis II

In order for a soot prediction model to be applied to different engine cycles,
it must contain a sizing methodology.

In the first research question, four factors, fuel-air ratio, air partitioning, flow properties, and residence time, were mentioned to be important in soot prediction. The flow properties can be achieved from the calculation of chemistry. The air partitioning and residence time are addressed in the discussion resulting in the first and second hypotheses. The technical approaches to calculate these two factors will be suggested later in the process of validating hypotheses. Now, it is time to discuss the fuel-air ratio.

The local fuel-air ratio is the factor mentioned first among four factors highly affecting soot prediction. This factor is closely related to the soot formation as Colket's experiment[46] shows in Figure 4.1. The importance of air partitioning in soot prediction also comes from the importance of fuel-air ratio. For typical combustors injecting all fuel at the front, the fuel-air ratio of a local zone is determined with given air mass flow and the properties required to determine the soot formation rates are calculated from the chemistry calculation. The fuel-air ratios of the local combustion zones of fuel-staging combustors that have their own fuel schedule are also determined after the air partitioning is determined.

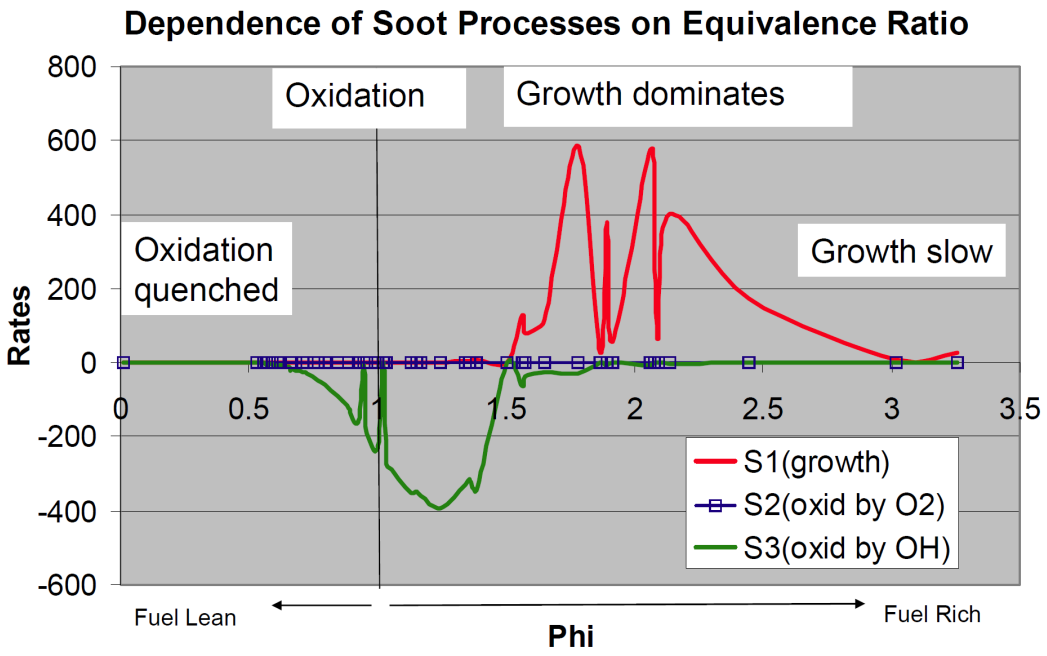

Dependence of soot processes on equivalence ratio[46] (repeated from Figure 4.1)

In addition to the fuel-air ratio of the local combustion zone, there is one more important phenomenon involving the fuel-air ratio affecting combustion characteristics. This is the burning of a non-uniform mixture of fuel and air flows. This is due to imperfect mixing after fuel is introduced into the combustor. Once the mixture is ignited, the mixture with various equivalence ratios as well as with the overall equivalence ratio is combusted and undesirable combustion characteristics, such as lower combustion efficiency or excessive NOx that can be theoretically achieved in the combustion of the mixture of given overall equivalence ratio, come out. For this reason, the combustion of non-uniform flow in the primary zone has been one of the major issues in the combustion study field.

In the early 70s, efforts to represent the non-uniform flow as a statistical distribution of fuel-air ratio were actively tried among scholars studying combustor design and NOx([59], [60], [61], [62], [63]). One of the major assumptions in these efforts is that the non-uniform flow consists of a large number of small eddies and that the equivalence ratios among these small eddies are showing Gaussian distribution around the overall equivalence ratio[63]. Sometimes, the mixture fraction instead of equivalence ratio is distributed in normal distri-

bution[61]. The mixture fraction is defined by the mass from the fuel divided by the mass of the total mixture. The value of this property is very close to the fuel-air ratio because the total mixture mass is the sum of the mass from the air and the mass from the fuel that is far smaller than the air mass. Since these efforts, representation of the non-uniform flow in the primary zone as the mass flow having a normal distribution of equivalence ratio becomes one of the typical assumptions and the concept of the mixing parameter, so-called unmixedness, is widely used. The unmixedness is defined by the standard deviation(σ) of the normal distribution of the equivalence ratio divided by the mean equivalence ratio($\bar{\phi}$) of the mixture[62], as shown in Equation (4.7), and its value has been typically determined by the measurement of the concentration of nitrogen oxide(NO) and oxygen(O_2) in the combustion product[63].

$$S = \frac{\sigma}{\bar{\phi}} \tag{4.7}$$

Many studies in the unmixedness have been conducted and these trials and efforts resulted in the unmixedness curve. Research results of unmixedness in various overall equivalence ratios were gathered together and one general curve was created from these data, as shown in Figure 4.8.

Even though the great improvement in the numerical simulation techniques has been achieved since the 1970s, the modeling approach of the primary zone with the assumption of a statistical distribution of equivalence ratio is still widely used because it efficiently represents the non-uniform flow characteristics. For this reason, many recent studies in the prediction of emissions utilized the concept of unmixedness rather than the detailed geometry and flow structure([30], [57], [36], [65], [66], [67]).

As the concept of unmixedness is still valid and widely used in emission studies, there is a research question for the soot prediction.

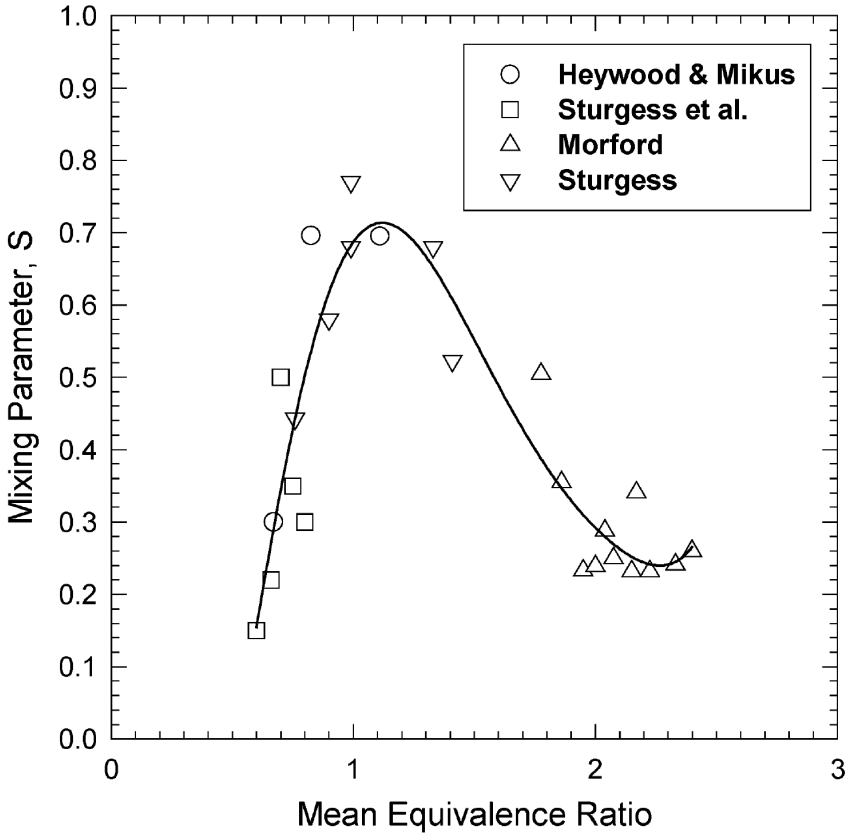

Figure 4.8: Unmixedness curve[64]

RQ6: Can the same statistical distribution in primary zone flow developed for NOx prediction be applied for the soot prediction?

The question is whether the same distribution is still valid for the soot prediction or not. To answer this question, further discussion on the statistical distribution of fuel-air ratio is required.

The statistical distribution used in the previous studies to represent the non-uniform flow characteristics was mainly applied to the NOx emission research. The major path producing NOx is the thermal mechanism. Although there are more NOx formation paths such as intermediate NO_2 mechanism and prompt mechanism, the contribution of the thermal mechanism to the total NOx formation is the most dominant. Because the high temperature is one of the most important factors activating the thermal mechanism, the equivalence ratio of the flow around the stoichiometric ratio is the most favorable condition for the

NOx formation. One of the reasons why the more NOx than the theoretical amount for the given overall equivalence ratio is produced in the lean or rich flow is that there exists the flow in the near-stoichiometric fuel-air ratio due to imperfect mixing of fuel and air mass. One of the basic ideas of the statistical distribution in the primary zone is to assign a specific amount of flow to the near-stoichiometric region so that the overall NOx formation predicted in the model matches the NOx produced in the real world.

However, when it comes to the soot emission, the rich fuel-air ratio region as well as near the stoichiometric region is important in soot formation mechanism. The results of Colket's simulation[46] implies that the soot is produced when the equivalence ratio is above 1.5 and oxidizes when the equivalence ratio is between 0.7 and 1.5. The fuel-air ratio region that is important in soot prediction is much wider than the region important in NOx prediction. For this reason, previous research that applied statistical distribution for the NOx prediction did not capture the region important in soot prediction. For example, the range of the statistical distribution implemented in the ASDL RQL model[57] is zero to twice the overall equivalence ratio of the primary zone. In this case, the equivalence ratio range cannot capture the region important in soot inception and growth for low power condition. The model developed by Rizk et al.[66] did not capture the far rich region and Sturgess[68] also did not pay attention on this region. The reason why these studies did not include far-rich region is that the mass flow that needs to be assigned to the far rich region is very small as this region is the tail of the normal distribution and that the contribution from this region to the NOx formation is almost negligible.

Based on these observations and discussion, it can be concluded that the model may not capture the physics required for soot prediction if the statistical distribution developed for the NOx prediction is applied. To evaluate this conjecture, two preliminary experiments are conducted.

The statistical distributions used by many NOx prediction models were developed for the NOx prediction purpose. The range of these distributions may be wide enough to

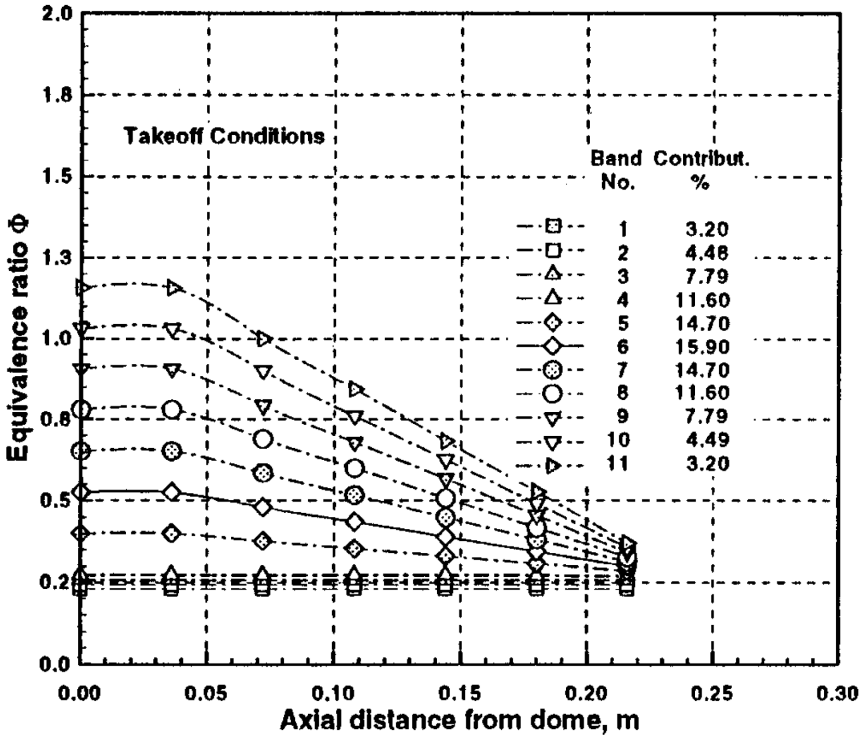

Figure 4.9: Statistical distribution of equivalence ratio (Rizk et al.[66])

capture NOx physics, but the range required for soot prediction may not be successfully accounted for. Therefore, the first experiment is about the range of the distribution. The model and cycle used in the first two preliminary experiments are also used in this experiment. The range of the current statistical distribution embedded in ASDL NOx prediction model of RQL combustor[57] is the independent variable. The dependent variables are also the four parameters($[C_2H_2]$, $[H]$, $[OH]$, $[H]$ $[C_2H_2]$). In this experiment, the approach cycle of PW6124A engine is used instead of other operating cycles. The range of the statistical distribution embedded in this combustor model is from zero to twice the mean equivalence ratio(0 - 2ϕ). Because the equivalence ratio of the primary zone at the approach cycle calculated by this model is 0.927, the range of the distribution becomes from zero to 1.854. The result of Colket's simulation[46] implies that the formation of soot occurs mainly in the equivalence ratio range between 1.5 and 3.0. The difference between the case accounting for this range and the case not accounting for it will be clear when the sensitivity study

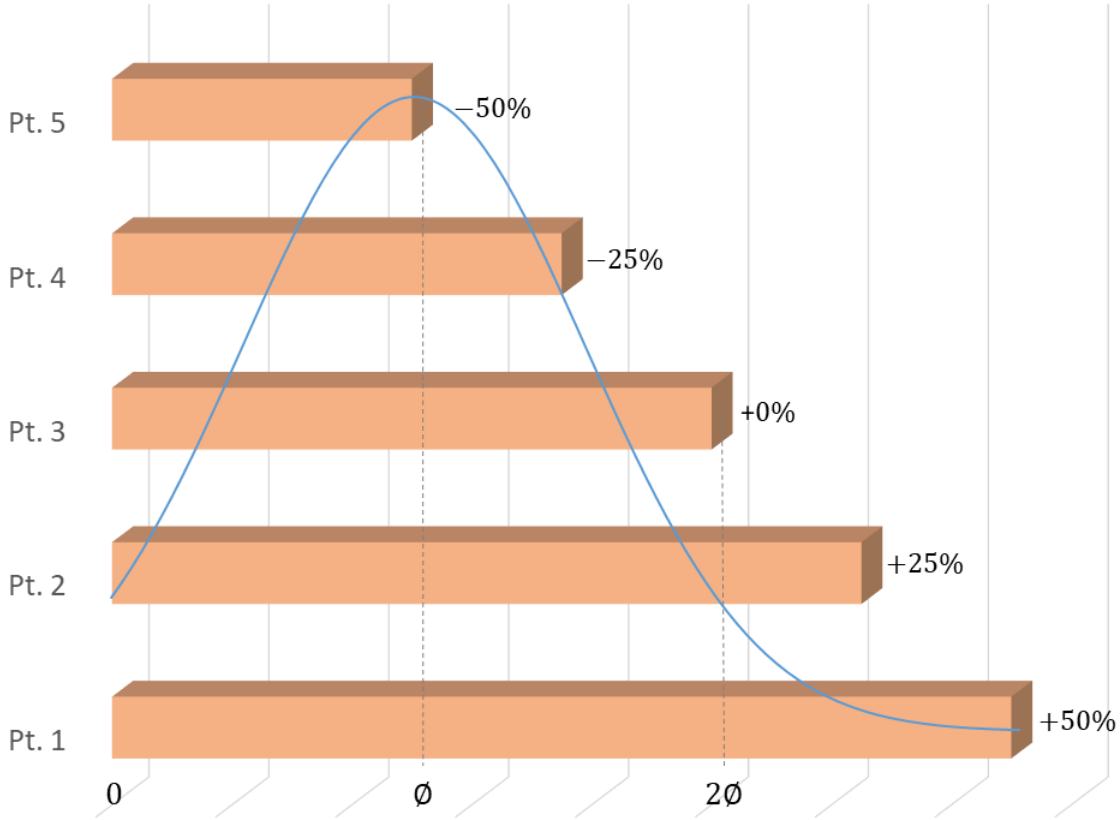

Figure 4.10: Different ranges of normal distribution

is performed for the range at the approach cycle because its upper limit(1.854) is close to 1.5. For this reason, the approach cycle is selected as an input cycle of this experiment.

The independent variable, that is range, is varied by $\pm 50\%$ from the original value. Five experimental points are illustrated in Figure 4.10. The results of this experiment is in Table 4.9, 4.10, and 4.11, and visualized in Figure 4.11 and 4.12.

The results agree with the expectation. As the more rich range is included, the parameters related to the soot inception and growth also noticeably increase. The local and overall sensitivities of these two parameters are high and sensitivities of other parameters are also not negligible. These results are enough to make a conclusion that the range of the statistical distribution generated for the NOx emission cannot fully capture the physics of soot formation.

This conclusion leads to another research question.

Table 4.9: Variation of species concentration parameters for variation of distribution range

% change of range	$[H]$	$[C_2H_2]$	$[OH]$	$[H]\,[C_2H_2]$
+50	0.0693	0.216	0.152	0.01499
+25	0.0723	0.196	0.158	0.01416
0	0.0728	0.081	0.168	0.00592
-25	0.0677	0.004	0.207	0.00028
-50	0.014	0.002	0.173	0.00003

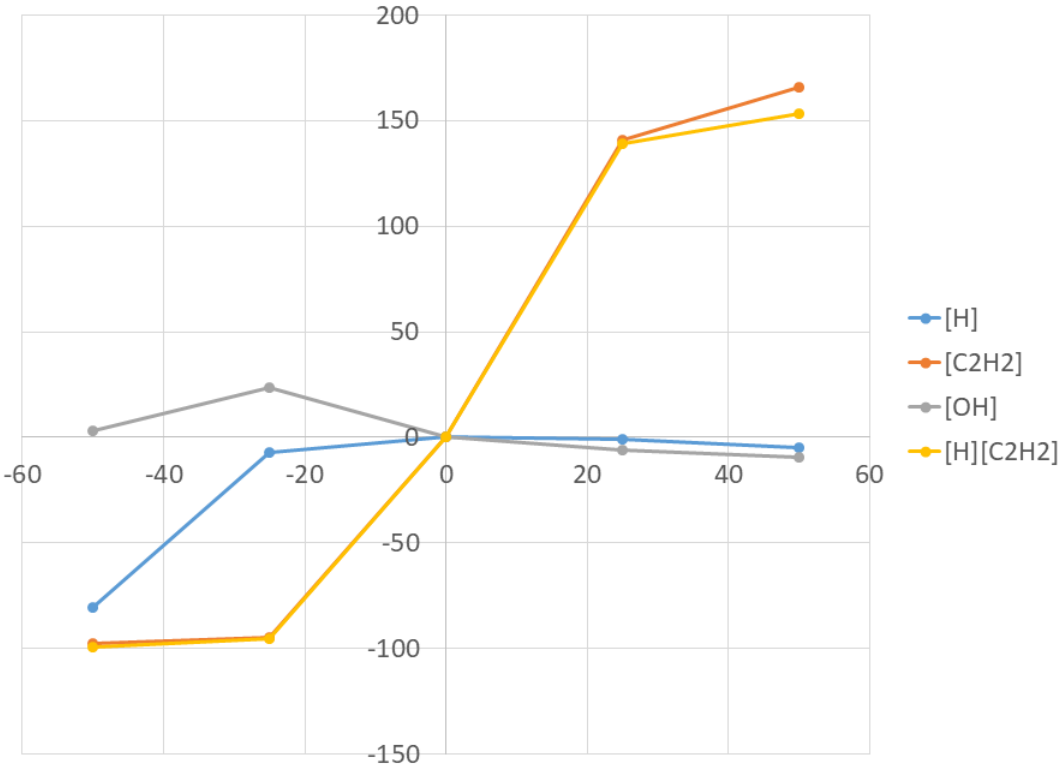

Figure 4.11: Variation of species concentration parmeters - range of distribution

Table 4.10: Local sensitivity of species terms to distribution range

% change of range	$S_{[H]}$	$S_{[C_2H_2]}$	$S_{[OH]}$	$S_{[H][C_2H_2]}$
+25	-0.095	3.313	-0.192	3.062
0	0.124	4.717	-0.587	4.689
-25	1.616	1.953	-0.059	1.991

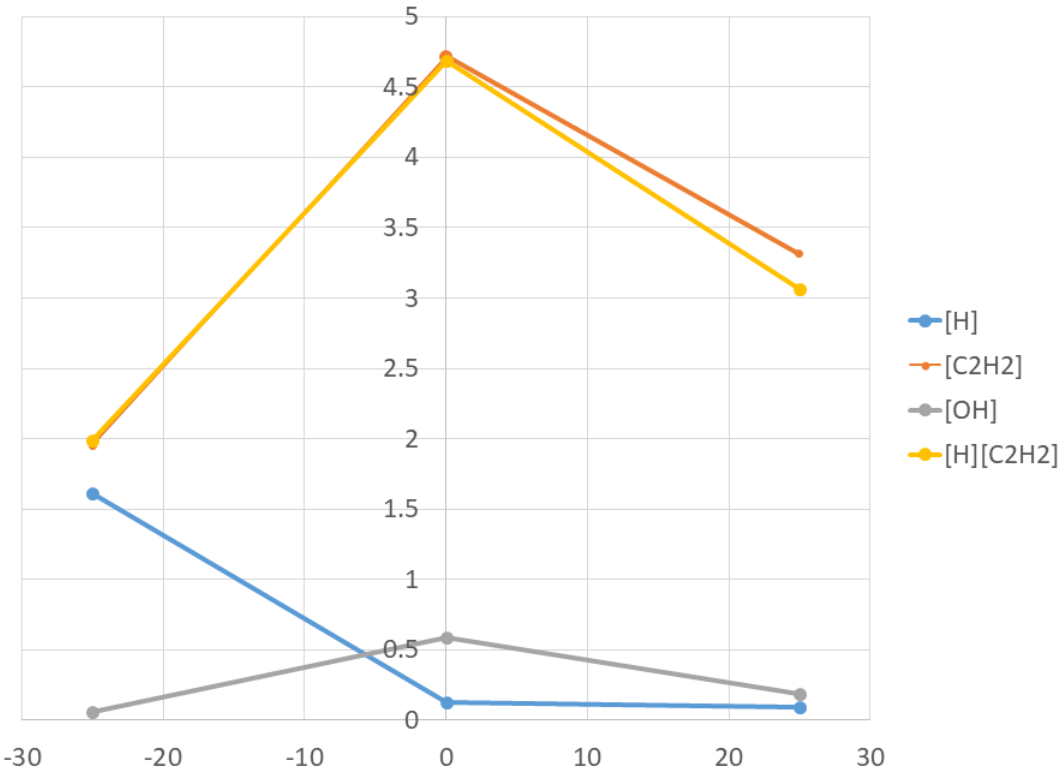

Figure 4.12: Local sensitivity of species - range of distribution

Table 4.11: Pearson correlation coefficient and overall sensitivity - range of distribution

	Correlation with distribution range	Overall sensitivity to distribution range
$[H]$	0.7180	0.7608
$[C_2H_2]$	0.9587	2.6326
$[OH]$	-0.6682	-0.1255
$[H]\,[C_2H_2]$	0.9558	2.5262

RQ7: Can the statistical distribution of fuel-air ratio representing a non-uniform mixture of fuel and air be applied to the soot prediction if the range of the distribution adequately covers the space important for soot prediction?

Another factor that may affect the soot prediction is the way of discretization of fuel-air ratio and mass of flow, or the shape of the distribution. Pompey and Heywood determined the unmixedness of the mixture by from the measurement of NO and O_2 species concentrations in the mixture[63]. This example infers that the shape of distribution used in the NOx study focuses mainly on the NOx concentration and other properties are not much considered. Therefore, the answer to the research question may be "*no*."

To get more hint about this issue, another preliminary experiment is performed. Because applying different distribution to the current model is not an easy task, the unmixedness parameter is varied to modify the shape of distribution while the type of the distribution still remains Gaussian. The unmixedness is varied by $\pm 90\%$ from the original value at the first experimental point of the previous experiment whose range was increased by 50%. By performing an experiment in the range covering the rich region where soot formation occurs, the effect of different shape can be more accurately evaluated. All experimental conditions are the same as the previous experiment except for the independent variable, unmixedness(S). The same model is used and the cycle is the approach mode of PW6124A

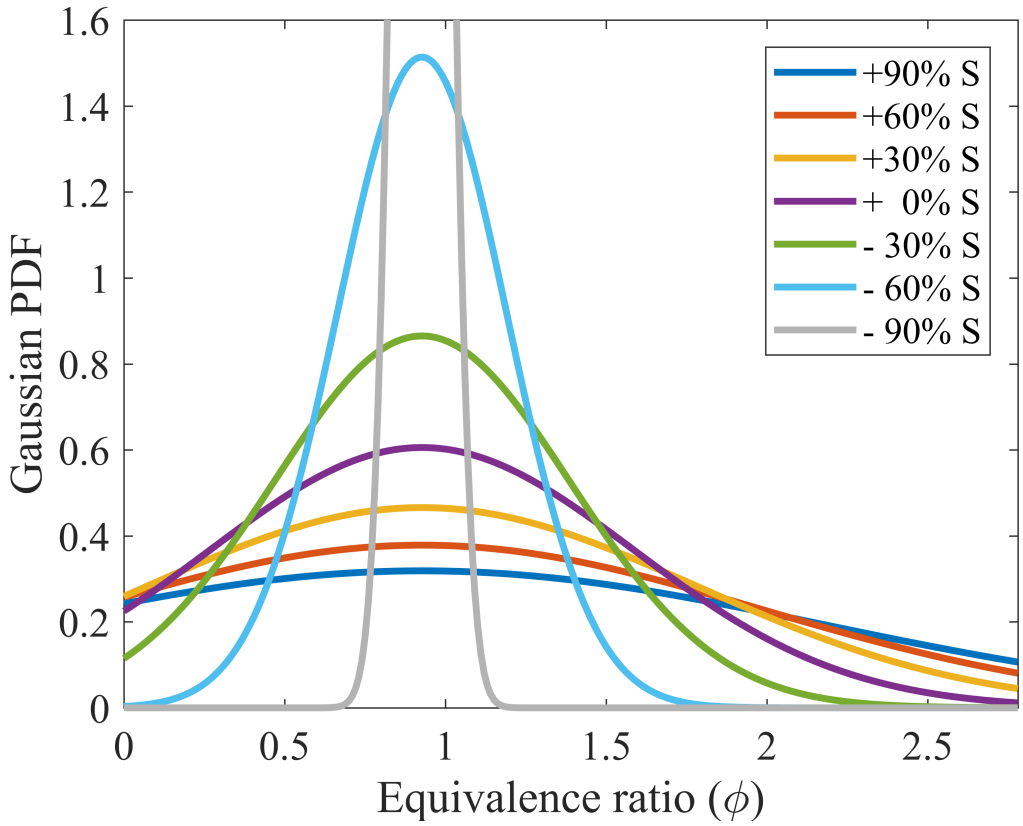

Figure 4.13: Normal distribution curves of different unmixedness

engine. The shape of the distribution corresponding to different unmixedness is illustrated in Figure 4.13. It is shown that the distribution spreads over the wide range as unmixedness increases. If the unmixedness increases even more than the specified limit, the distribution will be closer to the uniform distribution. It is also observed that the distribution makes a peak around the mean equivalence ratio when the unmixedness is low because zero of unmixedness means uniform mixture.

As the unmixedness of the distribution increases, more mass is assigned to the equivalence ratio far from the mean value. This means that there is less mass near the mean equivalence ratio and more mass is in the far lean and rich equivalence ratio. Therefore, positive correlation between the unmixedness and the number of species related to the formation process of soot is expected while the amount of species related to the oxidation is expected to have a negative correlation with the unmixedness. The results in Table 4.12, 4.13, and

4.14, and Figure 4.14 and 4.15 show agreement with the expectation. The local and overall sensitivities of soot to the formation-related parameters are positive while the one to the oxidization-related parameter is negative. Although the hydrogen concentration that is related to the growth of soot shows a negative correlation, this result does not have meaningful interpretation because soot sensitivity to this parameter is very low. These positive and negative correlations and sensitivities relationships are clearly demonstrated in Figure 4.14 and 4.15.

Table 4.12: Variation of species concentration parameters for variation of unmixedness

% change of unmixedness	[H]	[C2H2]	[OH]	[H][C2H2]
+90	0.0603	0.506	0.115	0.0305
+60	0.0624	0.439	0.122	0.0274
+30	0.0654	0.344	0.133	0.0225
0	0.0693	0.216	0.152	0.0150
-30	0.0729	0.082	0.183	0.00601
-60	0.0691	0.009	0.237	0.000598
-90	0.0607	0.002	0.273	0.000119

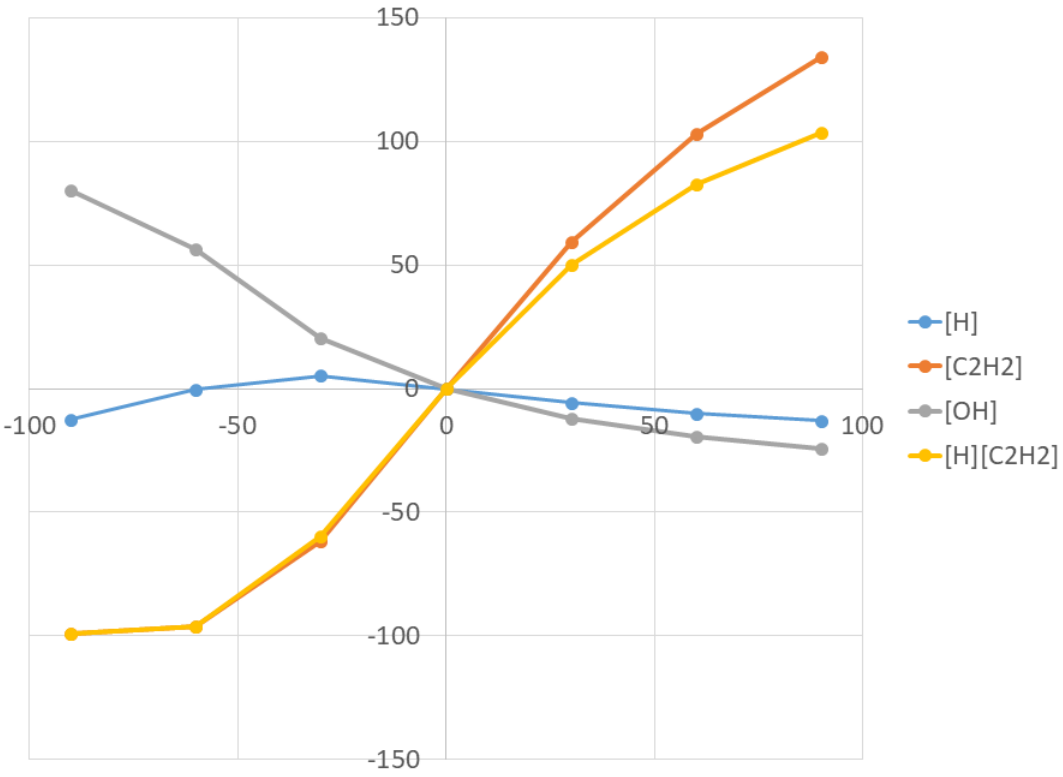

Figure 4.14: Variation of species concentration parameters - unmixedness

Table 4.13: Local sensitivity of species parameters to unmixedness

% change of unmixedness	$S_{[H]}$	$S_{[C_2H_2]}$	$S_{[OH]}$	$S_{[H][C_2H_2]}$
+60	-0.123	1.248	-0.203	0.890
+30	-0.168	1.719	-0.327	1.379
0	-0.182	2.015	-0.543	1.830
-30	0.007	1.600	-0.936	1.600
-60	0.293	0.621	-0.993	0.656

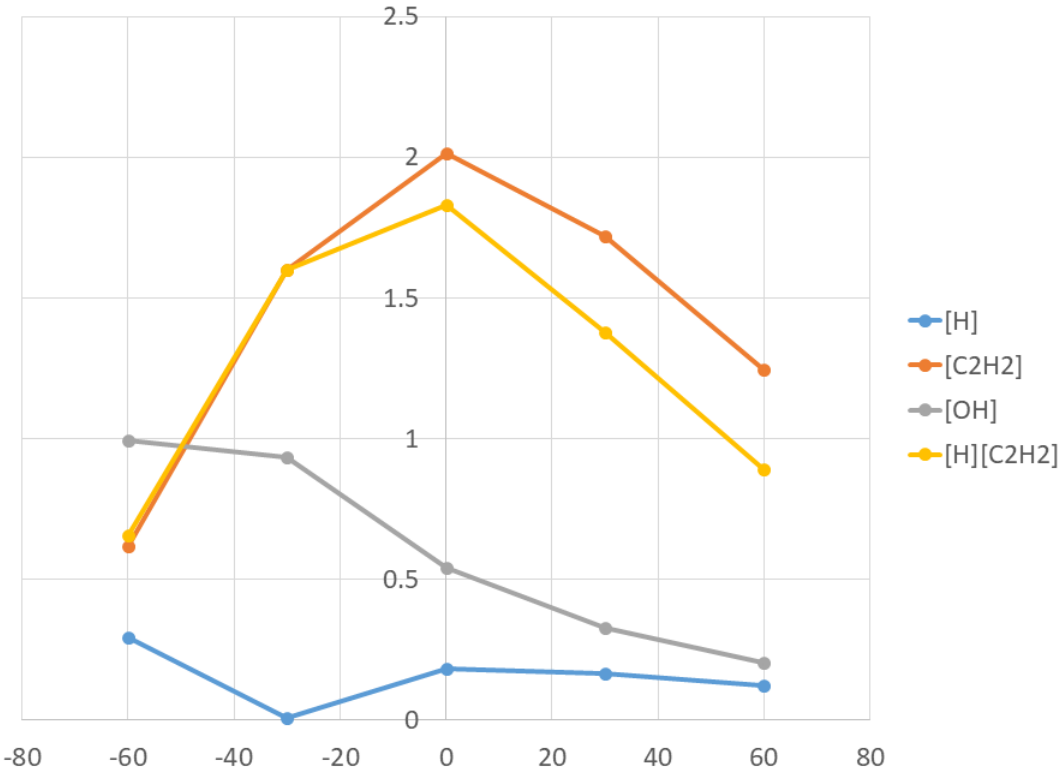

Figure 4.15: Local sensitivity of species - unmixedness

Table 4.14: Pearson correlation coefficient and overall sensitivity - unmixedness

	Correlation with unmixedness	Overall sensitivity to unmixedness
H	-0.3549	-0.004
C2H2	0.9843	1.2946
OH	-0.9563	-0.5798
H C2H2	0.9841	1.1253

The results of this experiment show a huge variation in the species parameters for the variation of the shape of the distribution. Therefore, it can be concluded that the way of distributing the mass of mixture in the wide range of fuel-air ratio space enough to capture the physics of the soot formation process may be important in soot prediction. To be more general,

Hypothesis III

Applying a statistical distribution of non-uniform flow to regions where soot phenomena are thermo-chemically active will improve predictive capability.

4.2 Summary of Hypotheses

From the research question asking what the important factors in soot prediction are, three hypotheses are derived after several preliminary experiments. They are

1. Incorporating air partitioning in combustor model during conceptual design improves soot prediction in different operating cycles,
2. In order for a soot prediction model to be applied to different engine cycles, it must contain a sizing rule,
3. Applying a statistical distribution of non-uniform flow to regions where soot phenomena are thermo-chemically active will improve the predictive capability.

The first hypothesis address the necessity of the calculation of air partitioning for soot prediction in off-design operating condition. Now that one of the research objectives is to create a parametric environment for soot prediction applicable to different engine cycles, the off-design operating conditions in the first hypothesis is not limited to the off-design conditions of a specific engine, but also include all engine cycles that do not provide calibration point during environment development. However, because the correct sizing of

engine volume is another factor required for the prediction of soot in different engine cycles, the sizing rule is addressed by the second hypothesis. Therefore, it can be said from these two hypotheses that the model can predict soot emission when the air partitioning and sizing rule are incorporated in the combustor model.

The third hypothesis addresses one of the important approaches representing a non-uniform mixture of fuel and air in the primary zone. By applying a statistical distribution, calculation of flow properties at the region where complex turbulent flow and drastic chemical reactions occur can be simplified. However, because current statistical distributions focus on the characteristics of NOx emission, the third hypothesis addresses the necessity of the statistical distribution for soot prediction.

These three hypotheses provide a direction that the parametric soot prediction model should follow. Based on these hypotheses, technical approaches to build a model will be addressed in the next chapter and the experiments to validate hypotheses will be addressed in the following chapter.

CHAPTER 5
TECHNICAL APPROACH

In this chapter, the overall approach and model structure as well as a detailed strategy of each subcomponent modeling are discussed. The goal of these approaches is to achieve the research objective that is to create a parametric soot prediction environment applicable to different engines during the conceptual design of the aircraft gas turbine engine. Three hypotheses established in the previous chapter provides directions to overcome the limits of current soot prediction methods. Based on these hypotheses, technical approaches to build a soot prediction model are suggested.

5.1 Overall Structure of Modeling and Simulation Environment

To establish an overall approach, it is required to remind the requirements of soot prediction method during conceptual design. There are three requirements in general, as discussed previously.

The soot prediction method should be

1. fast
2. parametric
3. able to predict soot with limited information

The execution time of the method should be short. Because the method is aimed at the conceptual design phase, lots of combinations of design alternatives will be evaluated. The method is not practical if the execution time is too long for this purpose.

The method also needs to be parametric. This means that the method can

- capture physics of input and output relationships
- explore wide design space
- handle different engine cycles

Because the conceptual design is a very early phase of the design process, detailed information of sub-components are not available. Therefore, the method for conceptual design must work despite the lack of information.

Many efforts to prediction soot emission are discussed in the literature search section. Approaches are mainly experiment, numerical simulation utilizing computational fluid dynamics techniques, and numerical simulation utilizing chemical reactor network. To determine the overall structure of the model, these methods will be evaluated again briefly based on the three requirements.

The experiment is preferred in many soot studies to discover the formation mechanism of soot for prediction. However, it does not satisfy all requirements. It is not fast. The experimental setup takes lots of time and budget. The experiment itself takes a long time, too. Therefore, it is not practical to explore large design space. Furthermore, it is not truly parametric. Small variation near the experimental condition may valid. However, a different experimental setup is required for an experiment of different combustors. The experiment is also not suitable when little information is available because the facility and device require lots of detailed information to replicate the real operating conditions.

To overcome these shortcomings of the experiment, correlations are often created based on the experimental results. Correlation provides results fast. It is parametric and requires very little information. However, these advantages are valid when there is an existing correlation. To create correlation expressions, lots of sample points are required from experiments. The shortcomings of the experiment apply again to correlation. If there is enough historical data, extra samples may not necessary. However, the combustor technology keeps improving as the new regulation targets future. The sample space is the only parametric re-

gion for correlation expression. The design space that the correlation can handle is limited to the sample space. To create new correlation expressions for future technology that are considered during conceptual design, additional experiments should be performed. New hardware needs to be developed, they need to be tested, and samples need to be generated. This process requires a long time and effort that is not acceptable for conceptual design. Furthermore, the correlation may work among a similar group of combustors. However, it may not work for the combustor that has different sizes and architectures. In this case, a new correlation for this type of combustor is required. In other words, the correlation expressions cannot be generalized. Therefore, correlation is not the method that is suitable for the research objective of this thesis work.

CFD is actively used in soot research as an efficient alternative of physical experiment. The time and cost required for CFD simulation are much lower than the ones for the physical experiment. However, CFD is still slow for soot prediction in the conceptual design phase. The simple simulation even takes at least several hours. As soot problems generally require the complex calculation of flow field and chemical reactions, the execution time is unacceptably long for conceptual design. In addition to the execution time, lots of detailed information on the geometry and boundary conditions are required to build a CFD environment. Due to this requirement, CFD simulation is also not truly parametric. It is not applicable to different engine cycles. The results may valid near the simulation conditions or for one engine cycle that is modeled. However, different engine cycle requires different CFD setup which takes another huge effort and time. Therefore, CFD simulation is not suitable for this thesis work.

The last option is the chemical reactor network(CRN). One of the strong advantages of CRN is its short execution time. CRN consists of lots of reactors and each reactor generally takes a few seconds even for very complex chemical mechanism. This is a huge reduction when it is compared to the CFD simulation or physical experiment. Another strong advantage is that the required information to build CRN is much less than CFD

simulation or physical information because CRN represents the approximated flow field with a network of idealized reactors.

Unfortunately, CRN approach does not satisfy the second requirement which is the parametric capability despite its two strong advantages. Examples are three groups that utilized CRN in soot prediction. Moniruzzaman and Yu[29] simulated the idle condition of CFM56-2C1 engine. Bisson's group[30] modeled CFM56-2C1 engine and simulated it for LTO cycles. Martini[28] modeled PW4090 engine and CFM56-2C engine. As already discussed in the previous chapter, their methods are not applicable to different engine cycles because their models are not capable of calculating air partitioning and sizing.

To overcome this shortcoming and add a parametric capability to CRN, Hypothesis I and Hypothesis II can be applied. The former addresses inclusion of air partitioning calculation and the later addresses inclusion of sizing rule. In addition to them, hypothesis III suggests the inclusion of statistical distribution specifically created for soot prediction to represent combustion of imperfectly mixed fuel and air mixture. With these three hypotheses, CRN is a great option to create parametric soot prediction environment suitable for conceptual design of aircraft gas turbine engine.

Based on these discussions, the overall structure and flow of the soot prediction with input and output properties of each sub-model are suggested in Figure 5.1.

The model starts from Combustor Model. This model includes two sub-components that are Combustor Flow Circuit model and Sizing Model. The Combustor Flow Circuit model is to compute air partitioning and the Sizing Model is to determine the size of geometry factors. More details of these two sub-component models are introduced later. Inputs of Combustor Model are cycle information.

Statistical Mixing Model takes some of the primary zone properties from Combustor Model as inputs. This model assigns mass, equivalence ratio, and volume determined by statistical distribution to parallel Perfectly Stirred Reactors(PSRs) in CRN representing combustion of the non-uniform mixture.

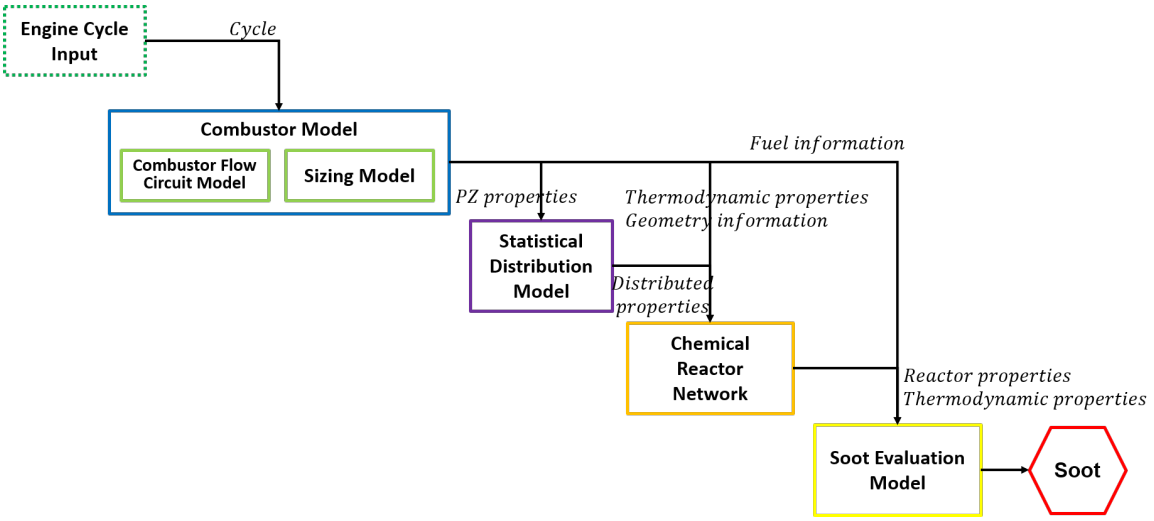

Figure 5.1: Model hierarchy

Chemical Reactor Networks (CRN) model mainly consists of PSRs and PFRs. In addition to them, there are non-reacting mixer and splitter components to construct a network of reactors. Thermodynamic properties and geometry information from Combustor Model and Statistical Distribution Model are used to define the reactor and flow properties. The thermodynamic properties of the flow and species information are computed and transferred to the Soot Evalueation Model.

Soot mainly consists of solid carbon and a little of other species such as hydrogen. Unlike NOx or CO, soot is not a chemical species. Therefore, soot is not a direct output from CRN. Thanks to many efforts on soot formation mechanism conducted for a long time, theoretical and empirical expressions of soot formation and oxidization rates have been created. They are mainly correlated to soot indicating species and oxidizers as well as gas temperature. A system of non-linear equations is formulated from these semi-empirical expressions of the soot formation process. The Soot Evaluation Model solves the formulated equation system for all reactors and time steps in CRN. Inputs of this model are thermodynamic properties of the flow and species concentrations. Outputs are soot mass and the number of soot particles. They will be out in the form of emission index.

The hierarchy of the overall environment with input and output flows are introduced in

this section. In the next following sections, technical strategy and theories to develop each sub-model element are introduced.

5.2 Combustor Flow Circuit Model

"Air Partitioning" is the design procedure of distributing air mass into discrete streams and delivering the appropriate amount to each part of the combustor for combustion and cooling. The stoichiometry of local combustor region is highly affected by air partitioning. This means that the temperature and reaction rate are also affected by air partitioning. The residence time is also affected because the amount of air in local combustion zones is determined by air partitioning. These properties affected by air partitioning are factors important in soot prediction, as already discussed in the previous chapter. Therefore, air partitioning is one of the key factors in soot prediction.

In this section, technical approaches to develop a combustor model incorporating air partitioning are introduced.

5.2.1 Modeling Approaches

A single or multiple components responsible for pressure losses are located in the pathways of flow streams in the combustor. Once the air enters the combustor, it is split into several streams. Split streams are split again at the hole and mixed at the liner. While the flow experiences loss of pressure during repeated slipt and mixing processes, it reaches station 4 as one stream. This process reminds a pipe network. When component responsible for pressure losses are replaced into equivalent pipes, a pipe network such as Figure 5.2 can be drawn.

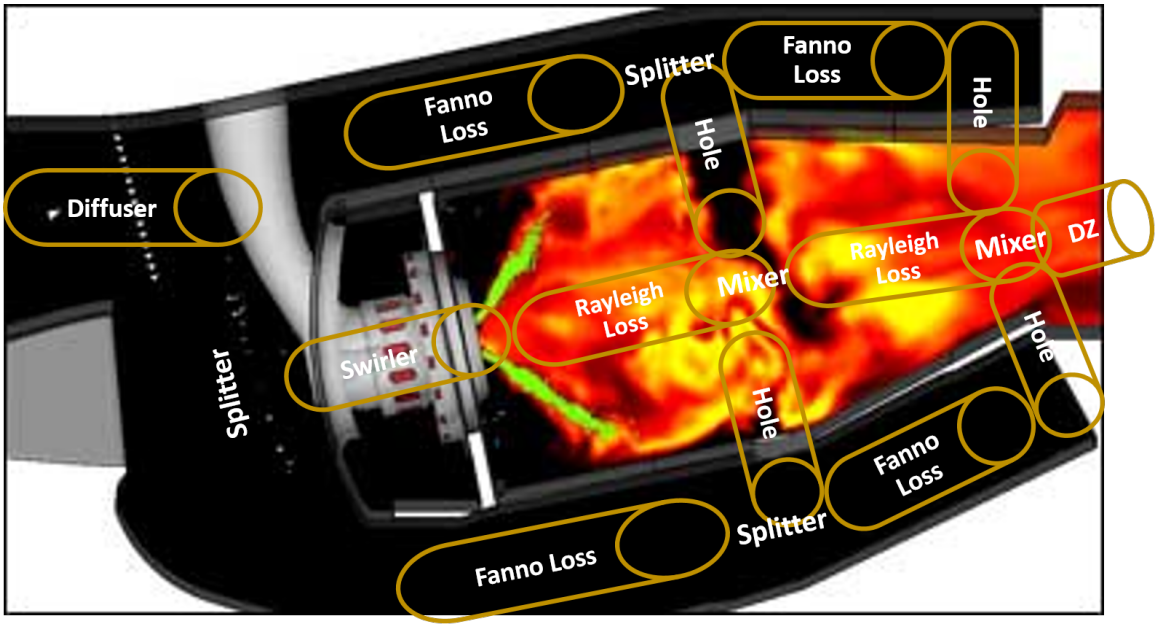

Figure 5.2: Concept of combustor flow circuit (figure editted from Referece [69])

This concept figure is for the typical single annular combustor(SAC). In this figure, diffuser, swirler, ducts, holes, and combustion zones are represented as pipes. To make it easier to see the flow streams, this system can be represented as a simple pipe diagram, as illustrated in Figure 5.3.

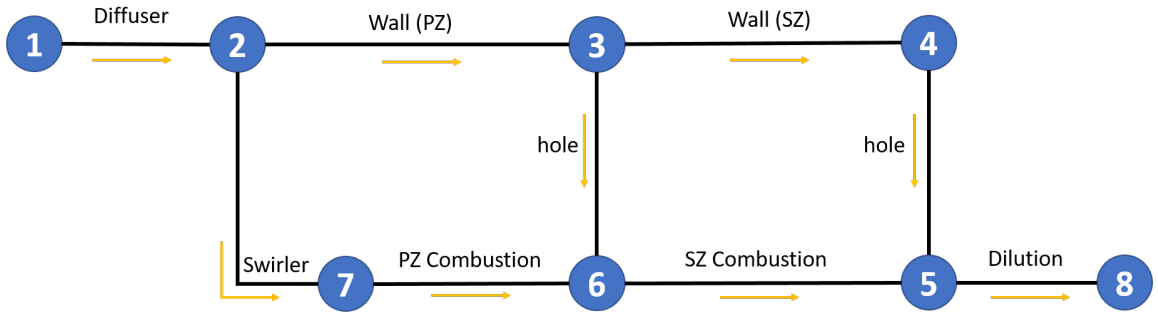

Figure 5.3: Pipe representation of combustor flow circuit

In this example of the SAC combustor system, there are three flow streams. They are 1-2-7-6-5-8, 1-2-3-6-5-8, and 1-2-3-4-5-8. The first path is the air flow enters the primary zone. The second stream is the air injected into the secondary zone through the

hole, the third stream directly injected into the dilution zone and this stream has almost no contribution to combustion. Although they all experience different pressure losses at a different component, they are mixed into one stream and reach the station 4 at the end. They start with flow properties of station 3 and ends their journey at the combustor with flow properties of station 4.

If we can figure out the amount of flow at each pipe, we can successfully achieve air partitioning. Generally, in the pipe network problem, head loss information can be achieved when the pipe geometry information is given. Darcy-Weisbach equation is one of examples(Equation (5.1)).

$$h_f = \frac{8fLQ^2}{g\pi^2 d^5} \tag{5.1}$$

In this equation, h_f is the head loss, f is the friction coefficient, L is the length of pipe, Q is the volumetric flow rate of the pipe, and d is the diameter of the pipe. Once these pipe information and inlet and outlet information are available, the amount of flow in each pipe can be calculated. Hardy Cross method is one of the famous methods for it.

In the Hardy Cross method, the volumetric flow rate of pipes is assumed first while keeping continuity. Then, head loss along the closed loop is calculated. In this example SAC system(Figure 5.4), loop 2-3-6-7 and loop 3-4-5-6 are closed loops to be evaluated. Whenever the head loss along the loops is calculated, volumetric flow rates are adjusted through iterations. This iteration is repeated until the head loss in closed loops makes zero balance.

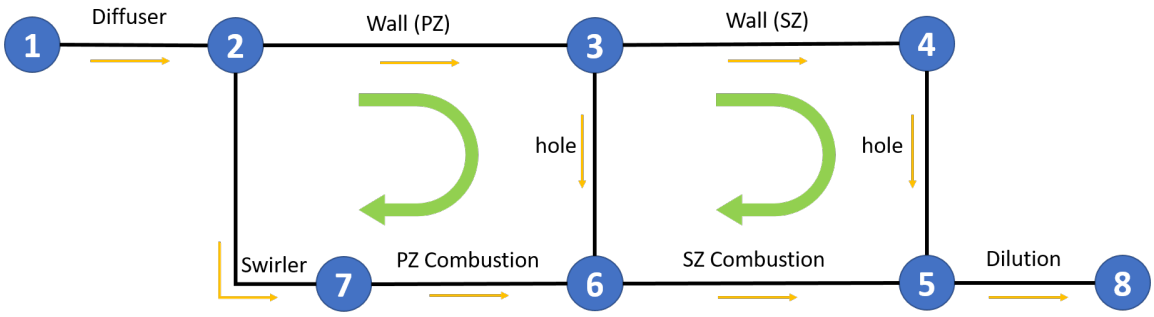

Figure 5.4: Closed loops of combustor flow circuit

At a glance, it seems that this method is applicable to the air partitioning of combustor flow. However, Hardy Cross method cannot be applied to the combustor problem for several reasons. This method is for the hydraulic system. Its base theory is based on the Bernoulli equation and its working fluid is incompressible. The amount of flow is represented as volumetric flow rate instead of mass flow rate because the density is constant. Because the flow speed inside the combustor is lower than Mach 0.3, compressibility effect of fluid is negligible. However, combustor flow experiences combustion. Flow properties including pressure, temperature, and density are significantly changed by chemical reactions. Bernoulli equation which has no energy source term is not applicable to the combustor flow circuit.

In addition, the flow properties of incoming streams are the same as the mixing point. However, the properties of two mixed streams can be different for combustor flow. In the example of Figure 5.4, node 5 and 6 are the mixing point. Flow from the 3 and 7 are mixed at node 6 and flow from 4 and 6 are mixed at node 5. If the static pressures of two mixed streams are same, other properties do not have to same. They are generally different in the most case because this process is the mixing of combustion product and fresh air. Therefore, the Hardy Cross method is not applicable to the combustor air partitioning problem.

Although the general pipe network problem is not applicable to combustor problem, there is still an advantage when the combustor air partitioning is considered as a circuit

flow consisting of components causing pressure losses. Pipe network gives us a hint to solve the combustor circuit flow problem. In the Hardy Cross method, a head loss can be calculated when the pipe information and flow rate are given. Similarly, pressure loss can be calculated when component information and mass flow rate are given.

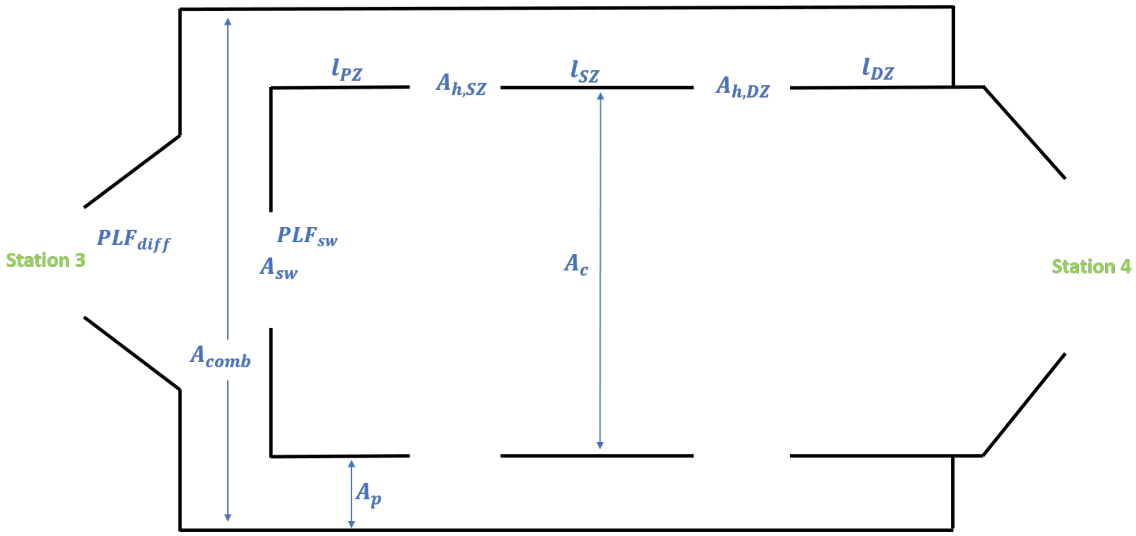

Figure 5.5: Schematic representation of combustor with some design variables

In this modeling, a simplified combustor illustrated in Figure 6.21 is used in order to minimize uncertainties coming from complexities accompanying with extra design variables. This simple structure is implemented in the Numerical Propulsion System Simulation (NPSS) version 1.6.4[70][71] environment. The thermodynamic package in NPSS is a great advantage because the flow properties are achieved from it very fast and easily. The overall flow diagram is in Figure 6.10.

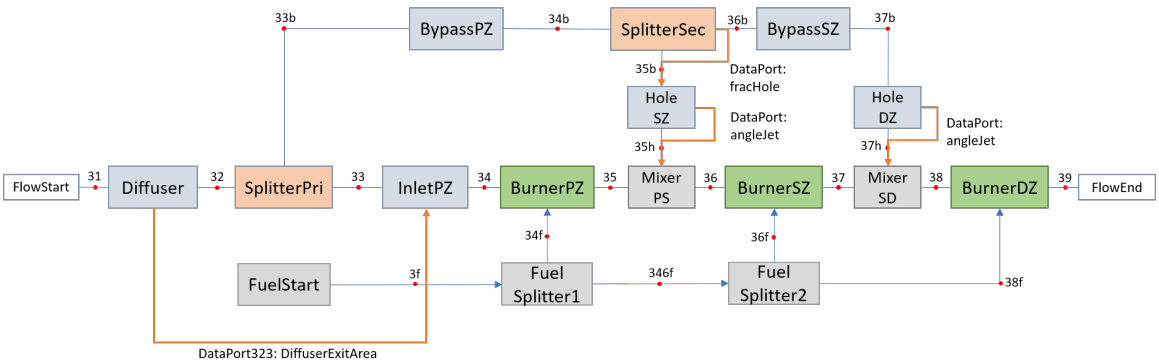

Figure 5.6: Diagram of Combustor Flow Circuit model

Once the cycle input is provided to the FlowStart element, the first pressure loss is calculated in the diffuser element. The first splitter, SplitterPri splits the core and bypass flow. The core flow enters the burners through InletPZ element. The bypass flow experiences Fanno loss at the BypassPZ element. This flow is splitted again at the SplitterSec element. One stream going to the HoleSZ element is mixed with the core stream at the MixerPS element. The mixed flow experience the second combustion and the secondary zone modeled with BurnerSZ element. The other stream experiences another Fanno loss at the BypassSZ element and goes to HoleDZ element. This stream is mixed with the core stream at the Mixer SD element. The flow finally enters the BurnerDZ element and one iteration is finished. Some parameters required for calculations but not included in the original NPSS elements are provided through DataPort. Fuels are provided to different burner elements via FuelSplitter elements. This is to model the combustion efficiency or the fuel consumption fraction in the different combustion zone.

5.2.2 Component Modeling

As the overall structure of the combustor model is introduced in the previous section, a more detailed modeling approach of individual components is introduced in this section. The user-defined sub-elements are used to model individual components. They are applied to the sockets in the original NPSS elements. These subelements have an internal solver in

many components for iterative calculations of losses. The whole system also utilizes the solver to compute air partitions. There are two independent variables and two dependent variables. The independent variables are bypass ratios in the splitter elements and the dependent variables are the static pressures in the mixers elements.

Diffuser

The axial flow velocity of the efflux from the compressor is very high especially when it is from the axial-flow compressors. This flow velocity may be higher than 170 m/s[34] or the order of 0.2-0.35 in Mach number[41]. This high velocity, however, is not desirable for the combustor stage for several reasons.

The first is that the pressure losses are significant for a high-speed flow. The pressure losses in the Rayleigh flow and the Fanno flow are a strong function of the incoming flow velocity. The high flow velocity after the compressor causes unacceptable cold and hot losses. For example, The pressure loss through the combustor is about a quarter of pressure raised from the compressor when the combustor inlet velocity is 170 m/s and the temperature ratio is 2.5[41].

Another reason is the combustion stability. The flow speed of the compressor efflux is usually much higher than the flame speed and this makes it extremely difficult to maintain the stable flame within the burner. For these reasons, a diffuser element is required to slow down the flow to the point where the total pressure loss is acceptable and the flame stability is manageable. The usual range of the diffused flow velocity is 0.05 to 0.1 in Mach number[41] or approximately one-fifth of the velocity at the compressor exit[34].

The diffuser has a simple geometry. It converts the velocity head to the static pressure head by increasing the cross-sectional area of the flow. The flow slows down due to the continuity when the area increases. This conversion process is not perfect and it accompanies with some amount of inevitable pressure losses. As the air flows along the wall, the skin friction causes friction loss and the boundary-layer separation causes the stall friction. While the pressure loss at the main burner contributes to the mixing process, the pressure

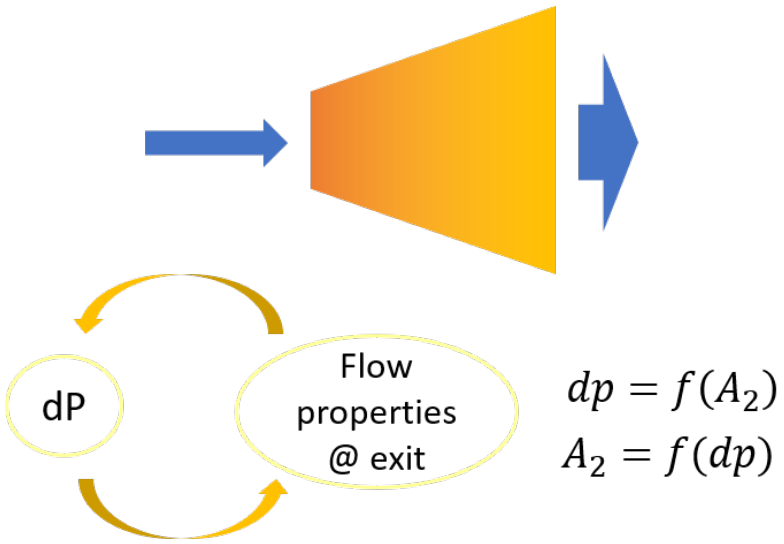

Figure 5.7: Diffuser element in Combustor Flow Circuit model

loss at the diffuser does not have merits and decreases the overall engine efficiency.

For this reason, it has been an important issue to measure, analyze, and predict the performance and losses at the diffuser. As a result of these efforts, there are lots of experimental data and research reports about the diffuser. Nevertheless, there is no general accurate method or chart to predict the performance of the diffuser at the combustor inlet. This is mainly due to the difference between the lab condition and the real gas turbine condition in terms of the velocity profile and the geometrical factors of the combustor. In the lab experiment or simulations, controlled inlet condition such as the symmetric uniform profile is often assumed. In the real world of the gas turbine, the efflux from the compressor has asymmetrical and peaked velocity profile with a swirl. Moreover, it varies with the operating conditions of the engine. Since the diffuser is a passage of the flow from the compressor to the combustor, the geometrical factors of the combustor also highly affect the performance of the diffuser. These factors include the size and shape of the combustor and its relative position to the diffuser. Because of these factors affecting the performance of the diffuser at the combustor inlet, it is very challenging to predict the pressure losses in the various operating conditions[34].

In the NPSS diffuser element, the pressure loss is calculated in the user-defined subele-

ment and applied via socket. The calculation of the pressure loss requires the exit area because the properties of the exit flow are involved in the calculation. When the Mach number of exit flow is specified by the user during the on-design phase, the pressure loss is required to calculate the exit area. Therefore, the diffuser element calculates the exit area via iteration.

Wiggert and Potter[72] introduced a diffuser efficiency, also known as pressure recovery factor, as

$$\mu = \frac{P_{t2} - P_{t1}}{P_{t2i} - P_{t1}} = \frac{q_1 - q_2 - \Delta P_t}{q_1 - q_2} \tag{5.2}$$

The subscript 1 is for the incoming flow and 2 is for the exit flow. The subscript is for the ideal property when there is no pressure loss. q is dynamic pressure. The pressure loss coefficient is

$$plc = 1 - \mu = \frac{q_2 - q_{2i} + \Delta P_t}{q_1 - q_{2i}} \tag{5.3}$$

Therefore, the pressure loss is

$$\Delta P_t = plc\,(q_1 - q_{2i}) + q_{2i} - q_2 \tag{5.4}$$

In this equation, q_{2i} is calculated in by the GasTbl, one of the thermodynamic packages in NPSS, without applying pressure loss. As q_2 and pressure loss are unknows, Secant solver is used to find pressure loss through iterations.

The pressure loss coefficient of components in the gas turbine engine is often defined as the ratio of the total pressure loss to the dynamic pressure of the incoming flow. In diffuser analyses, as the purpose of the diffuser is to slow down the flow and recover the static pressure, the pressure loss is often defined as the ratio of the static pressure loss to the dynamic pressure of the incoming flow.

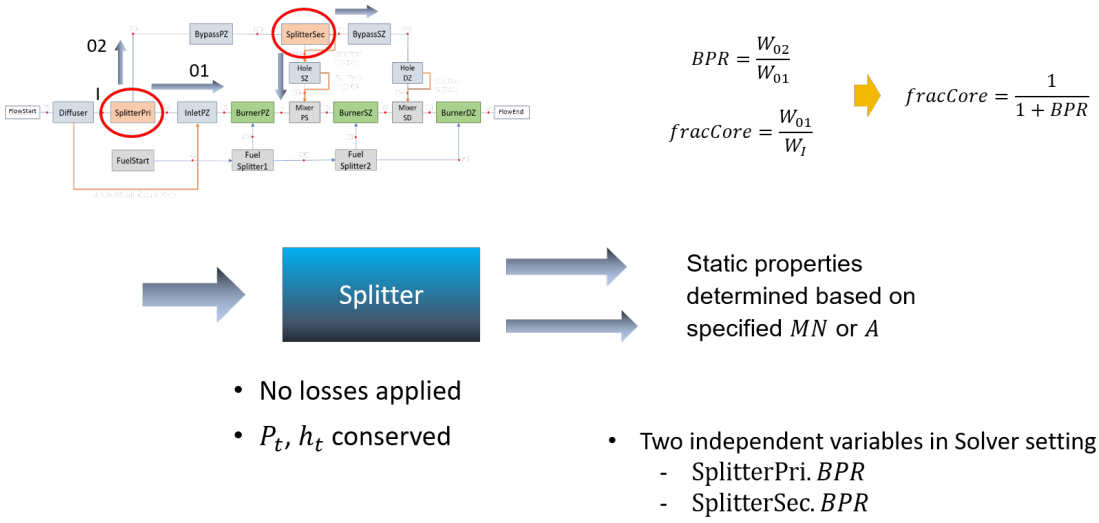

Figure 5.8: Splitter element in Combustor Flow Circuit model

All three definition of the pressure loss is tested in several test simulations. The results are almost identical regardless of the definition of the pressure loss coefficient. Therefore, the first definition is adopted in current modeling. During simulations, it is also observed that the pressure loss coefficient does not change for the off-design cycles. Therefore, the pressure loss coefficient is kept constant once it is determined for the on-design cycle.

Splitter

The splitter element divides the incoming flow into two streams, keeping the energy and the total pressure constant. The exit properties are calculated by the specified Mach numbers or the exit areas.

Because the NPSS is an engine simulation tool, the variable, BPR is used. The fraction of the core flow (fracCore) can be calculated as

$$\text{fracCore} = \frac{1}{1 + \text{BPR}} \tag{5.5}$$

There are two bypass ratio variables as the splitter element is deployed twice. The first splitter is in front of the swirler, splitting the exit flow from the diffuser into the core stream

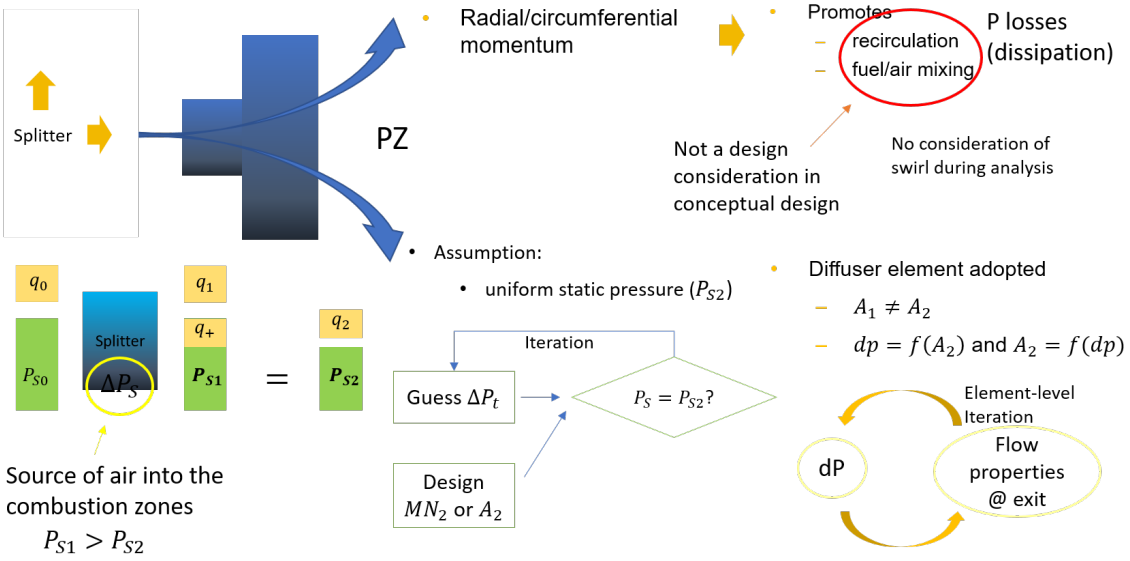

Figure 5.9: InletPZ element in Combustor Flow Circuit model

and the bypass stream. The second splitter is in front of the hole for the secondary air injection. The bypass ratio variables are the independent variables varied by the Solver during iterations in the current model.

InletPZ

The diffuser element is adapted for the InletPZ element because the calculation is similar to the diffuser pressure loss. First of all, the inlet and exit areas are different. The exit area is much larger than the inlet area. Second, the pressure loss is required for the calculation of the exit area while the exit area is required in the calculation of pressure loss. By adapting the diffuser calculation, the exit area and the pressure loss are calculated for the specified Mach number of the exit flow via iterations.

When the flow enters the swirler, some portion of the total pressure is converted into the dynamic pressure, accelerating the flow. The accelerated speed is dissipated when the flow enters the primary zone. During this process, the static pressure does not change. Therefore, keeping the static pressure constant, the pressure loss that satisfies the specified design Mach number of the exit flow and the static pressure condition is found via iterations. This calculation is performed by the user-defined subelement plugged in the socket.

Burner

Heat addition to the flow causes fundamental loss. As discussed in the background chapter, this loss is relatively small when the Mach number of the flow is low. In the previous simulation introduced with Figure 3.5 in the background chapter, the total pressure loss is less than 1% when the Mach number of incoming flow is 0.025.

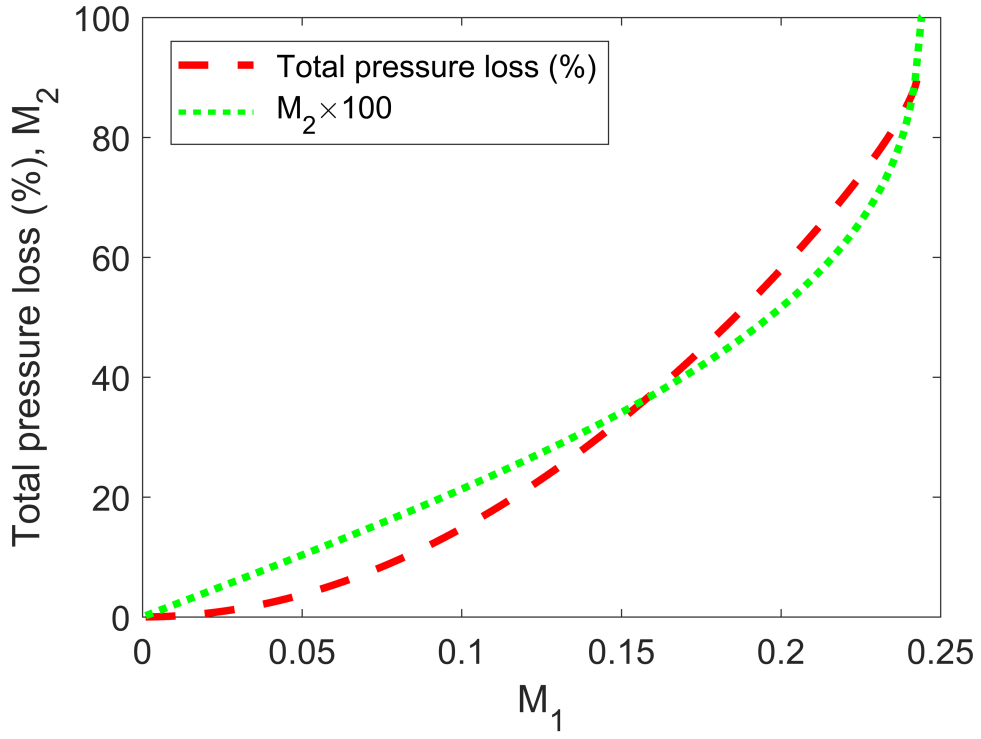

Hot loss and Mach number relationship (repeated from Figure 3.5)

The primary, secondary, and dilution zones are modeled with Burner element, denoted as BurnerPZ, BurnerSZ, and BurnerDZ. The burner element adds the lower heating value of the fuel, whose amount is specified by eps variable, to the flow. The enthalpy of the exit flow is calculated from the energy equation by the burn function. As the Rayleigh loss option is already embedded in the burner element, the pressure loss at the burner is calculated via this option.

The calculation starts by assuming the pressure loss. With calculated exit properties after assumed pressure loss is applied, the momentum equation is used to calculate the

static pressure of the exit flow. The calculated static pressure from the momentum equation is compared with the current static pressure of the exit flow calculated by GasTbl. This process is iteratively repeated until the static pressure is stabilized.

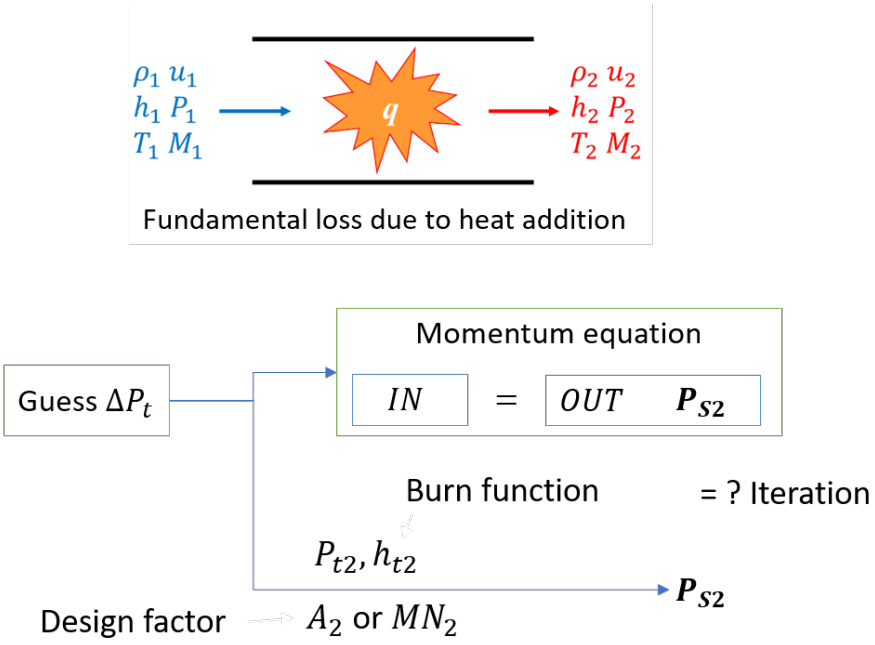

Figure 5.11: Burner element in Combustor Flow Circuit model

Bypass Duct

The bypass ducts (or outer annuli) are modeled with a diffuser element. Even though NPSS provides a duct element, it cannot handle the variable area duct. Because the momentum equation used in the calculation of the pressure loss requires the properties of the exit flow which are a function of the exit area, the diffuser element is appropriate for the modeling of bypass ducts.

The friction between the wall of the duct and flow also causes pressure loss. This is the Fanno flow. Because this loss is also a function of Mach number of the flow, its contribution is also relatively small. Therefore, a simple analysis is applied to duct flow.

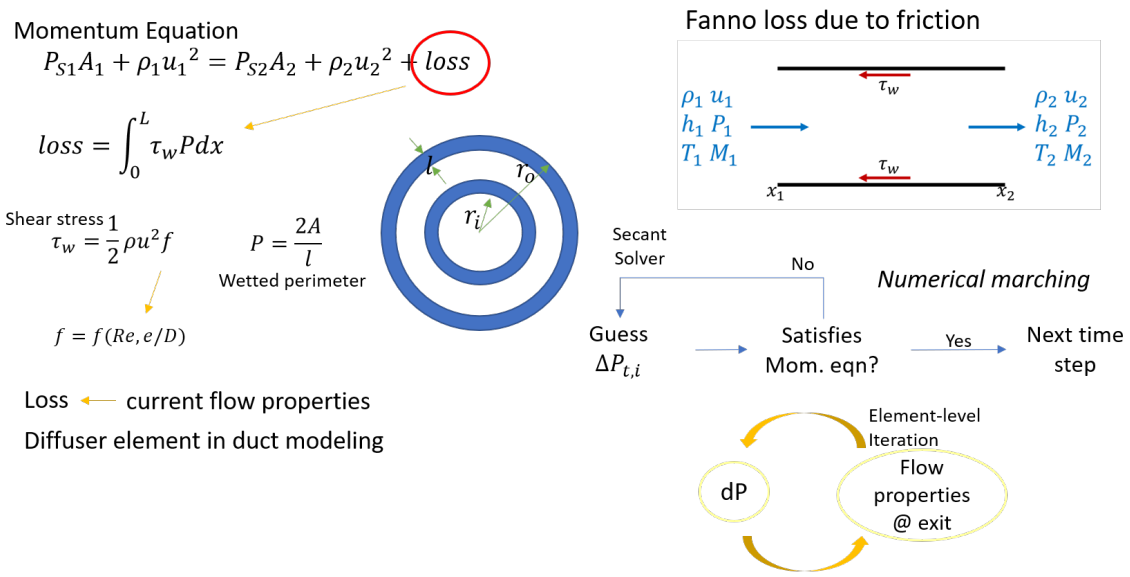

Figure 5.12: Bypass Duct element in Combustor Flow Circuit model

The shear stress(τ_w) and friction coefficient have a relationship of

$$\tau_w = \frac{1}{2}\rho u^2 \tag{5.6}$$

In general pipe system, there is a concept of hydraulic radius for the non-circular pipe. It is defined as

$$R = \frac{A}{P} \tag{5.7}$$

where A is the cross-sectional area and P is wetted perimeter[72]. The hydraulic diameter of the annulus is

$$R = \frac{l}{2} \tag{5.8}$$

where l is the width of the annulus. From Equation (5.7) and (5.8),

$$P = \frac{2A}{l} \tag{5.9}$$

The momentum equation can be established, as

$$P_{s1}A_1 = \rho_1 u_1^2 = P_{s2}A_2 + \rho_2 u_2^2 + loss \tag{5.10}$$

The loss term is

$$loss = \int_0^L \tau_w P dx \tag{5.11}$$

L is the length of the duct.

For a small step, $\Delta x_{i,i+1}$, the momentum equation in Equation (5.10) becomes

$$P_{si}A_i + \frac{\dot{m}_i u_i}{g_c} = P_{i+1}A_{i+1} + \frac{\dot{m}_{i+1} u_{i+1}}{g_c}$$
$$+\frac{1}{2}\left(\frac{\rho_i + \rho_{i+1}}{2}\right)\left(\frac{u_i + u_{i+1}}{2}\right)^2 f\left(2\left(\frac{A_i + A_{i+1}}{2}\right) / \, l \, / \, 12\right)\left(\Delta x_{i,i+1}/12\right)/g_c \tag{5.12}$$

The pressure loss is calculated in this momentum equation via iterations by Secant solver.

The width of the duct (l) and the friction coefficient are required in this calculation. In order to prepare the friction coefficient, the relative roughness and the Reynolds number are required. The Reynolds Number is calculated from the flow properties. A nominal value for the relative roughness is selected from the literature[72]. The width and the friction coefficients are fixed later because the soot result shows very little sensitivities to these parameters.

Hole

Figure 5.13 shows the flow pattern of the combustor.

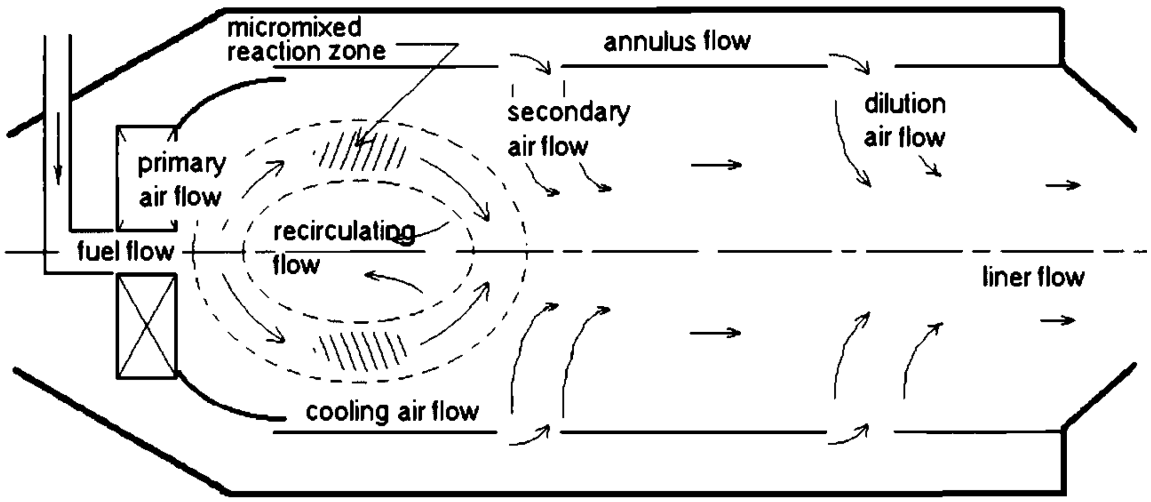

Figure 5.13: Flow pattern in combustor[50]

As shown in this figure, the flow enters the main burner through several holes in the wall. These air streams control the stoichiometry of the combustion zones to achieve expected performance goals such as stable combustion, high combustion efficiency, and low pollutant emissions. For this goal, the injected air should be mixed well with a hot product inside the burner liner. To achieve sufficient penetration and enhanced the mixing, the Mach number of the air streams through holes is of the order of 0.3[41]. This fast stream of air is one of the factors contributing to the total pressure loss because some of the pressure in the annulus air is converted to the dynamic pressure and eventually dissipated.

Because there is no NPSS element corresponding to the hole in the combustor, one of the simplest element, a duct is used and the calculation is implemented at the socket even though there is no press loss in the hole flow at this point. The pressure loss occurs at the mixer. The radial component of the momentum of the jet is dissipated while promoting the mixing between the secondary flow through the hole and the combustion product gas from the burner.

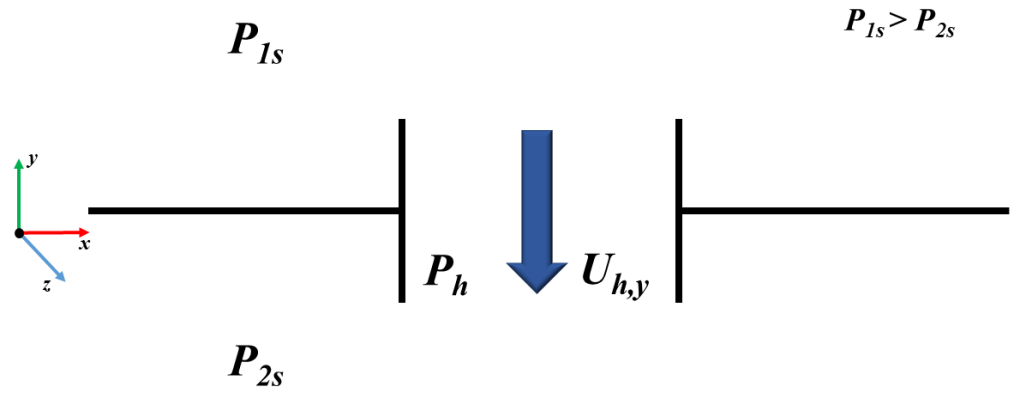

Figure 5.14: Transfer of mass through a hole

Figure 5.14 illustrates the mass transfer from the high-pressure state(state 1) to the low-pressure state(state 2) through a hole. In this figure, the static pressure of the state 1(P_{s1}) is higher than the static pressure of the state 2(P_{s2}). It is assumed that there is no velocity component in y-direction for both states except for the hole jet flow. When the flow whose Mach number is below 0.3, the compressibility effect is generally regarded as negligible. Therefore, the general relationships of incompressible flow such as Bernoulli Equation are valid in this case.

The difference between P_{s1} and P_{s2} is ΔP_s. Therefore,

$$P_{s1} = P_{s2} + \Delta P_s \tag{5.13}$$

This difference in pressure is the source of the mass transfer, or air injection from state 1 to state 2. The static pressure of the injected air stream at hole passage(P_h) is the same as the static pressure of the state 2.

$$P_h = P_{2s} \tag{5.14}$$

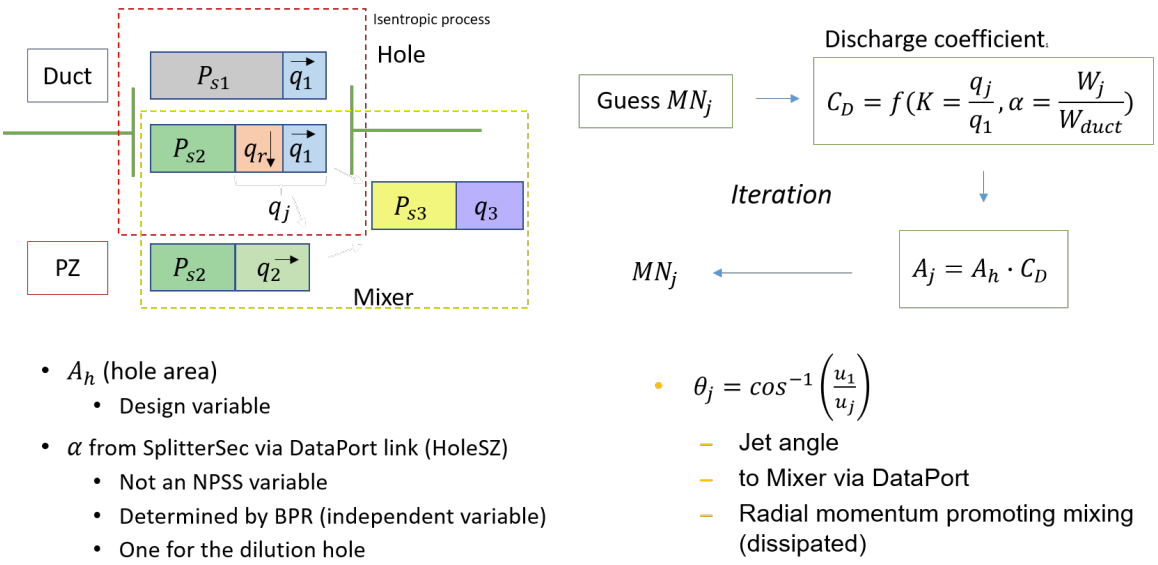

Figure 5.15: Hole element in Combustor Flow Circuit model

The calculation involves the Secant solver. Mach number of the jet flow is assumed. The assumed Mach number determines the jet flow properties because the total properties are conserved through the hole. The discharge coefficient is calculated in Equation (5.15)[34].

$$C_D = \frac{1.65\,(K-1)}{\left[4K^2 - K\,(2-\alpha)^2\right]^{0.5}} \tag{5.15}$$

where K is the ratio of the dynamic pressure of the jet to the dynamic pressure of the upstream and α is the ratio of the jet mass flow rate to the mass flow rate of the upstream flow.

With the calculated discharge coefficient, the cross-sectional area of the jet is

$$A_j = A_h \cdot C_D \tag{5.16}$$

where A_h is the actual hole area in the liner wall, which is an input parameter. The calculated jet area is compared to the jet area set by the assumed Mach number at the beginning. This process is repeated via iteration by the Secant solver until the jet area converges.

The axial momentum makes the jet injected with an inclined angle. The jet angle is

$$\theta = cos^{-1}(\frac{U_{h,x}}{U_j}) \tag{5.17}$$

The calculated jet angle is transferred to the mixer via DataPort.

Mixer

In the mixer, the core stream and the jet flow through the hole are mixed. Through the iterative calculations, the total pressure of the exit flow satisfying the momentum equation is achieved. The direction of the core flow is the same as the exiting flow while the jet flow is inclined with an angle. This angle is transported from the hole element via DataPort. The axial component of the momentum of the jet participates in the momentum equation while the radial component is dissipated.

The static pressures of two incoming flows are the dependent variables for the Solver. Because there are two mixers, there are two dependent variables in the combustor model. The NPSS Solver varies two BPRs in the splitter elements until the static pressures of the incoming flows in the mixer converge. The converged solution provides the air partitions of the primary, secondary, and dilution zones.

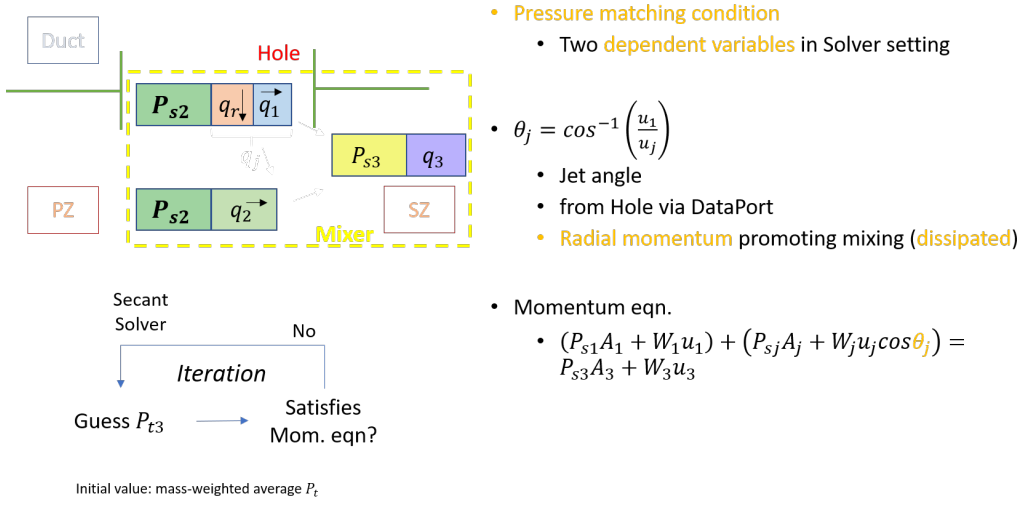

Figure 5.16: Mixer Duct element in Combustor Flow Circuit model

5.3 Combustion of Non-uniform Mixture

The Statistical Distribution model is to distribute mass into a range of fuel-air ratio. It is to represent non-uniform flow caused by imperfect mixing of fuel and air. This is one of the traditional methods modeling non-uniformly mixed fuel and air flows in the oxides of nitrogen studies (NOx). The thermal mechanism which highly contributes to the formation of NOx in the combustion process requires relatively high temperature. For this reason, the fuel-air ratio range near the stoichiometric ratio is the major contributor. NOx is produced even if the overall equivalence ratio is rich or lean because there exists combustion of a mixture whose fuel-air ratio is around stoichiometric value due to imperfect mixing. To represent this phenomenon, it is commonly assumed that primary zone flow consists of a large number of small eddies whose fuel-air ratio is in normal distribution around the mean value. By applying statistical distribution, an amount of mass is assigned near the stoichiometric region and the physics of the NOx formation path is captured.

A similar approach can be applied to soot research. Soot is mainly produced in the rich region and oxidized at the lean and near stoichiometric region. In order to represent the combustion of the non-uniform mixture and capture the physics of the soot formation process, a statistical distribution can be applied over a wide range of fuel-air ratio where soot is actively produced and oxidized.

The results of the preliminary experiment introduced in the Problem Formulation chapter implies that the statistical distribution created for NOx prediction may not cover enough range of fuel-to-air ratio for soot prediction. Nevertheless, the same approach is still valid for soot prediction because the soot is also produced due to the non-uniform fuel-to-air ratio in the flow field. One of the most important requirements of statistical distribution for soot prediction is that the distribution must include a rich region where soot is mainly produced as well as lean and near stoichiometric regions for oxidization. The unmixedness

parameter(S) is defined as

$$S = \frac{\sigma}{\phi_{ov}} \tag{5.18}$$

σ is the standard deviation of the distribution and the $\phi_o v$ is the overall equivalence ratio of the mixture. By adjusting this parameter, the normal distribution can capture the wide enough range, as shown in Figure 4.13

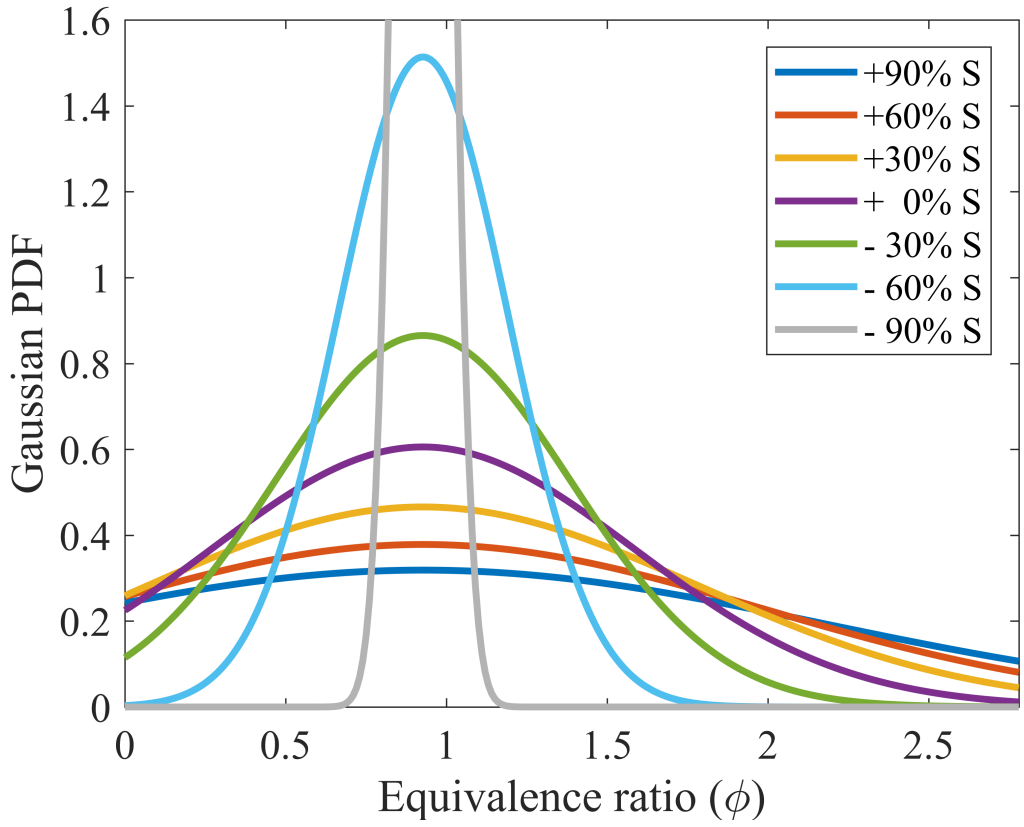

Normal distribution curves of different unmixedness (repeated from Figure 4.13)

The Statistical Distribution Model starts with computing the overall equivalence ratio of the primary zone. The fuel flow rate is provided from the cycle input and the air flow rate is provided from the CFC model after air partitioning. There is an unmixedness curve created for soot prediction in the later part of this research. The unmixedness curve is a

function of the equivalence ratio. The unmixedness will be achieved from the computed overall equivalence ratio. Once the unmixedness of the current flow is determined, the standard deviation is achieved from the definition of the unmixedness parameter explained in Equation (5.18).

When the unmixedness parameter is created, it is assumed that the equivalence ratios of small eddies in the turbulent primary zone are normally distributed. The normal distribution is traditionally adopted in emission studies to model the mixing of fuel and air. Its usefulness is proved by many successful studies[29][30][61][62][64][65][66][68][67][73]. If a different distribution is applied to model the non-uniform flow field, further analyses and measurement are required to prove its reasonable application. This is another topic of research and this is out of the scope of the current research. Therefore, in this research, the normal distribution is applied to model the non-uniformly mixed primary zone.

Now that the overall equivalence ratio and the standard deviation (σ) are available, the normal probability distribution function (PDF) can be achieved. Because the normal distribution has infinite range, +-2.5σ from the mean equivalence ratio range is applied. 98.8$\%$ is covered for +-2.5σ range. The contribution to soot prediction of the uncovered 0.6$\%$ at each tail is very small because these regions are extremely lean or rich. The lower bound of the equivalence ratio is the larger value between zero and -2.5σ from the mean value in order to prevent negative equivalence ratio.

Given the overall equivalence ratio, standard deviation, and the upper and lower boundaries, the normal PDF can be achieved. However, due to the uncovered range or the zero lower boundary, the area of the PDF curve is less than 1. This shape of distribution does not conserve mass. Therefore, the truncated normal distribution is applied. The truncated normal distribution is not an official statistical distribution. However, due to the infinite boundary of a normal distribution, the truncated normal distribution is often adopted in many studies. To have a truncated normal distribution, the PDF within the upper and lower boundaries is normalized by the area of the PDF curve within the boundaries. As a first

step, the range from the lowest equivalence ratio to the highest equivalence ratio is divided into 100,000 slices and the truncated PDF is numerically integrated. Then, each slice is normalized by the integrated area. This process gives the truncated normal probability density function.

Mass is distributed into slices based on this new pdf. However, because the equivalence ratio is not an additive property, here comes an issue: The fuel and air mass are not perfectly conserved. The sum of the fuel and air mass does not satisfy the overall mass of fuel and air. For example, if the equivalence ratios of two flows with same mass are 0.5 and 1.5, respectively, the sum of these two flow will have the equivalence ratio of 0.98, not 1.0 (see Figure 5.18). In order to conserve fuel and air mass and overall equivalence ratio, correction factors for fuel and air mass are applied to each splice. The correction factor for the air mass is the ratio of the overall mass of air to the sum of air mass in slices. The fuel correction factor is generated in the same manner. By applying these simple correction factors, total mass, air mass, fuel mass, and the overall equivalence ratio are conserved. The change in fuel and air mass is minimized in each slice.

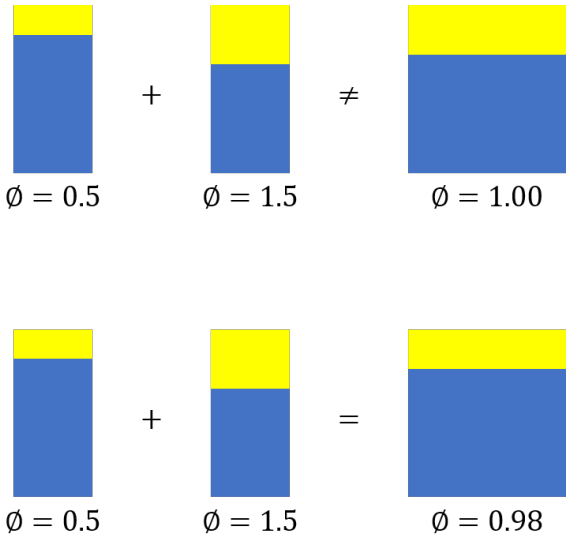

Figure 5.18: Flow addition and equivalence ratio

Although the mass and overall fuel-to-air ratio are conserved, the correction factor

makes a slight change in the fuel-to-air ratio of each slice are difference correction factors are applied to fuel and air. As a result, the PSR braches in the lean side is denser than the rich side. Figure 5.19 is an example of slices after correction when 20 slices are used for distribution. As long as enough number of slices is placed in the less dense side, the resolution of the equivalence domain is not an issue. The rich side can also be dense when the total number of slices is enough and 100,000 slices are enough to make a dense resolution.

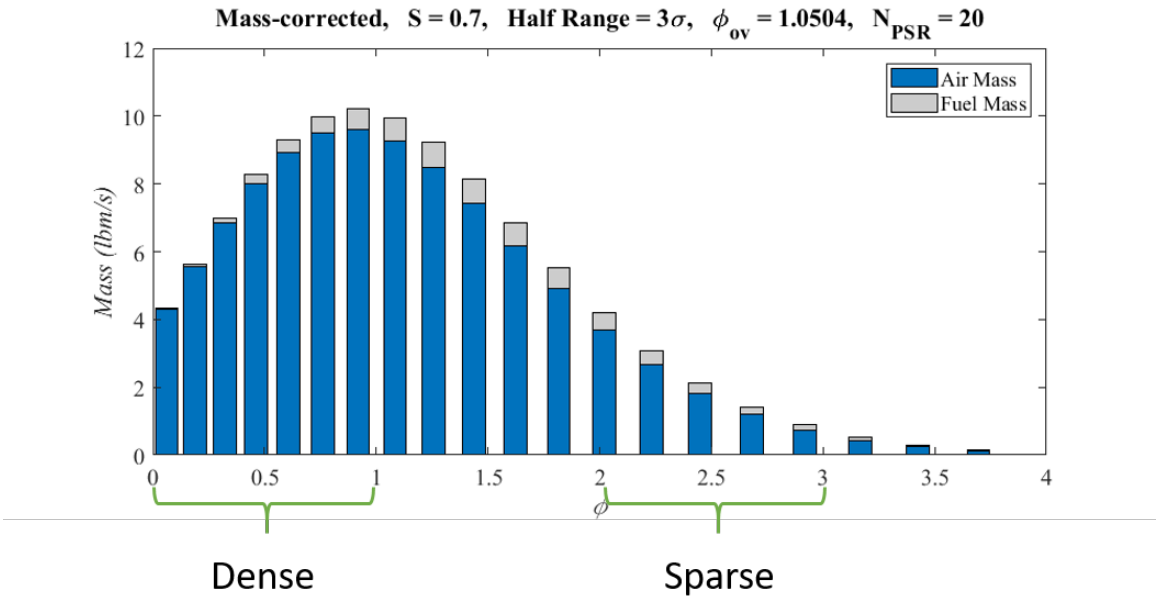

Figure 5.19: Relocation of slices after correction

Now that the slices are no longer equally spaced due to the slight movement of the equivalence ratio of each slice, the equal number of slices cannot be added up to form PSR branches anymore. Instead of summing up the same number of slices, the equivalence ratio domain is equally divided into N_PSR branches, where N_PSR is the number of PSRs, and the slices in the same branch are added up to form a PSR branch (see Figure 5.20). The equivalence ratio of PSR branches is determined by the fuel and air mass in each branch.

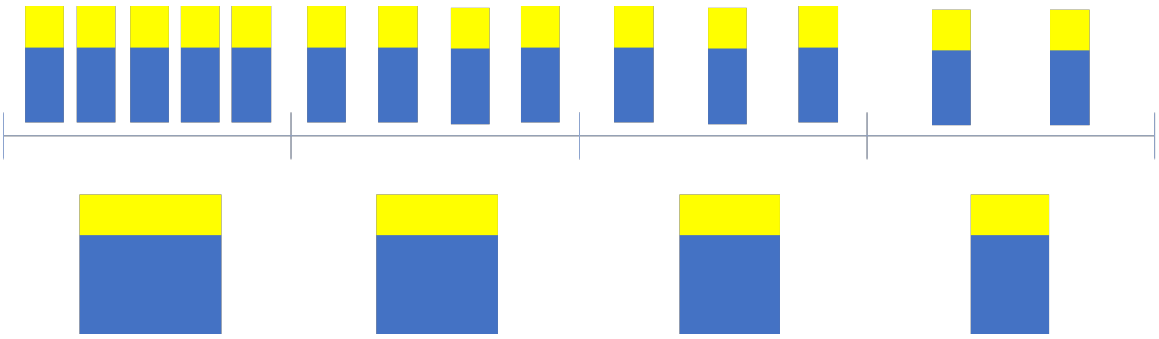

Figure 5.20: Flow distribution over PSR brach

The mass of fuel and air in each branch is passed to the Chemical Reactor Networks model. The overall process of distribution is illustrated in Figure 5.21.

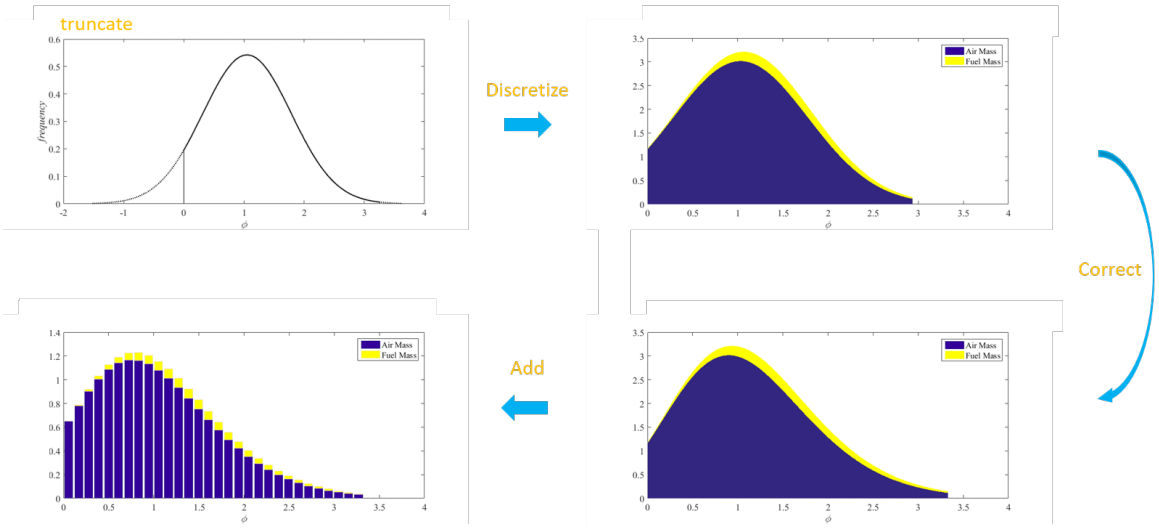

Figure 5.21: Procedure of statistical distribution

The fraction of the sum of fuel and air mass in each branch to the total mass is the probability of the flow to have the equivalence ratio of that branch. Each PSR brach has its probability and the volume is distributed based on this probability.

5.4 Chemical Reactor Network

A Chemical Reactor Networks (CRN) model represents the approximated combustion flow field of the combustor with a network of multiple idealized reactors. The CRN model consists of Perfectly Stirred Reactors and Plug Flow Reactors. These reactors are linked in serial and parallel to represent local combustion characteristics. A splitter and mixer elements are placed to control mass flow in the network.

The perfectly stirred reactor (PSR), also known as Well-Stirred Reactor is an idealized zero-dimensional reactor. One of the key characteristics of this reactor is that the mixing inside the control volume is perfect. Properties inside the control volume are uniform. Properties of incoming flow immediately change to outgoing properties which are the same as the properties inside the control volume. A major assumption defining the PSR is that the mixing process is much faster than the chemical reaction and the flow time is much shorter than chemical time. The PSR is usually used in the region where intense turbulence exists, such as the primary zone.

The continuity equation is simple for a steady-state flow. Outgoing mass remains the same as incoming mass. The momentum equation is not considered because the PSR is zero-dimensional. Species conservation equations for steady-state operation are [74]

$$\dot{\omega}_i MW_i + \dot{m}\left(Y_{i,in} - Y_{i,out}\right) = 0 \quad \text{for} \quad i = 1, 2, ..., N \text{ species} \tag{5.19}$$

where i is an arbitrary species, $\dot{\omega}$ is the net production rate, and Y is the mass fraction. The energy equation is[74]

$$\dot{Q} = \dot{m}\left(\sum_{i=1}^{N} Y_{i,out} h_i\left(T\right) - \sum_{i=1}^{N} Y_{i,in} h_i\left(T_{in}\right)\right) \tag{5.20}$$

where $\dot{Q}$ is the heat release rate and h is enthalpy. The kinetic and potential energies are neglected because this is a zero-dimensional reactor.

The residence time of a perfectly stirred reactor is defined as

$$\tau_{res} = \frac{\rho V}{\dot{m}} \tag{5.21}$$

These equations form a set of coupled nonlinear algebraic equations. The time differential terms are disappeared due to the steady-state assumption. Therefore, PSR reactor equations are easily solved in a fast manner.

However, equations of the plug flow reactor(PFR) which is the other ideal reactor in the CRN are a system of first-order ordinary differential equations. A PFR is a one-dimensional reactor. There are several assumptions made for a PFR. The flow is in a steady state. There is no mixing in the axial direction. The flow properties are uniform at any cross-section. The flow is frictionless[74].

Four governing equations for a steady state one-dimensional flow are[74]

Mass:

$$\frac{d\left(\rho u_x A\right)}{dx} = 0 \tag{5.22}$$

Momentum:

$$\frac{dP}{dx} + \rho u_x \frac{du_x}{dx} = 0 \tag{5.23}$$

Energy:

$$\frac{\left(h + u_x^2/2\right)}{dx} + \frac{\dot{Q}''\mathbf{P}}{dx} = 0 \tag{5.24}$$

Species:

$$\frac{dY_i}{dx} - \frac{\dot{\omega}_i \, MW_i}{\rho u_x} = 0 \tag{5.25}$$

where $\dot{Q}''$ is the heat flux and $\mathbf{P}$ is the local perimeter of the reactor.

When there is no heat flux, with assumptions made above, a system of ODEs is made

from these four conservation equations, as

$$\frac{d\rho}{dx} = \frac{\left(1 - \frac{R_u}{c_p MW_{mix}}\right)\rho^2 u_x^2 \left(\frac{1}{A}\frac{dA}{dx}\right) + \frac{\rho R_u}{u_x c_p MW_{mix}} \sum_{i=1}^{N} MW_i \, \dot{\omega}_i \left(h_i - \frac{MW_{mix}}{MW_i}\right) c_p \, T}{P\left(1 + \frac{u_x^2}{c_p T}\right) - \rho u_x^2} \tag{5.26}$$

$$\frac{dT}{dx} = \frac{u_x^2}{\rho c_p}\frac{d\rho}{dx} + \frac{u_x^2}{c_p}\left(\frac{1}{A}\frac{dA}{dx}\right) - \frac{1}{u_x \rho c_p}\sum_{i=1}^{N} h_i \dot{\omega} MW_i \tag{5.27}$$

$$\frac{dY_i}{dx} = \frac{\dot{\omega}_i MW_i}{\rho u_x} \tag{5.28}$$

The residence time in a PFR is defined as

$$\frac{d\tau_{res}}{dx} = \frac{1}{u_x} \tag{5.29}$$

The CRNs in the early days have a simple structure. They consist of a few reactors. These simple CRNs are generally alternatives to complicated numerical simulations of which computation hardware is not capable. As computation power is improved, more reactors are often used in CRNs while a simple structure of CRNs is still in use.

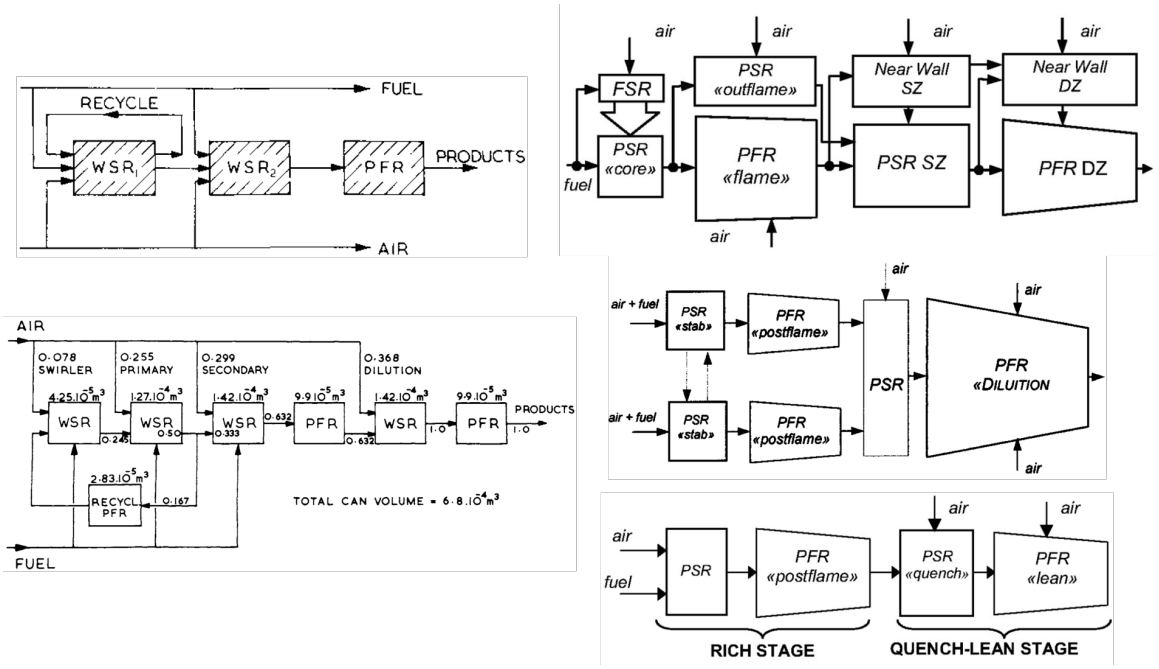

Figure 5.22: Simple chemical reactor networks

There are two types of structure among relatively complicated CRNs. The first type is based on the detailed geometry, similar to the CFD. This type of CRN is generally combined with CFD simulations. Reactor properties in the CRN are determined based on the CFD solutions. The opposite is also possible. The CRN results provide the information required for the CFD setup. Figure 5.23 is an example of the geometry-based CRN. This type of CRN is created based on the geometry details which is not available during conceptual design. Therefore, this approach is not suitable for the purpose of this research.

The second type of CRN is based on mixing characteristics. The statistical distribution of the fuel-to-air ratio is applied to construct the primary zone flow field where fuel and air are being mixed. In this type of the CRN, imperfect mixing of fuel and air is represented by parallel PSRs. This structure is based on the assumption that this region consists of a large number of small eddies with a different fuel-to-air ratio that is statistically distributed around the mean value. The downstream where there is relatively less turbulence is represented by PFRs.

Because imperfect mixing is one of the important phenomena in emissions, the mixing-

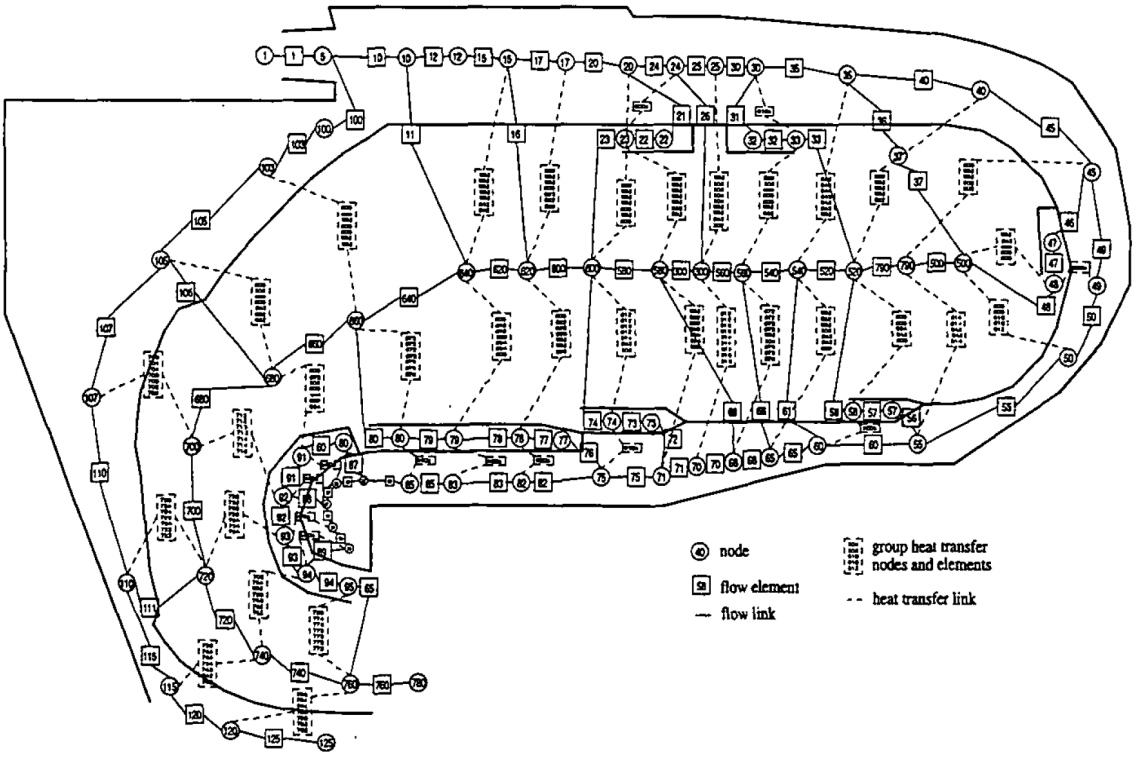

Figure 5.23: An example of geometry-based network[35] (repeated from Figure 2.13)

characteristics-based CRN is usually used in emission studies. The structure of this type of CRNs is relatively simple and relies less on the geometry details. The chemical mechanism used in soot studies is complex due to the aromatic species, which is minor species, involved in the soot formation mechanism. The mixing-characteristics-based CRN that has fewer reactors than the geometry-based CRN is more advantageous due to the heavy computational load caused by the massive amount of elementary reactions involved.

The geometry and flow properties required to construct reactor networks are provided from the Combustor Flow Circuit model and the Statistical Distribution Model. CHEMKIN[75], a software handling chemistry and solving reactor equations, is used to construct the CRN in this research. Calculated flow properties and species concentrations from all reactors are passed to the next model, the Emissions Evaluation Model to calculate predicted soot amount.

Figure 5.25 illustrates the structure of the CRN model constructed for the current re-

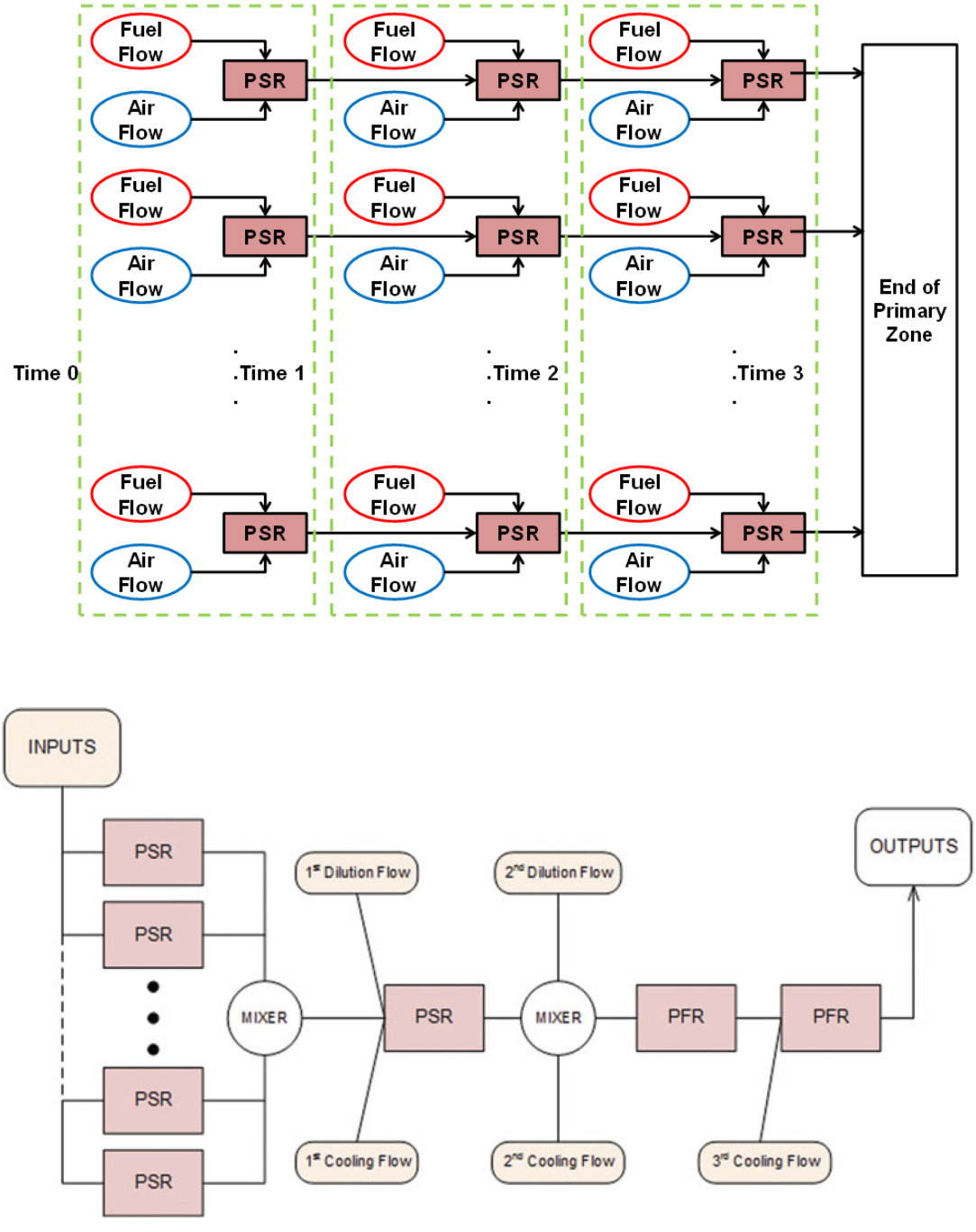

Figure 5.24: Examples of mixing-based network[10][36] (repeated from Figure 2.14)

search. The primary zone is modeled with a set of parallel PSRs. The volume, air flow rate, and fuel flow rate are provided from the Statistical Distribution Model. The thermodynamic properties of the flow including the initial temperature and pressure come from the Circuit Flow Model. The number of PSRs constructing parallel structure is 40. The required number of PSRs for soot prediction is tested after baseline modeling and validation of the whole environment. 40 PSRs turn out to be enough for soot prediction for LTO cycle from this test later. The flow leaving the PSRs are mixed at the mixer with the secondary air. The amount of secondary and dilution air is from the CFC model. The downstream combustions are modeled with the PFRs. The geometry information required for the PFR also comes from the CFC model.

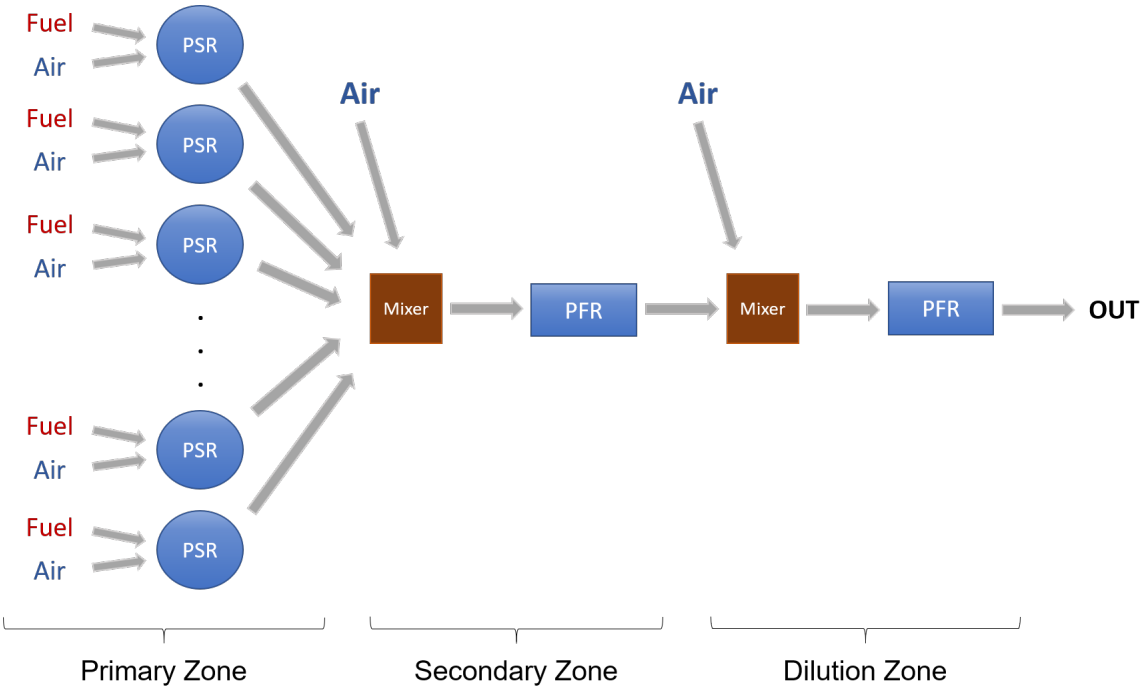

Figure 5.25: CRN structure

Even though the reactors are placed and connected, the CRN is not ready because the chemical mechanism consists of elementary reactions is not provided yet. The chemical mechanism, or fuel surrogate, provided for the soot prediction must satisfy requirements.

1. The fuel surrogate must represent jet fuel.

2. The chemical mechanism must include species involved in the soot formation mechanism.

3. The chemical mechanism should not be computationally expensive.

The first requirement address the type of fuel that the fuel surrogate is representing. Because this research is to predict soot from an aviation gas turbine engine, the chemical mechanism must represent the combustion of jet fuel. The jet fuel is loosely defined. Its combustion reaction is complicated because various hydrocarbons are in the jet fuel. Development of jet fuel surrogate is relatively a difficult task compared to the light fuel. For this reason, there are not many jet fuel surrogate available in the public domain.

The reactions in the fuel surrogate must involve species required for soot calculation. The purpose of the CRN is to provide thermodynamic properties of the flow and the species information to the Soot Evaluation Model. Therefore, the species involved in the selected soot formation mechanism must also be included in the chemical mechanism in the CRN.

The computationally expensive fuel surrogate is not realistic for conceptual design. The soot formation mechanism generally includes aromatic species which are minor species. These species are often omitted in the simplified fuel surrogate because their contribution to the overall heat release is small. Inclusion of many minor species increases the number of elementary reactions, causing heavy computational load. Many alternatives are reviewed and compared via design space exploration during the conceptual design phase. Unrealistically increased computation time caused by heavy mechanism is not desirable. Therefore, the jet fuel surrogate which is not too much heavy and involving species for soot formation mechanism must be selected.

Mattingly et al.[43] introduced Kollracks mechanism for jet fuel. It is a simple fuel surrogate consisting of two global reactions and 28 elementary reactions. The jet fuel is represented by C12H23. Two global reactions are to approximate the pyrolysis of heavy

fuel to small molecules. As a jet fuel surrogate, this mechanism satisfies the first condition. Due to its simplicity, this mechanism does not cause heavy computational loads. However, due to the limited number of elementary reactions and species, this mechanism cannot provide species information required for soot calculation.

The second generation surrogate developed in the MURI (Multidisciplinary University Research Initiative) project is a very detailed fuel surrogate targeting a real jet fuel[40]. The Jet-A fuel is represented by 40.4% of n-dodecane, 29.5% of iso-octane, 7.3% of 1,3,5 trimethylbenzene, and 22.8% of n-propylbenzene by mole. This mechanism consists of 2080 species and 8310 reversible reactions. All species for soot calculations are included in this fuel surrogate. However, due to a large number of species and reactions included, the computation for whole CRN takes too much time.

As fuel surrogates developed by Dagauts group utilized in soot studies very often, one of their fuel surrogate is reviewed. The jet A-1 fuel is represented by 69% of n-decane, 20% of n-propylbenzene, and 11% of n- propylcyclohexane by mole[76]. However, as this mechanism contains 2185 species and 8217 reversible reactions[77], this mechanism is not selected in the current research due to heavy computational load although it contains all required species.

Eventually, another fuel surrogate also developed by Dagauts group[78] is selected. The jet fuel is represented by 74% of n-decane, 15% of n-propylbenzene, and 11% of n-propylcyclohexane by mole. This mechanism consists of 209 species and 1673 reversible reactions. Despite relatively less number of species and reactions compared to other surrogates reviewed above, the combustion of jet fuel modeled in this fuel surrogate is still detailed, including all species required for the soot calculation in Soot Evaluation Model.

Table 5.1: Fuel representation

component	mol %
n-decane	74.0
n-propylbenzene	15.0
n-propylcyclohexane	11.0

After sub-models are integrated later, EINOx will serve as a baseline modeling target for unmixedness and the length of the combustor. As the selected fuel surrogate does not have NOx formation mechanism, the nitrogen chemistry from San Diego Mechanism[79] is added. The nitrogen chemistry of San Diego mechanism consists of 21 species and 40 reversible reactions. It includes various formation mechanisms of nitrogen oxides such as thermal, prompt, intermediate N_2O, etc. Reaction Workbench[80] is used to merge fuel surrogate and nitrogen chemistry. The merged mechanism consists of 209 species and 1673 reversible reactions. Negligible changes in concentrations of the species participating soot formation process in the Soot Evaluation Model are observed after several tests.

There are 14 pressure-dependent reactions in the selected fuel surrogate. For 1 atm, 10 atm, 20atm, and 40 atm, their Arrhenius coefficients are different. Although 14 is a small number compared to the number of total elementary reactions in the fuel surrogate, these pressure-dependent reactions include acetylene, involved in the inception and the surface growth phases, and hydroxyl radical, an oxidizer of soot. Therefore, it would be safe to use appropriate coefficients for a given cycle.

One option to handle pressure-dependent reactions is to interpolate results. However, there are two issues in this method. First, the CRN needs to be run twice for interpolation. Because the computation time significantly increases, this method is not desirable. Second, it is not realistic to interpolate all outputs. The results from the CRN model include thermodynamic properties of the flow and species information for the Soot Evaluation Model. The SEM model requires these outputs from all reactors. For PFR, results from every time

step are required. The total number of output parameters passed to the SEM model is approximately 3,000. It is unrealistic to interpolate 3,000 outputs.

Therefore, as an alternative method, parameters in the Arrhenius expressions are interpolated. There are three parameters in the Arrhenius expressions of the specific reaction rate constant (k); pre-exponential (collision) factor, exponent of temperature (b), and the activation energy (T_{atc}). Because there are 14 pressure-dependant reactions, there are 42 parameters to be interpolated.

$$k = A\,T^{b} exp(-T_{act}/T)$$

The simplest interpolation, a linear interpolation is applied first. 42 parameters in 14 pressure-dependent reactions are linearly interpolated. However, the CHEMKIN solver did not converge with this fuel surrogate.

The parameters in the Arrhenius expression of the reaction rate constants are interpolated for pressure. As pressure increases, the reaction rate also increases because the increased pressure causes denser molecules, shorter mean free path, and more collisions. Many analyses show a positive relationship between the p^n and the reaction rate[43][34] [81][42]. If the relationship $k \sim p^n$ is assumed,

$$p^n \sim k = AT^{b} e^{\frac{-T_{act}}{T}}$$

Transforming both sides with log derives

$$nlogP \sim logA + b\,logT - T_{act}/T$$

From this relationship, $logA$, b, and T_{act} are interpolated for $logP$. With interpolated coefficients, the CHEMKIN solver successfully converges and continuous results are achieved.

The interpolation is performed at the Mechanism Interpolator unit. It is a MATLAB[82] based code. The interpolated coefficients are passed to the Mechanism Generator unit and a new mechanism file is generated for the CRN.

5.5 Soot Evaluation Model

5.5.1 Calculation of Non-volatile Particulate Matter

There are four phases in soot formation; Inception, surface growth, oxidation, and coagulation phases. The initial nuclei are formed in the inception phase. The number of particles increases while this phase rarely contributes to the increase of the soot mass due to the tiny mass of soot nuclei. In the surface growth phase, the formed nuclei increase their mass, combining with more carbons. Because the mass increases via surface growth, this phase does not affect the number of soot particles. The mass of soot increased through the surface growth phase decreases in the oxidation phase. The soot particles lose their mass in the oxidation phase when the carbons on the surface of the particle react with oxidizers such as a hydroxyl radical. In the coagulation phase, the soot particles agglomerate together decreasing the number of particles. Figure (2.1) illustrates these four phases.

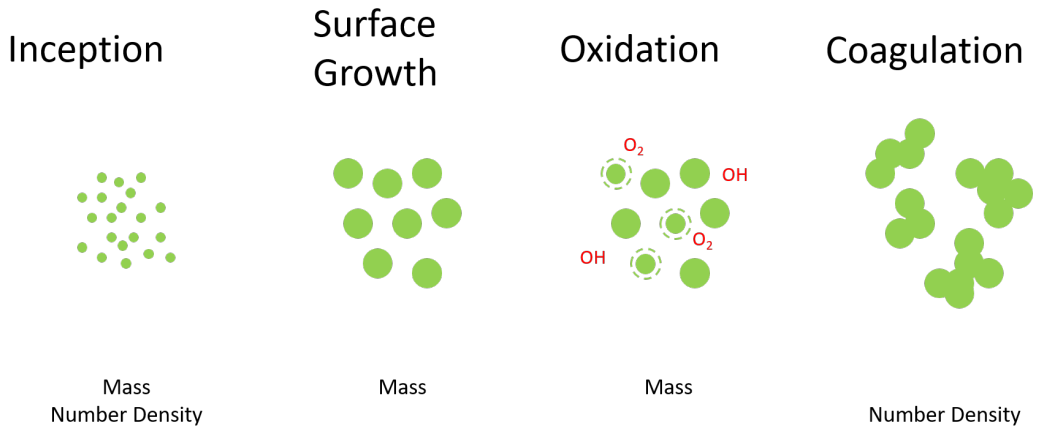

Soot Evolution Stages (repeated from Figure 2.1)

In the semi-empirical modeling method adopted in this research, each phase of soot formation is modeled as the functions of the soot mass and the soot particle number. These expressions form a non-linear differential equation system consisting of two equations; one for the time rate of the mass and the other for the time rate of the particle number.

This method is often called the two-equation system model. This modeling method is widely accepted in numerous soot research due to its simplicity while providing reasonable accuracy. The expressions of soot formation phases consisting of a two-equation system adopted in this research are introduced in the following sub-chapters.

Inception model

As an essential role of acetylene species in soot formation has been reported in numerous studies, the early attempts of inception modeling tried to build a direct correlation between the soot and acetylene. Many studies agreed with the assumed reaction introduced in Equation (5.30) and reported an Arrhenius form of the soot inception model. Equation (5.31) is one of the examples by Leungs group[14]. However, the pre-exponential factor and the activation energy of this model is not well agreed on by different studies.

$$C_2H_2 \rightarrow 2C_s + H_2 \tag{5.30}$$

$$R_1 = k_1\,(T)\,[C_2H_2], \qquad \text{where} \quad k_1 = 0.1 \times 10^5 e^{-21{,}100/T} \tag{5.31}$$

In the later studies, the significant PAH (Polycyclic Aromatic Hydrocarbon) contribution to the soot formation has been discovered. The importance of PAH is more emphasized in the flame burning heavy hydrocarbon fuels than in the flame burning light fuels. As one of the efforts to reflect this discovery, Lindstedt[53] added a benzene reaction to the acetylene reaction. His inception model is introduced in Equation (5.32) and Equation (5.33).

$$\begin{gathered} C_2H_2 \rightarrow 2C_s + H_2 \\ \\ C_6H_6 \rightarrow 6C_s + 3H_2 \end{gathered} \tag{5.32}$$

$$\begin{gathered} r_1 = k_1\,(T)\,[C_2H_2], \quad \text{where } k_1 = 0.63 \times 10^5 e^{-21{,}000/T} \\ \\ r_2 = k_1\,(T)\,[C_6H_6], \quad \text{where } k_1 = 0.75 \times 10^5 e^{-21{,}000/T} \end{gathered} \tag{5.33}$$

More recently, as an effort to include the PAH effect on the soot inception, Halls group[54] proposed an inception model based on the formation of two- and three-ringed aromatic species from acetylene, benzene, and a phenyl radical.

$$2C_2H_2 + C_6H5 \rightarrow C_{10}H_7 + H_2 \tag{5.34}$$

$$C_2H_2 + C_6H_6 + C_6H_5 \rightarrow C_{14}H_{10} + H + H_2 \tag{5.35}$$

Halls group simplified the model by applying a steady-state assumption to some minor species. The resultant inception rate is

$$S_1 = 8 \times \left(127 \times \frac{d\left[C_{10}H_7\right]}{dt} + 178 \times \frac{d\left[C_{14}H_{10}\right]}{dt} \right)$$

$$\text{where} \quad \frac{d\left[C_{10}H_7\right]}{dt} = 10^{11.88} e^{-4378/T} \frac{\left[C_2H_2\right]^2}{\left[H_2\right]} \left[C_6H_5\right] \tag{5.36}$$

$$\text{and} \quad \frac{d\left[C_{14}H_{10}\right]}{dt} = 10^{12.50} e^{-6390/T} \frac{\left[C_2H_2\right]}{\left[H_2\right]} \left[C_6H_6\right] \left[C_6H_5\right]$$

Hall and his colleagues multiplied eight at the beginning of this expression in order to match experimental results.

As two different forms of the soot inception model are reported, Wen et al.[18] compared them against the experimental measurement of turbulent kerosene flame conducted by Young et al.[83]. The better predictability of the model proposed by Halls group is observed in this comparison. Therefore, This inception model introduced in Equation (5.34) - (5.36) is adopted in this research.

In order to form a two-equation system, the expression introduced in Equation (5.36) is converted to the functions of the mass density (M_s) and the number density (N_s) of the

soot particles. The time rate of the mass density is in Equation (5.37).

$$\left(\frac{dM_s}{dt}\right)_{inc.}\left[\frac{kg}{m^3 s}\right] = k_1 MW_{C_{10}H_7}\frac{\left[C_2H_2\right]^2}{\left[H_2\right]}\left[C_6H_5\right] + k_2 MW_{C_{14}H_{10}}\frac{\left[C_2H_2\right]}{\left[H_2\right]}\left[C_6H_6\right]\left[C_6H_5\right] \tag{5.37}$$

The soot inception rate constants are $k_1 = 10^{8.88}e^{(-4378/T)}$ and $k_2 = 10^{9.50}e^{(-6390/T)}$

The molecular weight of species ($MW[kg/kmol]$) in Equation (5.37) is computed from the atomic weights provided in the periodic table. The concentrations of the species are computed from the relations in Equation (5.38) involving the mixture gas density (ρ) and the mass fraction of species (Y) provided by the Chemical Reaction Networks (CRN) model.

$$[M] = \frac{\rho\, Y_M}{MW_M} \tag{5.38}$$

The number of soot particles comes from the mass expression. When the Avogadro's number (N_{av}) divided by the molecular weight of soot is multiplied to the mass, the number of soot particles per unit mass is computed. In order to have the molecular weight of soot, the minimum number of carbon atoms forming soot nuclei (N_{Cmin}) is applied because one soot nucleus consists of multiple carbons. Leung et al.[14] and Wen et al.[18] used 100 for N_{Cmin}, and the same value is adopted in this research. The complete expression is introduced in Equation (5.39).

$$\left(\frac{dN_s}{dt}\right)_{inc.}\left[\frac{\#}{m^3\, s}\right] = \left(\frac{dM_s}{dt}\right) \times \frac{N_{av}}{MW_C\, N_{Cmin}} \tag{5.39}$$

Equation (5.37) and Equation (5.39) form the inception model. Although the mass of initial soot nuclei is tiny, a large number of soot particles formed at the inception phase gains massive weight through the surface growth phase.

Surface area and density of soot

The surface growth model and the oxidation model are surface-area-dependent. The soot grows when the carbon is attached to the surface of the soot particle. The soot loses its mass when it collides with oxidizer species and loses carbon on the surface. Therefore, the soot growth and oxidation processes are surface-area-dependent. The surface area should be modeled.

The total sum of the surface areas (S) of all soot particles is generally modeled in terms of the mean diameter (d_p) and the number density of soot particles(N_s). The mean diameter can be expressed in terms of the mass fraction of soot (Y_s), the density of the gas mixture(ρ), the number density of soot, and the density of the solid soot(ρ_s).

$$S = \pi d_p^2 N_s \tag{5.40}$$

$$d_p = \left(\frac{6}{\pi} \frac{1}{\rho_s} \frac{Y_s}{N_s/\rho} \right)^{\frac{1}{3}} \tag{5.41}$$

The soot density is generally assumed to be around 2000 kg/m^3 in many studies. Kim et al.[84] used 1850 kg/m^3, Lindstedt[53] and Wen et al.[18] assumed 2000 kg/m^3, and Puri et al.[15] assumed 1800 kg/m^3. These values imply 150-167 $kmol/m^3$ of the molar concentration of carbon. Even though slightly different values are applied for different studies, their differences are small and not likely cause significant difference in calculations. In this research, 1850 kg/m^3 is assigned to the soot density(ρ_s) because the surface growth model of Kim et al. is adopted.

Surface growth model

The early attempts to model soot surface growth is also focused on the direct correlation of acetylene concentration and the growth rate. Leung et al.s expression[14] in Equation (5.42) is one of the examples. They applied square root dependence to their Arrhenius form of growth rate.

$$R_2 = k_2(T)\sqrt{S}[C_2H_2]$$
$$k_2(T) = 0.6 \times 10^4 e^{-12{,}100/T} \tag{5.42}$$

In later studies, there have been many efforts to explain soot surface growth as PAH (Polycyclic Aromatic Hydrocarbon) growth via HACA, Hydrogen Abstraction Acetylene (C_2H_2) Addition, mechanism. As the name of HACA mechanism implies, the hydrogen and acetylene species are the major species involved in the soot formation process.

The model proposed by Kim et al.[84] is one of the simplest forms based on HACA theory, in Equation (5.43). Their simple expression does not have temperature dependence as the growth rate constant, k_H, is a constant number. Despite its simple form, a good agreement with measurement is reported by Kim et al. Another study by the same researchers[55] reported $2.85 \times 10^7\ kg\ m^4/(kmol^2 s)$ for k_H.

$$w_g \left[\frac{kg}{m^2\ s}\right] = k_H[C_2H_2][H]$$
$$k_H \left[\frac{kg\ m^4}{kmol^2\ s}\right] = 1.83 \times 10^7 \tag{5.43}$$

There is another popular form of growth first proposed by Frenklach and Wang[85], as

shown in Equation 5.44.

$$w_g \left[\frac{kg}{m^2\ s}\right] = \alpha_i R_i \tag{5.44}$$

.

Their model has been revised by several research groups in later studies. Colket and Hall[86] added reversibility in the acetylene addition process. Kim et al.[84] eliminated Reaction 3 from Colket and Hall's mechanism in Table 5.2 to obtain better pressure dependence. The growth rate proposed by Kim et al. is

$$w_g \left[\frac{kg}{m^2\ s}\right] = \alpha_{CH} R_{CH}$$

$$R_{CH} \left[\frac{kg}{m^2\ s}\right] = \frac{C_{HACA}\left(k_1\left[H\right] + k_{-2}\right) k_4 k_5 \left[C_2H_2\right]\left[C_s\text{-}H\right]}{\left(k_{-1}\left[H_2\right] + k_2\left[H\right]\right)\left(k_{-4} + k_5\right) + k_4 k_5 \left[C_2H_2\right]} \tag{5.45}$$

$$\alpha_{CH} = 0.35,\ C_{HACA} = 2MW_C/N_{av},\ \ [C_s\text{-}H] = 2.3 \times 10^{19}$$

In this research, Kim et al's HACA surface growth model in Equation (5.45) is adopted.

Table 5.2: CK reaction mechanism for soot surface growth[84]

No.	Reaction	A	n	E
1	C_s-$H + H \rightarrow C_s \cdot + H_2$	2.5×10^{11}	–	$50,200$
-1	$C_s \cdot + H_2 \rightarrow C_s$-$H + H$	4.0×10^{8}	–	$29,300$
2	$C_s \cdot + H \rightarrow C_s$-$H$	2.2×10^{11}	–	–
-2	C_s-$H \rightarrow C_s \cdot + H$	2.0×10^{17}	–	$456,000$
3	$C_s \cdot \rightarrow C_2H_2 + products$	3.0×10^{14}	–	$259,000$
4	$C_s \cdot + C_2H_2 \rightarrow C_sCH\dot{C}H$	2.0×10^{9}	–	$16,700$
-4	$C_sCH\dot{C}H \rightarrow C_s \cdot + C_2H_2$	5.0×10^{13}	–	$159,000$
5	$C_sCH\dot{C}H \rightarrow C_s$-$H + H$	5.0×10^{10}	–	–

Oxidation model

Soot loses its mass via oxidation phases. Oxygen has been considered as one of the major oxidizers in early studies. One of the famous models adopted to many studies is Nagle and Strickland-Constable model[87], shown in Equation (5.46).

$$Rate = \left(\frac{K_A p}{1 + k_z p}\right) x + k_B p (1 - x)$$

$$\text{where } x = \frac{1}{1 + \frac{k_T}{k_B p}},$$

$$\begin{aligned} k_A &= 20 \times e^{-30{,}000/RT}, \\ k_B &= 4.46 \times 10^{-3} e^{-15{,}200/RT}, \\ k_T &= 1.15 \times 10^{5} e^{-97{,}000/RT}, \\ k_z &= 21.3 \times e^{+4{,}100/RT} \end{aligned} \tag{5.46}$$

Lee et al.[88] suggested a simple oxidation reaction in Equation (5.47) and Equation (5.48).

$$C_s + \frac{1}{2} O_2 \rightleftharpoons CO \tag{5.47}$$

$$r = k\,(T)\, S[O_2] \tag{5.48}$$

These oxidation models involving O_2 as an oxidizer have adopted widely in soot studies. However, as measurement data are collected, it is revealed that these models significantly underpredict the oxidation effect. For instances, the collision efficiency of O_2 estimated by Strickland-Constable model is ten to a hundred times less than measurement

data[84]. Because of this issue, Leung and Lindstedt[14] used Lee et al.'s model[88] with eight times larger values for rate constant. For this reason, researchers think that there must be other species responsible for soot oxidation. According to Puri et al. [15], soot and carbon monoxide competes for the hydroxyl radical. The hydroxyl radical is generally accepted as a dominant oxidizer for soot in current studies[84].

The oxidation model involving hydroxy radical as an oxidizer is based on the collision efficiency from kinetic theory. The collision efficiency η_{OH} between OH radicals and soot particles is[84][55]

$$\eta_{OH} = \frac{4w_{OH}}{C_{OH}[OH]\bar{\nu}_{OH}} \tag{5.49}$$

and the rearranged expression is[10]

$$\frac{MW_s}{S}\frac{d\,[C_s]}{dt} = -\frac{1}{4}\eta_{OH}C_{OH}\bar{\nu}_{OH}\,[OH] \tag{5.50}$$

where w_{OH} is the oxidation rate, MW_s is the molar weight of soot particle, $[C_s]$ is molar concentration of soot, η is collision efficiency, C_{OH} is the mass of carbon removed from the soot surface per mole of OH, $[OH]$ is molar concentration of OH, and $\bar{\nu}_{OH}$ is the Boltzmann equilibrium mean molecular velocity of OH which is

$$\bar{\nu}_{OH} = \sqrt{\frac{8R_uT}{\pi MW_{OH}}} \tag{5.51}$$

The more rearranged form of oxidation rate introduced by Puri et al. is[15]

$$\frac{d\,[C_s]}{dt} = -4.6\times10^{-23}\eta_{OH}N_{av}d_p^2N_s\sqrt{T}\,[OH] \tag{5.52}$$

where N_{av} is Avogadro's number, and N_s is the number density of soot.

The collision efficiency (η_{OH}) is one of the factors adding uncertainties. The range

indicated by the experiment of Roth and Gersum[89][90] is around 0.2 (from 0.1 to over 0.3). Neoh et al.[91][12] suggests 0.13-0.28. Ma et al.[92]. In this research, the oxidation model involving hydroxyl radical with 0.13 for η_{OH}, one of the collision efficiency values by Neoh et al. is adopted.

Coagulation model

While the inception phase increases the number of particles, coagulation it. In this modeling, it is assumed that the coagulation processes occur when soot particles collide each other. The coagulation model derived from the collision frequency. From this assumption, a predominantly used coagulation expression can be derived from the definition of collision frequency is introduced in Equation (5.53).

$$r = k\left(T\right)\left[C_s\right]^{\frac{1}{6}}\left[N_s\right]^{\frac{11}{6}}$$
$$k\left(T\right) = -2C_a\left(\frac{6MW_s}{\pi\rho_s}\right)^{\frac{1}{6}}\left(\frac{6k_BT}{\rho_s}\right)^{\frac{1}{2}} \tag{5.53}$$

where MW_s is the molecular weight of soot which is 12.011 $kg/kmol$, and k_B is the Boltzmann constant which is 1.38×10^{-23} J/K[53]. C_a is the agglomeration constant. Different studies report different values for C_a. The common range of the agglomeration constant in various research is 1$\sim$9. In this research, 9 is assigned for it as Lindstedt[53] did.

Computation strategies

Models for the four phases of the soot formation are achieved in terms of the soot mass per unit volume and the soot particle number density. As assumed earlier, the inception and coagulation phases contribute to the mass of soot and the inception, surface growth, and oxidation phases contribute to the number density of the soot particles.

$$\frac{dN}{dt} = \left.\frac{dN}{dt}\right|_{inc.} - \left.\frac{dN}{dt}\right|_{coag.} \tag{5.54}$$

$$\frac{dM}{dt} = \left.\frac{dM}{dt}\right|_{inc.} + \left.\frac{dM}{dt}\right|_{gr.} - \left.\frac{dM}{dt}\right|_{oxi.} \tag{5.55}$$

When four models are added up and rearranged, they formulate a system of differential equations or so-called two-equation system.

$$\frac{dN}{dt} = A + BM^{\frac{1}{6}}N^{\frac{11}{6}} \tag{5.56}$$

$$\frac{dM}{dt} = C + DM^{\frac{2}{3}}N^{\frac{1}{3}} \tag{5.57}$$

where M is the soot mass per unit volume and N is the soot number density. Four coefficients A, B, C, and D are functions of temperature and species concentrations provided by Chemical Reactor Networks (CRN) Model. The first terms (A and B) in Equation (5.56) and Equation (5.57) are from the inception model. The second term ($BM^{\frac{1}{6}}N^{\frac{11}{6}}$) in Equation (5.56) is from the coagulation model and the second term ($DM^{\frac{2}{3}}N^{\frac{1}{3}}$) in Equation (5.57) is from the surface growth and oxidation models.

The CRN model consists of the Perfectly Stirred Reactors (PSRs) and the Plug Flow Reactors (PFRs). Because their assumptions are different, the strategies to compute soot quantity are different for different reactor types.

The PSRs in the CRN model are zero-dimensional and the instant mixing and steady-state conditions are assumed. Therefore, there is no transient state and the left-hand-sides of Equation (5.56) and Equation (5.57) become

$$\left.\frac{dN}{dt}\right|_{PSR} = \frac{N_{out} - N_{in}}{\tau_{PSR}} \tag{5.58}$$

$$\left.\frac{dM}{dt}\right|_{PSR} = \frac{M_{out} - M_{in}}{\tau_{PSR}} \tag{5.59}$$

Because the properties inside the reactors are the same as the properties of the efflux flows for PSRs, $M_{out} = M_{PSR}$ and $N_{out} = N_{PSR}$. Therefore, Equation 5.56 and 5.57 become

$$\frac{N_{PSR} - N_{in}}{\tau_{PSR}} = A + BM_{PSR}^{\frac{1}{6}} N_{PSR}^{\frac{11}{6}} \tag{5.60}$$

$$\frac{M_{PSR} - M_{in}}{\tau_{PSR}} = C + DM_{PSR}^{\frac{2}{3}} N_{PSR}^{\frac{1}{3}} \tag{5.61}$$

The initial properties (N_{in} and M_{in}) are from the previous reactors in the CRN model.

Equation 5.60 and 5.61 are no longer differential equations but a system of nonlinear algebraic equations. The computationally expensive calculations can be avoided due to the PSR assumptions.

However, this equation system is still not ready to be solved yet. The terms including species concentrations, soot mass and number densities, and soot formation rates vary in a broad order-of-magnitude range when a numerical solver attempts different conditions for iterations. Therefore, the functions in the system are very stiff and nonlinear and the solver often failed to converge. For this reason, log-transformation is applied to both independent and dependent variables so that the solver can handle various conditions without further

adjustment. This approach results in consistent convergence for all PSR reactors with a variety of fuel-to-air ratio regardless of the engine input cycle.

Plug Flow Reactor is a one-dimensional reactor. When the time is set to a parameter instead of the axial distance, the Euler method enables to approximate the soot properties at the next step ($i + 1^{th}$ step) in terms of the current soot properties (i^{th} step), as Equation (5.62) and Equation (5.63) show. This numerical marching technique is fast and efficient despite a large number of time steps because it does not involve a solver technique.

$$N_{i+1} \cong N_i + \left.\frac{dN}{dt}\right|_i \times (t_{i+1} - t_i) \tag{5.62}$$

$$M_{i+1} \cong M_i + \left.\frac{dM}{dt}\right|_i \times (t_{i+1} - t_i) \tag{5.63}$$

For both PSR and PFR, incoming soot properties before reactions occur at the current reactor are required to compute the current level of soot. The Soot Evaluation Model takes species and thermodynamic properties from all reactors in the CRN model and computes soot properties at every reactor.

5.5.2 Calculation of CO and NOx Emissions

After all sub-models are integrated, the unmixedness parameter and length of the combustor are calibrated for EINOx and EICO. Therefore, EINOx and EICO in addition to soot need to be achieved based on the CRN results.

Equation (5.64) explains the calculation method for EICO. The mass of CO is computed by multiplying the mass fraction of CO species to the gas mixture mass. The computed mass of CO is then divided by the fuel mass.

$$EICO\left[\frac{g}{kg-fuel}\right] = W \times Y_{CO} \,/\, W_f \tag{5.64}$$

Because most NO species produced by combustion are converted into NO_2 species in the atmosphere, the calculation method for EINIOx assumes all NO species are already converted into NO_2 species. Therefore, the total mass of NOx emission is the sum of the existing mass of NO_2 and the estimated mass of NO2. The calculation method is explained in Equation (5.65).

$$EINOx\left[\frac{g}{kg-fuel}\right] = W \times \left(Y_{NO} \times \frac{MW_{NO_2}}{MW_{NO}}\right) \,/\, W_f \tag{5.65}$$

CHAPTER 6

INTEGRATION OF ENVIRONMENT

In this chapter, the sub-models prepared in the previous chapter is integrated, forming a prediction environment. The baseline is modeled and the environment is extended with sizing and unmixedness curve for further predictability. Two engine cycles with different size are applied for validation against correlations results.

6.1 Hierarchy of Overall Environment

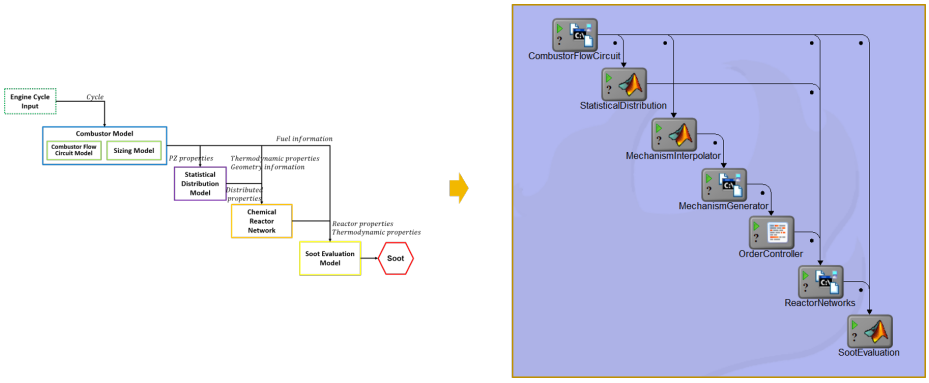

Figure 6.1: Integrated prediction environment

All models addressed in the Technical Approach chapter are integrated into the ModelCenter[104]. The overall hierarchy of the integrated environment is illustrated in Figure 6.1. The cycle inputs are pressure (P_{t3}), temperature (T_{t3}), air mass flow rate (W_3), fuel mass flow rate (W_f), and Mach number of the airflow (MN_3) of on-design and off-design phases. The Combustor Flow Circuit (CFC) model takes these inputs. After air partitioning and sizing calculations, the air mass of the primary zone and the fuel mass are transferred to the Statistical Distribution Model (SDM). The SDM model computes the air and fuel

mass and volume for each PSR in Chemical Reactor Networks (CRN) modeling combustion of non-uniform mixture in the primary zone. Before the CRN model, the fuel surrogate is prepared by the Mechanism Interpolator calculating coefficients in pressure-dependent reactions, and by the Mechanism Generator creating and providing a new chemical mechanism file for the CRN model. The geometry and air partition data from the CFC model, distributed properties of the primary zone flow from the SDM model, and the fuel surrogate from the Mechanism Generator component are provided to the CRN model. The CRN computes the thermodynamic properties and species concentrations of every reactor and transfers them to the Soot Evaluation Model (SEM). The SEM model computes quantitative soot via soot formation mechanism by solving the coupled non-linear equation system for PSRs and by numerical marching technique for PFR.

All input and output variables are connected among sub-models. As all sub-models are linked, the prediction processes are automized. Once the input cycle is given, the prediction environment starts computations from the CFC model to the SEM model to result in the quantitative soot amount automatically.

6.2 Baseline Modeling

The automated prediction environment is prepared as sub-models are integrated. This environment is a generic model at this point. The next task is to model the baseline. The baseline prediction environment is modeled, adjusting many design parameters in the sub-models via statistical analysis, surrogate modeling, and optimization techniques.

6.2.1 Selection of Cycle

Cycles for baseline modeling and validation of the environment needs to be prepared first as the input of the environment is an engine cycle. Among available engine cycles from the Environmental Design Space[93], a modeling and simulation framework for airframe and engine, three engine cycle models are selected for baseline modeling and validation of the environment. Selected cycle models are named Engine S, Engine M, and Engine L in the current research. The Engine S is a notional representation of CF34-8C5 engine, the Engine M is a notional representation of CFM56-7B27 engine, and the Engine L is a notional representation of CF6-80C2 engine. They are selected because CF34-8C5, CFM56-7B27, CF6-80C2 engines and their combustors are in a similar technology level while their engine sizes are different. The core flow rate, thrust, and pressure ratio of three engine series are compared to notional engine models in Table 6.1. Engine information in this table is from the ICAO Emissions Databank[94].

Table 6.1: Comparison of selected engines[93][94]

	W3 Take-off (lbm/s)	ICAO Take-off Thrust (kN)	ICAO Take-off Pressure Ratio
CF34-8C5	N/A	56.4 - 64.5	22.1 - 24.8
Engine S	58.6	63.4	22.1
CFM56-7B27	N/A	121.4	28.6 - 29.0
Engine M	100.7	121.4	28.6
CF6-80C2	N/A	231.1 - 272.5	27.5 - 32.9
Engine L	185.5	261.2	31.2

For CFM56-7B27 series, CFM56-7B27/2 engine is excluded because the combustor of this engine is a dual-annular combustor, not a traditional single annular type combustor[95]. Among 34 variations in CF6-80C2 engine series, the combustor type of 19 engines is 1862M39. Engine L is a notional representation of these 19 CF6-80C2 engines with the 1862M39 combustor because the power hook of the Engine L cycle model collapses with the power hook of CF6-80C2 engines equipped with the 1862M39 combustor. The power hooks are compared in Figure 6.2.

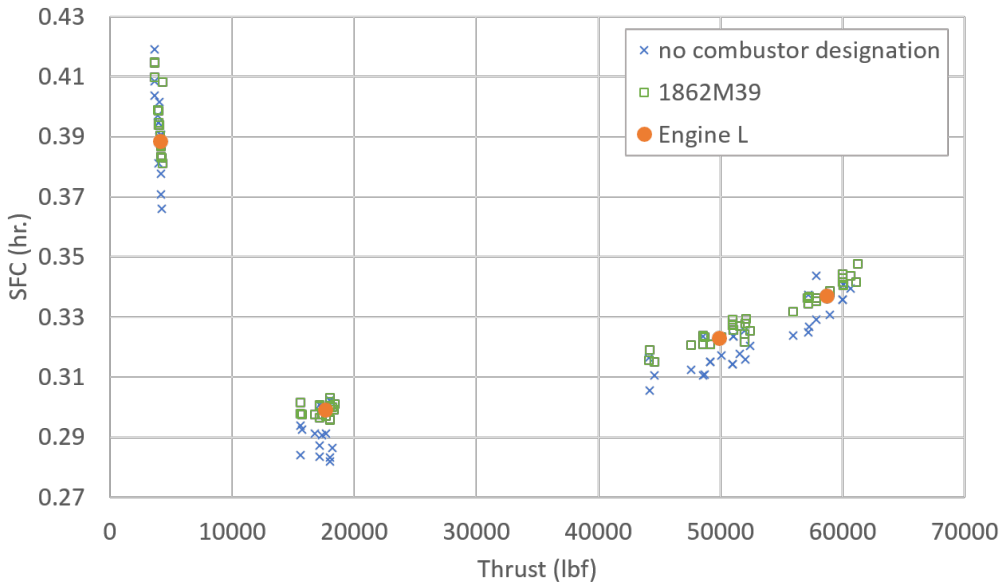

Figure 6.2: Comparison of selected engines

Among three engine cycle models, Engine M is selected as a baseline because its combustor size is estimated to be between the other two based on the core mass flow rate (W_3). Engine L with larger W_3 and Engine S with smaller W_3 are provided as validation points.

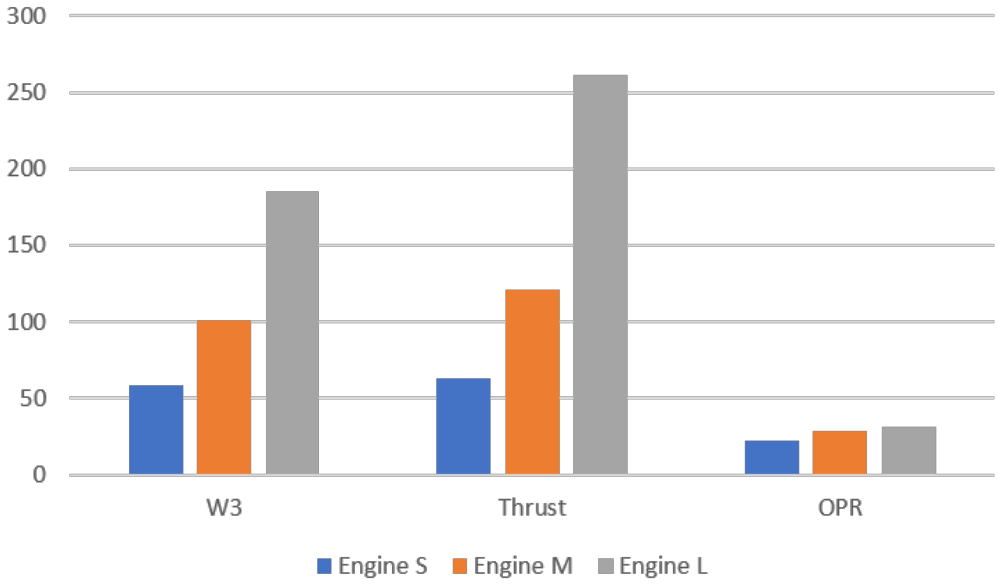

Figure 6.3: Comparison of selected engines

6.2.2 Correlations for Baseline and Validation

The sub-models are integrated and the cycles for the baseline modeling and validation are selected. The selected cycles are provided to the environment as an input. In addition to the cycle, quantitative soot information from these engines is required for modeling and validation. However, there are not available measurement data from these engines in public domain because soot is not easily measured.

The combustor of the operating gas turbine engine is highly pressurized and exceedingly hot. Plugging in the sampling probe and take the gas sample is a challenging task. The small size of the soot particles also makes measurement challenging. Different measurement instrument and techniques often report different measurement results. For example, emission indices in Table 6.2 are derived from the measurement of different instruments in the APEX II campaign[96]. Their disagreement is up to an order of magnitude. The PM particles quenched at the wall of the sampling probe also adds uncertainties in measurements. Due to these effects addressed here, the measurement is challenging and data includes high uncertainties. Table 6.3 is the average and standard deviations of black carbon measurements from the LTO cycle of CFM56-2C1 engine during APEX I campaign[96]. Compared to the average indices, significant standard deviations are observed.

Table 6.2: Derived PM mass emission indices from measurements of different instruments

	Derived average EI (mg/kg fuel)			
Test	Nano-SMPS	EEPS	TEOM	QCM
T1	34.4	132	262	89.9
T2	22.9	113	215	207
T3	39.6	167	272	326
T4	31.7	131	244	117

Table 6.3: Average and standard deviation of BC measurement from LTO cycle of CFM56-2C1 during APEX I

Cycle	EI BC (mg/kg)	SD (mg/kg)
Take-off	71.2	81.6
Climb out	402	113
Approach	99.5	174
Idle	33.6	46.2

For these reasons, there are not much measurement data in the public domain including the data corresponding to the selected three engine cycle models. Nevertheless, these cycles are selected as a baseline and validation points, because there are correlations enabling estimation of soot emitted from these engines. The ICAO Emissions Databank (EDB)[94] provides data required data for the black carbon correlations, such as the smoke number and fuel flow rate.

First Order Approximation Version 3.0

The information in ICAO EDB is measured and reported for the emissions certification process. As it is addressed in the Background chapter, the current aviation emitted PM is regulated via the smoke number (SN). SN is an empirical measure of filter stain because the purpose of the regulation is to reduce exhaust plume visibility. Because ICAO EDB provides publically accessible abundant SN data of fleets currently in operation, there have been many efforts to correlate SN to the mass of black carbon to estimate effects of BC on human health and environment.

The First Order Approximation 3.0 (FOA3) is a standard correlation method to estimate the mass of BC from SN[97]. The concentration index (CI) is calculated from the smoke number, the exhaust volumetric flow rate per fuel flow (Q) is from air-to-fuel ratio, and

the emission index of non-volatile PM is the product of CI and Q. The detailed process is explained by Wayson et al.[6].

The concentration index (CI) is the mass of soot per standard volume of engine exhaust gas. The standard conditions are 0 ^{o}C and 1 atm. The correlation between CI and SN is

$$CI = 0.0694\,(SN)^{1.24} \tag{6.1}$$

This correlation is valid for SN$\leq$30. The smoke number of most modern engines is generally below 30. However, some old engines whose smoke number is over 30 are still in operation. For these engines, the correlation is

$$CI = 0.0294\,(SN)^{2} - 1.802\,(SN) + 31.94 \tag{6.2}$$

The unit of CI is mg/m^3 and SN is a dimensionless parameter.

Next is to calculate the exhaust volumetric flow rate per fuel mass flow rate (Q). Q is correlated with the air-to-fuel ratio (AFR). For the separate flow turbofan engine whose core flow not mixed with bypass flow before exhaust, the correlation is

$$Q_{core} = 0.776\,(AFR) + 0.877 \tag{6.3}$$

For the mixed flow turbofan engine whose core flow is mixed with bypass flow before the exhaust is

$$Q_{mixed} = [0.776\,(AFR)\,(1 + BPR)] + 0.877 \tag{6.4}$$

The unit of Q is $m^3/kgfuel$ and AFR is non-dimensional.

AFR of the engine is usually proprietary and not available in the public domain. For this reason, representative AFRs are applied in this correlation.

Table 6.4: Representative air-to-fuel ratio for FOA3 correlation

Power	Representative AFR
Take-off	45
Climb out	51
Approach	83
Idle	106

The emission index of the mass of non-volatile PM is the product of CI and Q and the unit is $mg/kgfuel$.

$$EI_{non-vol.PM} = (Q) \times (CI) \tag{6.5}$$

The procedure of FOA3 method is illustrated in Figure 6.4.

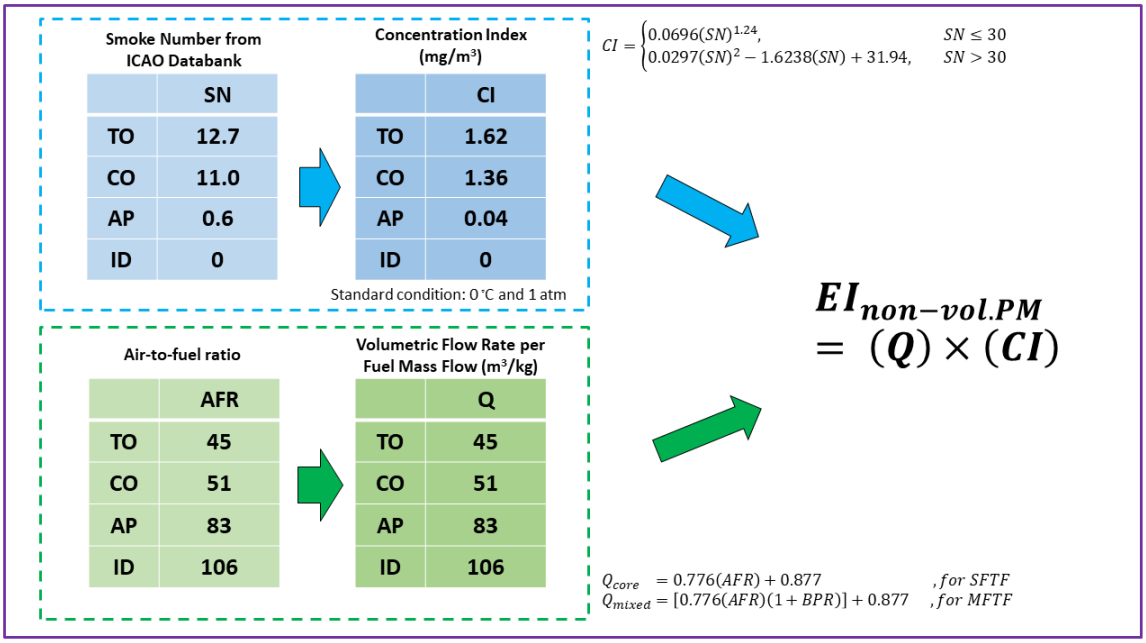

Figure 6.4: First Order Approximation 3.0 method[6]

First Order Approximation Upper Bound

Because the error in the smoke number measurement is estimated up to ± 3, Wayson et al.[6] created correlations for the upper bound of CI. For SN ≤ 30,

$$CI = 0.0012\,(SN)^2 + 0.1312\,(SN) + 0.2255 \tag{6.6}$$

For SN > 30,

$$CI = 0.0297\,(SN)^2 - 1.6238\,(SN) + 26.801 \tag{6.7}$$

Correlations for lower bound is not introduced by the authors because it can cause significant under-estimation.

Because there is much research arguing that FOA3 method greatly under-estimate non-volatile PM, this correlation for upper bound is often applied together with the standard correlation. In the current research, results from the upper bound correlation are denoted as FOAup.

Updated Correlation

According to Stettler et al.[98], a large fraction of their data shows that FOA3 method under-estimate mass of BC more than an order of magnitude. Stettler et al.[97] argue that the reason for under-estimation is the size of particles in the base measurement for the derivation of the FOA3 correlation. Dodds et al.[99] report that a correlation between SN and CI depends on the size of the particle. Stettler et al.[97] argue that the filter efficiency is affected by the size of particles when SN is measured. In their measurement, higher CI is measured for smaller particles even if measured smoke numbers are identical. The particle size in measurements used to derive FOA3 correlation is around the 100 nm range, which is

relevant to older aircraft engines[97], while the size of PM measured in APEX champaign is around 10-40 nm[100].

Stettler et al.[97] suggest a new correlation for the concentration of black carbon and the smoke number for different sizes of particles. The correlation for the geometric mean diameter of 20 30 nm is for the modern aircraft engine.

$$C_{BC}\left(GMD = 20 - 30nm\right)\left[\frac{mg}{m^3}\right] = 0.236\left(SN\right)^{1.126} \tag{6.8}$$

For older engines, the correlation for the geometric mean diameter of 60 nm is suggested.

$$C_{BC}\left(GMD = 60nm\right)\left[\frac{mg}{m^3}\right] = 0.0472\left(SN\right)^{1.42} \tag{6.9}$$

These updated correlations suggested by Stettler et al.[97] is denoted as FOAst in the current research. Because these correlations are an update of FOA3 method, the same FOA3 method is applied to calculate the exhaust volumetric flow rate per fuel flow rate (Q).

Formation and OXidation (FOX) Method

Stettler et al.[98] suggest a correlation independent of the smoke number due to the uncertainties in measurement and under-estimation issue of FOA3 method. The name of this correlation is Formation and Oxidation (FOX) method. They insist that their new correlation depends on the engine operating conditions.

Wen et al.[18] models soot formation mechanism with the two-equation system. The FOX method by Stettlers group takes the inception term and the oxidation term from Wen et al.s mechanism. The basic form of their correlation is

$$C_{BC} \sim \left[fuel\right] e^{-6390/T} - \left[air\right] e^{-19778/T} \tag{6.10}$$

The first term is for the formation and the second term is for the oxidation of soot. In this expression, they assume that the formation is related to the amount of fuel and inception phase, and the oxidation is related to the amount of air and oxidation by hydroxyl radical. For simplification, they omitted the surface growth phase, where mass increases, and the coagulation phase, affecting the number of particles. In addition, they use the flame temperature (T_{fl}) for temperatures in both exponential terms despite the fact that the zones mainly responsible for formation and oxidation are different.

After applying assumptions and simplification, the correlation of the concentration index of black carbon in the FOX method is

$$C_{BC}\left[\frac{mg}{m^3}\right] = \dot{m}_f\left(A_{form}\, e^{-6390/T_{fl}} - AFR\, A_{OX}\, e^{-19778/T_{fl}}\right) \tag{6.11}$$

The coefficients A_{form} is 356 $mg\ s/kg-fuel\ m^3$ and Aox is 608 $mg\ s/kg-fuel\ m^3$. The fuel flow rate comes from the ICAO emissions databank[94]. For the air-to-fuel ratio, while the FOA3 method uses the fleet-average AFR values, Stettler et al. linearly regressed the fuel-to-air ratio measured in APEX campaign, as shown in Equation 6.12.

$$AFR = \left(0.0121\left(\frac{F}{F_{00}}\right) + 0.008\right)^{-1} \tag{6.12}$$

For the flame temperature (T_{fl}), a correlation which is a function of T_3 is used, as in Equation 6.13.

$$T_{fl}\,[K] = 0.9\,T_3 + 2120 \tag{6.13}$$

To have T_3, P_3 is calculated first. Stettler et al. linearly approximate P_3 from the thrust ratio, as in Equation (6.14)

$$P_3\,[atm] = (\pi_{00} - 1)\left(\frac{F}{F_{00}}\right) + 1 \tag{6.14}$$

T_3 is calculated from Equation (6.15) when the polytropic efficiency is assumed to be 0.9, specific heat ratio is assumed to be 1.4, P_2 is approximated to 101325 Pa, and T_2 is approximated to 293 K.

$$\frac{T_3}{T_2} = \left(\frac{P_3}{P_2}\right)^{\frac{\gamma-1}{\gamma\,\eta_p}} \tag{6.15}$$

The same method from FOA3 is applied to the calculation of the exhaust volumetric flow rate per fuel flow. Because the concentration of black carbon at the exit of the core is assumed in the FOX method, there is no consideration for the bypass ratio.

The procedure of the FOX method is illustrated in Figure 6.5.

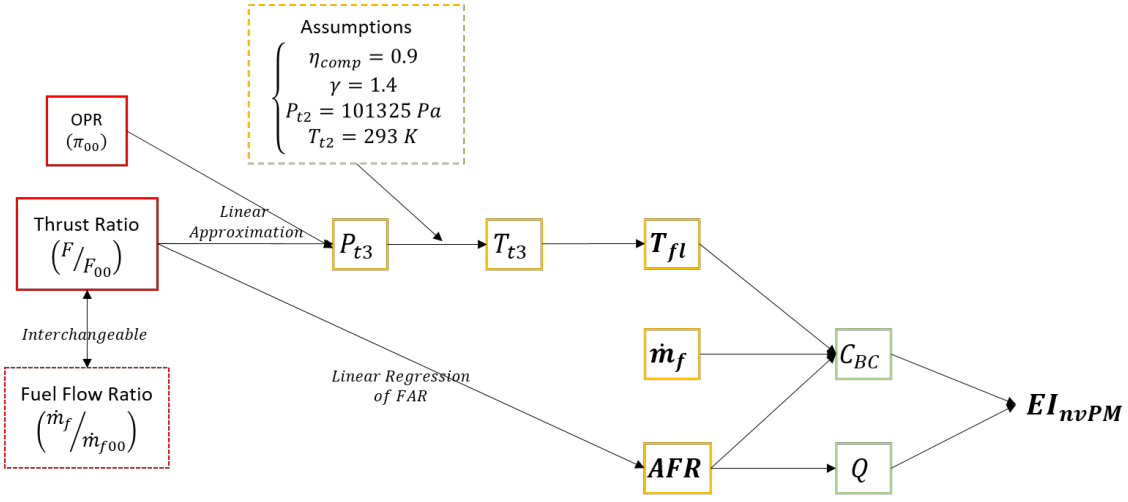

Figure 6.5: Procedure of FOX method

Improved Formation and OXidation Method (ImFOX)

Improved FOX method is the correlation maintaining a similar approach with the FOX method. Abrahamson et al.[101] developed ImFOX method by utilizing proprietary cycle deck and measurement data of CFM56-2C installed on DC-8 vehicle. They argue that the

FOX method highly over-predict their data and ImFOX method is more appropriate for the current engines predominantly equipped with RQL type combustors.

They evaluate ImFOX method as a thrust-dependent correlation. The only required input is the fuel flow rate. The formation coefficient in the FOX method is now a third-order polynomial of fuel flow ratio. They argue that the fuel flow ratio is a measure of thrust ratio.

$$A_{form} = 1013 - 4802\left(\frac{\dot{m}_f}{\dot{m}_{f00}}\right) + 7730\left(\frac{\dot{m}_f}{\dot{m}_{f00}}\right)^2 - 3776\left(\frac{\dot{m}_f}{\dot{m}_{f00}}\right)^3 \tag{6.16}$$

They argue that high degree of over-prediction is observed for the air-to-fuel ratio expression in the FOX method. They suggest a different expression for the air-to-fuel ratio, which is a function of fuel flow ratio.

$$AFR = 71 - 35.8\left(\frac{\dot{m}_f}{\dot{m}_{f00}}\right) \tag{6.17}$$

For the temperature in the exponential terms, T_4 is used instead of the flame temperature. T_4 is calculated from Equation 6.18.

$$T_4[K] = 490 + 42,266\left(AFR^{-1}\right) \tag{6.18}$$

The correlation of BC concentration in ImFOX method is in Equation (6.19). In order to handle fuels other than conventional fuel, a fuel term depending on the hydrogen content is added. The oxidation coefficient is the same as the FOX method.

$$C_{BC}\left[\frac{mg}{m^3}\right] = \dot{m}_f\, e^{(13.6-H)}\left(A_{form}\, e^{-3690/T_{fl}} \;-\; A_{OX}\, AFR\, e^{-19778/T_{fl}}\right) \tag{6.19}$$

The procedure of ImFOX method is demonstrated in Figure 6.6. The method to calculate exhaust volumetric flow rate is also the same as the FOX method, which is from FOA3 method.

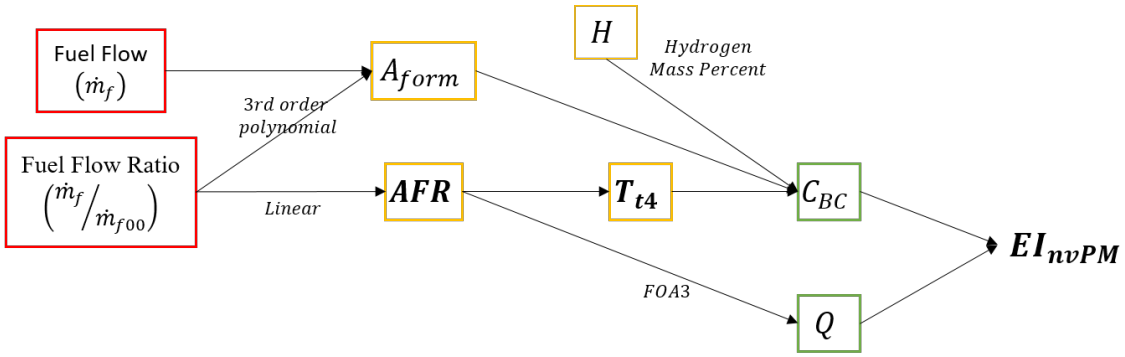

Figure 6.6: Procedure of ImFOX method

Based on five correlation methods addressed in this section, the expected scatter of non-volatile PM is illustrated for the engine series of CF34-8C5, CFM56-7B27, CF6-80C2, in Figure 6.7 and Figure 6.8. The baseline modeling Engine M cycle targets the scattered results of CFM56-7B27 series. The expected results of CF34-8C5 and CF6-80C2 in Figure 6.7 and Figure 6.8 are the validations points of prediction environment simulating Engine S and Engine L.

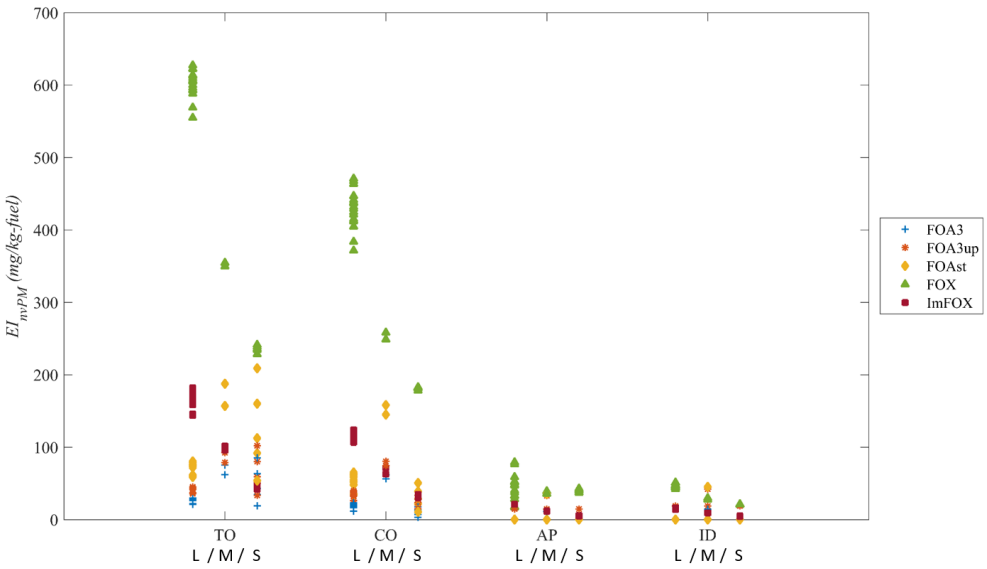

Figure 6.7: Expected emission indices of non-volatile PM from various correlations

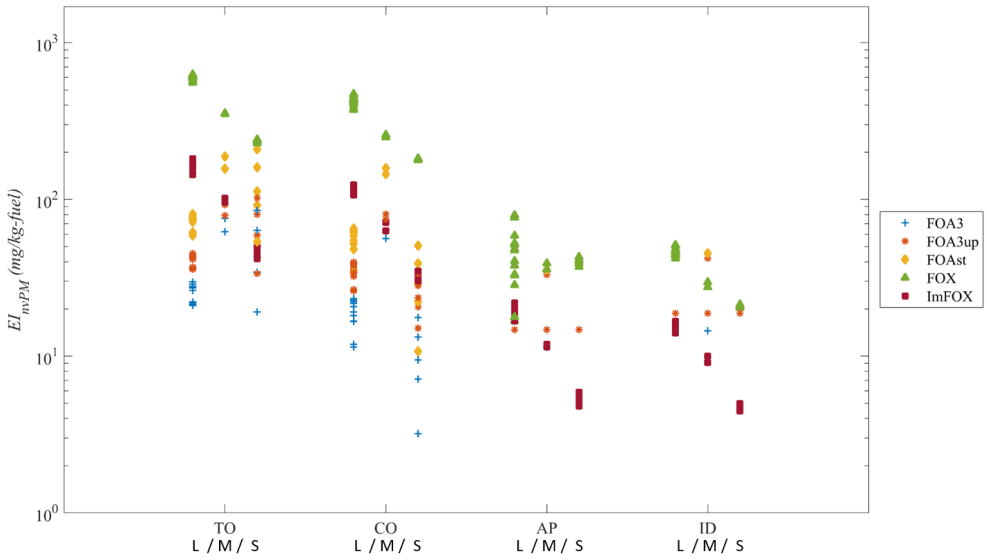

Figure 6.8: Expected emission indices of non-volatile PM from various correlations (log scale)

6.2.3 Modeling Baseline of Combustor Flow Circuit

In this section, the baseline combustor is modeled in the Combustor Flow Circuit (CFC) model. The baseline combustor is a generic combustor model demonstrating general characteristics of the conventional combustor. The general combustor characteristics include

- Overall Pressure loss
- Stoichiometry of different combustion zones
- Local Mach numbers

In this modeling, there is an assumption about the design parameter; Non-dimensional design variables defining generic properties of the baseline combustor model, such as the pressure loss coefficient and Mach number, are universal regardless of cycle inputs. Some dimensional parameters are scaled based on the cycle. These cycle-specific parameters are mainly geometry-related parameters such as the length of the combustion zones and the size of the hole. For these cycle-specific design variables in baseline modeling, the cycle from Engine M model, which is a notional representation of CFM56-7B27 engine, is utilized as a baseline cycle.

As introduced in the previous chapter, a simplified combustor configuration in Figure 6.9 is adopted in the CFC model. This is to minimize the number of design variables. As design variables are added, the complexity of modeling significantly increases and the uncertainties also greatly increase. Too many design variables are not affordable in the conceptual design phase where information is deficient.

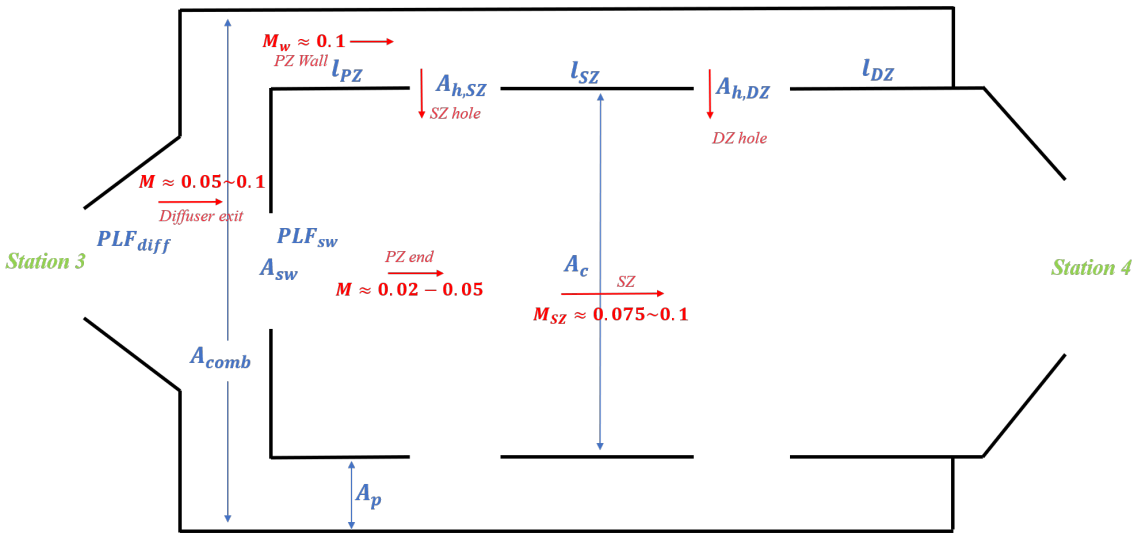

Figure 6.9: Simplified combustor configuration

The diagram of the CFC model and the following design variables are in Figure 6.10 and Table 6.5, respectively.

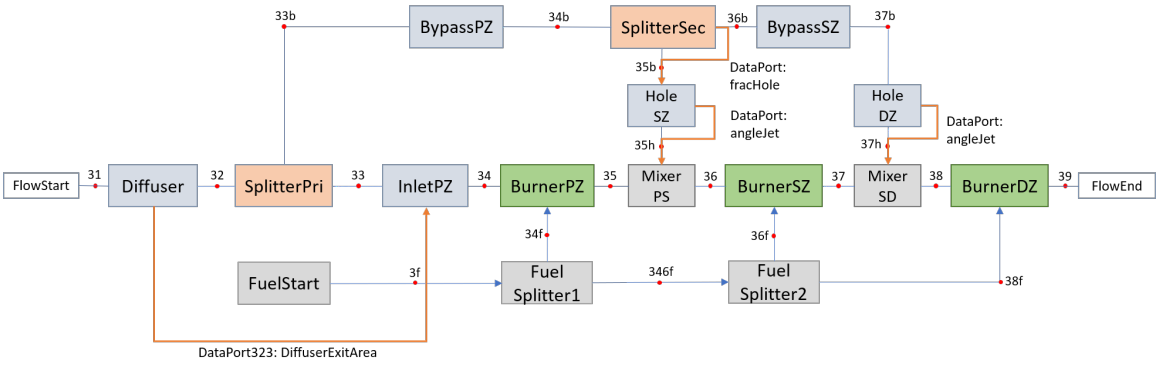

Figure 6.10: Diagram of Combustor Flow Circuit model

Table 6.5: List of design variables

Design Variables
Diffuser.plc
Diffuser.AR
SplitterPri.Aout_01
SplitterPri.Aout_02
InletPZ.Aout
epsPZ
epsSZ
epsDZ
BurnerPZ.AR
BypassPZ.l
BypassPZ.L
BypassPZ.fric
BypassPZ.AR
HoleSZ.A_h
BypassSZ.L
BypassSZ.AR
HoleDZ.A_h
BurnerSZ.AR
BurnerDZ.AR

Mach numbers play an essential role in this modeling because they deeply involve in the pressure losses inside the combustor. Incorrect combinations of design values often cause inappropriate local Mach numbers and pressures not satisfying the convergence conditions at the mixer elements. For this reason, the design of experiment (DOE) is not efficient. Many design combinations in the DOE table are often generated without consideration

on a physical relationship of variables. These combinations easily generate errors during iteration. Therefore, design values are found one by one from the beginning of the flow to the end of the combustor while following the flow of the diagram in Figure (CFCdiagram). This method accompanies iterative feedback loop.

While several different values are tried to design variables, these values are determined by referencing suggested values from the literature. For example, the friction coefficient, fric, is determined by referencing a Moody diagram with an estimation of Reynolds number and relative roughness from literature. The length and width, L and l, are determined to reference a schematic figure of CFM56-7B27 engine. The combustion efficiency or fuel consumption ratio, eps, is also determined from the literature. The area ratios of the primary zone and the secondary zone are set to unity in order to maintain a simplified geometry for the ease of modeling.

Once an initial set of design values are found, this sample provides a nominal baseline point. A DOE table can be generated while disturbing design parameters from this nominal point. A Monte-Carlo simulation of 50,000 sample points is performed. Latin-Hypercube design is used in this simulation due to its superiority over random sampleing[102][10].

The design values are found via filtering of samples generated in the Monte-Carlo simulation. The generic characteristics of the combustor are filtering parameters. Generic characteristics include the pressure loss, Mach numbers, and the equivalence ratio of combustion zones. Filtering ranges of these parameters are based on literature.

The pressure loss through the combustor is around 4-8$\%$[34][48]. The suggested value of equivalence ratio at the primary zone is around 1.02 and at the secondary zone is around 0.6[41]. Walsh and Fletcher[41] introduce a guide for Mach number inside the combustor. They suggest 0.05-0.1 at the exit of the diffuser, the order of 0.1 at outer annuli, 0.02-0.05 at the end of the primary zone, 0.2-0.3 at the hole, and 2.5 or more for the ratio of the hole Mach number to the outer annuli Mach number.

As the filtering ranges are gradually narrowed, clear clouds of sample points in the

design space are observed. When the cloud of samples is in a small range, the average of values is selected as a design value of that parameter. When the cloud is not clear or the size of the cloud is not small enough to specify a certain value, the preferred range of the design parameter is found. The preferred value is the point where the mode, average, and 50 percentile of the distribution of sample values of a design variable agree (see Figure 6.11). In this filtering experiment, many design variable values are found while some design variables still show variability. The design values of these variables are selected after additional simulations via the Latin-Hypercube DOE and filtering experiment. The selected design set is tested on the combustor model with off-design cycles, and the solver successfully converges.

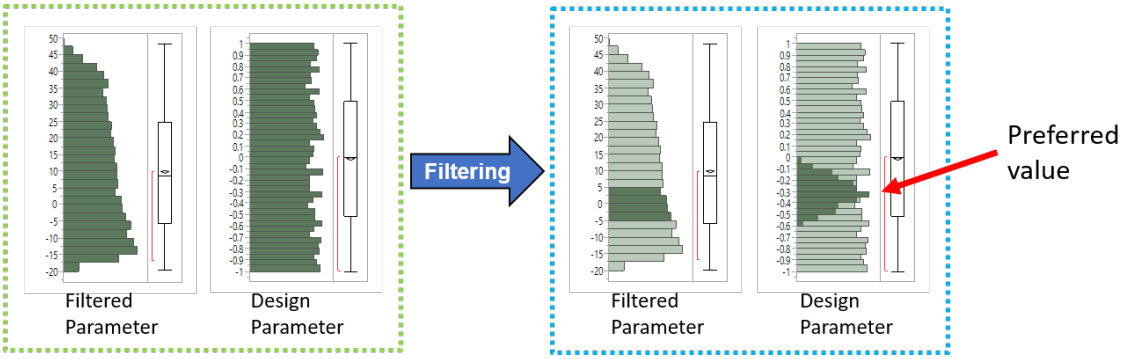

Figure 6.11: Filtering and preferred value

Table 6.6 shows the design variable of the combustor flow circuit model and the selected design values of the baseline model. The combustor properties are listed in Table 6.7. Note that the Mach numbers instead of areas are used as design variables because the Mach number is a non-dimensional flow property which belongs to general characteristics of a combustor while the area is a combustor-specific variable. As combustors have limited ranges of local Mach numbers, it is assumed that selected Mach numbers in filtering experiment are representative values common for all cycles in the same level of combustor technology in this modeling.

Table 6.6: List of design variables and design values

Design Variables	Design Value
Diffuser.plc	0.465
Diffuser.MNout	0.08
SplitterPri.MNout_01	0.233
SplitterPri.MNout_02	0.08
InletPZ.MNout	0.02
epsPZ	0.7
epsSZ	0.3
epsDZ	0
BurnerPZ.AR	1
BypassPZ.l	0.9
BypassPZ.L	2.75
BypassPZ.fric	0.02
BypassPZ.AR	1
HoleSZ.A_h	16.7
BypassSZ.L	3.9
BypassSZ.AR	1
HoleDZ.A_h	17.9
BurnerSZ.AR	1
BurnerDZ.AR	1

Table 6.7: Characteristics of baseline combustor at design point

Parameter	Value
$\frac{\Delta P}{P}$	5.40%
ϕ_{PZ}	1.02
ϕ_{SZ}	0.60
ϕ_{DS}	0.41

As one of the validations of the performance of the combustor model, the empirical expressions of pressure losses introduced by Walsh and Fletcher[41] are tested. For cold loss, the expression relating pressure loss to the cycle parameters is

$$\Delta P_{t,cold} = K_{cold} P_{t3} \left(\frac{W_3 \sqrt{T_{t3}}}{P_{t3}} \right)^2 \tag{6.20}$$

The hot loss expression is

$$\Delta P_{t,hot} = K_{hot} P_{t3} \left(\frac{T_{t4}}{T_{t3}} - 1 \right) \left(\frac{W_3 \sqrt{T_{t3}}}{P_{t3}} \right)^2 \tag{6.21}$$

The total loss is computed at the design point. The cold loss is computed when all eps variables are set to zero. The hot loss is calculated by subtracting the cold loss from the total loss. This is the procedure of the actual measurement of cold and hot losses of the combustor.

The coefficients for cold and hot losses are calculated at the design point from Equation 6.20 and 6.21. By applying calculated loss coefficients and off-design cycles back to Equation 6.20 and 6.21, pressure losses at the off-design cycle are calculated.

The computed pressure losses from the CFC model and the calculated pressure losses from empirical equations agree very well. This agreement supports that the combustor model demonstrates the generic characteristics of conventional combustors as expected.

6.2.4 Modeling Volumes and Mixing Characteristics of Baseline

Volume in this research is not the physical volume of the combustor. The volume in this context is the space providing the residence time to the combusting mixture. It is more conceptual and chemical volume rather than the real geometric volume of the combustor. Because this volume is for the general combustion phenomena, not only soot but also many combustion products are affected together.

Mixing performance is a combustor and flow property affecting general combustion phenomena. Oxides of nitrogen emission is a well-known combustion product highly affected by the mixing characteristics of the combustor flow. CO is also considered as a product related to the mixing performance[30][67].

The next procedure after volumes and mixing characteristics are modeled is the adjustment of the soot mechanism. Based on the previous experience[10] as well as related literature[30][28], quantitative soot amount varies in the order of magnitude scale during adjustment. If the soot mechanism is adjusted while modeling volume and mixing characteristics, significant complexity and non-linearity are added in the modeling process.

For these reasons, the modeling of volumes and mixing characteristics and the adjustment of the soot mechanism are decoupled in the current modeling.

The cross-section areas are determined by the design Mach number in the Combustor Flow Circuit model. Therefore, for the given simplified geometry in Figure 6.9, the length should be moded in order to model the volume. Therefore, lengths of the primary, secondary, and dilution zones (l_{PZ}, l_{SZ}, l_{DZ})are the design variable. The unmixedness is one variable in the Statistical Distribution Model. However, as many studies report[30][57][61][62][64][65][66][67][68][73], it varies with the power and the equivalence ratio of the primary zone. Therefore, four unmixedness parameters in LTO cycle (S_{TO}, S_{CO}, S_{AP}, S_{ID}) of Engine M are modeled.

The modeling targets are EINOx and EICO of CFM56-7B27/3 engine. There are nine CFM56-7B27 series in the ICAO Emissions Databank[94]. Among them, data of six vari-

ations are identical to CFM56-7B27/3 engine. CFM56-7B27/2 engine is excluded because its combustor type is a dual-annular combustor[95] which is different from the baseline modeling a conventional single annular combustor. Therefore, CFM56-7B27 and CFM56-7B27/3 variation are the available targets. The validation cycles, Engine S and Engine L models are notional representations of CF34-8C5 and CF6-80C2 engines. CF34-8C5 engine series are equipped with Low Emissions Combustor and CF6-80C2 series are equipped with the 1862M39 combustor. Based on these two types of combustors, NOx and CO emissions from CFM56-7B27/3 engine equipped with Tech Insertion technology combustor is selected as targets. Therefore, mixing characteristics and volumes are modeled via seven design variables against eight target emissions (four EINOx and four EICO from LTO cycle of CFM56-7B27/3).

To determine the design values of the unmixedness parameter and lengths of different combustion zones, four groups of sample data are prepared. Because emissions can be evaluated after the species information is achieved from the chemical reactor networks, sampling is a time-consuming task. Although the computation time depends on the CUP power, it took an hour to generate five sets of design samples in the current research. One set consists of four simulations of the model due to the four power modes in the LTO cycle. Therefore, in order to prepare data sets, the design of experiment followed by surrogate modeling is performed.

Two hundred samples are generated in the first simulations of the Latin-Hypercube design. Generated samples are analyzed via statistical techniques utilizing scatterplot matrix, empirical cumulative distribution, and histograms in JMP[103], a statistical tool. After the first round of analysis, the ranges of design variables are refined. The second round of DOE simulation is performed with 500 sets of samples whose ranges are adjusted based on the first DOE results. With these five hundred samples, eight surrogate models for target EINOx and EICO are created via Artificial Neural Networks (ANN) in JMP. From these surrogate models, four groups of samples are achieved.

With given ranges of design variables, the design space is not feasible for EINOx at Idle condition. EINOx at Idle is under-predicted. This is to match the target of EICO at Idle. While EICO at idle is very high, EINOx at Idle is very low. Design ranges satisfying both targets are not found in the test simulations. To match the NOx target, unrealistically high unmixedness range is required in the test simulations. It is considered that the high value of EICO is a better target demonstrating the mixing characteristics of the primary zone than the low value of EINOx. Because EINOx achieved by large unmixedness significantly degrades the EICO performance, the ranges of design variables are set to achieve EICO target at idle.

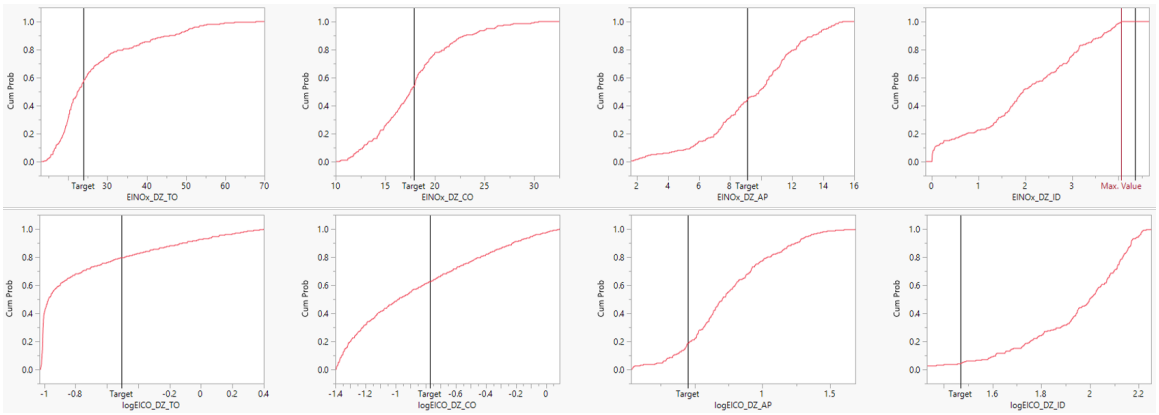

Figure 6.12: Empirical cumulative distribution of EINOx and EICO from 500 sample points

The empirical cumulative distribution functions in Figure 6.12 are drawn with 500 sample points. The upper four distributions are for EINOx and the lower four are for EICO. They are for take-off, climb out, approach, and idle conditions from left to right. The black vertical lines are the target values. Under-predicted EINOx values at idle condition are also observed in this figure.

The first group of a data set is from optimization utilizing Design Explorer in Model-

Center[104]. The objective function is in Equation (6.22)

$$obj = \sqrt{\sum_{LTO} (dev.EINOx)^2} + \sqrt{\sum_{LTO} (dev.EICO)^2} \tag{6.22}$$

, where dev.EINOx is the normalized deviation of EINOx from the target and dev.EICO is the normalized deviation of EICO from the target.

Two hundred seventy-five sample points are evaluated by the Design Explorer. Among them, samples of lower 10% in objective function value are selected as the first group.

The second optimization is performed via Evolve option in the optimizer in ModelCenter, which utilizes a genetic algorithm. Eleven thousand six hundred eighty-three sample points are evaluated the samples of lower 10% in objective function value are selected as the second group.

The third group is from multi-objective optimization. Objective functions are the root-mean-squared deviation of normalized emission indices. Therefore, there are eight objective functions and no weighting is applied to them. The Non-dominated Sorting Genetic Algorithm II (NSGA II) in the ModelCenter is applied. NSGA II algorithm does not search for a unique optimum solution. Instead, it identifies the Pareto set based on the non-dominated rank. Among 12,283 evaluated sample points, last 10% is selected as the third group.

The last group is from a Monte-Carlo simulation. One hundred thousand samples in Latin-Hypercube design are simulated. A filtering technique is applied to the simulation results up to ± 3 g/kg in EI, except for EINOx at idle because the surrogate model is created from the sample points not satisfying EINOx target at the idle condition.

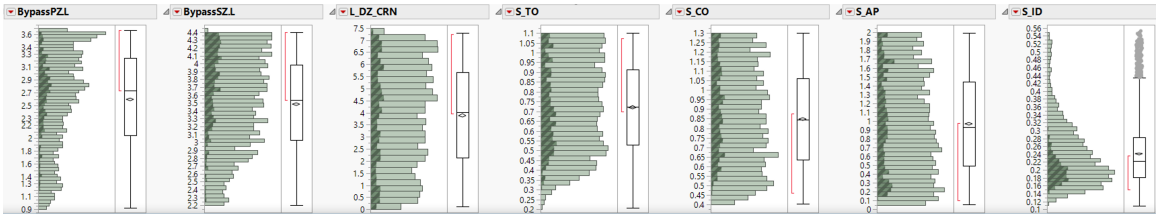

Figure 6.13: Change of distribution during filtering

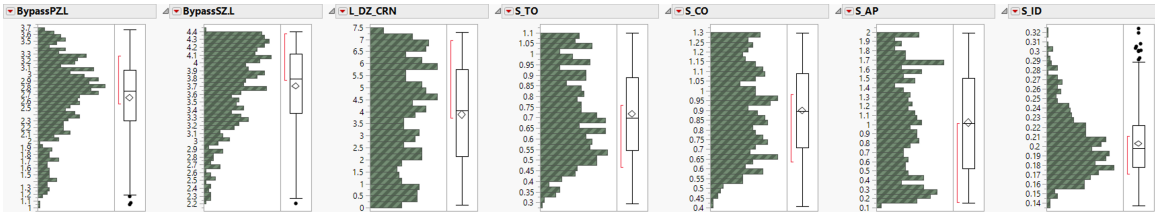

Figure 6.14: Distribution and trend after filtering

In Figure 6.13, the light colored histograms are the distribution of values of the design variables when $\pm$ 10 g/kg filtering range is applied to all emission indices. The dark color histograms are the distributions for $\pm$ 5 g/kg filtering range. Figure 6.14 shows the distributions for $\pm$ 5 g/kg filtering range alone. These two figures show the response of output distributions when filtering is applied. As the narrower filtering range is applied, the distributions reveal the trends which are not available before filtering is applied. In Figure 6.14, it is observed that l_{PZ} prefers values around 2.8 inches, l_{SZ} prefers larger values, S_{TO} prefers value near the lower bound, S_{CO} does not prefer values near the lower bound, and S_{ID} prefers values around 0.16 - 0.21.

Distributions of design values in the other three groups show some specific trends when a filtering technique is applied. When the preferred ranges of design variables from all four groups are overlapped, very small ranges of design variables are observed. The middle of these ranges are selected as design values of length parameters and unmixedness parameters. The final selection of design values are in Table 6.8 and the corresponding emission performances are in Table 6.9.

Table 6.8: Length and unmixedness of combustor M

L_{PZ}	L_{SZ}	L_{DZ}	S_{TO}	S_{CO}	S_{AP}	S_{ID}
2.75	9.90	2.56	0.65	0.97	1.70	0.19

Table 6.9: NOx and CO characteristics after modeling length and unmixedness

	EINOx				EICO			
	TO	CO	AP	ID	TO	CO	AP	ID
CFM56-7B27/3	23.94	17.89	9.09	4.36	0.31	0.17	2.82	29.39
Engine M	22.60	17.54	10.23	0.01	0.10	0.04	4.63	32.24

6.2.5 Adjustment of Soot Formation Mechanism

Even though the combustor model, mixing characteristics, and volumes are modeled for Engine M cycle, the integrated environment is not ready to predict soot. The current version of prediction environment does not predict soot correctly because of uncertainties embedded in the soot formation mechanism.

$$C_2H_2 \rightarrow 2C_{(s)} + H_2 \tag{6.23}$$

Equation (6.23) is one of traditional models of soot inception phase. Values of pre-exponential factor and the activation energy are not agreed in many different studies even in this simple model.

Disagreement in parameters in the phases of the soot formation mechanism is common. Because of the uncertainties due to the variability in these parameters, the soot formation mechanism is often modified by the user in soot studies. For instance, Martini[28] applied multiplicative constants, ranging over three orders of magnitude from 0.01 to 10, to each soot formation phase. The growth mechanism adopted by Bisson et al.[30] consists of four reactions. They had to multiply 0.01 to all four reactions in order to reduce errors of predicted soot amount. Because the specific reaction rate constants in different reactions are multiplied to each other when the expressions are rearranged to form a soot formation rate, the effect of multiplicative constant 0.01 is enormous.

The inception rate expression adopted in the Soot Evaluation Model is introduced by Colket and Hall[86]. They multiplied 8 to their inception rate in order to match the experimental measurement.

The surface growth rate in the SEM model is suggested by Kim et al.[84]. They eliminated one of the reactions from the growth mechanism of Colket and Hall[86]. This elimination significantly changes the soot growth rate because the pre-exponential factor of the eliminated reaction is relatively large among reactions in their mechanism.

The oxidization model has a collision efficiency in the oxidization rate expression. This parameter includes high uncertainties because various studies report large variability.

The coagulation rate expression has agglomeration constant. From one to eight, various values are reported for the value of this constant.

Because of uncertainties in the soot formation mechanism, correction factors are applied in the current model. In order to maintain the original forms of the mechanism and not to modify chemically important parameters such as the activation temperature, a linear coefficient is applied to each phase. They are corr_inc, corr_gr, corr_oxi, corr_coag.

Repeated design of experiments are performed followed by surrogate modeling, Monte-Carlo simulations, and adjustment of design range of correction factors. After several repetitions of this process, a surrogate model relating correction factors to the soot quantity is established. With this surrogate model, Monte-Carlo simulation of 20,000 sample points, whose design values are uniformly distributed, is performed. A filtering technique is applied to the simulation results. The filtering ranges are determined by the maximum and minimum quantity of soot estimated by five correlations for Engine M, introduced in the previous section (see Figure 6.7 and Figure 6.8).

In order to select a set of correction factors minimizing the change of the original soot formation mechanism, an objective function is established, as in Equation (6.24)

$$obj = \sqrt{\sum_{inc.,gr.,oxi.,coag} (log\ corr)^2} \tag{6.24}$$

Log scale is used because the multiplications of 10 and 0.1 are equivalent in the order of magnitude scale.

When the filtering is applied to the objective function value, values of the correction factors converge well. Therefore, no optimization is required in this step. The set of correction factors whose objective function value is the smallest is selected. The selected correction factors are listed in Table 6.10.

Table 6.10: Applied correction factors of soot formation mechanism

corr_inc	corr_gr	corr_oxi	corr_coag
0.05	0.45	0.02	1

6.2.6 Baseline Result and Sensitivity Study

The baseline of the Combustor Flow Circuit Model is modeled. The volume and the unmixedness for the Engine M cycle are also modeled. The soot mechanism is adjusted against correlation results. The integrated environment is ready to predict soot. This is the baseline. The results are in Table 6.11. Predicted emission indices of soot from Engine M is also illustrated in Figure 6.15 with estimated EI soot of CFM56-7B27 engine from five correlations.

Table 6.11: Predicted emission index of non-volatile PM emitted from notional Engine M

Power mode	EI non-volatile PM (mg/kg)
Take-off	141.61
Climb out	138.48
Approach	13.18
Idle	0.0

The emission indices of soot are well predicted within the expected range estimated by various correlations. Zero soot is predicted at the idle condition. This is in agreement with FOA3 and FOAst methods. The measured smoke number of CFM56-7B27 engine at Idle, reported in ICAO Emissions Databank[94], is zero.

Figure 6.16 illustrate baseline results in log scale. This figure demonstrates the good predictability of the environment. Because this is log scale and the log of zero is negative infinity, predicted EI from baseline and estimated EI from some correlations are not shown in this figure.

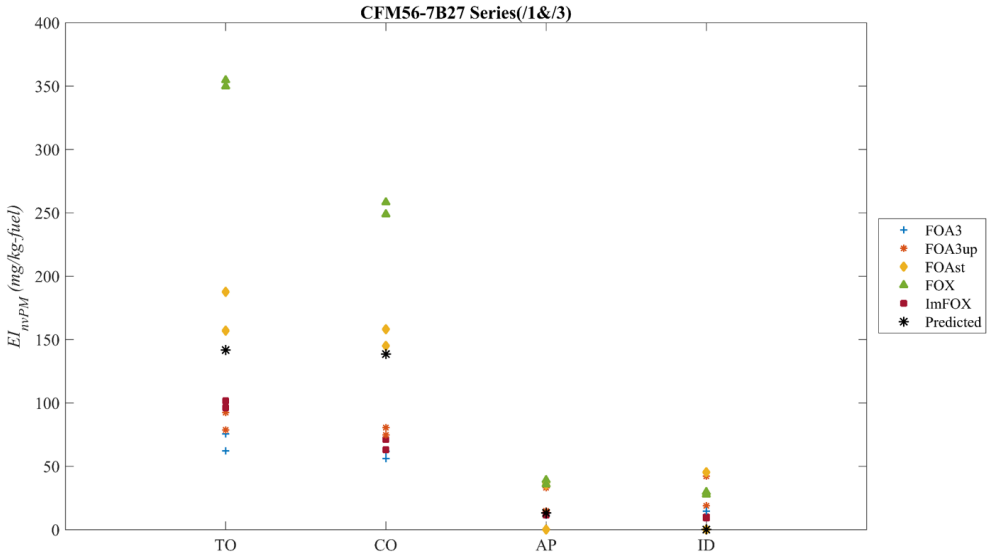

Figure 6.15: Predicted emission index of non-volatile PM emitted from notional Engine M

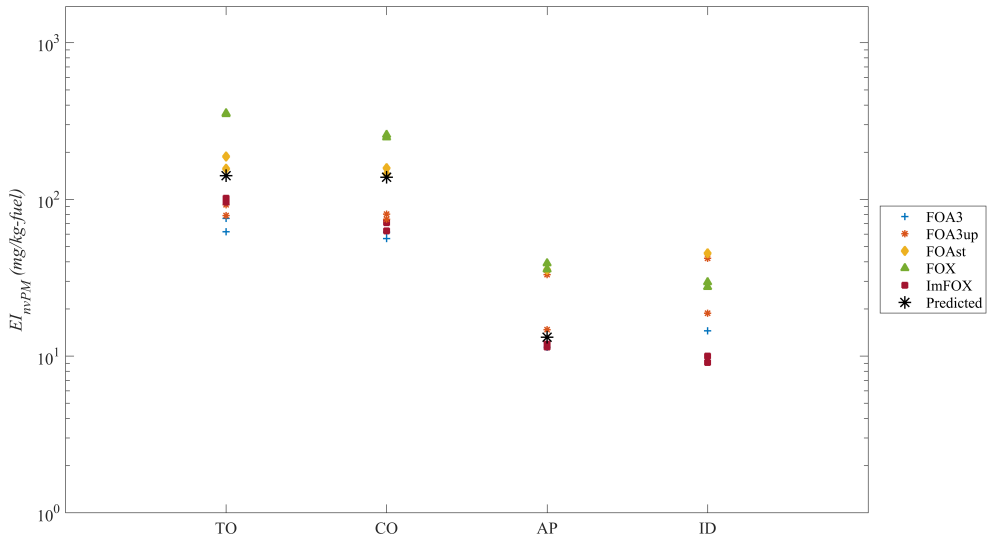

Figure 6.16: Predicted emission index of non-volatile PM emitted from notional Engine M in log scale

As the baseline model shows good predictability for given Engine M cycle, the next step is to extend the environment so that it is capable of a variety of cycles. However, before

it is extended for further capability, the sensitivity study should be performed so that the minor parameters not contributing much to soot prediction are excluded in the following modeling.

Two types of sensitivity studies are conducted. The first one is to perturb each design variable $\pm 5\%$ from a baseline value one by one. Total 24 design variables in the CFC model, the SDM model, and the SEM model are perturbed. The sensitivity is defined as

$$Sensitivity \equiv \frac{\% \text{ change in EIsoot}}{\% \text{ change in design variable}} \tag{6.25}$$

The evaluated rank of sensitivities of design variables are listed in Table 6.12.

Table 6.12: Sensitivity rank of design variables

	TO	CO	AP	ID
Diffuser.plc	17	17	14	12
Diffuser.MNout	21	23	19	17
SplitterPri.MNout_01	12	4	1	1
SplitterPri.MNout_02	14	13	4	13
InletPZ.MNout	3	3	8	5
epsPZ	23	20	18	16
BurnerPZ.AR	7	6	11	4
BypassPZ.l	19	21	15	14
BypassPZ.L	2	2	9	19
BypassPZ.fric	20	22	16	15
BypassPZ.AR	13	14	5	11
HoleSZ.A_h	4	5	2	2
BypassSZ.L	5	8	10	18
BypassSZ.AR	22	19	12	6
HoleDZ.A_h	15	15	3	3
BurnerSZ.AR	10	12	17	8
BurnerDZ.AR	18	18	21	24
c_range	9	11	13	9
nn	24	24	24	22
L_DZ_CRN	16	16	20	23
Cal_inc	11	10	6	7
Cal_gro	1	1	22	21
Cal_oxi	6	9	7	10
Cal_coag	8	7	23	20

nn is the number of slices in the statistical distribution model. As the sensitivity of this parameter is in low rank, it can be concluded that nn is large enough to maintain the continuous characteristics of the distribution. The width of the outer annuli (l) and the friction coefficient in the duct element (fric) are expected to vary for different cycles. However, as they show low sensitivities, the baseline values of these two variables are used for all other cycles. The value of epsPZ, the combustion efficiency of the primary zone or the fuel consumption fraction is from literature[43]. Due to the low sensitivity of eps variable, the same baseline value can be used for all cycles. The high sensitivity ranks of the lengths of the primary and the secondary zone prove that the sizing methodology is required.

The same conclusions are made from the second sensitivity study. For the second sensitivity study, a hundred Latin Hypercube design samples are simulated within the range of $\pm 5\%$ from the baseline. The predictor screening function in JMP[103] is utilized to identify the contribution of each design variable to EIsoot results. The predictor screening utilizes the partition algorithm. The results are demonstrated in Figure 6.17. The importance of sizing methodology is also found in this study. nn, l, fric, and eps parameters show low sensitivity again in this study.

	EIBC_TO			EIBC_CO			EIBC_AP			EIBC_ID		
Predictor	Contribution	Portion	Rank	Contribution	Portion	Rank	Contribution	Portion	Rank	Contribution	Portion	Rank
Diffuser.plc	111.68	0.0068	20	103.62	0.0082	21	3.2903e-7	0.0161	17	1.953e-11	0.0071	21
Diffuser.MNout	110.17	0.0067	21	109.36	0.0087	20	4.0285e-7	0.0197	15	9.821e-11	0.0356	6
SplitterPri.MNout_01	195.17	0.0119	16	612.32	0.0485	4	8.8052e-6	0.4296	1	1.1434e-9	0.4147	1
SplitterPri.MNout_02	144.59	0.0088	17	261.41	0.0207	7	5.5237e-7	0.0270	8	9.205e-11	0.0334	7
InletPZ.MNout	3163.91	0.1923	3	1940.48	0.1537	3	1.8264e-7	0.0089	22	5.675e-11	0.0206	10
epsPZ	291.73	0.0177	13	209.82	0.0166	11	4.2061e-7	0.0205	13	1.185e-11	0.0043	24
epsSZ	202.53	0.0123	15	195.59	0.0155	12	4.6125e-7	0.0225	9	2.058e-11	0.0075	20
BurnerPZ.AR	232.59	0.0141	14	239.79	0.0190	10	2.6501e-7	0.0129	20	7.704e-11	0.0279	8
BypassPZ.l	62.49	0.0038	25	156.38	0.0124	16	4.3098e-7	0.0210	11	3.501e-11	0.0127	17
BypassPZ.L	3446.33	0.2094	2	3125.29	0.2475	2	7.5667e-7	0.0369	4	1.783e-10	0.0647	4
BypassPZ.fric	337.73	0.0205	12	167.67	0.0133	15	1.3706e-7	0.0067	25	4.461e-11	0.0162	12
BypassPZ.AR	381.87	0.0232	10	331.76	0.0263	5	7.2625e-7	0.0354	5	1.251e-10	0.0454	5
HoleSZ.A_h	604.17	0.0367	6	139.68	0.0111	19	1.5545e-6	0.0758	2	3.417e-11	0.0124	18
BypassSZ.L	357.81	0.0217	11	146.00	0.0116	18	2.5367e-7	0.0124	21	3.768e-11	0.0137	15
BypassSZ.AR	74.77	0.0045	24	168.82	0.0134	14	1.5101e-7	0.0074	23	3.051e-11	0.0111	19
HoleDZ.A_h	459.21	0.0279	8	176.25	0.0140	13	1.3239e-6	0.0646	3	2.809e-10	0.1019	2
BurnerSZ.AR	673.01	0.0409	5	258.56	0.0205	8	3.7885e-7	0.0185	16	1.63e-11	0.0059	22
BurnerDZ.AR	117.03	0.0071	18	80.10	0.0063	25	6.5834e-7	0.0321	6	6.05e-11	0.0219	9
c_range	106.50	0.0065	22	92.82	0.0073	23	4.154e-7	0.0203	14	1.065e-11	0.0039	25
nn	111.78	0.0068	19	99.94	0.0079	22	2.8663e-7	0.0140	19	1.927e-10	0.0699	3
CRN.Inputs.DZ_PFR.L_DZ_CRN	477.98	0.0290	7	153.75	0.0122	17	1.5023e-7	0.0073	24	4.098e-11	0.0149	14
Cal_inc	101.52	0.0062	23	91.80	0.0073	24	4.5766e-7	0.0223	10	5.537e-11	0.0201	11
Cal_gro	3582.39	0.2177	1	3206.82	0.2539	1	3.2102e-7	0.0157	18	1.478e-11	0.0054	23
Cal_oxi	710.32	0.0432	4	245.66	0.0195	9	4.2884e-7	0.0209	12	3.574e-11	0.0130	16
Cal_coag	397.21	0.0241	9	315.22	0.0250	6	6.4525e-7	0.0315	7	4.444e-11	0.0161	13

Figure 6.17: Sensitivity of design variables

Based on the results of sensitivity studies as reference information, design variables

showing low sensitivity are excluded from the further modeling.

6.3 Extension of Environment

After the sensitivity study, the baseline prediction environment is extended to handle different cycles. Because the unmixedness parameter values are found for the baseline conditions, a generalized unmixedness curve is applied to the preiction environment. The geometry is also scaled for different input cycles.

6.3.1 Unmixedness Curve

With the aid of statistical techniques and optimization, the unmixedness values are achieved for the four different power settings of Engine M model. However, this discovery does not mean that the unmixedness issue is entirely resolved. The found values are different for different inlet conditions of the combustor. The different engine cycles as well as the different power settings other than the ICAO LTO cycle will cause different unmixedness values. Therefore, the unmixedness parameter needs to be a continuous function corresponding to the condition of the primary zone.

Abrahamson et al.[101] argue that the thrust and the fuel flow rate are the parameters involving the mixing effect of the flow inside the combustor because the thrust determines the fuel flow rate, the fuel flow rate affects the equivalence ratio of the combustion zones, and the equivalence ratio affects the mixing characteristics of the flow. Therefore, it is a reasonable approach to relate the unmixedness to the fuel-to-air ratio of the flow. This approach is commonly applied to many studies in emission research [28][36][57][60][61][62][63][64][65][66][68]. Figure 4.8 is one of the examples of the unmixedness curve. In this research, the unmixedness curve is created as a function of the equivalence ratio of the primary zone.

The found values of unmixedness parameter are interpolated for the corresponding equivalence ratios of the primary zone. When the unmixedness curve is created from the experimental measurement, the regression method is preferred because the measured sam-

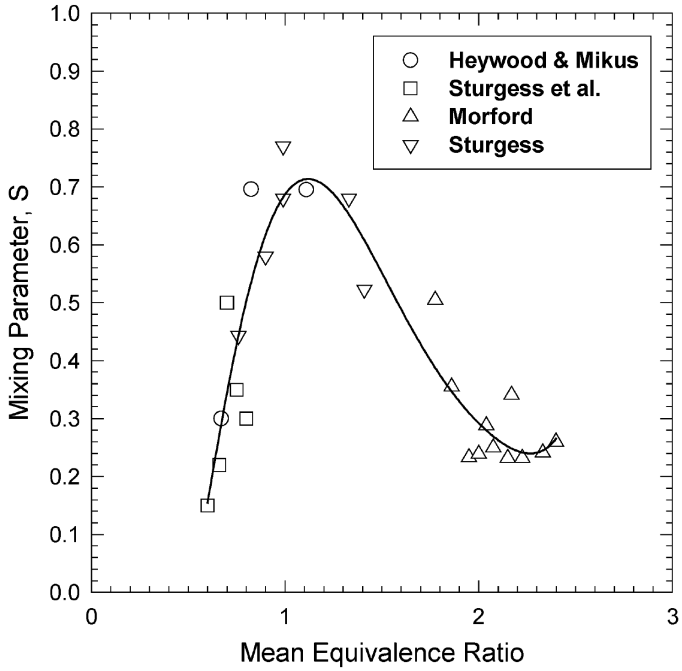

Unmixedness Curve by Sturgess et al.[64] (repeated from Figure 4.8)

ples are scattered due to the measurement uncertainties, forming a trend. However, as the found four sample points are from the baseline model, these values are valid only for baseline soot results. Therefore, the four sample points are deterministic values for the soot results in this simulation environment. For this reason, the interpolation technique is adopted instead of the regression method.

As one of the simplest methods, the linear interpolation can be tried if the sample points are closely placed in the equivalence ratio domain. However, there are just four samples and their deviations of unmixedness values are not small. The use of the linear model will not capture the adequate trend of unmixedness in the equivalence ratio domain. Furthermore, it will add severe discontinuity to the parametric prediction environment. Therefore, the continuous interpolation method must be considered.

Because the number of the samples are four, the third-order polynomial interpolation is one of the available continuous methods. However, when this method is applied and tested for given samples, an oscillating curve through the sample points, implying overfitting, is observed.

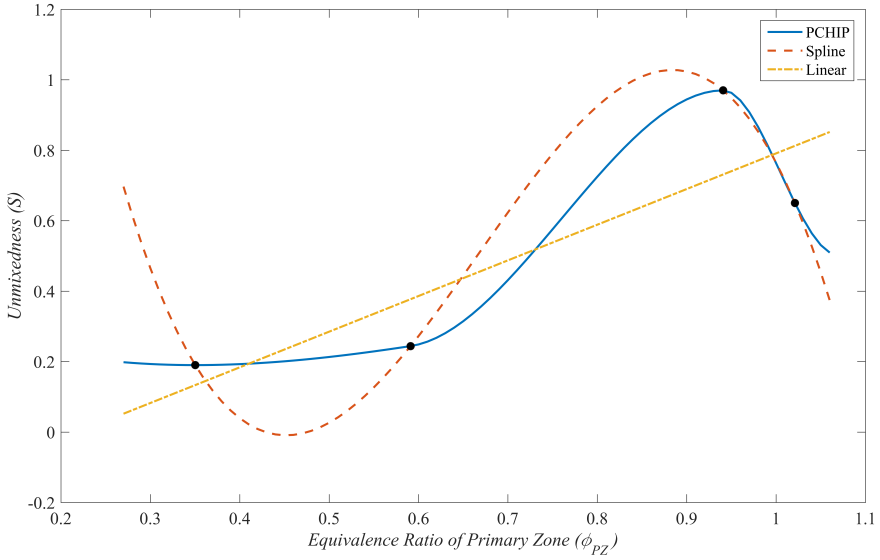

Figure 6.19: Comparison of Interpolation Functions

The cubic spline method is another method considered. It is a piecewise method consisting of third-order polynomials. It creates a smooth curve with less possibility of Runges phenomenon. The first- and the second-order derivatives of the created spline curve are continuous. However, this method is not completely free from overfitting for given samples of unmixedness. The results are the same as the third-order polynomial method because there are only four samples.

The next considered and selected interpolation method is a piecewise cubic Hermite interpolating polynomials. This method is also based on the third-order polynomials as the spline method is. However, one of the conditions, continuous second-order derivatives, is eliminated[105]. This modification significantly reduces the oscillation of the curve while keeping the curve smooth.

Figure 6.19 compares the standard cubic interpolation function and the piecewise cubic Hermite interpolating polynomials function as well as the linear regression model. This comparison was performed during the baseline modeling processes before the unmixedness values for the Engine M model is not finalized.

The yellow straight line is created by the linear regression. At a glance, this line reason-

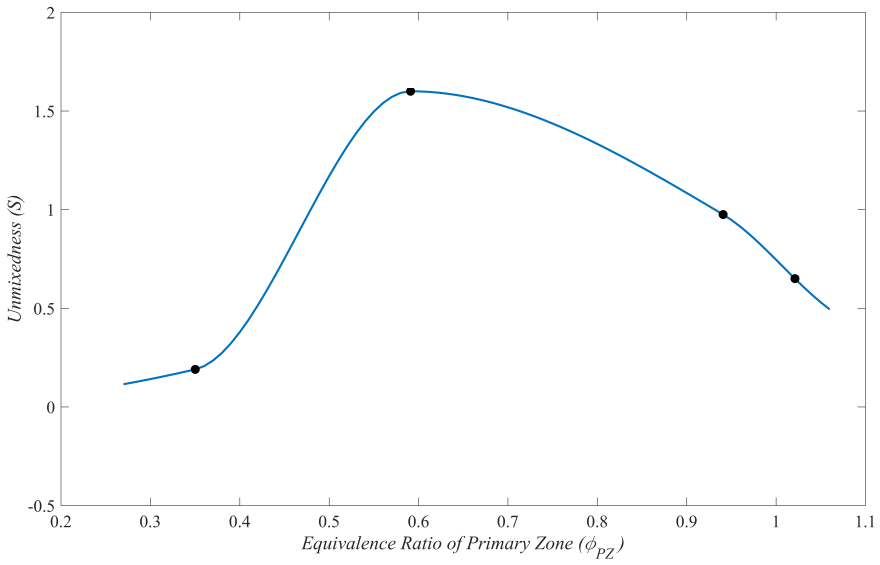

Figure 6.20: Created Unmixedness Curve

ably represents the variation of unmixedness for the change of equivalence ratio. However, the errors at the sample points are not negligible. For instances, the unmixedness deviation at the climb out power is more than 0.2, large enough to cause significant deviation in the soot result.

The red dotted line highly curved and goes to the negative unmixedness region is created with the spline function. The variation of unmixedness is too much drastic for the equivalence ratio lower than 0.6. The negative value of the unmixedness is not physically possible because the definition of the unmixedness is the standard deviation divided by the mean value. The standard deviation is always positive, and the mean of the equivalence ratio, a normalized fuel-to-air ratio, is also positive.

The solid blue line is created from the piecewise cubic Hermite interpolating polynomials function. The variations of unmixedness between sample points are smooth. The curve shape is overall smooth while there are no signs of overfitting.

Figure 6.20 illustrates the finalized unmixedness curve with four calibrated samples. There is one more sample point used to generate this curve. The unmixedness for the leaner equivalence ratio than the idle value must be extrapolated due to the lack of samples

for this region. Because the unmixedness of the idle power is low close to zero, the negative values can be leaded in extrapolation. To avoid negative unmixedness, (0, 0) sample point is additionally included in interpolation. However, the cubic spline method still created highly oscillating curve going through the negative unmixedness between the idle and the zero-equivalence-ratio region. On the other hand, with the added sample, an unmixedness curve for the prediction environment is successfully created from the piecewise cubic Hermite interpolating polynomials function, as shown in Figure 6.20. Once the input cycle is given, the Combustor Flow Circuit model calculates air partitions. The calculated air flow rate of the primary zone and the fuel flow rate are passed to the statistical distribution (SDM) model. Then, the SDM model calculates the unmixedness value for the given input cycle from the created unmixedness curve.

6.3.2 Sizing Methodology

The unmixednesses and the lengths of the different combustion zones are achieved via the calibration process. The integrated environment can now predict the soot from Engine M cycle. When a different cycle is provided, all sub-models in the prediction environment(the circuit flow mode, the statistical distribution model with implemented unmixedness curve, the chemical reactor model, the mechanism generator, and the emissions evaluation model) are working together to compute predicted soot emission. However, the environment is not fully parametric yet. The computed prediction soot result will not correspond to the provided cycle because the size of the combustor for a given cycle is not considered.

As it is addressed in the previous chapters, the amount of the soot produced and oxidized depend on the residence time. An adequate volume correctly corresponding to the cycle must be considered in the soot prediction. This issue is addressed via Hypothesis II.

Hypothesis II

In order for a soot prediction model to be applied to different engine cycles, it must contain a sizing methodology.

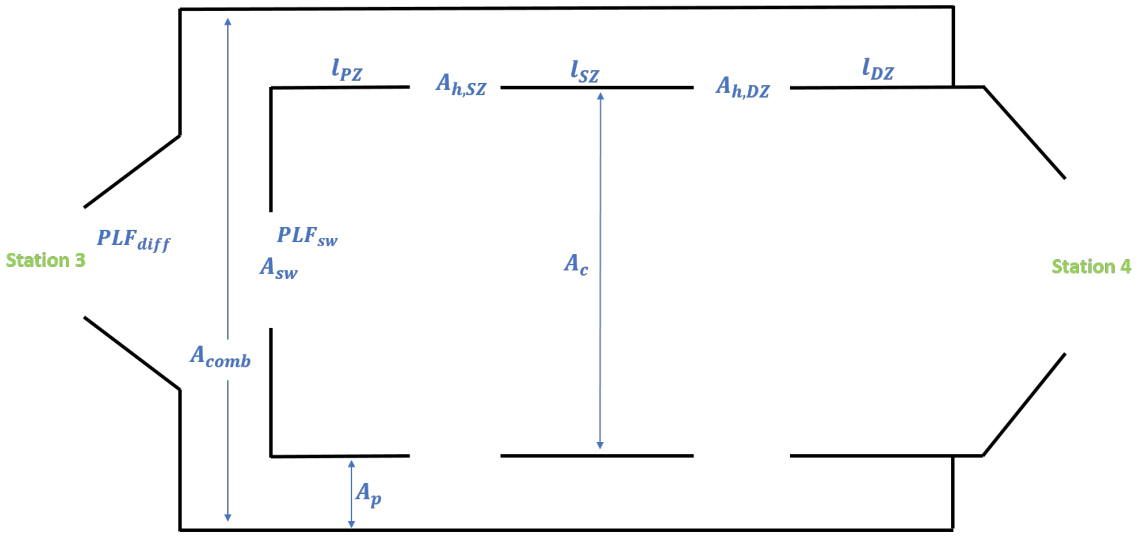

Schematic representation of combustor with some design variables (repeated from Figure 4.8)

In Figure 6.21, the factors determining volumes are the cross-section areas (A_{comb}, A_{sw}, A_p, A_c) and the lengths of the combustion zones (l_{PZ}, l_{SZ}, l_{DZ}). The cross-section areas of the primary, the secondary, and the dilution zones are A_c as the area ratio of these zones are set to unity in order to maintain the simplicity of the analysis. In addition to these factors, the hole size ($A_{h,SZ}$, $A_{h,DZ}$) must be scaled so that the air partitioning is adequately determined for the given cycle.

In the old literature, the theta parameter and the combustor loading parameter are interchangeably used. It is defined as[47]

$$CLP = \theta = \frac{P_{t3}\, A_{ref}\, H\, e^{\frac{T_{t3}}{b}}}{W_3} \tag{6.26}$$

This parameter has been correlated with combustion efficiency in many studies[34][42][47][81]. One of the advantages of this parameter for the combustor designers is that it

correlates efficiency to the cycle and the geometry of the combustor.

The coefficient b is a function of an equivalence ratio[81].

$$b = 220\left(\sqrt{2} \pm ln\frac{\phi}{1.03}\right) \tag{6.27}$$

After correlating theta parameter to 22 test points from several types of combustors, Lefebvre and Halls[106] slightly modified the form of theta parameter. They assigned 300 Kelvin to the coefficient b and 0.75 to the exponent of H. Their theta parameter is

$$\theta = \frac{P_{t3}^{1.75}\ A_{ref}\ H_{ref}^{0.75}\ e^{\frac{T_{t3}}{300}}}{W_3} \tag{6.28}$$

Even though the theta parameter involves both geometry factors and cycle parameters, this expression is not useful to size the current soot prediction environment because the involved geometry factors are the cross-section area and the height of the combustor. The Combustor Flow Circuit model handles the cross-section area based on the design Mach number. The factor required for sizing is either volume or length. Theta parameter cannot be utilized for current sizing issue. However, there are several parameters whose form is similar to theta, involving volume and cycle.

Lefebvre and Ballal[34] introduced a stirred reactor model based on the analysis of the reaction rate in addition to the theta parameter. This model looks similar to the theta, but it has volume in it instead of area and height. This parameter is also called theta in many studies. It is defined as

$$\theta = \frac{P_{t3}^{1.75}\ V\ e^{\frac{T_{t3}}{300}}}{W_3} \tag{6.29}$$

Because of the volume factor included in this expression, this form of theta is widely adopted in many sizing applications[34][43][107][108].

Walsh and Fletcher[41] introduced a parameter for sizing of a combustor, called combustor loading(CL). It is defined as

$$CL = \frac{W_3}{VP_{t3}^{1.8} 10^{0.00145(T_{t3}-400)}} \tag{6.30}$$

This parameter looks similar to the inverse of the theta introduced in Equation (6.29) because the combustor loading is also derived from the kinetic theory. The theta and CL derive similar but slightly different volumes.

Walsh and Fletcher introduced Combustion Intensity(CI) as one of the factors considered in sizing. The combustion intensity is a measure of the heat release rate per unit volume of the combustor. The CI is applied to the sea-level-static maximum rating condition to set the minimum volume[41].

$$CI = \frac{W_3 \, \eta_{comb} \, LHV}{VP_{t3}} \tag{6.31}$$

The volume of the total combustor and the volume of the primary zones are separately sized, in general, because the requirements are different[41]. In order to ensure high combustion efficiency, the whole volume is considered because the whole combustor is responsible for the heat release required for engine operation. The primary zone volume is considered for the stability requirement because the area where combustion starts is the most vulnerable point. Once the stable combustion starts at the primary zone, the lean blow out is not an issue at the downstream. For this reason, the inlet properties are applied to size the whole volume and the primary zone properties calculated in the CFC model is applied to the sizing of the primary zone.

These three parameters are measures of a minimum volume satisfying combustor requirements such as heat release, combustion efficiency, and stability. There are more factors to be considered in combustor including ignition, mixing, and emissions. The actual loading and intensity are not available at the conceptual design phase. Nevertheless, it can

be assumed that the theta parameter, the combustor loading, and the combustion intensity of the combustors in the same technology level are close. Based on this assumption, the scaling from the reference combustor is available. If the theta is used for scaling,

$$V_i \approx V_{ref} \left(\frac{W_i}{W_{ref}} \right) \left(\frac{P_{t,ref}}{P_{t,i}} \right)^{1.75} e^{\frac{\left(T_{t,ref} - T_{t,i}\right)}{300}} \tag{6.32}$$

If the combustor loading is used for scaling,

$$V_i \approx V_{ref} \left(\frac{W_i}{W_{ref}} \right) \left(\frac{P_{t,ref}}{P_{t,i}} \right)^{1.8} 10^{0.00145\left(T_{t,ref} - T_{t,i}\right)} \tag{6.33}$$

If the CI is used for scaling, as the low heating value of the fuel and the combustion efficiency can be assumed to be identical for the same technology level of the combustors, the scaling expression is

$$V_i \approx V_{ref} \left(\frac{W_{f,i}}{W_{f,ref}} \right) \left(\frac{P_{t,ref}}{P_{t,i}} \right) \tag{6.34}$$

Because all three parameters are widely accepted in sizing analyses, the average volume derived from three scaling is applied to new cycles. Both theta parameter and the combustor loading are closely related to the combstion efficiency and stability because they are derived from a simple analysis of global reaction rate. High reaction rate is advantageous to both efficiency and stability. Due to the low temperature and pressure, the stability efficiecy issues arise the most during the low power operation. For this reason, the idle oprating power or the windmilling condition is the design point for sizing, in general. Therefore, the idle power condition, one of four available power modes, is selected for the sizing point when theta parameter and the combustor loading are used in the current research. For sizing utilizing the combustion intensity, however, the take-off power mode condition is used because the high efficiency close to 100% is a strong requirement for the high power operation mode.

When the scaling rules in Equation (6.32) - (6.34) are applied, the new volume corresponding to the input cycles is computed and applied to SDM, CRN, and SEM models. The change of volume size results in large changes in soot prediction. The effects of sizing methodology are demonstrated in the latter chapter when the hypotheses are evaluated. After scaling, the volume of Engine S, whose thrust and flow rate are smaller than the reference engine, becomes 75% of the reference volume. The scaled volume of the Engine L engine, whose thrust and flow rate are larger than the reference engine, increases 65% from the reference volume.

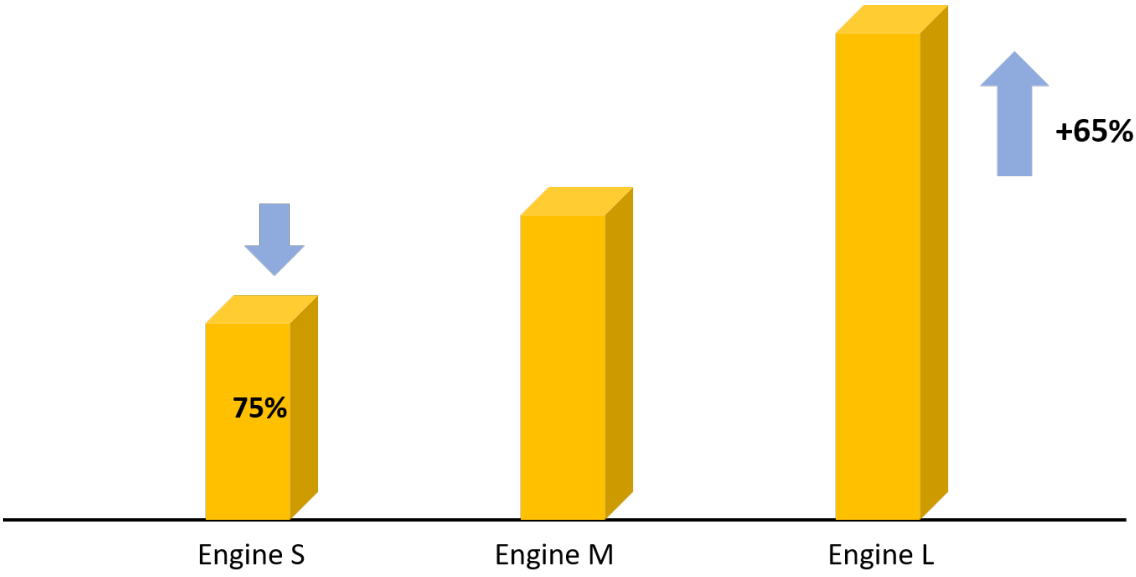

Figure 6.22: Volume change after scaling

Another essential factor to be sized is the hole area. The secondary and the dilution airs are introduced through the holes. Without appropriate sizing of the hole area, air partitioning cannot be correctly achieved for different cycles.

The purpose of the holes is to introduce the huge amount of the secondary air into the combustion zone. The introduced air occupies the combustor volume. It can be argued for the appropriately designed combustor that the more air is introduced through the hole as the combustor volume is larger. From this argument, a proportional relationship can be

assumed between the combustor volume(V) and the volumetric flow rate of the secondary air(Q_h).

$$V_{combustor} \sim Q_h \tag{6.35}$$

The volumetric flow rate is the product of the cross-section area and the flow speed. The normalized non-dimensional flow speed, Mach number of the hole flow is one of the design factors. It is a designers choice ensuring efficient mixing of the secondary air and the combustion product gas from the upstream. As other components in the combustor have their acceptable range for Mach number, the hole flow also has its Mach number range similar for the combustors in the similar technology level. Therefore, if the Mach number is a constant factor, the flow speed(U) can be assumed to be proportional to the square-root of T_{t3}.

$$U = MN_h\sqrt{\gamma R\, T_h} \qquad \text{and} \qquad U \sim \sqrt{T_{t3}}$$

Therefore, from Equation (6.35),

$$V_{combustor} \;\sim\; A_h U \;\sim\; A_h\sqrt{T_{t3}}$$

and

$$A_h \sim \frac{V_{combustor}}{\sqrt{T_{t3}}}$$

From this relationship,

$$A_h = A_{ref}\left(\frac{V_{combustor}}{V_{ref}}\right)\sqrt{\frac{T_{ref}}{T_{t3}}} \tag{6.36}$$

Equation (6.36) scales the hole area based on the reference area, volume, and temperature. The reference values are from the baseline engine model (Engine M).

CHAPTER 7

CONCLUSION AND DISCUSSION

7.1 Validation and Evaluation

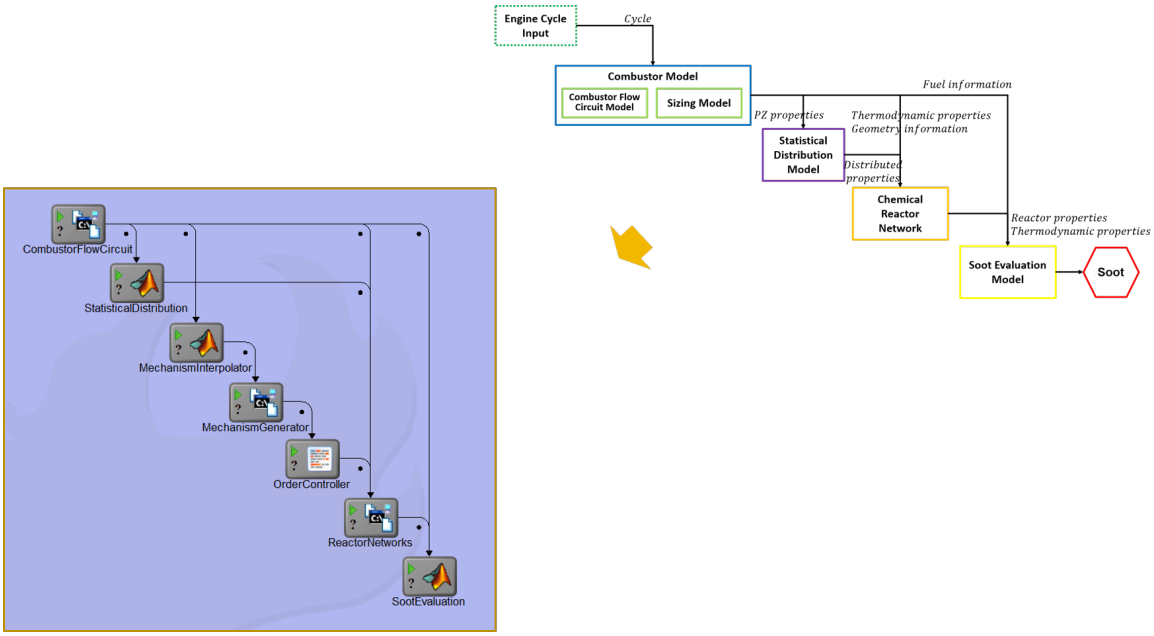

Figure 7.1: Integrated Prediction Environment

As the unmixedness curve and the sizing methodology are implemented, the automation process of soot prediction is ready for input cycles. The predicted emission indices of soot from notional Engine L, M, and S are listed in Table 7.1. They are also demonstrated in Figure 7.2 with estimated EI nvPM from CF6-80C2, CFM56-7B27, and CF34-8C5 engine series. Predicted values are in black markers. The estimated EIs from correlations are illustrated together in colored markers. Different correlation estimations are in different colors.

Table 7.1: Emission indices of non-volatile PM from notional Engine L, M, and S

	Engine L	Engine M	Engine S
Take-off	121.34	141.61	146.73
Climb out	124.62	138.48	128.35
Approach	10.98	13.18	10.39
Idle	0.00	0.00	0.00

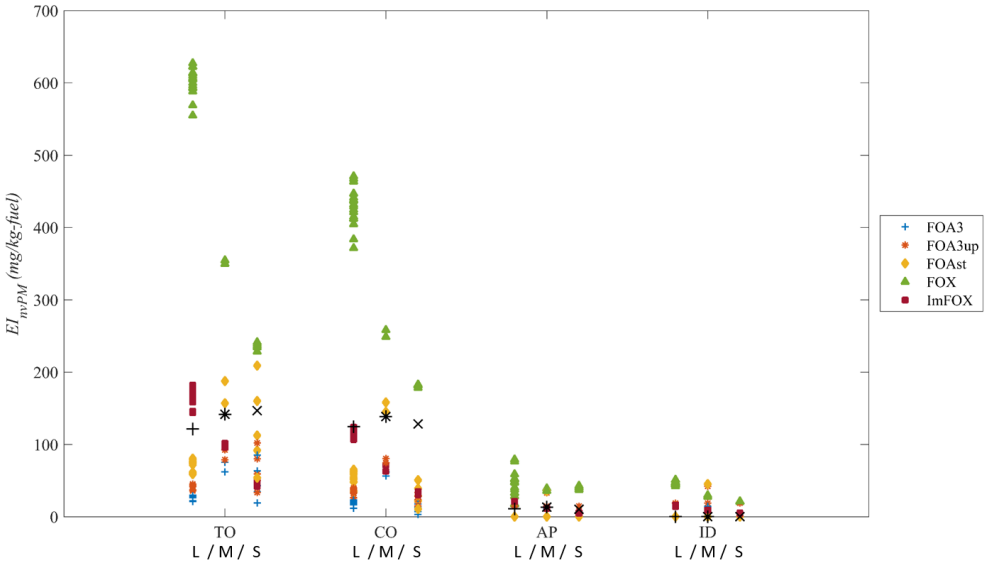

Figure 7.2: Emission indices of non-volatile PM from notional Engine L, M, and S

The predicted soot quantities are well placed within the ranges estimated by correlations. Due to the difficulties and uncertainties in soot prediction, the predicted amount of soot is often compared in the order of magnitude scale with deviations within a few orders of magnitude[28][29][30]. Nevertheless, the prediction environment shows successful predictions in Figure 7.2.

No soot is predicted at the idle power for all three notional engine cycles. In the ICAO emissions databank[94], the smoke numbers of CFM56-7B27 engine and all series of CF6-80C2 and CF34-8C5 engine variations at the approach and idle power are zero. This means

that these engines actually produced no or almost no soot and the stain is not detected in the filter during the certification process.

The number of black carbon particles predicted by the developed prediction environment is in the order of 10^{16} per kg of fuel at the take-off power. The mean size of the particles is approximately 20 nm in diameter at take-off power. The number and the mean size of the particles are in good agreement with APEX measurement data[96][100].

The trend of soot for different thrust is not observed while the trend of soot by different power are shown in Figure 7.2. The more soot is produced at high power settings at low power settings. These trends are in good agreement with APEX measurement. In APEX campaign, more soot is generally measured during high power operations and less soot is measured at low power operations. This is a general trend, but not a strict trend. More soot is often observed at the climb out power than at the take-off power and less soot is also often measured at the approach power than at the idle power, during APEX campaign. Measured black carbon data is in the appendix with estimated emission indices from correlations.

There are not much difference in EIs for different engine cycles regardless their different thrust, pressure ratio, and mass flow rates. This is because the computations of air partitioning and sizing are applied. For example, the higher EI is predicted without the air partitioning and the lower EI is expected without sizing for the high power of Engine L cycle. In contrast, the smaller EI is predicted without the air partitioning and the higher EI is expected without sizing for the high power of Engine S cycle. As a result of air partitioning and sizing, three engine EIs are in the similar level. These effects of air partitioning and sizing are discussed in the latter section with experiments.

The predicted emission indices of soot are also in Figure 7.3 in log scale. The predictability of the environment is observed better in this log scale figure as the correlation-estimated values form noticeable clouds. Note that the log scale plot has long tails to the low EI values because the log of zero is negative infinity. As addressed, the smoke numbers of most engines referenced for comparison in this research are zero at the approach and idle

power modes, in the ICAO emissions databank. 25 engines among 26 engine data in EDB used for the correlation estimation show zero SN in the approach and idle power modes. The estimations by FOA3 method and FOAst method, which are based on the smoke number, are zero for zero smoke number at low power. For this reason, the predicted soot at idle power and estimated soot by FOA3 and FOAst correlations at the approach and idle power are not shown in Figure 7.3.

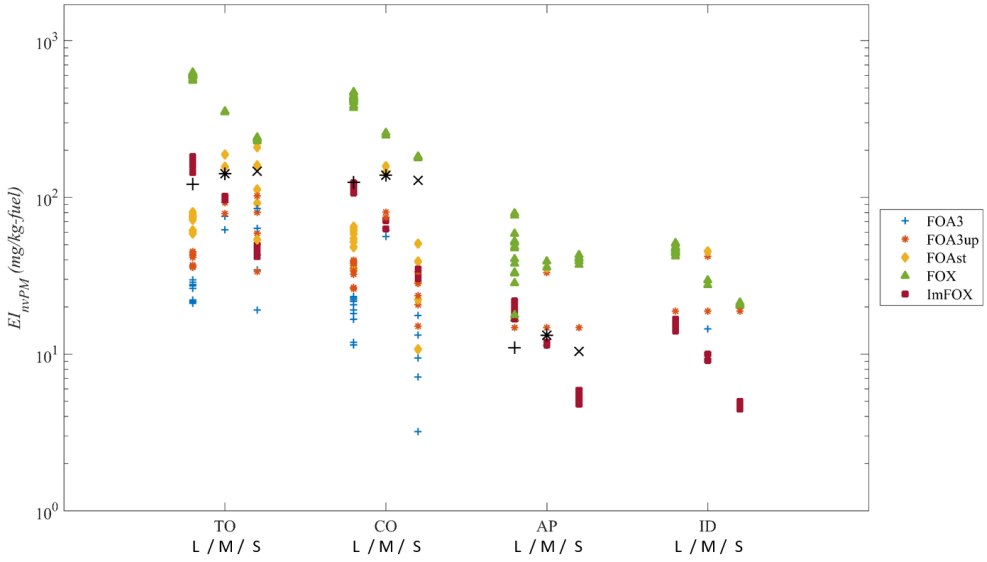

Figure 7.3: Emission indices of non-volatile PM from notional Engine L, M, and S in log scale

The predicted EIs are generally located between the SN-based correlation estimations and the thrust-based correlations. The First Order Approximation version 3.0 method, the current standard method of estimating the effect of non-volatile PM emitted from the aircraft currently in operation[98], is criticized by many studies that it significantly underestimates the mass of the non-volatile PM[97][98][101]. The thrust-based methods such as FOX and ImFOX methods are developed due to the under-estimation issue in FOA methods and the uncertainties in Smoke Number. The prediction environment predicts Emission Index of non-volatile PM in the middle level of the correlation estimations, demonstrating

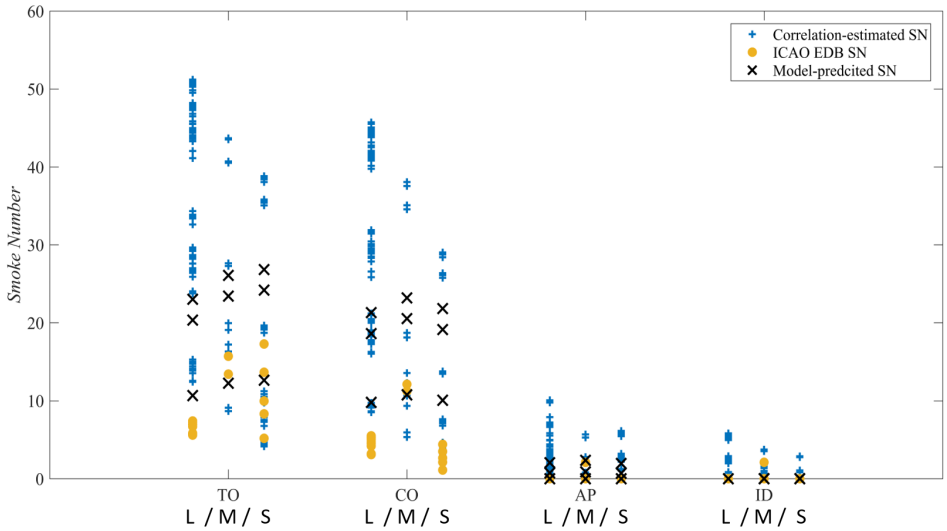

Figure 7.4: Comparison of results in SN metric

good agreement with trends in different power modes, for different cycles. Because the current regulation metric is the Smoke Number, the results are also compared in the SN metric, in Figure 7.4 and 7.5.

The Smoke Numbers in yellow circle markers are from the ICAO Emissions Databank[94]. The estimated EIs by FOX and ImFOX methods are converted to SN metric by the reverse procedure of the FOA3, FOAup, and FOAst methods. These are in blue + markers. The EIs by prediction environment are also converted to SN metric by the FOA3, FOAup, and FOAst methods. They are in black x markers. Because the FOX and ImFOX methods are developed due to the under-estimation issue of the FOA methods, blue + markers are generally in the upper location and the yellow circle markers are in the lower location. The black markers are in between, in general.

The trends of the SN results are the same as the EI results. Predicted values and estimated values are in good agreement. There are also many SN values not shown in the log-scale plot due to their zero or near-zero values in low power modes.

The upper limit of the current SN regulation is 50 and all aircraft passed the current SN regulation since it was introduced. However, in Figure 7.4 and 7.5, there are a few points

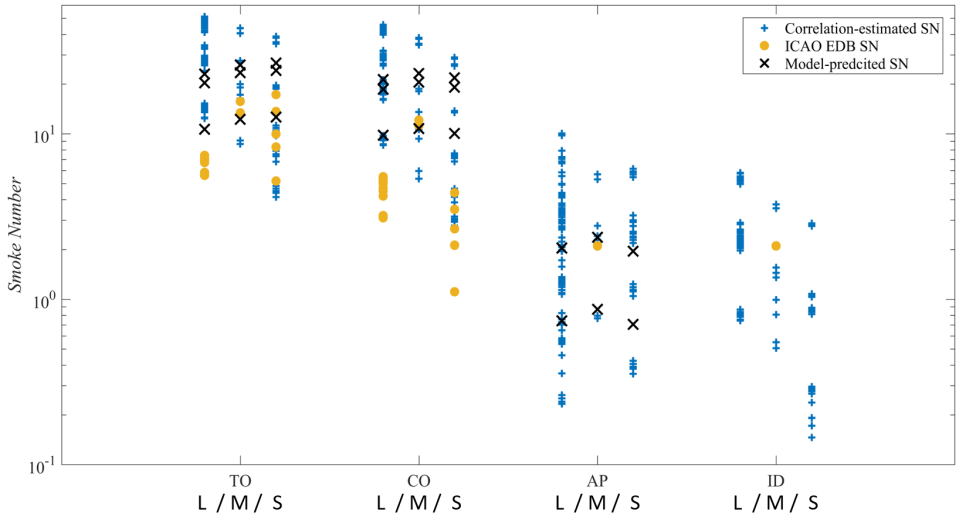

Figure 7.5: Comparison of results in SN metric (log-scale)

not satisfying the regulation standard limit. This is possibly due to the under-estimation issue of the FOA3 method. If the FOA methods are truly under-estimate emission index of non-volatile PM with a given Smoke Number, the reverse conversion methods over-predict the Smoke Number with a given emission index value.

The SN limit set by the current regulation standard is $83.6(F_{oo}^{-0.274})$ or a value of 50, whichever is lower[11]. From this formula, the regulation limit of SN for Engine L cycle is 18.20, for Engine M cycle is 22.44, and for Engine S cycle is 26.81. Some predicted and estimated SNs in the figures are over these limits. It possibly proves the over-estimation of inverse FOA methods, or the under-estimation of FOA methods.

7.2 Experiment and Evaluation of Hypotheses

The first hypothesis is

Hypothesis I

Air partitioning in different combustion zones must be modeled
in order to predict soot in different cycles

Based on this hypothesis, a circuit flow model computing air partitions of different combustion zones is modeled in the Combustor Flow Circuit model. The CFC model successfully performs air partitioning via computations in the flow circuit. In order to evaluate this hypothesis, simulations of the prediction environment are performed after the air partition model is replaced. Because there is no air partition, the CRN structure is also modified to have a set of parallel PSRs only without discretion of different combustion zones. Sizing methodology is also applied to the total volume of the combustor. In these simulations, no soot production is predicted for all three notional engine cycles of LTO cycles.

Different zones are responsible for different phases of soot formation. In the primary zone, due to the non-uniform mixing, the formation of soot is more dominant than oxidation. In the downstream of the combustor, oxidation is dominant due to the lean mixture. Without consideration of different combustion zone, the soot formation phenomena are not correctly captured. Because air partitioning is not considered, there is one burner instead of three different combustion zones with different equivalence ratio. The fuel-to-air ratio of of the one burner is the same as the input cycle fuel-to-air ratio and the equivalence ratio of one burner is very lean. Even though the statistical distribution is applied to model non-uniform mixture, the overall equivalence ratio is not rich enough to produce soot more than oxidation amount. The zero soot result implies that air partitioning must be modeled in order to predict soot. Without it, soot cannot be predicted correctly in any cycles. Therefore, the hypothesis I is proved at this point.

In order to evaluate the effect of air partitioning, an additional experiment is conducted.

Table 7.2 shows the air partitions of different combustion zones of notional Engine L, M, and S. While air partitions of Engine L and M are close each other, the air of different combustion zones are slightly differently partitioned. In this experiment, air partitioning model is de-activated while the air partition of the baseline is maintained for all cycles. The resultant changes are in Table 7.3.

Table 7.2: Air partitions at take-off power mode

	Engine L	Engine M	Engine S
PZ	40.94%	39.79%	34.02%
SZ	27.45%	27.98%	30.54%
DZ	31.61%	32.23%	35.44%

Table 7.3: Change in EI nvPM with assumed air partitions

	Take-off	Climb out	Approach	Idle
Engine L	+ 8.07	+ 10.9	+ 5.44	+ 0.00
Engine S	- 54.12	- 48.97	- 9.82	- 0.00

The predicted EI nvPM of Engine L increases with assumed air partitions in this simulation. The change is very small due to similar air partitions computed for Engine L and Engine M. In contrast, the EI nvPM predicted for the cycle of Engine S decreases a lot with assumed air partitions. The computed air partition of the primary zone for Engine S is 34.02% while the one for Engine M is 39.79%. The more air in the primary zone causes the leaner mixture in the primary zone and the less amount of soot is predicted in this experiment. This is in the opposite of Engine L case. Slightly smaller air partition causes richer primary zone for Engine L and more soot is predicted. In this experiment, the importance of air partitioning model addressed in the first hypothesis is emphasized again.

The second hypothesis is

Hypothesis II

In order for a soot prediction model to be applied to different engine cycles,
it must contain a sizing methodology.

In order to evaluate the second hypothesis addressing the importance of the sizing methodology, soot predictions for the cycles of Engine L and Engine S are simulated without sizing methodology. Without sizing methodology, the size of the combustor is the baseline size.

Table 7.4 shows the effects of sizing on soot prediction of Engine S cycle. In this experiment, the size of the combustor is for Engine M cycle while the mass flow rate of the Engine S cycle is less than Engine M cycle. The relatively larger volume of the combustor for the given cycle causes longer residence time for the flow. Therefore, more soot is produced at the high power modes in this experiment. However, less soot is predicted due to more oxidation caused by the lean primary zone in the low power modes.

Table 7.4: Effect of Sizing on EI nvPM (Engine S)

	Take-off	Climb out	Approach	Idle
with Sizing	146.73	128.35	10.39	0.00
without Sizing	267.86	239.19	1.31	0.00
% change	+82.55%	+86.35%	- 87.35%	N/A

Table 7.5 shows the effects of sizing on soot prediction of Engine L cycle. Due to the relatively large mass flow of Engine L cycle for the given baseline volume, the residence time is decreased and the flow does not stay long enough to produce soot. For this reason, the emission indices in all power modes are decreased.

Table 7.5: Effect of Sizing on EI nvPM (Engine L)

	Take-off	Climb out	Approach	Idle
with Sizing	121.34	124.62	10.98	0.00
without Sizing	28.46	25.85	1.59	0.00
% change	- 76.55%	- 79.26%	- 85.51%	N/A

From these two experiments, the substantial effect of sizing on soot prediction is observed. It can be concluded that the size must be computed for the given input cycle in order to predict the correct amount of soot. This conclusion proves the second hypothesis.

The third hypothesis is about the statistical distribution of non-uniformly mixed flow

Hypothesis III

Applying a statistical distribution of non-uniform flow to regions where soot phenomena are thermo-chemically active will improve predictive capability.

Two experiments to evaluate the third hypothesis are conducted. In the first experiment, the soot prediction environment is simulated without statistical distribution in the Statistical Distribution Model and the Chemical Reactor Networks model. The primary zone is modeled with one Perfectly Stirred Reactor instead of a set of parallel PSRs. In this experiment, no soot is predicted for all cycles. It is straight forward that no reactors are in the equivalence ratio region where soot is actively produced while the oxidation process is active in the primary zone modeled with one PSR having mean equivalence ratio computed via air partitioning. This result proves that the statistical distribution must be applied to model the non-uniformly mixed flow in order to predict soot.

The second experiment tests the range covered by the statistical distribution. In this experiment, the range of the distribution is limited to $\pm$ one standard deviation. The simulation results are in Table 7.6.

Table 7.6: EI nvPM with the reduced covered range in the statistical distribution

	Engine L	Engine M	Engine S
Take-off	2.47	34.16	53.70
Climb out	108.31	138.72	38.00
Approach	0.00	0.00	0.00
Idle	0.00	0.00	0.00

In overall, soot is under-predicted with reduced range of statistical distribution for all cycles. The produced soot amount is determined by the balance between formation and oxidation processes. The active regions of formation and oxidation phenomena are not correctly captured due to the reduced range in this experiment. When the region for formation is not captured, less soot is produced in the simulation. When the region where the oxidation process is active is not captured, less oxidation causes over-prediction. The active region for the formation is roughly 1.5 or richer equivalence ratio and the active region for the oxidation is around 0.7 to 1.5. When the statistical distribution does not fully capture these ranges due to the reduced covering range, the formation region is lost more than the oxidation region because the overall equivalence ratio at the primary zone is at one or less. For this reason, the emission indices in Table 7.6 are under-predicted in overall.

The results of these two experiments prove that the statistical distribution modeling non-uniform flow capturing soot formation phenomena are thermo-chemically important plays a crucial role in soot prediction.

7.3 Conclusion

7.3.1 Review

Due to the growing concern about the effect of PM on the environment and human health, aviation-emitted PM is one of the factors to be considered during the design of the gas turbine engine. However, there are not adequate methods to predict PM at the conceptual design phase. Current soot prediction methods utilize engine-specific information. They do not successfully compute combustor characteristics, which highly affects soot formation. For this reason, three hypotheses addressing air partitioning, sizing methodology, and the statistical distribution of the non-uniform mixture are established to provide a methodology to develop a prediction environment, capable of a variety of cycles.

The prediction environment consists of a Combustor Flow Circuit model, Statistical Distribution Model with the unmixedness curve, Chemical Reactor Networks (CRN), and Soot Evaluation Model. The Combustor Flow Circuit model, built on NPSS, computes air partitioning and sizes the combustor. The air partitioning model consists of NPSS elements, computing air distribution in the flow circuit via loss calculations in the combustor components. The Statistical Distribution Model is to model the imperfectly mixed primary zone over the parallelly organized Perfectly Stirred Reactors with statistically distributed equivalence ratio. The Chemical Reactor Networks model, built on CHEMKIN, computes and provides thermodynamic properties of flow and species information from all reactors to the Soot Evaluation Model. The Soot Evaluation Model computes quantitative non-volatile PM based on the soot formation mechanism applied to the semi-empirical two-equation system. These sub-models are integrated on ModelCenter and provides automated computations.

The integrated prediction environment developed with the proposed methodology shows good predictability for cycles of different size and thrust engines. The baseline environment is developed first and extended for different cycles. The unmixedness curve is generalized and embedded in the Statistical Distribution Model. The sizing model, scaling the length of

combustion zones and the sizes of the holes based on the combustor requirements and input cycles, are embedded in the Combustor Flow Circuit Model. The extended prediction environment provides automated computations to predict non-volatile PM emission for given input cycles.

The predicted emissions for two engine cycles of different size and thrust are compared and validated against a group of correlations whose inputs are the Smoke Number measurement and engine operating conditions. The results demonstrate good predictability, agreeing with estimations from correlations. With the developed prediction environment, three hypotheses, the basis of the development, are evaluated via a set of experiments. The effects of air partitioning, sizing, and statistical distribution modeling on the prediction of the non-volatile PM emission are evaluated while hypotheses are proved.

A methodology for the prediction of the non-volatile particulate matter emitted from the aircraft gas turbine engine is introduced via the development of the integrated prediction environment. The air partitioning, sizing, and non-uniform mixture modelings are incorporated in the prediction environment providing the capability of handling cycles of a variety of sizes and thrust classes. As the input of the prediction environment is a cycle, the proposed methodology is adequate for the prediction of non-volatile PM during the conceptual design of an aircraft engine.

7.3.2 Limitations and Future Works

Despite its good predictability, the proposed methodology has a few limitations. The first is that the methodology cannot capture the minor combustion phenomena producing soot. Soot is produced not only at the major combustion flow field but also at the unwanted place such as the near-wall field. Due to the interaction with the cooling flow and liner wall accompanying heat transfer, incomplete combustion occurs at the near-wall field and the soot is often produced here.

The current structure of the chemical reactor network and the statistical distribution

model cannot handle this phenomenon. In order to capture it, CRN may need to have additional structure modeling combustion at the near-wall flow field. Multi-modal distribution in the Statistical Distribution Model is also one of the possible approaches. In addition to the main distribution modeling the core flow, extra distributions for near-wall flow field may be required. The combustor model may also need to be modified in order to transfer useful information to the CFN and the SDM model. There are not many published studies on this issue. To implement these approaches in the prediction environment, more experiment and studies are required due to the increased complexity and following uncertainties. For this reason, these works are left to a future task.

Another limitation is the average flow field in the primary zone modeling. The current structure of the parallel PSRs in the CRN and the statistical distribution is to model the average flow field of the primary zone, where soot is actively produced. In the real combustor, the recirculating flow transfer heat to the fresh air and fuel and the diffusion flame starts before air and fuel are perfectly mixed at the early stage of combustion. The current structure of a single-layer PSRs cannot capture this phenomenon. In order to improve the structure,

1. More layer of PSRs in the CRN may be required. The multi-layer structure will model the transient state of mixing of the fuel and air. However, due to the increased number of reactors, not only increased computation time but also the increased number of design parameters for the additional layers such as volume and unmixedness parameters will significantly increase the complexity of the model.

2. Multi-modal distribution may be required. This solution is already suggested for the first issue. The extra distribution in addition to the main distribution modeling the core flow may be useful in modeling the combustion of the early stage when the fuel and air are not mixed well. However, this approach also causes more design variables and uncertainties due to increased complexity.

3. Recirculation modeling may be required in the CRN. However, there are several

issues in recirculation model. The fraction of recirculating flow, volume and residence time for the recirculation, these factors significantly increase the uncertainties. Moreover, the computations caused by recirculation accompanies iterations, significantly increases computation time.

Implementation of these three approaches while maintaining the computation speed to the adequate level for the conceptual design is another task to be studied in the future.

Another future work may be the implementation of the methodology to combustors of different architecture. As the methodology utilizes an object-orient code, NPSS, it has excellent expandability. By re-organizing elements, different architecture such as dual annular, twin annular, and staged combustors can be modeled. The statistical distribution model can also be applied to the region where fuel is injected in different architectures. The CRN is also flexible to handle different architecture.

7.3.3 Contributions

One of the major contributions of the current research is the suggestion of the methodology to develop integrated and automated non-volatile particulate matter prediction environment. As the cycle is the only required input in this methodology, the sub-models in the prediction environment are automatically executed and computes the predicted quantitative amount of non-volatile PM. Due to the fast computation speed, the proposed methodology is adequate for the soot prediction during the conceptual design of the aircraft engine.

The methodology to compute air partitioning is another contribution of the current research. The proposed methodology utilizes the flow circuit of the combustor. The air partitions, which are assumed or not considered in many studies, are now computed based on the given cycles.

In addition to air partitioning methodology, the sizing methodology also enables to handle different cycles. With the methodology, the appropriate size of volume can be applied to the combustor model based on the given cycles.

The use of Mechanism Interpolator and Generator models help to maintain continuous response of the model to the variation of cycles. The chemical mechanism is automatically generated via interpolation for given cycle input.

The unmixedness is generalized to respond to different conditions of the primary zones. As the values are found for two different combustion emissions whose trends are opposite, the created general curve is applicable not only to soot but also to other general combustion products.

With the implementation of air partitioning model, sizing methodology, and the generalized unmixedness curve, the proposed prediction environment is applicable to various cycles with different sizes and thrust classes. Therefore, the soot prediction methodology proposed in the current work can be utilized to predict soot emission during the conceptual design.

Appendices

APPENDIX A

A BRIEF REVIEW ON ADVERSE EFFECTS OF OXIDES OF NITROGEN

The photochemical smog in Los Angeles area in the mid 1940s was one of the most famous disasters associated with NO_X. The sunlight initiated chemical reactions of NO_X and subsequent reactions associated with unburned hydrocarbons caused severe photochemical smog in this region[45]. After this disaster, a lot of researches were conducted with public concerns to figure out the reasons of this smog and many adverse effects of NO_X were revealed.

There are several well-known negative aspects of NO_X. With carbon-based particulate matters, NO_X reduces visibility. Lakes and soils are damaged by the acid rain caused by NO_X[74]. More important aspects are associated with the ozone balance[45]. NO_X contributes to produce ozone species in the troposphere where people breathe. Exposure to the higher ozone concentration than normal atmospheric ozone concentration is harmful to human health. Respiratory illness, impaired vision, headache, and allergies can be caused by NO_X[34]. Another adverse aspect is the ozone depletion at the stratosphere. The depleted stratospheric ozone layer increases the chance of the skin cancer[34]. Because these depletion is catalytic reactions, small amount of NO_X results in the large amount of depletion. The reaction mechanism is[74]:

$$NO + O_3 \rightarrow NO_2 + O_2 \tag{A.1}$$

$$NO_2 + O \rightarrow NO + O_2 \tag{A.2}$$

Another major concern associated with human health is that NO_X reacts with various

compounds to form small particles which penetrate deeply into lungs. This penetration can cause respiratory disease and heart disease, and it can even cause premature death[3]. This is the formation of the secondary particulate matters discussed in the introduction chapter.

APPENDIX B

APEX MEASUREMENT AND CORRELATIONS

Emission indices of black carbon measured for LTO cycles during APEX I, II, III campaign[96] and estimated EIBC from various correaltions are in Figure B.1 - B.4, for different power modes. Measured data are in black markers with error bars indicating $\pm$ one standard deviation. higher thrust engines are in the left side and the lower thrust engines are in the right side. No trend in thrust is observed in these figures.

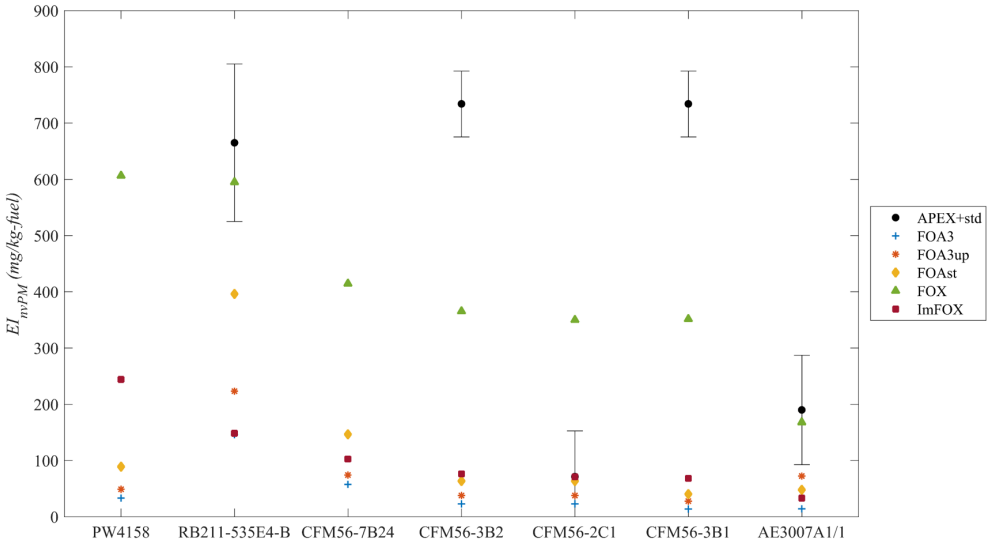

Figure B.1: Emission indices of non-volatile PM from APEX engines

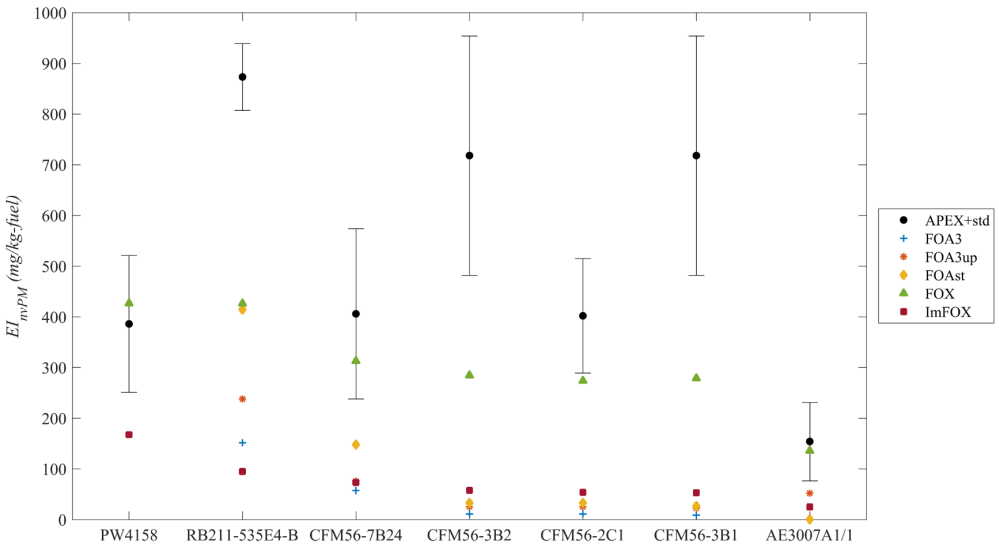

Figure B.2: Emission indices of non-volatile PM from APEX engines

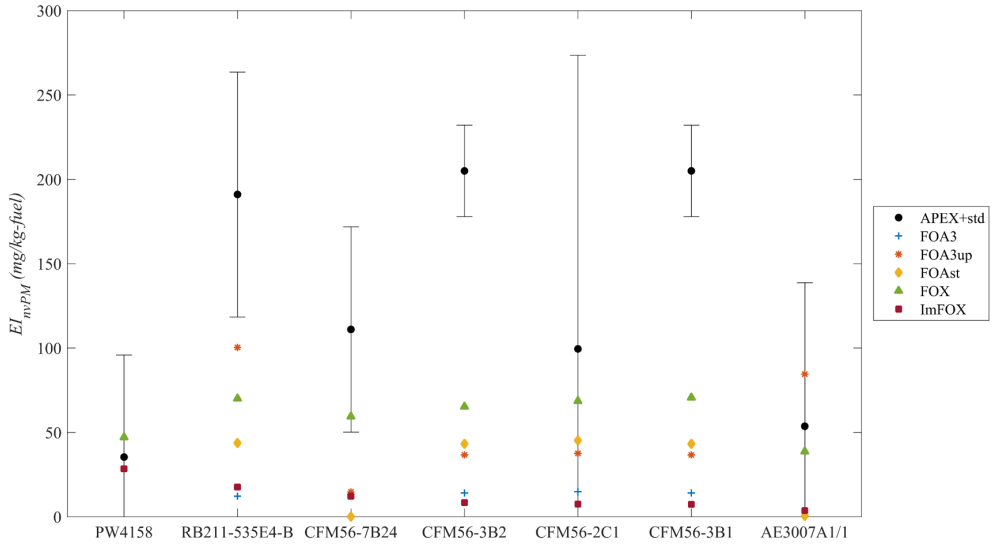

Figure B.3: Emission indices of non-volatile PM from APEX engines

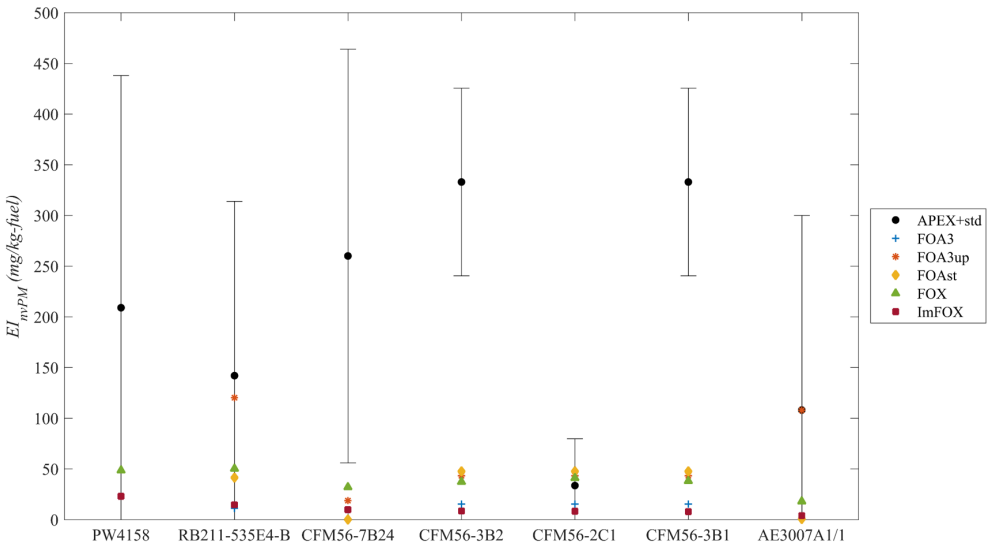

Figure B.4: Emission indices of non-volatile PM from APEX engines

Emission indices of black carbon measured for LTO cycles during APEX I, II, III campaign[96] and estimated EIBC from various correaltions are demonstrarted in Figure B.5 - B.11 for different engines. In general, more soot is measured at the higher power operation. However, this is not always true. More soot is observed at the climb out power than at the take-off power. Measured soot at the approach power mode is often less than at the idle power mode.

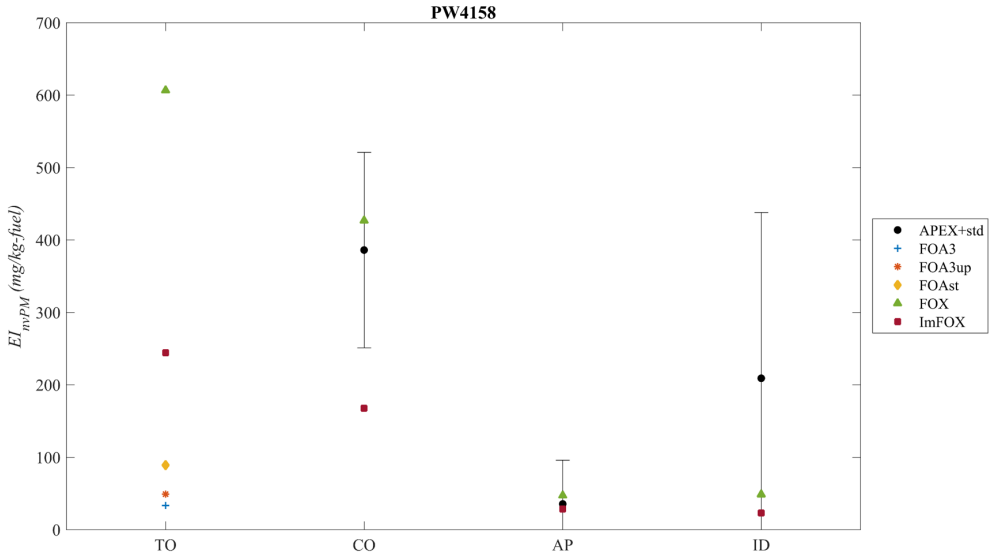

Figure B.5: Emission indices of non-volatile PM from APEX engines

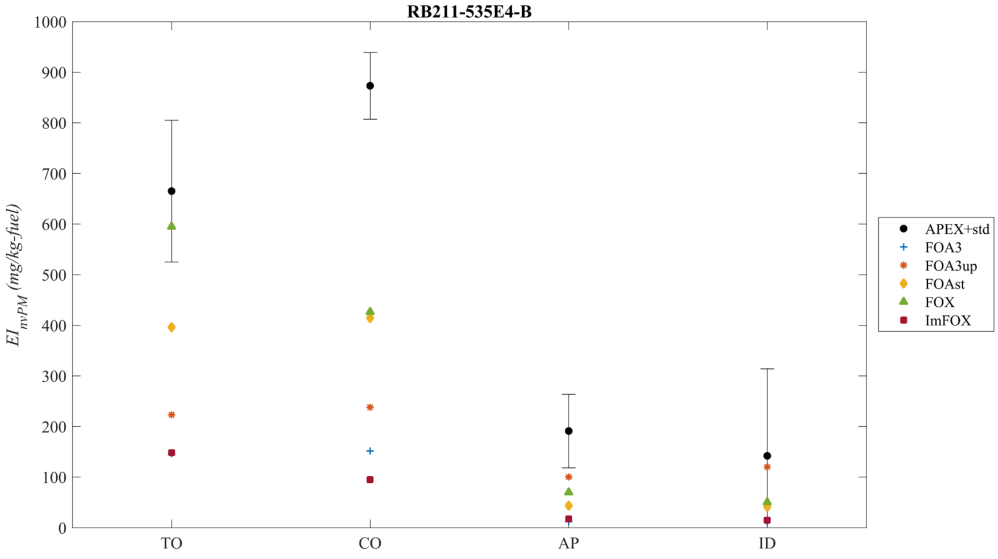

Figure B.6: Emission indices of non-volatile PM from APEX engines

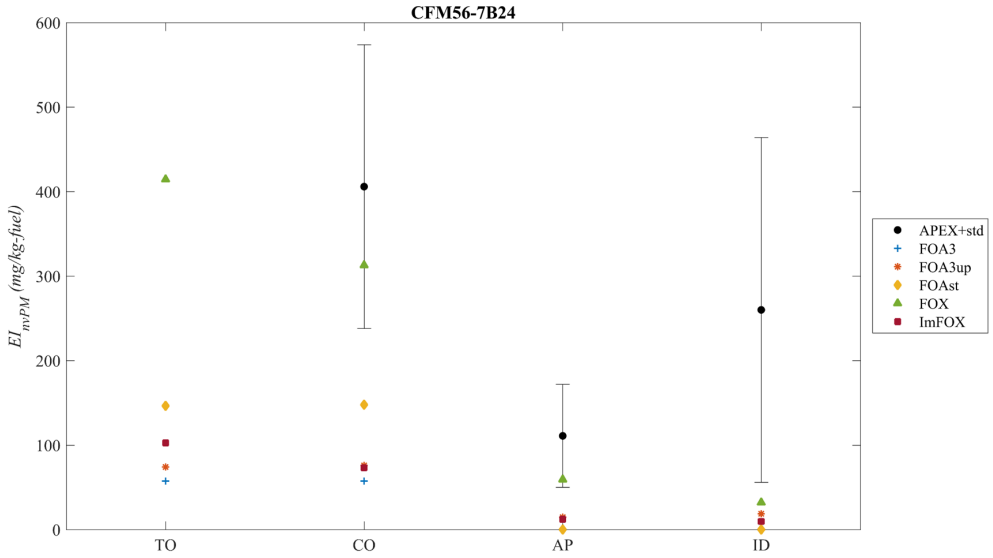

Figure B.7: Emission indices of non-volatile PM from APEX engines

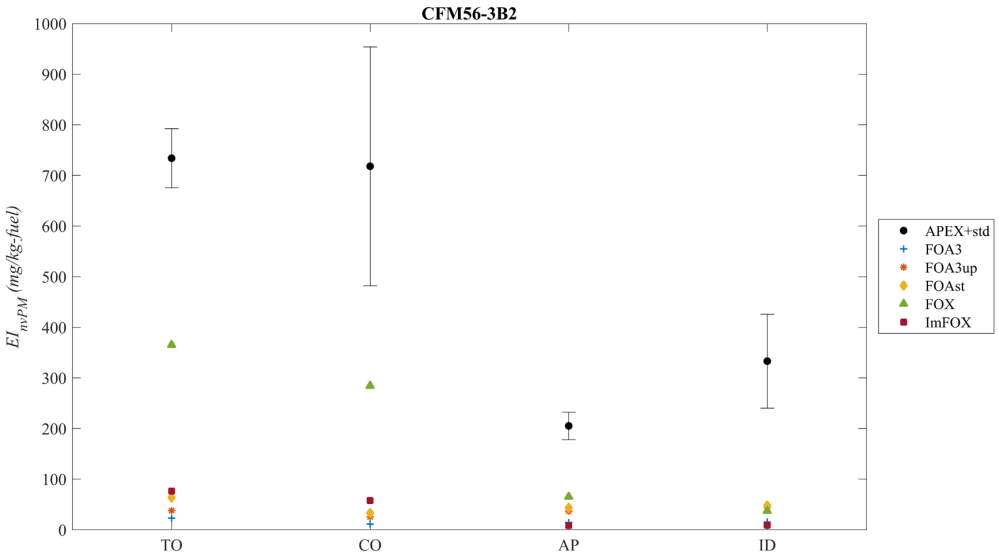

Figure B.8: Emission indices of non-volatile PM from APEX engines

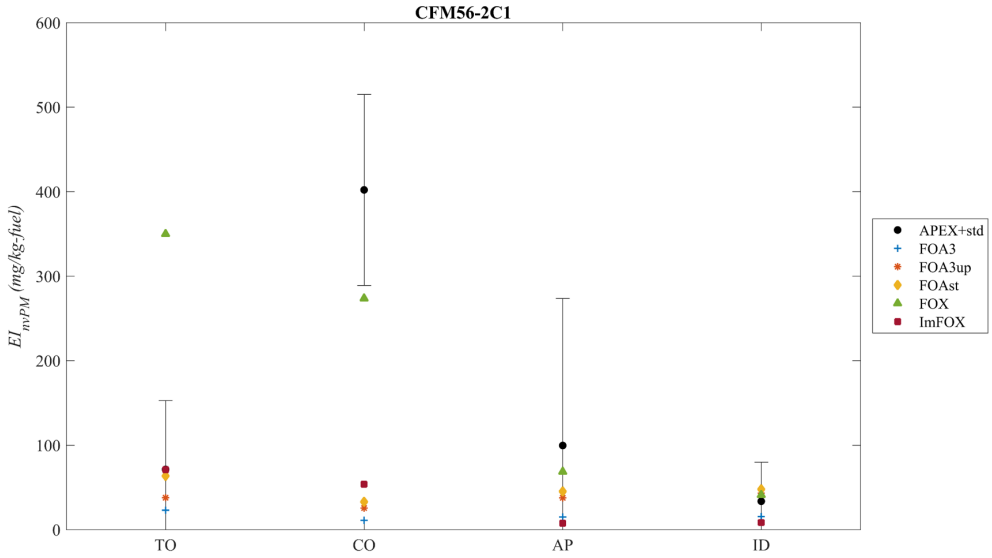

Figure B.9: Emission indices of non-volatile PM from APEX engines

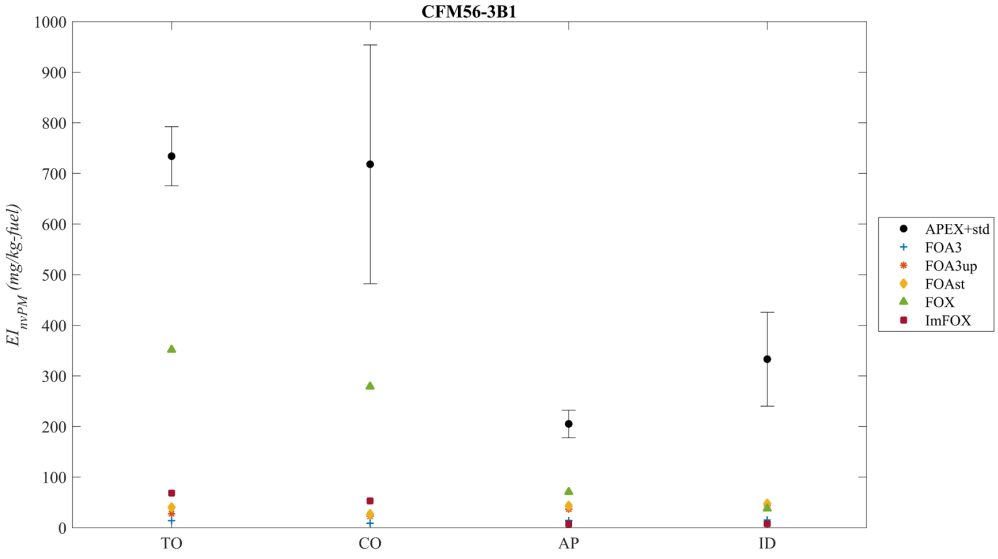

Figure B.10: Emission indices of non-volatile PM from APEX engines

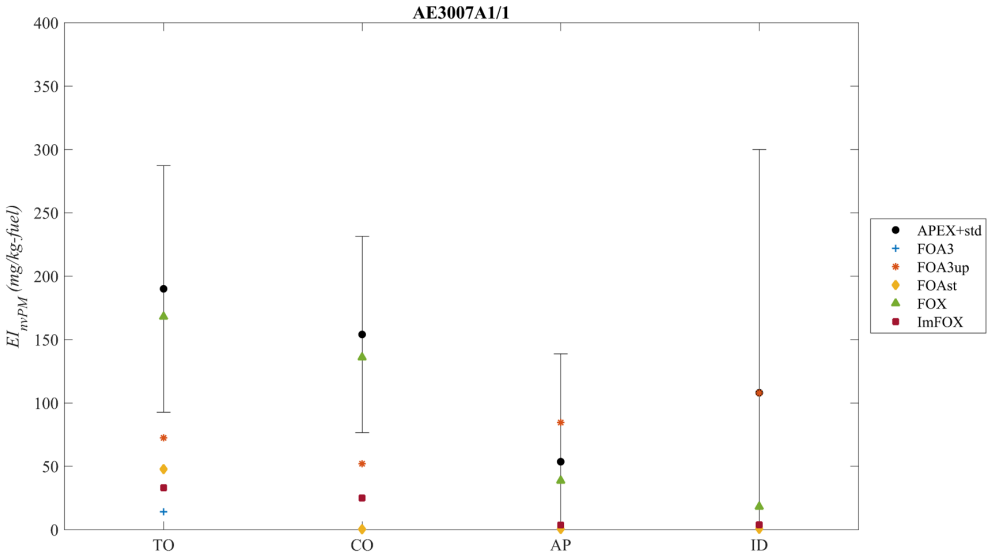

Figure B.11: Emission indices of non-volatile PM from APEX engines

The measurement results show considerable variability. Some standard deviation bars are larger than the average EIs. Many bars are over a few hundred EIs.

Measurement is usually larger than the correlation-estimated EIs. This is possibly due to the different measurement conditions of APEX and ICAO SN. In the APEX campaign, the engine is installed in the aircraft and the fuel is also from the same aircraft. The sampling is performed after 30 m from the exhaust. The operating time varies by tests. The ambient condition is also different from the standard condition. This is very different from the condition of SN measurement in ICAO certification process.

REFERENCES

[1] Airbus, Airbus Global Market Forecast, *Forecast 2015-2034*.

[2] World Health Organization and others, "Health aspects of air pollution with particulate matter, ozone and nitrogen dioxide: Report on a who working group, bonn, germany 13-15 january 2003," World Health Organization, Tech. Rep., 2003.

[3] United States Environmental Protection Agency. (2015). Health. `https://www3.epa.gov/airquality/nitrogenoxides/health.html` (accessed January 18, 2016).

[4] C. E. Kolb, "Atmospheric chemistry: Iodine's air of importance," *Nature*, vol. 417, no. 6889, pp. 597–598, 2002.

[5] J. Tollefson, "Climate's smoky spectre," *Nature*, vol. 460, no. 7251, p. 29, 2009.

[6] R. L. Wayson, G. G. Fleming, and R. Iovinelli, "Methodology to estimate particulate matter emissions from certified commercial aircraft engines," *Journal of the Air & Waste Management Association*, vol. 59, no. 1, pp. 91–100, 2009.

[7] R. L. Wayson, G. G. Fleming, B. Kim, and J. Draper, "Derivation of a first order approximation of particulate matter from aircraft," in *96th Annual Meeting of the Air & Waste Management Association*, 2006.

[8] A. Bhargava, D. Liscinsky, R. McKinney, B. Anderson, A. Petzold, and R. C. Miake-Lye, "Characterizing particulate matter emissions from aircraft engines," in *ASME Turbo Expo 2012: Turbine Technical Conference and Exposition*, American Society of Mechanical Engineers, 2012, pp. 1185–1194.

[9] G. Ratliff, C. Sequeira, I. Waitz, M. Ohsfeldt, T. Thrasher, M. Graham, T. Thompson, M Graham, and T Thompson, "Aircraft impacts on local and regional air quality in the united states," *PARTNER report (Report No. PARTNER-COE-2009-002)*, 2009.

[10] K. Choo, S. Lee, R. K. Denney, and D. N. Mavris, "A semi-empirical model to predict aircraft soot emission in rich zone of rql combustor," in *ASME Turbo Expo 2015: Turbine Technical Conference and Exposition*, American Society of Mechanical Engineers, 2015.

[11] International Civil Aviation Organization, *ICAO Annex 16: Environmental Protection, Volume II – Aircraft Engine Emissions*, Third. 2008.

[12] K. Neoh, J. Howard, and A. Sarofim, "Effect of oxidation on the physical structure of soot," in *Symposium (International) on Combustion*, Elsevier, vol. 20, 1985, pp. 951–957.

[13] J. Moss, C. Stewart, and K. Syed, "Flowfield modelling of soot formation at elevated pressure," in *Symposium (International) on Combustion*, Elsevier, vol. 22, 1989, pp. 413–423.

[14] K. M. Leung, R. P. Lindstedt, and W. Jones, "A simplified reaction mechanism for soot formation in nonpremixed flames," *Combustion and flame*, vol. 87, no. 3-4, pp. 289–305, 1991.

[15] R. Puri, R. J. Santoro, and K. C. Smyth, "The oxidation of soot and carbon monoxide in hydrocarbon diffusion flames," *Combustion and Flame*, vol. 97, no. 2, pp. 125–144, 1994.

[16] P. Sunderland and G. Faeth, "Soot formation in hydrocarbon/air laminar jet diffusion flames," *Combustion and flame*, vol. 105, no. 1-2, pp. 132–146, 1996.

[17] S. Brookes and J. Moss, "Predictions of soot and thermal radiation properties in confined turbulent jet diffusion flames," *Combustion and Flame*, vol. 116, no. 4, pp. 486–503, 1999.

[18] Z Wen, S Yun, M. Thomson, and M. Lightstone, "Modeling soot formation in turbulent kerosene/air jet diffusion flames," *Combustion and Flame*, vol. 135, no. 3, pp. 323–340, 2003.

[19] M Saffaripour, P Zabeti, S. Dworkin, Q Zhang, H Guo, F Liu, G. Smallwood, and M. Thomson, "A numerical and experimental study of a laminar sooting coflow jet-a1 diffusion flame," *Proceedings of the Combustion Institute*, vol. 33, no. 1, pp. 601–608, 2011.

[20] B. Franzelli, E. Riber, B. Cuenot, and M. Ihme, "Numerical modeling of soot production in aero-engine combustors using large eddy simulations," *submitted to ASME IGTI*, 2015.

[21] C. Eberle, P. Gerlinger, and M. Aigner, *A Comparison of URANS and LES for Soot Predictions in an Aero-Engine Model Combustor*. Deutsche Gesellschaft für Luft- und Raumfahrt-Lilienthal-Oberth eV, 2015.

[22] C. Eberle, P. Gerlinger, K. P. Geigle, and M. Aigner, "Numerical investigation of transient soot evolution processes in an aero-engine model combustor," *Combustion Science and Technology*, vol. 187, no. 12, pp. 1841–1866, 2015.

[23] H. Koo, M. Hassanaly, V. Raman, M. E. Mueller, and K. P. Geigle, "Large-eddy simulation of soot formation in a model gas turbine combustor," *Journal of Engineering for Gas Turbines and Power*, vol. 139, no. 3, p. 031 503, 2017.

[24] H. Moriai, R. Kurose, H. Watanabe, Y. Yano, F. Akamatsu, and S. Komori, "Large-eddy simulation of turbulent spray combustion in a subscale aircraft jet engine combustorpredictions of no and soot concentrations," *Journal of Engineering for Gas Turbines and Power*, vol. 135, no. 9, p. 091 503, 2013.

[25] M. E. Mueller and H. Pitsch, "Large eddy simulation of soot evolution in an aircraft combustor," *Physics of Fluids*, vol. 25, no. 11, p. 110 812, 2013.

[26] F. Dupoirieux and N. Bertier, "Methodology for the numerical prediction of soot formation in turbulent reactive flows and application to aircraft engine combustors," *International Journal of Sustainable Aviation*, vol. 2, no. 1, pp. 15–33, 2016.

[27] P. Ghose, J. Patra, A. Datta, and A. Mukhopadhyay, "Prediction of soot and thermal radiation in a model gas turbine combustor burning kerosene fuel spray at different swirl levels," *Combustion Theory and Modelling*, vol. 20, no. 3, pp. 457–485, 2016.

[28] B. Martini, "Development and assessment of a soot emissions model for aircraft gas turbine engines," PhD thesis, Massachusetts Institute of Technology, 2008.

[29] C. G. Moniruzzaman and F. Yu, "A 0d aircraft engine emission model with detailed chemistry and soot microphysics," *Combustion and Flame*, vol. 159, no. 4, pp. 1670–1686, 2012.

[30] J Bisson, P Seers, M Huegel, and F Garnier, "Numerical prediction of gaseous aerosol precursors and particles in an aircraft engine," *Journal of Propulsion and Power*, 2016.

[31] W. J. Fabrycky and B. S. Blanchard, *Life-cycle cost and economic analysis*. Prentice Hall Englewood Cliffs, NJ, 1991.

[32] M. J. Foust, D. Thomsen, R. Stickles, C. Cooper, and W. Dodds, "Development of the ge aviation low emissions taps combustor for next generation aircraft engines," *AIAA Paper*, vol. 936, p. 2012, 2012.

[33] D. Bahr, "Technology for the design of high temperature rise combustors," *Journal of propulsion and power*, vol. 3, no. 2, pp. 179–186, 1987.

[34] A. H. Lefebvre and D. R. Ballal, *Gas Turbine Combustion: Alternative Fuels and Emissions*, Third. CRC Press, 2010.

[35] P. J. Stuttaford and P. A. Rubini, "Preliminary gas turbine combustor design using a network approach," PhD thesis, Cranfield University, 1997.

[36] Z Saboohi and F Ommi, "Emission prediction in conceptual design of the aircraft engines using augmented crn," *The Aeronautical Journal*, pp. 1–24, 2017.

[37] T. C. Lieuwen and V. Yang, *Gas turbine emissions*. Cambridge University Press, 2013, vol. 38.

[38] European Aviation Safety Agency. (2017). European aviation environmental report. https://www.easa.europa.eu/eaer/figures-tables/reference-landing-and-take-lto-cycle(accessed September 11, 2017).

[39] Lenntech. (2017). Molecular weight calculator. http://www.lenntech.com/calculators/molecular/molecular-weight-calculator.htm(accessed September 12, 2017).

[40] F. L. Dryer, Y. Ju, K. Brezinsky, R. J. Santoro, T. A. Litzinger, and C.-J. Sung, "Generation of comprehensive surrogate kinetic models and validation databases for simulating large molecular weight hydrocarbon fuels," Princeton University NJ Dept of Mechanical and Aerospace Engineering, Tech. Rep., 2012.

[41] P. P. Walsh and P. Fletcher, *Gas turbine performance*. Blackwell Science and ASME, 2004.

[42] R. E. Henderson and W. S. Blazowski, "Turbopropulsion combustion technology," *Aircraft Propulsion Systems Technology and Design*, pp. 105–165, 1989.

[43] J. D. Mattingly, W. H. Heiser, and D. T. Pratt, "Aircraft engine design, american institute of aeronautics and astronautics," *Inc., Reston, VA*, vol. 2, 2002.

[44] R. G. McKinney and J. B. Hoke, "Aero gas turbine combustion: Metrics, constraints, and system interactions," *Gas Turbine Emissions*, vol. 38, p. 3, 2013.

[45] I. Glassman and R. A. Yetter, *Combustion*, Fourth. Academic press, 2008.

[46] M. Colket, "Modeling of particulate emissions," United Technologies Research Center East Hartford CT, Tech. Rep., 2011.

[47] S. Farokhi, *Aircraft propulsion*. John Wiley & Sons, 2014.

[48] H Cohen, G. Rogers, and H. Saravanamuttoo, "Gas turbine theory 4th ed," *Padstow, Cornwall, UK*, 1996.

[49] W. R. Hawthorne, "Some aerodynamic problems of aircraft engines," *Journal of the Aeronautical Sciences*, vol. 24, no. 10, pp. 713–730, 1957.

[50] J. D. Anderson, *Modern compressible flow: with historical perspective*. McGraw-Hill New York, 1990, vol. 12.

[51] S. Samuelsen, "Rich burn, quick-mix, lean burn (rql) combustor," *The Gas Turbine Handbook, US Department of Energy, Office of Fossil Energy, National Energy Technology Laboratory, DOE/NETL2006-1230*, pp. 227–233, 2006.

[52] P. Whitney and G. E. A. Engines, "Critical propulsion components, volume 2: Combustor," National Aeronautics and Space Administration Glenn Research Center, NASA/CR2005-213584/VOL2, Tech. Rep., 2005.

[53] P. R. Lindstedt, "Simplified soot nucleation and surface growth steps for non-premixed flames," in *Soot Formation in Combustion*, Springer, 1994, pp. 417–441.

[54] R. Hall, M. Smooke, and M. Colket, "Predictions of soot dynamics in opposed jet diffusion flames," *Physical and Chemical Aspects of Combustion: A Tribute to Irvin Glassman*, vol. 4, pp. 189–229, 1997.

[55] A. M. El-Leathy, C. H. Kim, G. M. Faeth, and F. Xu, "Soot surface reactions in high-temperature laminar diffusion flames," *AIAA journal*, vol. 42, no. 5, pp. 988–996, 2004.

[56] G. P. Smith, D. M. Golden, M. Frenklach, N. W. Moriarty, B. Eiteneer, M. Goldenberg, C. T. Bowman, R. K. Hanson, S. Song, W. C. Gardiner Jr, *et al.*, "Gri 3.0 mechanism," *Gas Research Institute (http://www. me. berkeley. edu/gri_mech)*, 1999.

[57] D. N. Mavris and J. S. Schutte, "Application of deterministic and probabilistic system design methods and enhancements of conceptual design tools for era project," NASA Langley Research Center; Hampton, VA, United States, Tech. Rep., 2016.

[58] Kent State University Libraries. (2017). Spss tutorials: Pearson correlation. `https://libguides.library.kent.edu/SPSS/PearsonCorr` (accessed October 18, 2017).

[59] E. Demetri, "Effects of major design and operating parameters on achieving low emissions from gas turbine combustors," *Journal of Fluids Engineering*, vol. 97, no. 3, pp. 303–309, 1975.

[60] R Fletcher and J Heywood, "A model for nitric oxide emission from aircraft gas turbine engines," in *9th Aerospace Sciences Meeting*, 1971, p. 123.

[61] J. B. Heywood and T. Mikus, "Parameters controlling nitric oxide emissions from gas turbine combustors," in *AGARD Atmospheric Pollution by Aircraft Engines*, 1973.

[62] T. Mikus and J. B. Heywood, "The automotive gas turbine and nitric oxide emissions," *Combustion Science and Technology*, vol. 4, no. 1, pp. 149–158, 1971.

[63] F. Pompei and J. B. Heywood, "The role of mixing in burner-generated carbon monoxide and nitric oxide," *Combustion and Flame*, vol. 19, no. 3, pp. 407–418, 1972.

[64] G. Sturgess, J. Zelina, D. T. Shouse, and W. Roquemore, "Emissions reduction technologies for military gas turbine engines," *Journal of Propulsion and Power*, vol. 21, no. 2, pp. 193–217, 2005.

[65] D. L. Allaire, I. A. Waitz, and K. E. Willcox, "A comparison of two methods for predicting emissions from aircraft gas turbine combustors," in *Proceedings of the ASME Turbo Expo*, vol. 2, 2007, p. 899.

[66] N. K. Rizk, J. S. Chin, A. W. Marshall, and M. K. Razdan, "Predictions of nox formation under combined droplet and partially premixed reaction of diffusion flame combustors," *Journal of Engineering for Gas Turbines and Power*, vol. 124, no. 31–38, V002T02A059–V002T02A059, 2002.

[67] R. Rezvani, "A conceptual methodology for the prediction of engine emissions," PhD thesis, Georgia Institute of Technology, 2010.

[68] G. Sturgess, "An account of fuel/air unmixedness effects on nox generation in gas turbine combustors," Innovative Scientific Solutions Inc. Dayton, OH (US), Tech. Rep., 1998.

[69] Center for Integrated Turbulence Simulations, Stanford University. (2004). LES of Multiphase Reacting Flows in PW Combustors. `https://web.stanford.edu/group/cits/simulation/pw_combustors.html` (accessed November 8, 2017).

[70] J. K. Lytle, "The numerical propulsion system simulation: A multidisciplinary design system for aerospace vehicles," 1999, NASA / TM–1999-209194.

[71] ——, "The numerical propulsion system simulation: An overview," 2000, NASA / TM–2000-209915.

[72] M. Wiggert and D. Potter, *Mechanics of fluids*, 2002.

[73] G. Sturgess, R. McKinney, and S. Morford, "Modification of combustor stoichiometry distribution for reduced n0x emission from aircraft engines," *Journal of Engineering for Gas Turbines and Power*, vol. 115, 23 1993.

[74] S. R. Turns, *An Introduction to Combustion: Concepts and Applications*, Second. MCGRAW-HILL, 2000.

[75] ANSYS CHEMKIN-PRO 18.1, ANSYS: San Diego, 2017.

[76] P. Dagaut and S. Gaïl, "Chemical kinetic study of the effect of a biofuel additive on jet-a1 combustion," *The Journal of Physical Chemistry A*, vol. 111, no. 19, pp. 3992–4000, 2007.

[77] P. Dagaut, F. Karsenty, G. Dayma, P. Diévart, K. Hadj-Ali, A. Mzé-Ahmed, M. Braun-Unkhoff, J. Herzler, T. Kathrotia, T. Kick, *et al.*, "Experimental and detailed kinetic model for the oxidation of a gas to liquid (gtl) jet fuel," *Combustion and Flame*, vol. 161, no. 3, pp. 835–847, 2014.

[78] P. Dagaut and M. Cathonnet, "The ignition, oxidation, and combustion of kerosene: A review of experimental and kinetic modeling," *Progress in energy and combustion science*, vol. 32, no. 1, pp. 48–92, 2006.

[79] Nitrogen Chemistry, "Chemical-Kinetic Mechanisms for Combustion Applications", San Diego Mechanism web page, Mechanical and Aerospace Engineering (Combustion Research), University of California at San Diego (http://combustion.ucsd.edu), (accessed September 9, 2018).

[80] Reaction Workbench 18.1, ANSYS: San Diego, 2017.

[81] M. Herbert, "Combustion researches and review, 1957," in *AGARDograph 15*, Pergamon, 1957, p. 76.

[82] MATLAB, *version R2015b*. Natick, Massachusetts: The MathWorks Inc., 2015.

[83] K. Young, C. Stewart, and J. Moss, "Soot formation in turbulent nonpremixed kerosine-air flames burning at elevated pressure: Experimental measurement," in *Symposium (International) on combustion*, Elsevier, vol. 25, Elsevier BV, 1994, pp. 609–617.

[84] C. Kim, A. El-Leathy, F Xu, and G. Faeth, "Soot surface growth and oxidation in laminar diffusion flames at pressures of 0.1–1.0 atm," *Combustion and flame*, vol. 136, no. 1, pp. 191–207, 2004.

[85] M. Frenklach and H. Wang, "Detailed modeling of soot particle nucleation and growth," in *Symposium (International) on Combustion*, Elsevier, vol. 23, 1991, pp. 1559–1566.

[86] M. B. Colket and R. J. Hall, "Successes and uncertainties in modeling soot formation in laminar, premixed flames," in *Soot formation in combustion*, Springer, 1994, pp. 442–470.

[87] J. Nagle and R. Strickland-Constable, "Oxidation of carbon between1000–2000c," in *Proceedings of the Fifth Conference on Carbon*, Elsevier, 1962, pp. 154–164.

[88] K. Lee, M. Thring, and J. Beer, "On the rate of combustion of soot in a laminar soot flame," *Combustion and Flame*, vol. 6, pp. 137–145, 1962.

[89] S Von Gersum and P Roth, "High temperature oxidation of soot particles by o atoms and oh radicals," *Journal of Aerosol Science*, vol. 21, S31–S34, 1990.

[90] P. Roth and S. von Gersum, "High temperature oxidation of soot particles by o, oh, and no," in *Turbulence and molecular processes in combustion*, Elsevier, 1993, pp. 149–163.

[91] K. Neoh, J. Howard, and A. Sarofim, "Soot oxidation in flames," in *Particulate Carbon*, Springer, 1981, pp. 261–282.

[92] G Ma, J. Wen, M. Lightstone, and M. Thomson, "Optimization of soot modeling in turbulent nonpremixed ethylene/air jet flames," *Combustion Science and Technology*, vol. 177, no. 8, pp. 1567–1602, 2005.

[93] M Kirby and D Mavris, "The environmental design space," in *26th International Congress of the Aeronautical Sciences*, vol. 26, 2008.

[94] International Civil Aviation Organization. (2017). ICAO Aircraft Engine Emissions Databank v25a. `https://www.easa.europa.eu/document-library/icao-aircraft-engine-emissions-databank` (accessed September 22, 2018).

[95] Type Certificate Data Sheet E00055EN, REVISION 9, Federal Aviation Administration, U.S. Department OF Transportation, 2011.

[96] J. S. Kinsey, *Characterization of emissions from commercial aircraft engines during the Aircraft Particle Emissions eXperiment (APEX) 1 to 3*. Office of Research and Development, US Environmental Protection Agency, 2009.

[97] M. E. J. Stettler, J. J. Swanson, S. R. H. Barrett, and A. M. Boies, "Updated correlation between aircraft smoke number and black carbon concentration," *Aerosol Science and Technology*, vol. 47, no. 11, pp. 1205–1214, 2013.

[98] M. E. Stettler, A. M. Boies, A. Petzold, and S. R. Barrett, "Global civil aviation black carbon emissions," *Environmental Science & Technology*, vol. 47, no. 18, pp. 10 397–10 404, 2013.

[99] W. Dodds, M. Colket III, A. Mellor, and J. Peters, "Preliminary study of smoke formed in the combustion of various jet fuels," *Journal of Energy*, vol. 1, no. 2, pp. 115–120, 1977.

[100] J. S. Kinsey, Y. Dong, D. C. Williams, and R. Logan, "Physical characterization of the fine particle emissions from commercial aircraft engines during the aircraft particle emissions eXperiment (APEX) 1–3," *Atmospheric Environment*, vol. 44, no. 17, pp. 2147–2156, 2010.

[101] J. P. Abrahamson, J. Zelina, M. G. Andac, and R. L. V. Wal, "Predictive model development for aviation black carbon mass emissions from alternative and conventional fuels at ground and cruise," *Environmental Science & Technology*, vol. 50, no. 21, pp. 12 048–12 055, 2016.

[102] M. Keramat and R. Kielbasa, "Latin hypercube sampling monte carlo estimation of average quality index for integrated circuits," *Analog Integrated Circuits and Signal Processing*, vol. 14, no. 1-2, pp. 131–142, 1997.

[103] JMP, Version 14.1. SAS Institute Inc., Cary, NC, 1989-2019.

[104] ModelCenter, Version 11.2.3. Phoenix Integration, Inc., 2016.

[105] K. Song, K. H. Choo, and D. Mavris, "A spline-based modeling algorithm for application to aerodynamic shape optimization based on CFD analysis," *SAE International Journal of Passenger Cars - Mechanical Systems*, vol. 10, no. 2017-01-1510, pp. 541–552, 2017.

[106] A. H. Lefebvre and G. A. Halls, *Some experiences in combustion scaling*. Pergamon, 1959.

[107] N. Pegemanyfar, M. Pfitzner, R. Eggels, R. von der Bank, and M. Zedda, "Development of an automated preliminary combustion chamber design tool," in *ASME Turbo Expo 2006: Power for Land, Sea, and Air*, American Society of Mechanical Engineers, 2006, pp. 327–336.

[108] S. Tietz and T. Behrendt, “Development and application of a pre-design tool for aero-engine combustors,” *CEAS Aeronautical Journal*, vol. 2, no. 1-4, pp. 111–123, 2011.

VITA

Kyung Hak Choo was born and raised in Seoul, Korea. He received Bachelor in Mechanical Engineering at the Korea University in 2009. During his college, he served for two years as military police in the Eighth United States Army in Yongsan, and he was a visiting student at the University of California, Davis.

He was an undergraduate research assistant in the Aerostructure/Vibration Control Laboratory at Korea University, working on the fuzzy logic and data analysis. He joined the Ben T. Zinn Combustion Laboratory at the Georgia Institute of Technology as a graduate research assistant, researching optical diagnostics. He earned his Master of Science degree in 2011.

He joined the Aerospace Systems Design Laboratory at the School of Aerospace Engineering at the Georgia Institute of Technology to pursue his doctoral degree. He studied the propulsion system, combustion modeling, and emission predictions, mainly sponsored by the National Aeronautics and Space Administration. He earned his Doctor of Philosophy in August 2019.